Constraints on Petrogenesis and Elemental Recycling of the Tonga-Kermadec Island Arc System and the associated Lau and North Fiji Basins

Raul Brens Jr

B.A. Earth Science and History

Boston University

M.Sc. Geosciences

Florida International University

Department of Earth and Planetary Sciences

Faculty of Science and Engineering

Macquarie University

Sydney, Australia

This thesis is submitted for the degree of Doctor of Philosophy

June 2018

DECLARATION

I declare that this work is original except where indicated by reference in the text and that no part of the thesis has been submitted for a higher degree to any other university or institution unless otherwise noted as written collaboratively. This thesis comprises seven chapters, four of which have been written in journal article format. As such, there is some repetition of introduction and summary material but has been included for completeness. The following table acknowledges the work of co-authors and outlines their respective contributions to the work present herein.

In addition, I certify that all information sources and literature used are indicated in the thesis.

Raul Brens Jr.

19th of December 2017

LIST OF ORIGINAL PUBLICATIONS

The following original publications are presented in this thesis investigation. They are referred to throughout by their respective roman numerals defined here. A table outlining the division of labor in the co-authored papers is provided on the next page. These publications, co-authored with me, comprise the principal chapters of my thesis.

I. Lithium isotopic composition of the Tonga-Kermadec Arc and constraints on subduction recycling

Co-Authors: Xiaoming Liu, Roberta Rudnick, Tracy Rushmer, and Simon Turner

Status: submitted (the submitted version is in Appendix B)

II. Volatile contents reveal mid-ocean basalt tapping an ocean island magma source

Co-Authors: Frances Jenner, Allison Price, Emma Bullock, Erik Hauri, Simon Turner, Tracy Rushmer, and Richard Arculus

Status: prepared

III. Geodynamic implications for zonal and meridional isotopic patterns across the northern Lau and North Fiji Basins

Co-Authors: Allison Price, Frances Jenner, Matthew Jackson, Janne Blichert-Toft, Jim Gill, Jerzy Blusztajn, and Richard Arculus

Status: accepted

IV. Using experimental petrology to constrain genesis of wet, silicic magmas in the Tonga-Kermadec island arc: a case study of the volcanic island of Late

Co-Authors: Tracy Rushmer, John Adams, and Simon Turner

Status: prepared as a thesis chapter only

List of Contributors/Contributions

DIVISION OF LABOR IN CO-AUTHORED ARTICLES

AP – Allison Price; EB – Emma Bullock; EH – Erik Hauri; FJ – Frances Jenner; JA – John Adam; JB – Jerzy Blusztajn; JBT – Janne Blichert-Toft; JG – Jim Gill; MJ – Matthew Jackson; MK – Mark Kurz; RA – Richard Arculus; RB – Raul Brens; RR – Roberta Rudnick; ST – Simon Turner; TR – Tracy Rushmer; XL – Xiaoming Liu (* indicates supervision from TR and ST; ** indicates supervision from JBT and MJ)

	I	II	III	IV
Concept & Design	RB, ST, TR	RB, FJ, AP, RA	AP, RB, FJ, RA	RB, TR, ST
Planning & Implementation	RB, RR, XM	RB, FJ, AP	AP, RB, FJ, MJ, JG, MK	RB, JA
Data Collection	RB, XM	FJ, EB, RB	AP, JBT	RB
Analysis & Interpretation	RB, ST, RR	RB, FJ	AP, RB, FJ	RB, JA
Writing the article	RB*	RB*	AP, RB, FJ**	RB*
Overall responsibility	RB	RB	AP	RB

CONSTRAINTS ON PETROGENESIS AND ELEMENTAL RECYCLING OF THE TONGA-KERMADEC ISLAND ARC SYSTEM AND THE ASSOCIATED LAU AND NORTH FIJI BASINS

RAUL BRENS JR.

Macquarie University, 2017

Sydney, Australia

Principal Supervisor: Dr Tracy Rushmer, Associate Professor

ABSTRACT OF THESIS

Subduction zones are sites where subducted materials achieve one of two opposing outcomes, either recycling back to the crust or being transferred to the deep mantle. The composition of arc magmas, and to a lesser extent the associated extensional back-arc basin, reflects the reservoirs that influence the chemical composition of arc lavas and subducted materials: the altered oceanic crust, the mantle, the overlying crust, and occasionally hotspots. To better understand the complex processes occurring in subduction zones, a series of studies investigate the process in which subducting elements recycle and interact with various upper mantle components and ultimately form into igneous rocks. This investigation takes a multifaceted approach to further understand the history and source of magmatism in intra-oceanic arcs, using as an example the Tongan arc from inception (subduction) to completion (petrogenesis and eruption). Constraining petrogenesis and elemental recycling within the Tonga-Kermadec Island arc and Lau back-arc basin system is integral to understanding crust-mantle exchange. The Tonga-Kermadec arc setting is ideal to test the chemical

influences imparted on the lavas from a range of dynamic forces because these magmas are not contaminated with continental crust.

This research focuses on magmas associated with the plate tectonic cycle at both convergent and divergent plate margins within the Tonga-Kermadec volcanic arc, Lau basin, and North Fiji basin system. In order to untangle the intricacies associated with constraining the contributions to intra-oceanic arc magmas (Tonga-Kermadec arc) and to identify the sources affecting mantle evolution over time in the accompanying back-arc basins (Lau basin and North Fiji basin), a range of geochemical, geothermobarometric, and high and low pressure experimental techniques have been applied. This study consists of 1) analyzing and quantifying how elements recycle within a subduction zone through the use of Li isotopes; 2) experimentally constraining pressure, temperature and water conditions that drive melting and magma generation at Late volcano, located on the active volcanic front; and 3) by using the major, trace, volatile elements along with radiogenic isotope data to create an intricate and cohesive dataset from back-arc samples collected during the 2012 Northern Lau Transit Expedition (NoLauTe) of the R/V Southern Surveyor (cruise name: ss2012_v02).

This study concludes that addition of up to 3.5% sediment is present in the arc front lavas and that back-arc lavas equilibrate with the mantle wedge, which may reflect a longer slab-to-surface path traversed by the magmas. This study also questions the utility of lithium as a possible tracer of recycled material. The (mid-ocean ridge basalt) MORB-like lithium isotopic composition of the Tonga-Kermadec lavas suggests that the lithium elemental and isotopic characteristics reflect either, or a combination of, equilibration with the mantle wedge or sequestration and removal of the heavy Li in the system, possibly linked to slab-convergence rate. Pyroxene thermobarometry for the subaerial volcano studied (Late) suggests fractional crystallization at 1020-1070 ^{o}C at 0.8-1.8 kbar. A lack of hydrous mineral phases in all of the experiments as well as in the

natural rock sample negates the influence of an amphibolite melt. The experimental results support shallow crustal (2-6 km) crystal fractionation of basalt that produces an evolved magmatic composition. Whereas the lavas from the Lau basin and connecting North Fiji basin indicate a primary influence from a wet plume source (Samoa) and additional extreme geochemical contributions (high $^{3}He/^{4}He$, high $^{87}Sr/^{86}Sr$, HIMU: high-μ = $^{238}U/^{204}Pb$) from the Samoa, Rarotonga, and Rurutu hotspots. For the first time, it is possible to map a clear north-south and east-west geochemical gradient in $^{87}Sr/^{86}Sr$ across the northern Lau and North Fiji basin: lavas with the most geochemically enriched radiogenic isotopic signatures are located to the northeastern Lau Basin, while signatures of geochemical enrichment are diminished to the south and west away from the Samoan hotspot.

ACKNOWLEDGEMENTS

First and foremost, I would like to thank my principal supervisor, Dr Tracy Rushmer. Tracy granted me the freedom to pursue projects I felt passionate about while encouraging, challenging, and imparting valuable insights and opinions that drove the research forward. She has been a great mentor who has always been there to answer my questions, both academic and philosophical, even before I started as a PhD student. Similarly, my secondary advisor, Dr Simon Turner, has always challenged me to think in outside the box in unconventional ways. Through him, I have continually enhanced my skills in geochemistry for which I will forever be grateful. Tracy and Simon allowed me to meet numerous scientists from all over the world that have taught me valuable lessons throughout my PhD. I thank Dr Roberta Rudnick, for allowing me to collaborate and undertake research in her laboratory at UMaryland. Without her knowledge, my project would not have been possible. Dr Xiaoming Liu, who taught me techniques for analyzing lithium, that formed one of the biggest facets of my project. Dr Frances Jenner and Dr Allison Price, who both helped me carve out supporting aspects of my project. Their eagerness and passion are infectious, and that excitement helped me to build my project. Without the help of Dr Richard Arculus, I would not have had the samples for my PhD. He was the Chief Scientist on the research vessel. I am grateful for all the long hours of conversation about back-arc geochemistry. Finally, Dr John Adam, who has an entire library of knowledge ready to be utilized at all times. He taught me everything I know about experiments, and I am very thankful for his time and care.

I would like to thank the professors and professional staff at Macquarie University who have been there for me when I have had many questions, since starting as a postgrad from the other side of the world. I thank David Adams and Peter Wieland for their many hours help and support in the laboratories. I also thank Dr Kelsie Dadd, who became my professional mentor. Observing her teach was captivating and made me

want to be a better teacher. Dr Stephen Foley, who has always been more than happy to help me with any research problem. Dr Dorritt Jacob, who has continually looked for me in the office to say hello and see how I was doing. The administrative staff in our department have also been very supportive and helpful with any and every question.

I would also like to thank my previous supervisors Dr Terry Plank and Dr Rosemary Hickey-Vargas because it is due to their encouragement and guidance that I decided to pursue a PhD in Australia. They have changed my life and am truly grateful for it.

My friends have been the cornerstone of my support system. Being a postgraduate is not easy, and adding moving to a new country makes that task seem entirely unmanageable. However, I am very fortunate to have very supportive friends that have been there to support me and cheer me on through all the highs and lows of a PhD as well as migrating to a new country. I am eternally thankful to Duncan Jones who has had one of the most significant impacts in my life and during my PhD, Lars Wijers who has a heart of gold and taught me a great deal about computer programs, mainly Illustrator, and Ben Keast who has always found a way to break me with laughter and help me see the fun side of life. Dr Alex Gold has been one of my friends who has known me the longest. He is someone I can always turn to for a wise lesson delivered with a cat emoji resembling his two cats, Squat and Nacho. David Silk, who was the first friend I made in Australia. He has provided support in many ways including helping me settle into Australia and lending me a place to stay when I came to Sydney without a place to live. Back at home, Michael Boucher has been someone who is consistently calling to check up on me and see the next time we will see each other. He has taught me an entirely new meaning of friendship for which I am grateful. Fernando Grullon and Thiem Ly have always been there to be a sounding board and have given me unconditional love and support. Lastly, my two childhood friends Carla

Maldonaldo-Santos and Milena Lopez who have always been two of my biggest cheerleaders. Their thoughtful conversations were what got me through my homesickness my first year, and without their support, I do not think I would have stayed in Australia. For those, I have not named know that it is because of word limit and not absent-mindedness.

Lastly and most importantly, I thank my family. My grandmother who does her word search to stay mentally active (she could have proofread this). She is one of my first memories of love and always gets even more excited than I do about the places, volcanoes, and field areas I have been. My aunt Maria and my siblings Zulaika, Victor, and Emmanuel who love me unconditionally and are always there at the drop of a hat. Growing up in a household full of people that are always asking questions and wanting to know more information is most likely the main reason why I grew up to become a scientist. My parents are the only reason I am here today. They fostered an environment where academics, curiosity, and learning were the highest priority. They moved to Boston, from Puerto Rico where we came from very little, to ensure their children were well educated. My dad, Victor Vazquez, works two to three jobs without complaining. He has taught me the value of hard work and to not let circumstance dictate your future. My mother has been my biggest supporter since I was a child, and through her, I have learned resilience, perseverance, and the importance of doing what I love. My parents have always reminded me how much I am loved and how proud they are of all my achievements. Because of their support I have been able to reach all these milestones in my life. Lastly, my partner James Douglas has been a fantastic support system for me. The word “Thank You” does not seem enough for patiently tolerating a partner in graduate school. He has ridden the roller coaster of emotions with me and not asked to get off. I am grateful and do not know that I could have done it without his support. I love you, thank you!

CONTENTS

LIST OF TABLES

List of Figures

List of Appendices

1 INTRODUCTION

1.1 General Introduction

Convergent plate boundaries transport crustal material and their associated chemistry into the mantle in the subducting plate. Convergent plate boundaries form subduction zones which remove old oceanic crust along with their associated components (e.g., sediments) from the Earth's surface. The density of the lithosphere is an integral factor in subduction zone dynamics where a typically older and denser plate descends beneath a younger and more buoyant plate. This convergence and subduction produce enough force to move the entire plate. Tonga is an end member subduction zone with an old cold subducting oceanic plate and active spreading along the Lau back-arc basin that causes increased convergence along the trench.

Several physical features are typically produced at subduction zones: a trench that is formed by the intersection of the two plates, a volcanic arc which generates most of the volcanism, and in many cases within oceanic systems, a back-arc which is an extensional feature associated with local faulting and magmatism (Stern, 2002). The majority of subduction zones prescribe to this profile with the primary two types of convergent margins being oceanic or continental arcs. Oceanic arcs (or intra-oceanic

arcs) incorporate two adjacent converging plates with oceanic lithosphere that produce a volcanic island arc on the upper plate, whereas continental arcs involve oceanic lithosphere that subducts beneath mature continental lithosphere. However, not all subduction zones are the same, and when continental crust reaches the subduction zone, it begins to terminate subduction. What does remain constant is the production of magma along most of the convergent zones.

As the subducting plate penetrates the Earth's mantle, it re-equilibrates and drags the adjacent mantle with it, causing a pull of the asthenospheric mantle beneath the arc towards the top of the subduction channel. Through this process, the cold (oceanic) subducting slab introduces aqueous fluids into the mantle which lowers the solidus temperature and allows magma production in an area that would otherwise be too cold to melt. Components of the subducted material are transferred to the magmas through dehydration and partial melting of the downwelling slab. These include volatile elements, dehydration and partial melting of pelagic and terrigenous sediments, altered oceanic crust and serpentinized oceanic lithosphere. They are recycled to the crust through magmas that ascend, recycling their chemical signatures, and either stagnate in the crust or erupt at the surface as volcanoes. While similar in many ways, the process that magmas undergo to erupt varies, and as a result, their chemistry reflects these processes. In general, more evolved rocks are associated with continental arcs, and more primitive rocks are found in intra-oceanic arcs. Therefore, magmas generated at intra-oceanic arcs provide a clearer insight into the subduction zone process because they do have continental crust complicating their chemistry. The igneous rocks of Tonga reveal an array of extrusive igneous rocks (basalt to dacite). Since the mantle cannot be directly sampled, we study these primitive volcanic rocks to constrain the recycling processes and to study primitive oceanic arcs by establishing which elements from the subducted material are redistributed between crustal and mantle reservoirs. This

augments our understanding of the long-term contributions that recycling makes to the evolution of mantle and crustal reservoirs on Earth.

1.1.1 Geochemical characteristics of arc magmas

Unravelling the inputs and outputs of subduction zones to understand magma processes is difficult to study directly, particularly because the composition of arc magmas varies from arc to arc. However, through the use of geoanalytical tools, we can methodically dissect these complex processes. Arc magmas often have a distinct general geochemical signature that allows us to differentiate them from magmatic products in other geodynamic environments, such as ocean-island, mid-ocean ridge, and intra-plate volcanism (Tatsumi & Eggins, 1995; Gill, 2012). Magmas generated at subduction zones are typically identified by 1) high large ion lithophile elements (LILE)/ high field strength elements (HFSE) ratios, 2) high light rare earth elements (LREE)/ heavy rare earth elements (HREE) ratios (with some exceptions), and 3) enrichment in fluid-mobile elements relative to mid-ocean ridge basalt (MORB) and ocean-island basalt (OIB). Subduction zone magmas also exhibit lower abundances of Ti and the transition elements relative to MORB and OIB (Hawkesworth et al., 1991; Manning, 2004; Stern, 2004; Gill, 2012). These enrichments/depletions may indicate the addition of subduction fluid, sediment, altered oceanic crust to the mantle wedge and overlying crust, as well as crustal contamination.

Recognizing these chemical trends is fundamental to understanding crust-mantle exchange over time. Demonstrating recycling of crustal material to subduction zone magmas has for the most part been determined by proxies for element behavior in the inputs versus outputs (Plank & Langmuir, 1993; Plank & Langmuir, 1998; Plank, 2005). However, the most robust tracer of recycled sediments has been ^{10}Be, a short-lived cosmogenic nuclide that is strongly enriched in ocean sediments, and which is the

only direct proof that subducted sediment melt is present in the mantle wedge (Morris et al., 1990; Morris et al., 2002). However, it remains important to characterize intra-oceanic arcs and their recycled products through the use of other geochemical tools, such as the ones presented in this thesis, which include radiogenic isotopes (e.g., Sr, Nd, Pb, Hf, He) and more recently stable isotopes like lithium.

1.1.2 Geochemical characteristics of back-arc basins

Two significant processes dominate the general chemistry of back-arc basins basalts (BABB): 1) variable influence from hydrous fluids in the mantle wedge with high LILE/HFSE ratios, and 2) repeated melt extraction which produces basalts enriched in incompatible elements (Saunders & Tarney, 1984). The basalts generated in the extensional zones are a direct result of the force imparted by slab pull which thins the upper plate and leads to decompression melting behind the arc. These magmas typically have compositions intermediate between N-MORB and island arc lavas with an initial LILE/HFSE ratio that resembles N-MORB. However, as the arc matures, the LILE/HFSE ratio evolves towards a transitional type of magma that incorporates geochemical signals from both of these sources producing a progressively higher LILE/HFSE ratio. Back-arc basin basalts are also enriched in LREE relative to N-MORB (Fryer et al., 1981, Wood et al., 1981). These BABBs also exhibit enrichment in volatile elements, most notably water, which is often physically visible through vesicles in the erupted lavas (Garcia et al., 1979; Saal et al., 2002). The presence of water in the melting regime stimulates an increased rate of melt production with a lower FeO content. Plagioclase crystallization is commonly suppressed in BABB which results in high Al2O3 and Na2O and low MgO contents in the more fractionated lavas (Yoder & Tilley, 1962; Nicholls & Ringwood, 1973).

1.2 Scope of the Thesis

This work adopts an integrated approach to assess the subducted slab and plume source contributions involved at the convergent plate margin within the Tongan arc and the zones of extension in the adjacent (Lau and North Fiji) back-arc basins. Additionally, it addresses the conditions in which evolved magmas form in an example volcano (Late) in the Tongan arc. An extensive range of geochemical methods, isotopic systems and petrological observations are combined with an analysis of previous studies to achieve a more thorough understanding of the generation and composition of Tongan arc magmatic products.

1.3 An overview of the Tonga-Kermadec arc and Lau Basin

1.3.1 Geologic setting

The Tonga-Kermadec island arc forms a nearly uninterrupted, continuous volcanic chain that extends 2,800 km from the Taupo Volcanic Zone in the North Island, New Zealand, and concludes at the Vitiaz strike-slip fault south of Samoa (Fig. 1.1). Present day subduction of the Pacific plate beneath the Australian plate (12-18 km thick) has continued since the Oligocene (Burns et al., 1973; Ewart et al., 1977; Sutherland et al., 2010; Bache et al., 2012). Initiation of a back-arc extensional basin formation commenced around 6 Ma, forming the Lau basin that is confined to the west by the Lau Ridge and the east by the Tonga arc (Parson and Hawkins, 1994). The Louisville Ridge, a seamount chain located on the Pacific plate, has migrated southward and has been subducted beneath the Australian plate for the last 4 Ma years (Dupont & Herzer, 1985). The Louisville Ridge bisects the arc and splits it into the Tonga segment to the north, and the Kermadec segment to the south. The subducting plate dips at an

angle of 30^{o} to a depth of ~120-130 km beneath both segments of the Tonga-Kermadec arc and afterwards steepens beneath both segments. The convergence rate increases northward along the arc from 5 to 24 cm/yr, and the back-arc respectively follows a similar trend northward with an extension from 6 to 16 cm/yr (Bevis et al., 1995).

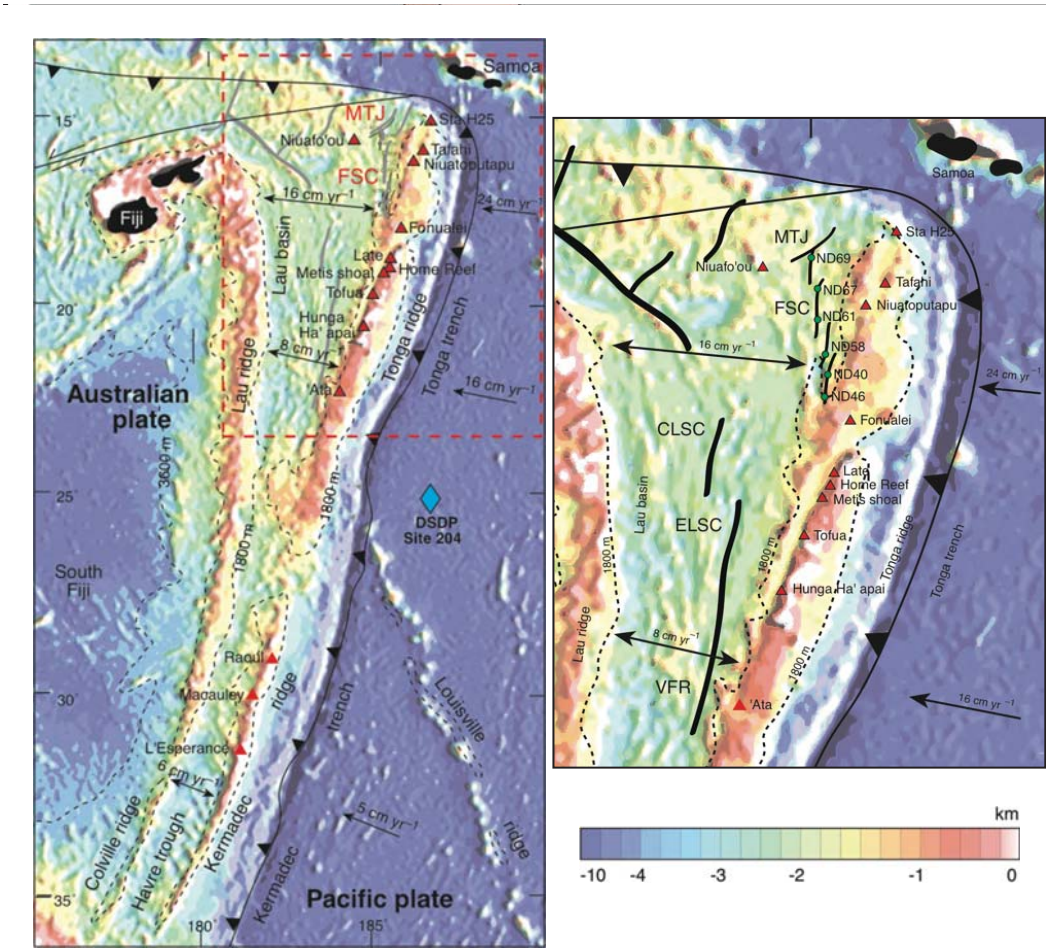

Figure 1.1 Map of Tonga-Kermadec island arc (adapted from Turner & Hawkesworth, 1997; and satellite altimetry-derived gravity data from: Fernando Martinez & Brian Taylor, University of Hawaii and David Sandwell, Scripps Institution of Oceanography), highlighting sample location for samples in this study: the arc volcanoes, (Lau Basin) Fonualei Spreading Center (FSC), Mangatolu Triple Junction (MTJ) and sediments from DSDP Site 204. The dotted red line indicates the area where the map has been magnified (right panel) to show in greater detail the samples from the FSC & MTJ. The red triangles represent volcanoes along the arc, green circles represent the back-arc (FSC & MTJ) and the blue diamond (left panel) on the Pacific Plate is the DSDP Site 204. The DSDP Site 596 lies ~1,000 km east of DSDP Site 204. Also illustrated are bathymetric contour lines and colors to illustrate different aquatic depths (scale for color scheme is the same for both

panels). Black arrows indicate directions and rates of convergence along the arc and spreading rates in the Lau Basin back-arc spreading center.

1.3.2 Petrology and Mineralogy

The rocks of the Tongan arc vary from basalt to dacite. The phenocrysts in the lavas exhibit highly calcic normative and modal plagioclase (An_{80-89}), strongly magnesian augite, and hypersthene. Titanomagnetite appears as the rock suite evolves towards a higher silica content (in andesites and dacites). Olivine is found only in basaltic andesite lavas from Tofua (~Fo_{90-93}) and Kao (and Metis Shoal as xenocrysts; Bauer, 1970; Melson et at., 1970; Bryan and Ewart, 1971). The groundmass of the lavas varies in mineral proportions; pigeonite is the most common groundmass mineral and is typically observed with plagioclase (labradorite-bytownite). Minor groundmass material, such as titanomagnetite, minor quartz, and rare K-feldspar in the evolved lavas has also been reported. All studies of the Tongan lavas show an absence of amphibole as a primary phase, although secondary alteration amphibole has been reported on Eua Island; Ewart et al., 1973; Ewart, 1976.

1.3.3 Geochemical characteristics of Tongan lavas

The Tongan lavas are low-K tholeiites (Ewart et al., 1973, 1977; Ewart 1976). The lavas from the Tongan arc are inferred to have originated by melting of highly depleted mantle wedge peridotite. The mantle wedge beneath the Tongan arc is believed to be refractory with a depletion in high field strength elements (HFSE) relative to light rare earth elements (LREE). This depletion is attributed to varying degrees of back-arc melt extraction (Ewart & Hawkesworth, 1987; Woodhead et al., 1993; Ewart et al., 1994; Caulfield et al., 2008; Cooper et al., 2010). In addition to the geochemical signatures derived from the depleted mantle wedge, other signatures influencing the overall chemistry of the Tongan lavas have been detected, such as a fluid flux from the

altered oceanic crust and melts of sedimentary rocks. The altered oceanic crust fluid, which is derived from dehydration of the subducting oceanic crust, is characterized in lavas by high large ion lithophile elements (LILE)/ HFSE ratios that decrease southward along the arc (Regelous et al., 1997, 2010; Turner et al., 1997). The addition of sediment melts in the Tonga-Kermadec arc have been identified using a variety of trace element and isotopic signatures, and in particular through the most unambiguous tracer, ^{10}Be, which has been used to narrow down the sediment flux to 0.25-1% (Plank & Langmuir, 1993; Turner et al., 1997; George et al., 2005).

1.3.4 Geochemical characteristics of Lau back-arc basin

The Lau Basin samples contain several isotopically distinct hotspot components. Firstly, the Samoan hotspot has been suggested to influence the geochemistry of Lau Basin lavas, where distinctive high-^{87}Sr/^{86}Sr and high-^{3}He/^{4}He signatures – associated with the Samoan plume – have been identified in the Rochambeau Rifts in the northern Lau Basin (e.g. Lytle et al., 2012, Lupton et al., 2009, Poreda and Craig, 1992). Also, a possible contributor to the geochemical diversity in the southern Lau Basin is the Louisville hotspot, which is currently being subducted into the Tonga trench at ~26°S. The Louisville hotspot exhibits relatively high ^{206}Pb/^{204}Pb (up to 19.6060; Vanderkluysen et al., 2015) and ^{208}Pb/^{204}Pb (up to 39.3695; Beier et al., 2011, when considering only fresh lavas) and has been suggested to contribute to the elevated Pb isotopic compositions observed in a subset of volcanoes from both the northern (e.g. Turner and Hawkesworth, 1998; Ewart et al, 1998) and southern (e.g. Timm et al., 2013) Tonga arc. Lastly, the subduction of seamounts from the Cook-Austral Volcanic Lineament (Falloon et al., 2007; Todd et al., 2009), in particular, volcanoes associated with the Rarotonga and Rurutu hotspots, influence the geochemistry of Lau Basin lavas (Price et al., 2016). Based on plate reconstructions (Wessel and Kroenke, 2008), the

Rarotonga hotspot, which exhibits Enriched Mantle 1 (EM1) isotopic signatures, subducted into the northern Tonga Trench. The same plate reconstructions show that the Rurutu hotspot, which hosts HIMU signatures, also likely subducted into the northernmost Tonga Trench. In conclusion, up to three hotspots originating in the South Pacific superswell influence the geochemistry of the *northern* Lau and North Fiji Basins, either by toroidal advection of under-plated plume material (Samoa) or by subduction of older portions of hotspot tracks (Rarotonga and Rurutu).

1.4 An outline of the geochemical approaches in addressing chemical recycling, fingerprinting, and magmatic processes in intra-oceanic arcs

1.4.1 Why is lithium of interest to potentially trace recycled material?

The addition of subducted crustal material to the mantle wedge has been studied and refined for many years (e.g., Armstrong, 1971; Elliot et al., 1997; Class et al., 2000; Turner et al., 2003). However, the nature and rates of transfer of subducted components are still not as constrained in arcs, yet it contains the key essential information for understanding and modeling the chemical evolution through wedge dynamics and melt generation. U-series isotopes have conventionally been used to trace the fluid movement from slab to eruption, providing insight on the mechanism and timing of fluid addition (Hawkesworth et al., 1997; Turner et al., 1997; Turner et al., 2003). However, sensitive tracers of sediment addition have further broadened the issue of mechanisms and timing of processes in subduction zones (Woodhead et al., 2001; Regelous et al., 2010). Lithium has gained significant attention as a sensitive tracer of sediment addition because of its higher concentrations in sediments and altered oceanic crust due to the

interaction with seawater characterised by heavy Li (high $^{7}Li/^{6}Li$ ratio) (Ryan and Langmuir, 1987; Chan & Edmond, 1988; Chan et al., 1992; Moriguti and Nakamura, 1998). Because Li is moderately incompatible during mantle melting and has a high fluid mobility, and strong isotopic fractionation at low temperatures, its potential as a powerful tracer of recycled material in the mantle has been highly debated recently (e.g., Ryan & Langmuir, 1987; Brenan et al., 1998; Moriguti & Nakamura, 1998; Tomascak et al., 2000; Chan et al., 2002; Elliott et al., 2004; Tang et al., 2014).

1.4.2 What is the role of volatile elements in magmatic processes in the Tonga-Kermadec region?

Volatile elements (in particular water and carbon dioxide) are an essential factor in magmatic processes by influencing melting (Asimow & Langmuir, 2003), fractional crystallization (Huppert et al., 1982), and degassing (Métrich & Wallace, 2008). Volatile elements are incompatible elements that prefer to partition into the liquid when melting occurs. They differ from standard lithophile elements as they prefer to be in the vapor phase, if present, and are dependent on high pressure to remain dissolved in melts. Lithophile elements, in contrast, have traditionally been used to assess the fertility of melts at mid-ocean ridges, establishing particular elemental affinities (e.g. LREE/HREE ratios) for deeper mantle signatures (e.g. plumes) (Weaver, 1991; Halliday et al., 1995). Several studies have improved our ability to constrain the volatile content of the mantle (Hirth & Kohlstedt, 1996; Saal et al., 2002; Eiler, 2003; Leeman et al., 2017). However, there is still work to be done to fully characterize and understand the reservoirs that occupy the upper mantle.

Lavas from the Samoan hotspot volcanoes span a broad range in H_2O (0.63 – 1.50 wt.%) and CO_2 (6 – 233 ppm) contents. The water contents of Samoan lavas

exceed the range of MORB (<0.7 wt.%) but do not exceed arc lavas (<8 wt.%) (e.g. Grove et al., 2002). Furthermore, it is well documented that the Samoan plume has infiltrated into the Lau Basin through an opening in the Pacific plate that originates at the northern termination of the Tonga-Kermadec arc (e.g., Giardini & Woodhouse, 1986; Volpe et al., 1988; Turner & Hawkesworth, 1998; Price et al., 2014). Therefore, by analyzing volatile elements, it is possible to examine how far the Samoan source extends under the Australian plate.

1.4.3 What are the geochemical influences related to mantle flow around the subducting Pacific slab edge?

The Tonga Trench – Samoan plume system provides an opportunity to evaluate mantle flow in the vicinity of a subducting slab experiencing rapid rollback. The unique geochemistry associated with the Samoan plume can be likened to a geochemical dye that can be traced as it infiltrates the depleted upper mantle of the Lau and North Fiji back-arc basins (e.g., Druken et al., 2014). Tracking the shape and extent of the incursion of this Samoan "dye" in the back-arc basins through geochemical analyses of lavas in the region can reveal how mantle flows around the nearby down-going Tonga slab. Previous studies have used the geochemical signatures associated with the Samoan plume (e.g., high $^{3}He/^{4}He$ and high $^{87}Sr/^{86}Sr$) to assess the extent to which the Samoan mantle material has infiltrated around the northern edge of the subducting Pacific lithosphere (e.g., Volpe et al., 1988; Gill & Whelan, 1989; Poreda & Craig, 1992; Wendt et al., 1997; Ewart et al., 1998; Pearce et al., 2007; Tian et al., 2008, 2011; Lupton et al., 2009; Hahm et al., 2012; Lytle et al., 2012; Price et al., 2014, 2016; Nebel and Arculus, 2015). Conversely, other hotspot tracks in the region (Louisville, Rurutu, and Rarotonga), it has been argued, influence the geochemistry of back-arc lavas that have erupted in the vicinity of the subducting hotspot tracks (e.g., Turner and

Hawkesworth 1998; Falloon et al. 2007; Regelous et al. 2008; Timm et al. 2013; Price et al. 2016).

1.4.4 How do silicic magmas form in intra-oceanic subduction settings?

Most previous studies have focused on along-arc characterization (Ewart et al., 1973; Ewart & Hawkesworth, 1987; Gamble et al., 1993; Turner et al., 1997, 2000, 2009; Turner & Hawkesworth, 1997; Ewart et al., 1998; George et al., 2005; Hergt & Woodhead, 2007; Castillo et al., 2009) with specific studies in this region mostly focusing on the Taupo volcanic zone or the Kermadec arc (Gamble et al., 1997; Smith et al., 2003, 2006, 2009; Haase et al., 2006, 2011, 2014; Cameron et al., 2010; Shane & Wright, 2011; Timm et al., 2011; Price et al., 2012). Recently, two studies analyzed volcanic islands near Late, Tofua and Fonualei, relative to the Late volcano discussed in this study (Caulfield et al., 2012; Turner et al., 2012). Tofua has predominantly erupted basaltic andesite lavas, with minor dacitic lavas, whereas the eruptive products of Fonualei have mainly been dacitic for the last 165 years, with recorded basaltic andesite and andesitic basal flows that underlie the current dacitic flows. The petrogenetic model proposed for these two volcanic islands, based on combining linear least-square models with mineralogy and major and trace element chemistry, is consistent with the general model proposed by Ewart et al. (1973) which suggests that the genesis of evolved lavas in the Tongan arc is due to low-pressure fractional crystallization of the parental magmas and not a history of partial melting. Yet the origin of felsic magmas in intra-oceanic arc settings has continued to be constantly debated (Wade et al., 2005; Smith et al., 2003, 2008; Brophy, 2008; 2009; Reubi & Blundy, 2009; Caulfield et al., 2012; Turner et al., 2012).

1.5 Aims of study

Given the gaps in knowledge defined in the literature review/state of the art, several focal questions are addressed in this thesis. The principal lines of investigation are:

I: Examining mass and chemical changes in the inputs to subduction across different locations in the subduction zone and how recycling influences the evolution of the crustal and mantle composition in the Tonga-Kermadec arc through the use of Li isotopes.

II: Investigating the geochemical reservoirs that occupy the upper mantle to explain heterogeneities in the North Fiji Basin.

III: Unraveling the contributions of various geochemical plume signatures to constrain the origin of the geochemical signals in the Lau and North Fiji back-arc basin lavas and illuminate shallow mantle flow patterns in the region.

IV: Constraining the depth and pressures at which the geochemically evolved arc magmas from Late volcano (in the Tonga-Kermadec arc) were formed by crystal fractionation, and establish the fractionating assemblage.

This thesis consists of four primary chapters, each of which employs geochemical tools to understand chemical recycling and magmatic evolution in the mantle and crust. As such, each chapter stands on its own for intended submission to peer-review to scientific journals. Thus, there is some repetition in introduction and summary material, but this is included for completeness.

1.6 General introduction to the fieldwork and samples used in the thesis collection

1.6.1 CSIRO Research Voyage

I undertook field work to collect samples from 47 dredged lavas from 40 dredge localities in the Lau and North Fiji Basins during the 2012 cruise of the R/V Southern Surveyor, expedition SS_V02; all samples have the prefix NLTD (Northern Lau Transect Dredges). Eight prime target areas were successfully mapped in detail with a multibeam echo sounder Kongsberg Simrad EM300. Dredged samples were collected on the research cruise to provide samples with a high proportion of glass. The dredge has a chain bag and trailing buckets which collected large rock samples as well as glass chips. The majority of the samples collected are fresh black glass-rimmed pillow and sheet flow fragments. However, a subset of samples contained mud that varied in color (dark red) in the North East Fiji Triple Junction and (tan) near the Fijian islands.

The primary aim of this research cruise was to recover fresh volcanic glass samples from a ~1,000km-wide transect, ranging from the northeast of the North Fiji basin to the northwest of the northern Lau basin. We undertook detailed mapping of the tectonic fabric of the boundary between the Pacific and Australian plates around Fiji. Appendix A has descriptions of each dredge sample, maps, images, localities, and bathymetric map (swath maps) collected in the research cruise. The fresh volcanic glass was harvested from all dredge lavas examined here. All of the samples were examined for major, trace, volatile and radiogenic isotopes (Hf, Pb, Sr, and Nd).

1.6.2 Additional lavas and sediments samples examined in this thesis

The remaining lavas and sediments analyzed in this thesis have been collected from multiple sources. IODP provided the sediments (DSDP 204) investigated in this study. A. Price provided the samples from Rotuma Island. J. Gill provided the majority of the Fijian samples. S. Turner provided the samples from the Tongan arc. T. Green provided samples from Late.

1.7 References

Armstrong, R. L. (1971) Isotopic and chemical constraints on models of magma genesis in volcanic arcs. *Earth and Planetary Science Letters*, *12*(1), 137-142.

Asimow, P. D., & Langmuir, C. H. (2003) The importance of water to oceanic mantle melting regimes. *Nature*, 421(6925), 815-820.

Bache, F., Sutherland, R., Stagpoole, V., Herzer, R., Collot, J., & Rouillard, P. (2012) Stratigraphy of the southern Norfolk Ridge and the Reinga Basin: a record of initiation of Tonga–Kermadec–Northland subduction in the southwest Pacific. *Earth and Planetary Science Letters*, 321, 41-53.

Bauer, G.R. (1970) The geology of Tofua Island, Tonga. *Pacific Science* 24, 333-350.

Beier C., Vanderkluysen L., Regelous M., Mahoney, J.J., & Garbe-Schonberg, D. (2011) Lithospheric control on geochemical composition along the Louisville Seamount Chain. Geochemistry Geophysics Geosystems 12:Q10008, doi: 10.1029/2011GC003690

Bevis, M., Taylor, F.W., Schutz, B.E., Recy, J. & Isacks, B.L., Helu, S., Singh, R., Kendrick, E., Stowell, J. (1995) Geodetic observations of very rapid convergence and back-arc extension at the Tonga arc. *Nature* 374, 249-251.

Brenan, J.M., Ryerson, F.J. & Shaw, H.F. (1998) The role of aqueous fluids in the slab-to-mantle transfer of boron, beryllium, and lithium during subduction; experiments and models. *Geochimica et Cosmochimica Acta* 62, 19-20, 3337-3347.

Brophy, J. G. (2008) A study of rare earth element (REE)–SiO_2 variations in felsic liquids generated by basalt fractionation and amphibolite melting: a potential test for discriminating between the two different processes. *Contributions to Mineralogy and Petrology*, *156*(3), 337-357.

Brophy, J. G. (2009) Decompression and H_2O exsolution driven crystallization and fractionation: development of a new model for low-pressure fractional crystallization in calc-alkaline magmatic systems. *Contributions to Mineralogy and Petrology*, *157*(6), 797.

Bryan, W. B., & Ewart, A. (1971) Petrology and geochemistry of volcanic rocks from Tonga: Carnegie Inst. *Washington Year Book*, *69*, 249-258.

Burns, R. E., Andrews, J. E., van der Lingen, G. J., Churkin, M., Jr., Galehouse, J. S., Packham, G., Davies, T. A., Kennett, J. P., Dumitrica, P., Edwards, A. R. & Von Herzen, R. P. (1973) Site 204. *Initial Reports of the Deep Sea Drilling Project* 21, 33-56.

Cameron, E., Gamble, J., Price, R., Smith, I., McIntosh, W., & Gardner, M. (2010) The petrology, geochronology and geochemistry of Hauhungatahi volcano, SW Taupo Volcanic Zone. *Journal of Volcanology and Geothermal Research*, *190*(1), 179-191.

Castillo, P. R., Lonsdale, P. F., Moran, C. L., & Hawkins, J. W. (2009) Geochemistry of mid-Cretaceous Pacific crust being subducted along the Tonga–Kermadec Trench: Implications for the generation of arc lavas. *Lithos*, *112*(1), 87-102.

Caulfield, J. T., Turner, S. P., Dosseto, A., Pearson, N. J., & Beier, C. (2008) Source depletion and extent of melting in the Tongan sub-arc mantle. *Earth and Planetary Science Letters*, *273*(3), 279-288.

Caulfield, J. T., Turner, S. P., Smith, I. E. M., Cooper, L. B., & Jenner, G. A. (2012). Magma evolution in the primitive, intra-oceanic Tonga arc: petrogenesis of basaltic andesites at Tofua volcano. *Journal of Petrology*, *53*(6), 1197-1230.

Chan, L. & Edmond, J.M. (1988) Variation of lithium isotope composition in the marine environment; a preliminary report. *Geochimica et Cosmochimica Acta* 52, 6, 1711-1717.

Chan, L. H., Edmond, J. M., Thompson, G., & Gillis, K. (1992) Lithium isotopic composition of submarine basalts: implications for the lithium cycle in the oceans. *Earth and Planetary Science Letters*, *108*(1-3), 151-160.

Chan, L.H., Leeman, W.P. & You, C.F. (2002) Lithium isotopic composition of Central American Volcanic Arc lavas: Implications for modification of the subarc mantle by slab-derived fluids: Correction. *Chemical Geology* 182, 293-300.

Class, C., Miller, D. M., Goldstein, S. L., & Langmuir, C. H. (2000) Distinguishing melt and fluid subduction components in Umnak Volcanics, Aleutian Arc. *Geochemistry, Geophysics, Geosystems*, *1*(6).

Cooper, L. B., Plank, T., Arculus, R. J., Hauri, E. H., Hall, P. S., & Parman, S. W. (2010) High-Ca boninites from the active Tonga Arc. *Journal of Geophysical Research: Solid Earth*, *115*(B10).

Druken, K. A., Kincaid, C., Griffiths, R. W., Stegman, D. R., & Hart, S. R. (2014) Plume–slab interaction: the Samoa–Tonga system. *Physics of the Earth and Planetary Interiors*, *232*, 1-14.

Dupont, J., & Herzer, R. H. (1985) Effect of subduction of the Louisville Ridge on the structure and morphology of the Tonga Arc.

Elliott, T., Plank, T., Zindler, A., White, W., & Bourdon, B. (1997) Element transport from slab to volcanic front at the Mariana arc. *Journal of Geophysical Research: Solid Earth*, *102*(B7), 14991-15019.

Elliott, T., Jeffcoate, A., & Bouman, C. (2004) The terrestrial Li isotope cycle: light-weight constraints on mantle convection. *Earth and Planetary Science Letters*, *220*(3-4), 231-245.

Eiler, J. (2003) Inside the subduction factory. Washington DC American Geophysical Union Geophysical Monograph Series, 138.

Ewart, A. (1976) A petrological study of the younger Tongan andesites and dacites, and the olivine tholeiites of Niua Fo'ou Island, SW Pacific. *Contributions to Mineralogy and Petrology*, *58*(1), 1-21.

Ewart, A., Brothers, R.N. & Mateen, A. (1977) An outline of the geology and geochemistry, and the possible petrogenetic evolution of the volcanic rocks of the Tonga-Kermadec-New Zealand island arc. *Journal of Volcanology Geothermal Research* 2, 205-250.

Ewart, A., Bryan, W. B., Chappell, B. W., & Rudnick, R. L. (1994) Regional geochemistry of the Lau-Tonga arc and backarc systems. In *Proceedings of the Ocean Drilling Program. Scientific Results* (Vol. 135, pp. 385-425). Ocean Drilling Program.

Ewart, A., Bryan, W. B., & Gill, J. B. (1973) Mineralogy and geochemistry of the younger volcanic islands of Tonga, SW Pacific. *Journal of Petrology*, *14*(3), 429-465.

Ewart, A., Collerson, K. D., Regelous, M., Wendt, J. I., & Niu, Y. (1998) Geochemical evolution within the Tonga–Kermadec–Lau arc–back-arc systems: the role of varying mantle wedge composition in space and time. *Journal of Petrology* 39:331–368.

Ewart, A., & Hawkesworth, C. J. (1987) The Pleistocene-Recent Tonga-Kermadec arc lavas: interpretation of new isotopic and rare earth data in terms of a depleted mantle source model. *Journal of Petrology*, *28*(3), 495-530.

Falloon, T. J., Danyushevsky, L. V., Crawford, T. J., Maas, R., Woodhead, J. D., Eggins, S., Bloomer, S. H., Wright, D.J., Zlobin, S.K., & Stacey, A. R. (2007)

Multiple mantle plume components involved in the petrogenesis of subduction-related lavas from the northern termination of the Tonga Arc and northern Lau Basin: Evidence from the geochemistry of arc and backarc submarine volcanics. *Geochemistry, Geophysics, Geosystems*, *8*(9).

Fryer, P., Sinton, J. M., & Philpotts, J. A. (1981) Basaltic glasses from the Mariana Trough: Initial Reports of the Deep Sea Drilling Project, v. 60, p. 601–609.

Gamble, J. A., Christie, R. H. K., Wright, I. C., & Wysoczanski, R. J. (1997) Primitive K-rich magmas from Clarke volcano, southern Kermadec arc: A paradox in the K-depth relationship. *Canadian Mineralogist* 35, 195-211.

Gamble, J. A., Smith, I. E. M., McCulloch, M. T., Graham, I. J., & Kokelaar, B. P. (1993) The geochemistry and petrogenesis of basalts from the Taupo Volcanic Zone and Kermadec Island Arc, SW Pacific. *Journal of volcanology and geothermal research*, *54*(3-4), 265-290.

Garcia, M. O., Liu, N. W., & Muenow, D. W. (1979) Volatiles in submarine volcanic rocks from the Mariana Island arc and trough. *Geochimica et Cosmochimica Acta*, *43*(3), 305-312.

Giardini, D., & Woodhouse, J. H. (1986) Horizontal shear flow in the mantle beneath the Tonga arc. *Nature*, *319*, 551-555.

Gill, J. B. (2012) *Orogenic andesites and plate tectonics* (Vol. 16). Springer Science & Business Media.

Gill, J., & Whelan, P. (1989) Postsubduction ocean island alkali basalts in Fiji. *Journal of Geophysical Research: Solid Earth*, *94*(B4), 4579-4588.

George, R., Turner, S., Morris, J., Plank, T., Hawkesworth, C., & Ryan, J. (2005) Pressure–temperature–time paths of sediment recycling beneath the Tonga–Kermadec arc. *Earth and Planetary Science Letters*, *233*(1), 195-211.

Grove, T., Parman, S., Bowring, S., Price, R., & Baker, M. (2002) The role of an H2O-rich fluid component in the generation of primitive basaltic andesites and andesites from the Mt. Shasta region, N California. *Contributions to Mineralogy and Petrology*, *142*(4), 375-396.

Haase, K. M., Stroncik, N., Garbe-Schönberg, D., & Stoffers, P. (2006) Formation of island arc dacite magmas by extreme crystal fractionation: an example from Brothers Seamount, Kermadec island arc (SW Pacific). *Journal of Volcanology and Geothermal Research*, *152*(3), 316-330.

Haase, K. M., Krumm, S., Regelous, M., & Joachimski, M. (2011) Oxygen isotope evidence for the formation of silicic Kermadec island arc and Havre–Lau backarc magmas by fractional crystallisation. *Earth and Planetary Science Letters*, *309*(3), 348-355.

Haase, K. M., Lima, S., Krumm, S., & Garbe-Schönberg, D. (2014) The magmatic evolution of young island arc crust observed in gabbroic to tonalitic xenoliths from Raoul Island, Kermadec Island Arc. *Lithos*, *210*, 199-208.

Hahm, D., Hilton, D. R., Castillo, P. R., Hawkins, J. W., Hanan, B. B., & Hauri, E. H. (2012) An overview of the volatile systematics of the Lau Basin: Resolving the effects of source variation, magmatic degassing and crustal contamination. Geochimica et Cosmochimica Acta 85:88–113. doi: 10.1016/j.gca.2012.02.007

Halliday, A. N., Lee, D. C., Tommasini, S., Davies, G. R., Paslick, C. R., Fitton, J. G., & James, D. E. (1995) Incompatible trace elements in OIB and MORB and source enrichment in the sub-oceanic mantle. *Earth and Planetary Science Letters*, *133*(3), 379-395.

Hawkesworth, C. J., Hergt, J. M., Ellam, R. M., & Mc Dermott, F. (1991) Element fluxes associated with subduction related magmatism. *Philosophical Transactions*

of the Royal Society of London A: Mathematical, Physical and Engineering Sciences, *335*(1638), 393-405.

Hawkesworth, C. J., Turner, S. P., McDermott, F., Peate, D. W., & Van Calsteren, P. (1997) U-Th isotopes in arc magmas: Implications for element transfer from the subducted crust. *Science*, *276*(5312), 551-555.

Hergt, J. M., & Woodhead, J. D. (2007) A critical evaluation of recent models for Lau–Tonga arc–backarc basin magmatic evolution. *Chemical Geology*, *245*(1), 9-44.

Hirth, G., & Kohlstedt, D. L. (1996) Water in the oceanic upper mantle: implications for rheology, melt extraction and the evolution of the lithosphere. *Earth and Planetary Science Letters*, *144*(1), 93-108.

Huppert, H. E., Sparks, R. S. J., & Turner, J. S. (1982) Effects of volatiles on mixing in calc-alkaline magma systems. *Nature*, *297*(5867), 554-557.

Leeman, W. P., Tonarini, S. and Turner, S. (2017) Boron isotope variations in Tonga-Kermadec-New Zealand arc lavas: implications for origin of subduction components and mantle influences. *Geochem. Geophys. Geosys.* 18, doi:10.1002/2016GC006523.

Lupton, J. E., Arculus, R. J., Greene, R. R., Evans, L. J., & Goddard, C. I. (2009) Helium isotope variations in seafloor basalts from the Northwest Lau Backarc Basin: Mapping the influence of the Samoan hotspot. Geophysical Research Letters. doi: 10.1029/2009GL039468

Lytle, M. L., Kelley, K. A., Hauri, E. H., Gill, J. B., Papia, D., & Arculus, R. J. (2012) Tracing mantle sources and Samoan influence in the northwestern Lau back-arc basin. Geochemistry Geophysics Geosystems 13:Q10008 doi: 10.1029/2012GC004233

Manning, C. E. (2004) The chemistry of subduction-zone fluids. *Earth and Planetary Science Letters*, *223*(1), 1-16.

Melson, W. G., Jarosewich, E., & Lundquist, C. A. (1970) Volcanic eruption at Metis Shoal, Tonga, 1967-1968: description and petrology. *Smithsonian Contributions to the Earth Sciences*, *4*, 1-18.

Métrich, N., & Wallace, P. J. (2008) Volatile abundances in basaltic magmas and their degassing paths tracked by melt inclusions. *Reviews in mineralogy and geochemistry*, *69*(1), 363-402.

Moriguti, T., & Nakamura, E. (1998) High-yield lithium separation and the precise isotopic analysis for natural rock and aqueous samples. *Chemical Geology*, *145*(1-2), 91-104.

Morris, J.D., Leeman, W.P. & Tera, F. (1990) The subducted component in island arc lavas; constraints from B-Be isotopes and Be systematics, *Nature* 344, 6261, 31-36.

Morris, J.D., Gosse, J., Brachfeld, S. & Tera, F. (2002) Cosmogenic Be-10 and the solid Earth; studies in geomagnetism, subduction zone processes, and active tectonics, in: Beryllium Mineralogy, Petrology, and Geochemistry, *Reviews in Mineralogy and Geochemistry* 50, 207-270.

Nebel, O., & Arculus, R. J. (2015) Selective ingress of a Samoan plume component into the northern Lau backarc basin. *Nature communications*, *6*.

Nicholls, I. A., & Ringwood, A. E. (1973) Effect of water on olivine stability in tholeiites and the production of silica-saturated magmas in the island-arc environment. *The Journal of Geology*, *81*(3), 285-300.

O'Brien, P. J. (2001) Subduction followed by collision: Alpine and Himalayan examples. *Physics of the Earth and Planetary Interiors*, *127*(1), 277-291.

Parson, L. M., & Hawkins, J. W. (1994) Two-stage ridge propagation and the geological history of the Lau backarc Basin, *Proceedings of the Ocean Drilling Program, Scientific Results*, 135, 819-828, 1994.

Pearce, J. A., Kempton, P. D., Gill, J. B. (2007) Hf-Nd evidence for the origin and distribution of mantle domains in the SW Pacific. Earth and Planetary Science Letters 260:98–114.

Plank, T. (2014) The chemical composition of subducting sediments. *Treatise on geochemistry*, *4*, 607-629.

Plank, T., & Langmuir, C. H. (1993) Tracing trace elements from sediment input to volcanic output at subduction zones. *Nature*, *362*(6422), 739-743.

Plank, T., & Langmuir, C. H. (1998) The chemical composition of subducting sediment and its consequences for the crust and mantle. *Chemical geology*, *145*(3), 325-394.

Poreda, R. J, & Craig, H (1992) He and Sr isotopes in the Lau Basin mantle: depleted and primitive mantle components. Earth and Planetary Science Letters 113:487–493.

Price, A. A., Jackson, M. G., Blichert-Toft, J., Hall, P. S., Sinton, J. M., Kurz, M. D., & Blusztajn, J. (2014) Evidence for a broadly distributed Samoan-plume signature in the northern Lau and North Fiji Basins. *Geochemistry, Geophysics, Geosystems*, *15*(4), 986-1008.

Price, A. A., Jackson, M. G., Blichert-Toft, J., Blusztajn, J., Conatser, C. S., Konter, J. G., Koppers, A.A. & Kurz, M. D. (2016) Geochemical evidence in the northeast Lau Basin for subduction of the Cook-Austral volcanic chain in the Tonga Trench. *Geochemistry, Geophysics, Geosystems*.

Price, R. C., Gamble, J. A., Smith, I. E., Maas, R., Waight, T., Stewart, R. B., & Woodhead, J. (2012) The anatomy of an Andesite volcano: a time–stratigraphic study of andesite petrogenesis and crustal evolution at Ruapehu Volcano, New Zealand. *Journal of Petrology*, *53*(10), 2139-2189.

Regelous, M., Collerson, K. D., Ewart, A., & Wendt, J. I. (1997) Trace element transport rates in subduction zones: evidence from Th, Sr and Pb isotope data for Tonga-Kermadec arc lavas. *Earth and Planetary Science Letters*, *150*(3), 291-302.

Regelous, M., Gamble, J. A., & Turner, S. P. (2010) Mechanism and timing of Pb transport from subducted oceanic crust and sediment to the mantle source of arc lavas. *Chemical Geology*, *273*(1), 46-54.

Regelous, M., Turner, S., Falloon, T. J., Taylor, P., Gamble, J., & Green, T. (2008) Mantle dynamics and mantle melting beneath Niuafo'ou Island and the northern Lau back-arc basin. Contributions to Mineralogy and Petrology 156:103–118. doi: 10.1007/s00410-007-0276-7.

Reubi, O., & Blundy, J. (2009) A dearth of intermediate melts at subduction zone volcanoes and the petrogenesis of arc andesites. *Nature*, *461*(7268), 1269.

Ryan, J. G., & Langmuir, C. H. (1987) The systematics of lithium abundances in young volcanic rocks. *Geochimica et Cosmochimica Acta*, *51*(6), 1727-1741.

Saal, A. E., Hauri, E. H., Langmuir, C. H., & Perfit, M. R. (2002) Vapor undersaturation in primitive mid-ocean ridge basalt and the volatile content of the Earth's upper mantle. *Nature*, *419*(6906), 451-455.

Saunders, A. D., & Tarney, J. (1984) Geochemical characteristics of basaltic volcanism within back-arc basins. *Geological Society, London, Special Publications*, *16*(1), 59-76.

Shane, P., & Wright, I. C. (2011) Late Quaternary tephra layers around Raoul and Macauley Islands, Kermadec Arc: implications for volcanic sources, explosive volcanism and tephrochronology. *Journal of Quaternary Science*, *26*(4), 422-432.

Smith, I. E., Stewart, R. B., & Price, R. C. (2003) The petrology of a large intra-oceanic silicic eruption: the Sandy Bay Tephra, Kermadec Arc, Southwest Pacific. *Journal of Volcanology and Geothermal Research*, *124*(3), 173-194.

Smith, I. E., Worthington, T. J., Price, R. C., Stewart, R. B., & Maas, R. (2006) Petrogenesis of dacite in an oceanic subduction environment: Raoul Island, Kermadec arc. *Journal of Volcanology and Geothermal Research*, *156*(3), 252-265.

Smith, I. E., Price, R. C., Stewart, R. B., & Worthington, T. J. (2009) An assessment of the mantle and slab components in the magmas of an oceanic arc volcano: Raoul Volcano, Kermadec arc. *Journal of Volcanology and Geothermal Research*, *184*(3), 437-450.

Stern, R. J. (2002) Subduction zones. *Reviews of geophysics*, *40*(4).

Stern, R. J. (2004) Subduction initiation: spontaneous and induced. *Earth and Planetary Science Letters*, *226*(3), 275-292.

Sutherland, R., Collot, J., Lafoy, Y., Logan, G. A., Hackney, R., Stagpoole, V., & Wood, R. (2010) Lithosphere delamination with foundering of lower crust and mantle caused permanent subsidence of New Caledonia Trough and transient uplift of Lord Howe Rise during Eocene and Oligocene initiation of Tonga-Kermadec subduction, western Pacific. *Tectonics*, *29*(2).

Tang, M., Rudnick, R.L., Chauvel, C. (2014) Sedimentary input to the source of Lesser Antilles lavas: A Li perspective. *Geochimica et Cosmochimica Acta* 144, 43-58.

Tatsumi, Y., & Eggins, S. (1995) Subduction zone magmatism, 211 pp., Blackwell, Cambridge.

Tian, L., Castillo, P. R., Hawkins, J. W., Hilton, D. R., Hanan, B. B., & Pietruszka, A. J. (2008) Major and trace element and Sr–Nd isotope signatures of lavas from the Central Lau Basin: Implications for the nature and influence of subduction components in the back-arc mantle. Journal of volcanology and Geothermal Research 178:657–670. doi: 10.1016/j.jvolgeores.2008.06.039

Tian, L., Castillo, P. R., Hilton, D. R., Hawkins, J. W., Hanan, B. B., & Pietruszka, A. J. (2011) Major and trace element and Sr-Nd isotope signatures of the northern Lau Basin lavas: Implications for the composition and dynamics of the back-arc basin mantle. Journal of geophysical Research 116:B11201. doi: 10.1029/2011JB008791

Timm, C., Bassett, D., Graham, I.J. de Ronde, C.E., Woodhead, J., Layton-Matthews, D. & Watts, A.B. (2013) Louisville seamount subduction and its implication on mantle flow beneath the central Tonga–Kermadec arc. Nat Comms 4:1720. doi: 10.1038/ncomms2702

Timm, C., Graham, I. J., de Ronde, C. E., Leybourne, M. I., & Woodhead, J. (2011) Geochemical evolution of Monowai volcanic center: New insights into the northern Kermadec arc subduction system, SW Pacific. *Geochemistry, Geophysics, Geosystems*, *12*(8).

Todd, E., Gill, J. B., & Freymuth, H. (2009, December) Sr-Nd-Hf-Pb Isotope Ratios in Recent NE Lau Lavas. In *AGU Fall Meeting Abstracts* (Vol. 1, p. 1721).

Tomascak, P.B., Ryan, J.G. & Defant, M.J. (2000) Lithium isotope evidence for light element decoupling in the Panama subarc mantle. *Geology* 28, 507-510.

Turner, S., Bourdon, B., & Gill, J. (2003) Insights into magma genesis at convergent margins from U-series isotopes. *Reviews in Mineralogy and Geochemistry*, *52*(1), 255-315.

Turner, S., Bourdon, B., Hawkesworth, C., & Evans, P. (2000) 226 Ra–230 Th evidence for multiple dehydration events, rapid melt ascent and the time scales of differentiation beneath the Tonga–Kermadec island arc. *Earth and Planetary Science Letters*, *179*(3), 581-593.

Turner, S., Caulfield, J., Rushmer, T., Turner, M., Cronin, S., Smith, I., & Handley, H. (2012) Magma evolution in the primitive, intra-oceanic Tonga arc: rapid petrogenesis of dacites at Fonualei volcano. *Journal of petrology*, *53*(6), 1231-1253.

Turner, S., Handler, M., Bindeman, I., & Suzuki, K. (2009) New insights into the origin of O–Hf–Os isotope signatures in arc lavas from Tonga–Kermadec. *Chemical Geology*, *266*(3), 187-193.

Turner S, & Hawkesworth C (1998) Using geochemistry to map mantle flow beneath the Lau Basin. Geology 26:1019–1022.

Turner, S., Hawkesworth, C., Rogers, N., Bartlett, J., Worthington, T., Hergt, J., Pearce, J., & Smith, I. (1997) 238 U-230 Th disequilibria, magma petrogenesis, and flux rates beneath the depleted Tonga-Kermadec island arc. *Geochimica et Cosmochimica Acta*, *61*(22), 4855-4884.

Vanderkluysen, L., Mahoney, J. J., Koppers, A. A., Beier, C., Regelous, M., Gee, J. S., & Lonsdale, P. F. (2014) Louisville Seamount Chain: Petrogenetic processes and geochemical evolution of the mantle source. *Geochemistry, Geophysics, Geosystems*, *15*(6), 2380-2400.

Volpe, A. M., Macdougall, J. D., Hawkins, J. W. (1988) Lau Basin basalts (LBB): trace element and Sr-Nd isotopic evidence for heterogeneity in backarc basin mantle. Earth and Planetary Science Letters 90:174–186.

Wade, J. A., Plank, T., Stern, R. J., Tollstrup, D. L., Gill, J. B., O'Leary, J. C., Eiler, J. M., Moore, R. B., Woodhead, J. D., Trusdell, F., Fischer, T. P. & Hilton, D. R. (2005) The May 2003 eruption of Anatahan volcano, Mariana Islands: Geochemical evolution of a silicic island-arc volcano. *Journal of Volcanology and Geothermal Research*, *146*(1), 139-170.

Weaver, B. L. (1991) The origin of ocean island basalt end-member compositions: trace element and isotopic constraints. *Earth and Planetary Science Letters*, *104*(2), 381-397.

Wendt, J. I., Regelous, M., Collerson, K. D., Ewart, A (1997) Evidence for a contribution from two mantle plumes to island-arc lavas from northern Tonga. Geology 25:611–614.

Wessel, P., & Kroenke, L. W. (2008) Pacific absolute plate motion since 145 Ma: An assessment of the fixed hot spot hypothesis. *Journal of Geophysical Research: Solid Earth (1978–2012)*, *113*(B6).

Wood, D. A. (1981) Geochemistry of igneous rocks recovered from a transect across the Mariana Trough, arc, fore-arc and trench, sites 453 through 461, Deep Sea Drilling Project leg 60. *Initial Report of Deep Sea Drilling Project*, *60*, 611-646.

Woodhead, J., Eggins, S., & Gamble, J. (1993) High field strength and transition element systematics in island arc and back-arc basin basalts: evidence for multi-phase melt extraction and a depleted mantle wedge. *Earth and Planetary Science Letters*, *114*(4), 491-504.

Woodhead, J. D., Hergt, J. M., Davidson, J. P., & Eggins, S. M. (2001) Hafnium isotope evidence for 'conservative'element mobility during subduction zone processes. *Earth and Planetary Science Letters*, *192*(3), 331-346.

Yoder Jr, H. S., & Tilley, C. E. (1962) Origin of basalt magmas: an experimental study of natural and synthetic rock systems. *Journal of Petrology*, *3*(3), 342-532.

2 Lithium Isotopic Composition of the Tonga-Kermadec Arc and Constraints on Subduction Recycling

Abstract

I analyzed lithium concentrations [Li] and isotopic compositions of a suite of lavas from the Tonga-Kermadec island arc and the Fonualei back-arc spreading center, along with a depth profile through the forearc marine sediments from DSDP Site 204. The [Li] and δ^7Li isotope variations in the subducting sediments greatly exceed those observed in the lavas and change systematically with depth and sediment type. Li concentration of pelagic sediments from DSDP Site 204 is high (32–133 ppm), and δ^7Li (+1.2 to +10.2) is low while the underlying volcanogenic sediments encompass an even larger [Li] range and extend to higher δ^7Li (+7.2 to +14.4). MORB-like Li isotopic compositions in many of the Tonga-Kermadec lavas make it difficult to detect

contributions from subducted components. The models presented in this study permit the addition of up to 3.5% sediment in the arc front lavas whereas lavas from the back-arc spreading center (δ^7Li = +3.0 to +5.0) show no deviation from MORB δ^7Li (+4 ± 2.0). Either much of the heavy δ^7Li is removed from the system in the forearc or else there is significant Li isotope equilibration with the mantle wedge. Still, the high lithium concentration in the mantle creates a barrier in the ability to differentiate the slab Li signatures through the MORB-like mantle fingerprint. In the case of the back-arc lavas, this may reflect the longer slab-to-surface path which the magmas traverse.

2.1 Introduction

Subduction recycles oceanic crust into the mantle. All subducting plates carry sediments that are either scraped off to create an accretionary prism or, in many cases, subduct with the plate itself. Depending on the quantity of sediment added to the source region for the arc magma, the isotopic signatures of these sediments may be observed in the erupted lavas, the most unambiguous tracer being ^{10}Be (Morris et al., 1990; Morris et al., 2002). Lithium being a light, water-soluble common trace element in rocks, and widely evaluated, operates as a potential tracer of subduction zone recycling (Ryan & Langmuir, 1987; You et al., 1996, Brenan et al., 1998; Penniston-Dorland et al., 2010; Tang et al., 2014). The utility of Li in this regard reflects low-temperature isotopic fractionation that occurs during weathering and the uptake of seawater into the altered oceanic crust (e.g., Brant et al., 2012; Chan et al. 1992, 2002a; Rudnick et al., 2004; Liu & Rudnick, 2011; Liu et al., 2013, 2015).

Lithium has two stable isotopes ^{6}Li and ^{7}Li that have a ~15% mass difference. These isotopes fractionate at low temperatures (<350^{o}C), but equilibrium fractionation is minor at higher temperatures with a fractionation factor ($\alpha_{\text{sediment-fluid}}$) <1.011 (Chan et

al., 1994). Fractionation factor at higher temperatures (>500^{o}C) causes a minor shift to heavier fluid compositions (Wunder et al., 2006). However, while the mantle wedge temperatures in subduction zones greatly exceed 350^{o}C some eclogites exhibit low δ^{7}Li values (δ^{7}Li down to –22‰) (Marschall et al., 2007b). This has been attributed to kinetic fractionation as a result of prograde metamorphism; accordingly, the fractionation can be corrected through the addition of up to 3‰ δ^{7}Li (Marschall et al., 2007a). Thereafter the lithium that is released into the wedge has had a contentious fate.

Figure 2.1 shows a cross-section of the oceanic crust and upper mantle in an idealized subduction zone with ranges in δ^{7}Li based on published values for rocks and sediments in the Pacific Ocean and Lau Basin. The accepted δ^{7}Li values for MORB range from ~+2.0 to ~+6.0‰ (Elliott et al., 2004; Tomascak et al., 2008). The sediment has a range in δ^{7}Li of +1.2 to +14.4‰ (this study) while the altered oceanic crust has a range in δ^{7}Li of -10.9 to +20.8‰ (Chan et al., 1994, 2002b; Brant et al., 2012). These values are selected for proximity to the arc; we recognize that they are values that do span a large range. However, these values are the best representation of the area in both literature and analysis.

A negative δ^{7}Li value for in altered oceanic crust is indicative of loss of Li through leaching during low-temperature alteration (Millot et al., 2010; Verney-Carron et al., 2011). However, in most cases, there is an increase in lithium, which is attributed to the exchange of lithium in seawater (~+31‰) within both the subducted sediments and (altered) oceanic crust (Chan & Edmond, 1988). [Li] decreases in the slab as dehydration occurs, leading to a variably positive δ^{7}Li signature similar to the bulk solid in the fluid released (0 to +15 ‰) (You et al., 1996; Zack et al., 2003; Marschall et al., 2007a,b). This enriched δ^{7}Li fluid potentially interacts with the subarc mantle imparting a sensitive tracer of lithium recycling in subduction zones (Ryan & Langmuir, 1987; Brenan et al., 1998; Moriguti & Nakamura, 1998; Tomascak et al., 2000; Tang et al.,

2014). However, not all studies have reached the same conclusion. For example, Tomascak (2002) and Tang et al. (2014) found no correlation between lithium and other geochemical tracers of subduction fluids (Kurile, Sunda, Aleutians, and Lesser Antilles (Martinique)). Tomascak et al. (2002) also found a lack of difference in δ^7Li between arc lavas and MORB which they explain as the result of a chromatographic exchange with subarc mantle peridotite. In contrast, other studies have found clear evidence for sediment-derived lithium isotope signals in the arc lavas (Moriguti & Nakamura, 1998; Chan et al., 2002b; Tang et al., 2014).

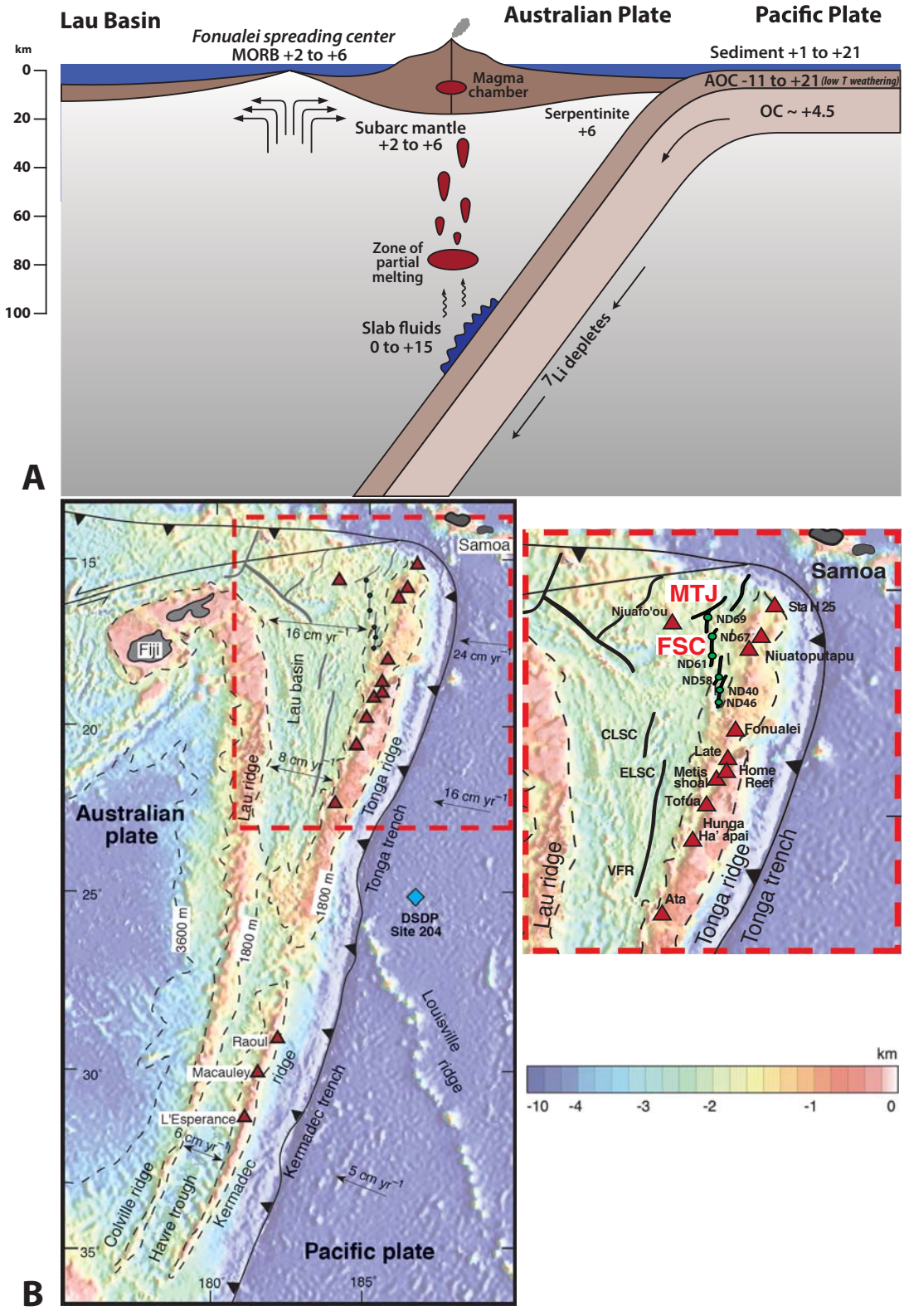

Figure 2.1 A) Cross-section of the Tonga-Kermadec arc illustrating lithium isotope systematics. The Fonualei Spreading Center is staggered obliquely from the arc front with a minimum distance of 20 km and a maximum distance of 120 km from the Tofua arc (not shown in illustration). The lithium isotopes for the back-arc are consistent with the MORB range along the entire spreading

center. Ranges are given for each area because of lithium's mobility in fluid. (Data ranges were compiled from Chan et al., 1994; You et al., 1996; Zack et al., 2003; Benton et al., 2004; Elliott et al., 2004; Marschall et al., 2007a,b; Tomascak et al., 2008; Vils et al., 2009; Brant et al., 2012.) B) *Left panel*: Map of Tonga-Kermadec island arc (adapted from Turner & Hawkesworth, 1997; and satellite altimetry-derived gravity data from: Fernando Martinez & Brian Taylor, University of Hawaii and David Sandwell, Scripps Institution of Oceanography), highlighting sample location for samples in this study: the arc volcanoes, (Lau Basin) Fonualei Spreading Center (FSC), Mangatolu Triple Junction (MTJ) and sediments from DSDP Site 204. The dotted red line indicates the area where the map has been magnified (*right panel*) to show in greater detail the samples from the FSC & MTJ. The red triangles represent volcanoes along the arc, green circles represent the back-arc (FSC & MTJ) and the blue diamond (*left panel*) on the Pacific Plate is the DSDP Site 204. The DSDP Site 596 lies ~1,000 km east of DSDP Site 204. Also illustrated are bathymetric contour lines and colors to illustrate different aquatic depths (scale for color scheme is the same for both panels). Black arrows indicate directions and rates of convergence along the arc and spreading rates in the Lau Basin back-arc spreading center.

In some arc lavas, lithium isotopes correlate with tracers of slab-derived fluids (e.g., Izu, Central America, and Western Anatolia; Moriguti & Nakamura, 1998; Chan et al., 2002b; Agostini et al., 2007, respectively) and behave similarly to boron. Boron and Li may also be decoupled tracers in arcs, showing a divergent relationship with B (e.g., Panama; Tomascak et al., 2000, 2002), irrespective of their similarities in enrichment in subducted materials, and correlated patterns of depletion during metamorphism in slabs. Alternatively, and most commonly, the lavas do not show any correlation with slab fluid tracers (e.g., Kurile, Sunda, Aleutians, and Lesser Antilles (Martinique); Tomascak et al., 2002; Tang et al., 2014). Although Tang et al. (2014) observed no correlation between Li isotopic composition and slab fluid indicators, they were able to detect a light Li isotopic signature derived from subducting sediments.

Here I present new Li data to investigate mass and chemical changes during subduction and the way recycling influences the evolution of the crustal and mantle

composition in the Tonga-Kermadec arc. This study aims to improve our understanding of element recycling in this arc by assessing whether these subducting slab fluids influence the lithium signature in the arc lavas and also whether they impact the lithium signal of back-arc lavas. The samples analyzed have been selected for their comprehensive geochemical background. Since some marine sediments and altered oceanic crust are enriched in ^{7}Li ($\delta^{7}Li$ up to ~+14) relative to fresh mid-ocean ridge basalt (MORB) ($\delta^{7}Li$ +2 to +6) (Chan et al., 1992), one of the aims is to test whether lithium isotopes correlate with subduction-related, fluid-sensitive elements as suggested in some previous studies (Moriguti & Nakamura, 1998; Chan et al., 2002b).

2.2 Geologic Setting and Samples

The 2,800-km long Tonga-Kermadec island arc extends from the Taupo Volcanic Zone in New Zealand to the Vitiaz strike-slip fault south of Samoa and results from subduction of the Pacific plate beneath the Australian plate (12–18 km thick) (Fig. 2.1, Burns et al., 1973; Ewart et al., 1977; Plank & Langmuir, 1998). The arc is composed of more than 80 volcanoes, both above and below sea level (Stoffers et al., 2006; Wright et al., 2006). The Louisville seamount chain, an aseismic ridge, intersects the arc, effectively splitting it into the Tonga segment to the north, and the Kermadec segment to the south. The subducting Pacific plate is 85–144 Ma old (Billen & Stock, 2000; Sutherland & Hollis, 2001) based on biostratigraphy of radiolarian chert and dating of ferrobasalts near to and from DSDP Holes 595/595A and 596/596A (Fig. 2.1). Both the dip of the slab and the convergence rate increase from south to north. The plate dips at an angle of 30^{o} to a depth of ~120–130 km beneath both segments of the Tonga-Kermadec arc and steepens to $55–60^{o}$ in the Kermadec segment and $43–45^{o}$ in the Tonga segment (Isacks & Barazangi, 1977). The convergence rate along the Kermadec

segment is 5 cm/yr, while in the Tonga segment the rate increases to 16–24 cm/yr (Bevis et al., 1995). As shown in Figure 2.2, the Tonga-Kermadec lavas consist predominantly of low-K basalts, basaltic andesites, andesites and minor dacites (Ewart, 1976; Ewart et al., 1973, 1977, 1998).

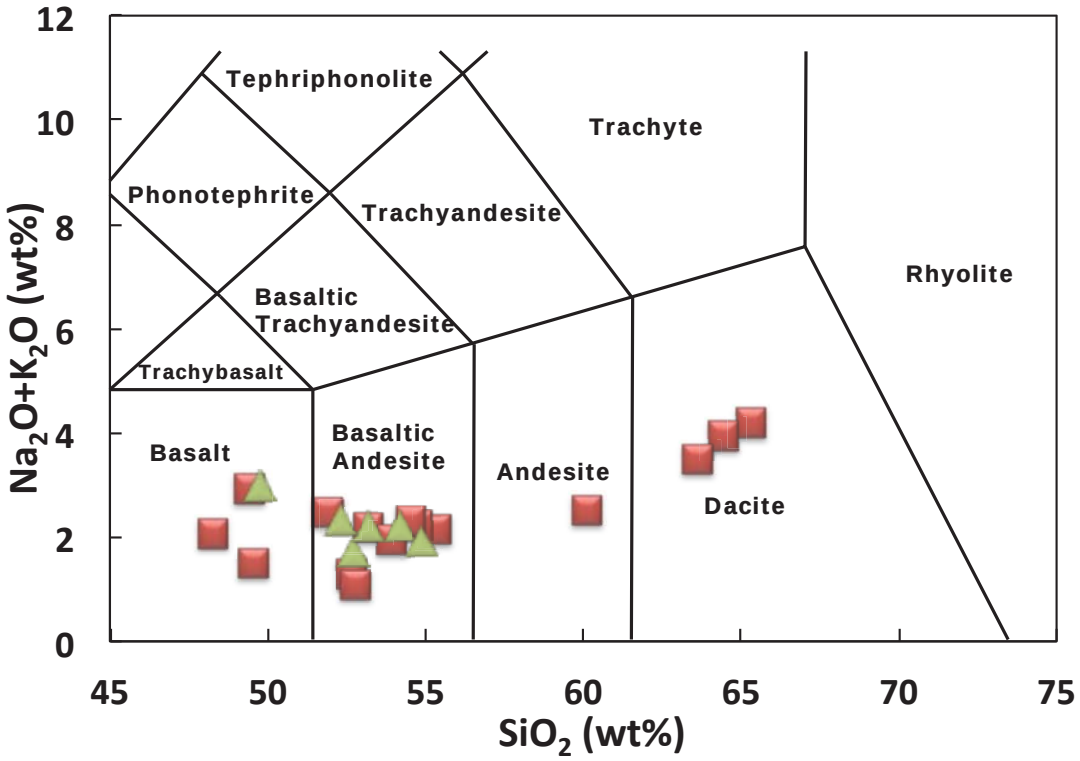

Figure 2.2 Total Alkali Silica (TAS) diagram classifying the arc lavas from the Tonga-Kermadec volcanic arc (red squares) and back-arc lavas from the Lau Basin back-arc spreading center (FSC & MTJ) (green triangles) (Ewart & Hawkesworth, 1987; Ewart et al., 1994; Acland, 1996; Keller et al., 2008; Caulfield et al., 2012b).

The composition of the sediments on the Pacific plate are well constrained (Burns et al., 1973; Turner et al., 1997; Plank & Langmuir, 1998). Figure 2.4 and Table 2.1 describe the types of sediments that are found in the southwest portion of the Pacific plate, with most being pelagic clays. Close to the Louisville Ridge, these are underlain by volcaniclastics derived from this seamount chain. The thickness of sediment decreases northwards from 200–70 m (Plank & Langmuir, 1998) and it is thought that

the full sediment packet is subducted beneath this arc (Bloomer & Fisher, 1986). Mass balance calculations show that only a minor amount (~0.25–1 %) of the pelagic sediment is recycled into the lavas (Turner et al., 1997; George et al., 2005). Enrichment in $^{206}Pb/^{204}Pb$ is observed in the volcanoes at the northern end of the arc (Tafahi and Niuatoputapu), and this has been interpreted to reflect the incorporation of the Louisville Ridge volcaniclastic sediments (Turner et al., 2007; Wendt et al., 1997).

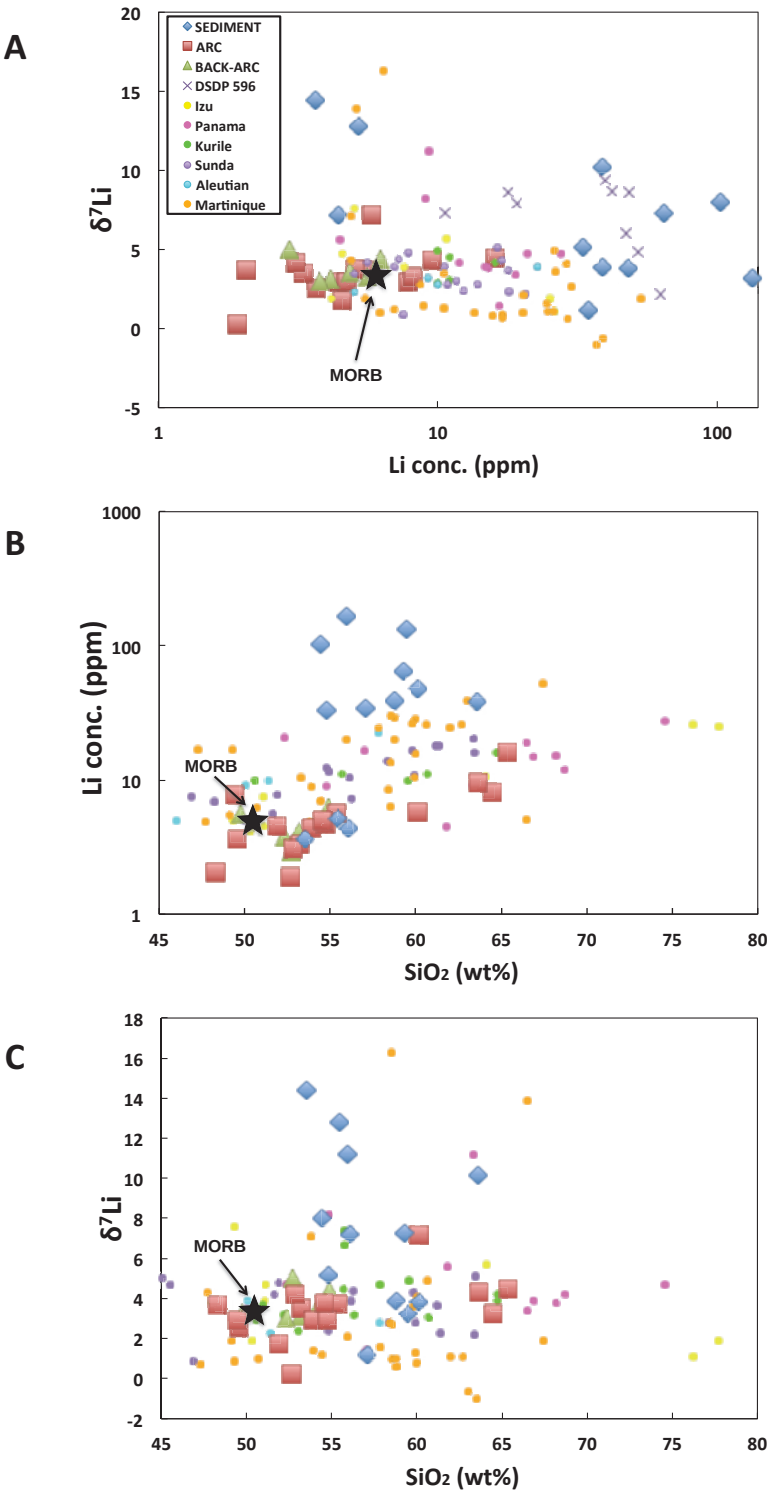

Figure 2.3 A) [Li] concentrations versus δ^7Li for the three areas of the Tonga-Kermadec arc analyzed here. Sediment compositions (blue diamonds) are for DSDP Site 204 with the DSDP 596 (X-symbols) core samples (Table 2.3). Also plotted are average MORB ranges (black star) (McDonough & Sun, 1995; Tomascak et al., 2008) along with previously studied arcs (Moriguti & Nakamura, 1998; Tomascak et al. 2000; Tomascak et al. 2002; Tang et al., 2014). SiO_2 versus (B) [Li] content and (C) δ^7Li for the Tonga-Kermadec

System. Black star is the average composition of MORB from (McDonough & Sun, 1995; Tomascak et al., 2008). Data sources for arcs in Table 2.1.

Westward of the Tonga-Kermadec arc lies two active back-arc basins, the Havre Trough to the south, and the Lau Basin to the north. The rate of spreading increases northward, opening in a "V" shape, with a 6 cm/yr spreading rate in the Havre Trough increasing northward to a maximum of 16 cm/yr in the upper portion of the Lau Basin (Bevis et al., 1995). In the northeastern section of the Lau Basin, the Fonualei Spreading Center (FSC) is an active spreading center that is located north of the volcanically active island of Fonualei (Keller et al., 2008). This spreading center extends obliquely away from the active volcanic front northward to the Mangatolu Triple Junction (MTJ) and is punctuated by a series of transform faults that extend into the MTJ (Fig. 2.1).

The Lau back-arc basin basalts (BABB) range from near MORB-like compositions (Hawkins, 1995) when erupted far from the arc, to arc-like compositions when erupted close to the arc (Pearce et al., 1995). BABBs, including those erupted along the Fonualei Spreading Center and Valu Fa Ridge, show subduction signatures that are characterized by enrichment in Large Ion Lithophile Elements (LILE) and volatile elements (e.g., they have up to 2.5 wt.% H_2O), and show a relative depletion in HFSE (Langmuir et al., 2006; Pearce & Stern, 2006; Keller et al., 2008; Caulfield et al., 2012a).

The samples analyzed here come from three regions in the Tonga-Kermadec arc: 1) sediments from the Pacific plate; 2) lavas from the arc, and 3) lavas from a traverse along the Fonualei Spreading Center (Fig. 2.1). The sediment samples come from DSDP Site 204, on the Pacific Plate near the trench (Fig. 2.4). In total, seven sediments were analyzed, and Figure 2.4 illustrates the lithological units, which span a total of 147 m in length. Unit 1, from which four samples were analyzed, consisted of pelagic clay

and ash and dates from the Quaternary to early Miocene or Oligocene (Burns et al., 1973). The two samples from the top of the clay unit are composed of dark brown clay that contains plagioclase (andesine), glass shards, mica, quartz, montmorillonite, zeolite, augite, and secondary clay phillipsite (Burns et al., 1973). The two samples from the bottom of the clay unit are dark reddish-brown iron-oxide clay composed of montmorillonite, potash feldspar, quartz, amorphous iron oxide, glass shards, and some authigenic carbonate layers. The bottom two units are composed of volcanogenic sediments derived from the Louisville Seamount Chain. Unit 2, from which three samples were analyzed, is a tuffaceous sandstone and conglomerate of early Cretaceous age. The clasts are composed of glass shards, andesine, calcite, pumice, and andesitic and basaltic rock fragments. The matrix is mainly altered ash with secondary minerals of epidote, zeolites, calcite, chloritic minerals, serpentine, and amorphous iron oxide (Burns et al., 1973). Unit 3, where two samples were analyzed, is a vitric tuff composed of basaltic to andesitic glass with pyroxene and feldspar crystals in a glass matrix.

Table 2.1 [Li] concentrations and δ^7Li values for lavas from the Tonga-Kermadec island arc, marine sediments from DSDP Site 204, and lavas from the Lau Basin back-arc spreading center (Ewart & Hawkesworth, 1987; Ewart et al., 1994; Acland, 1996; Regelous et al., 1997; Turner et al., 1997; George et al., 2005; Keller et al., 2008; Caulfield et al., 2012a,b).

Tonga-Kermadec Island Arc					
Sample name	**Location**	**SiO_2, wt%**	**δ^7Li**	**[Li], ppm**	**Y/Li**
	Volcanic Front				
7125	Raoul	49.5	+2.5	3.7	3.7
Late 7	Late	53.2	+3.5	3.3	3.6
45658	Macaulay	48.3	+3.7	2.1	6.1
26835	Tofua	53.9	+2.9	4.4	3.0
HH Topflow	Hunga	55.4	+3.7	5.7	2.5
ATA 8-1	Ata	51.9	+1.9	4.5	3.3
Replicate	-		+1.6		
FON 39	Fonualei	65.3	+4.5	16.0	1.3
14831	L'Esperance	52.7	+0.3	1.9	11.5
NTT 29/3	Niuatoputapu	60.1	+6.4	5.8	3.1
Replicate	-		+7.9		
Sta H25-7-17-18	N. Tonga - Boninite	54.7	+2.9	4.7	2.3
26833	Tofua	54.6	+3.8	5.0	3.0
31461	Niuafo'ou	49.4	+2.9	7.8	3.8
T116	Tafahi	52.8	+4.2	3.1	2.5
HR06	Home Reef	64.5	+3.3	8.1	2.7
TLi7	Metis Shoal dacite	63.7	+4.3	9.5	1.5
	Back-arc Basin				
ND-40	Fon spreading center	52.7	+5.0	2.9	
ND-46	Fon spreading center	53.2	+3.1	4.1	
ND-58	Fon Spreading center	54.2	+3.5	4.8	
ND-61	Fon spreading center	54.9	+4.4	6.2	
ND-67	Fon spreading center	52.3	+3.0	3.8	
ND-69	MJT	49.7	+3.3	5.6	
	DSDP 204				
204-1R-3W-60-61	Sediment (pelagic clay)	57.1	+1.2	34.5	0.8
204-2R-1W-109-110	Sediment (pelagic clay)	59.3	+7.3	64.1	0.7
204-2R-4W-60-61	Sediment (pelagic clay)	60.1	+3.8	47.9	1.4
204-3R-2W-59-60	Sediment (pelagic clay)	63.6	+10.2	38.8	0.7
204-4R-1W-75-76	Sediment (pelagic clay)	59.5	+3.2	133.3	1.4
204-4R-4W-140-141	Sediment (pelagic clay)	54.8	+5.2	32.9	0.7
204-5R-4W-60-61	Sediment (pelagic clay)	58.8	+3.9	38.8	4.7
204-6R-3W-48-50	Sediment (volcaniclastic)	54.4	+8.0	102.6	0.2
204-7R-1W-92-93	Sediment (volcaniclastic)	56.0	+7.2	4.4	4.6
204-8R-3W-86-87	Sediment (volcaniclastic)	55.9	+11.2	165.3	0.1
204-9R-1W-108-110	Sediment (volcaniclastic)	55.4	+12.8	5.2	4.4
204-9R-3W-24-27	Sediment (volcaniclastic)	53.5	+14.4	3.6	6.1
	Standards				
BHVO-1	USGS		+3.6	4.9	
BHVO-1	USGS		+3.2	4.8	
Replicate	-		+4.4		
Replicate	-		+3.9		
AGV-2	USGS		+5.2	11.1	
AGV-2	USGS		+5.6	10.5	
BCR-2	USGS		+2.1	10.3	

Table 2.1 lists the location and rock type of the 21 samples that were analyzed from the arc volcanoes and along the Fonualei Spreading Center. The arc lavas range from basalt to dacite (Fig. 2.2) and include some pumaceous samples, while the back-arc lavas are basalt to basaltic andesite. Full petrographic and geochemical data for these samples can be found elsewhere (Ewart & Hawkesworth, 1987; Ewart et al., 1994; Acland, 1996; Regelous et al., 1997, 2010; Turner et al., 1997, 2009; George et al., 2005; Keller et al., 2008; Caulfield et al., 2012a,b).

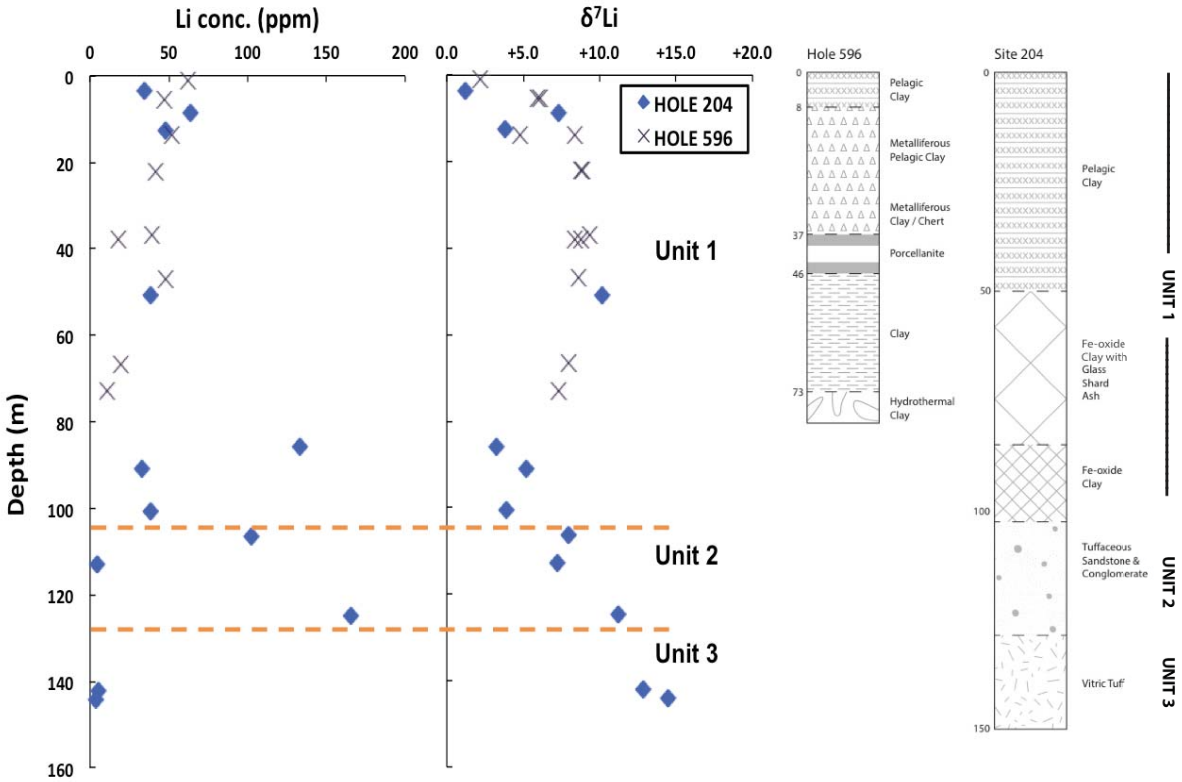
Li conc. (ppm)
δ7Li
Depth (m)
HOLE 204
HOLE 596
Unit 1
Unit 2
Unit 3
Hole 596
Pelagic Clay
Metalliferous Pelagic Clay
Metalliferous Clay / Chert
Porcellanite
Clay
Hydrothermal Clay
Site 204
Pelagic Clay
Fe-oxide Clay with Glass Shard Ash
Fe-oxide Clay
Tuffaceous Sandstone & Conglomerate
Vitric Tuff
UNIT 1
UNIT 2
UNIT 3

Figure 2.4 Depth profile (in meters) for the sediments analyzed in this study (DSDP Site 204) & published data from DSPD 596 (~1,000 km east) for [Li] and δ^7Li (Chan et al., 2006). Core logs (in meters) of DSDP Site 204 and published data of DSDP 596 (Chan et al., 2006). The core analyzed in this study (DSDP Site 204) is twice the length of the nearby DSDP 596 core (~1,000 km to the east). The main compositional difference between both cores is that DSDP Site 204 has Louisville volcaniclastic sediments in the lower third of the core.

2.3 Analytical Methods

Whole rocks were pulverized at Macquarie University (Australia), the University of Queensland (Australia), Durham University (U.K.), the Open University (U.K.), and Florida International University (Miami, Florida USA). Samples (and standards) were prepared for Li isotopic analysis at the University of Maryland by digesting the powders with a 3:1 mixture of concentrated HF and HNO_3 in Savillex® screw-top beakers on a hot plate (T~90^{o}C). This was followed by the addition of HNO_3 and HCl, with drying between each stage of acid addition. The residue was then re-dissolved in 4 N HCl in preparation for chromatographic separation following the methods outlined by Rudnick et al. (2004).

Lithium separation was achieved through ion-exchange chromatography, adapted from Moriguti and Nakamura (1998), where four chromatographic columns were used. For each column, 1 ml of cation exchange resin of AG50w-X12, 200-400 mesh (Bio-Rad), was cleaned with HCl and Milli-Q water followed by conditioning, chemical separation and sample collection using an eluent mixture of HCl and ethanol. The first two columns remove major element cations with 2.5M HCl and subsequently 0.15M HCl. The third and fourth columns separate Na from Li with 30% ethanol in 0.5M HCl through a N_2 pressurized ion exchange column (Rudnick et al., 2004).

The samples were analyzed for ^{6}Li and ^{7}Li on a Nu Plasma multi-collector, inductively-coupled mass spectrometer (MC-ICP-MS) using faraday cups. Li isotopic

compositions were analyzed by bracketing the sample, before and after, with the L-SVEC standard. The δ^7Li value ($\delta^7Li = [[^7Li/^6Li]_{sample} / [^7Li/^6Li]_{standard} - 1 \times 1000]$) is expressed as per mil deviations from the L-SVEC standard (Flesch et al., 1973). External reproducibility of the isotopic compositions is ≤ ±1.0‰ (2σ) based on repeat runs of pure Li standard solutions: in-house standard UMD-1 and international standard reference material IRMM-016 (Teng et al., 2006; Liu et al., 2010, 2013). The data for these solutions measured over the course of the analyses are provided in Table 2.2. The in-house and the international standard reference materials were analyzed at the beginning and end of each session and often a third time between runs in which more than eight samples were analyzed.

Table 2.2 Standard values

	δ^7Li	[Li] ppm
IRMM		
Value 1	0.12	
Value 2	0.12	
Value 3	-0.10	
Value 4	0.14	
Value 5	0.21	
Mean	0.10	
UMD-1		
Value 1	55.43	
Value 2	54.93	
Value 3	55.12	
Value 4	55.13	
Value 5	55.09	
Mean	55.14	
BHVO-1		
Value 1	+3.6	4.9
Value 2	+3.2	4.8
Replicate	+4.4	
Replicate	+3.9	
AGV-2		
Value 1	+5.2	11.1
Value 2	+5.6	10.5
BCR-2		
Value 1	+2.1	10.3

Comparing signal intensities for the whole rock with that measured for the 50 ppb L-SVEC standard and then adjusting for sample weight determined the lithium concentrations. These measurements have a 2σ uncertainty of ≤ ±10‰ (Teng et al., 2006).

Results for United States Geological Survey (USGS) international rock standards BHVO-1, AGV-2 and BCR-2 are reported in Table 2.1. The results are within analytical error of the recommended values from the U.S. Geological Survey and within the ranges for data that has been published (Gladney & Goode, 1981; Ryan & Langmuir, 1987; Govindaraju, 1994; James & Palmer, 2000; Chan & Frey, 2003; Rudnick et al., 2004; Bouman et al., 2004; Penniston-Dorland et al., 2012; Shihong et al., 2012; Tang et al., 2014; Liu et al., 2015). The only exception is BHVO-1 that initially had slightly lower values than the published data (Magna et al., 2004). Replicating the analysis produced a value within the accepted range (Shihong et al., 2012).

2.4 Results

Lithium concentrations and δ^7Li isotopic values for the lavas are presented in Table 2.1. As illustrated in Figure 2.3a, [Li] in the arc lavas range between 2–16 ppm, and δ^7Li varies from +0.3 to +7.9 (mean = +3.4). [Li] increases with SiO_2 (Fig. 2.3b) although there are no correlations between SiO_2 and δ^7Li in the lavas (Fig. 2.3c). The concentrations of Li in the back-arc lavas show a much smaller range, between 3–6 ppm, as do the δ^7Li values (+3.0 to +5.0, mean = +3.7).

Table 2.3 presents a comparison of the new [Li] and δ^7Li for sediments from DSDP Site 204 with published data from DSDP Site 596. The sediments from DSDP Site 204 exhibit a wide range of [Li] from 4 to 165 ppm, and δ^7Li values of +1.2 to

+14.4 (unweighted mean = +7.4). [Li] and δ^7Li in the sediments show no correlation with SiO_2 (Fig. 2.3), although they do correlate with lithology.

Table 2.3 A comparison of [Li] concentration and Li isotopic composition for DSPD Site 204 and published data for DSDP 596 (Chan et al., 2006) along with a comprehensive description of the sediments and values for depth.

Depth (m)	Sample name	Type	Li conc (ppm)	δ^7Li
3.6	204-1R-3W-60-61	Fe-oxide clay	34.5	+1.2
8.6	204-2R-1W-109-110	Fe-oxide clay	64.1	+7.3
12.6	204-2R-4W-60-61	glass shard ash	47.9	+3.8
50.9	204-3R-2W-59-60	glass shard ash rich clay	38.8	+10.2
85.8	204-4R-1W-75-76	Fe-oxide clay	133.3	+3.2
90.9	204-4R-4W-140-141	Fe-oxide clay	32.9	+5.2
100.6	204-5R-4W-60-61	Fe-oxide clay	38.8	+3.9
106.5	204-6R-3W-48-50	tuffaceous ss & congl.	102.6	+8.0
112.9	204-7R-1W-92-93	tuffaceous ss & congl.	4.4	+7.2
124.9	204-8R-3W-86-87	tuffaceous ss & congl.	165.3	+11.2
142.1	204-9R-1W-108-110	vitric tuff	5.2	+12.8
144.2	204-9R-3W-24-27	vitric tuff	3.6	+14.4

(Tonga Hole 596 from Chan et al., 2006)

Depth (m)	Sample name	Type	Li conc (ppm)	δ^7Li
1.05	596-1-1-105-108	pelagic clay	62.4	+2.2
5.5	596-1-cc	pelagic clay	47.2	+6.0
5.5	Repeat	-		+6.1
13.7	596-2-6-70-72	metalliferous pelagic clay	52.1	+4.8
22.1	596-3-5-100-102	metalliferous pelagic clay	42.0	+8.9
13.7	Repeat	-		+8.4
22.1	Repeat	-		+8.8
36.94	596-5-2-114-116	metalliferous clay/chert	39.6	+9.4
38	596-5-2-cc	porcellanite	17.7	+8.8
38	Repeat	-		+8.4
46.84	596-6-5-104-106	clay	48.3	+8.7
66.7	596-1-1-70-75	hydrothermal clay	19.2	+7.9
72.97	596A-1-5-97-101	hydrothermal clay	10.6	+7.3

2.5 Discussion

2.5.1 DSDP Site 204 sediment profile

To constrain the lithium inputs to the Tonga-Kermadec arc, I have analyzed and compared the DSDP Site 204 data with published data from DSDP 596, situated around 1,000 km to the east (Fig. 2.1; Table 2.3). Since it is thought that the full sediment packet is subducted beneath this arc (Bloomer & Fisher, 1986), the depth profile on Figure 2.4 provides a robust constraint on the lithium budget of the quantity of sediment subducted. The bulk composition of the sedimentary sections was determined following the method of Plank and Langmuir (1998). I calculate a weighted mean for each lithological unit and average each unit proportionally to its mass. Two sets of bulk compositions were used in this study, pelagic and pelagic + volcaniclastic. [Li] and δ^7Li for the weighted bulk sediments of DSDP Site 204 are as follows: pelagic [Li] is 55.8 ppm and δ^7Li = +5.0, whereas pelagic + volcaniclastic [Li] is 54.2 ppm and δ^7Li = +6.1.

At DSDP Site 204, the sediments display an inverse relationship between [Li] and δ^7Li, with a systematic increase in δ^7Li (+1.2 to +14.4) and decrease in [Li] with depth (see Table 2.3 and Fig. 2.4). This reflects the sediment type: lithium isotopic signatures for pelagic sediments are often lighter than MORB because of Li isotope fractionation during weathering, while volcanoclastic sediments can be either lighter or heavier than MORB, depending on the style of their alteration (Chan et al., 2006). The δ^7Li values of pelagic clays for DSDP Site 204 overlap those of fresh MORB, but extend to values both lower and higher (+1.2 to +10.2), while the δ^7Li of the volcanoclastic sediments are higher than fresh MORB (+7.2 to +14.4). This suggests that the volcanogenic sediments may have experienced uptake of seawater lithium in secondary minerals, much in the way MORB becomes isotopically heavier due to more

extensive time-integrated exchange in seafloor weathering (Chan et al., 1992; Bouman et al., 2004). The pelagic clays may have a smaller variation in δ^7Li than the volcanoclastic sediments due to their higher overall concentration of lithium.

2.5.2 Tracers of slab fluids

The data show that relatively high δ^7Li sediments are being subducted beneath the Tonga-Kermadec arc. However, while some of the arc lavas have δ^7Li values that extend beyond the range MORB to both heavier and lighter extremes, most have MORB-like compositions (Elliott et al., 2004; Tomascak et al., 2008).

Elemental pairs such as B/Be, Ba/La, B/Nb, and Li/Y are strongly fractionated between aqueous fluids and residual clinopyroxene and garnet during eclogitisation of subducting altered oceanic crust (Kelemen et al., 1993; Brenan et al., 1998; Caciagli et al., 2011). In the Tonga-Kermadec lavas, there is no obvious correlation between δ^7Li and ratios of soluble to insoluble elements (Fig. 2.5). This contrasts with findings in both the Central American (Chan et al., 2002b) and Izu arcs (Moriguti & Nakamura, 1998) where a positive correlation between δ^7Li and ratios of soluble elements was reported. In contrast, Tomascak et al. (2000) observed an inverse correlation between B and Li isotopes in arc lavas from Panama. The observations presented in this study are similar to those of Tomascak et al. (2002) for the Kurile, Sunda, and Aleutian arcs, and Tang et al. (2014) for the Lesser Antilles arc, where no obvious correlations exist.

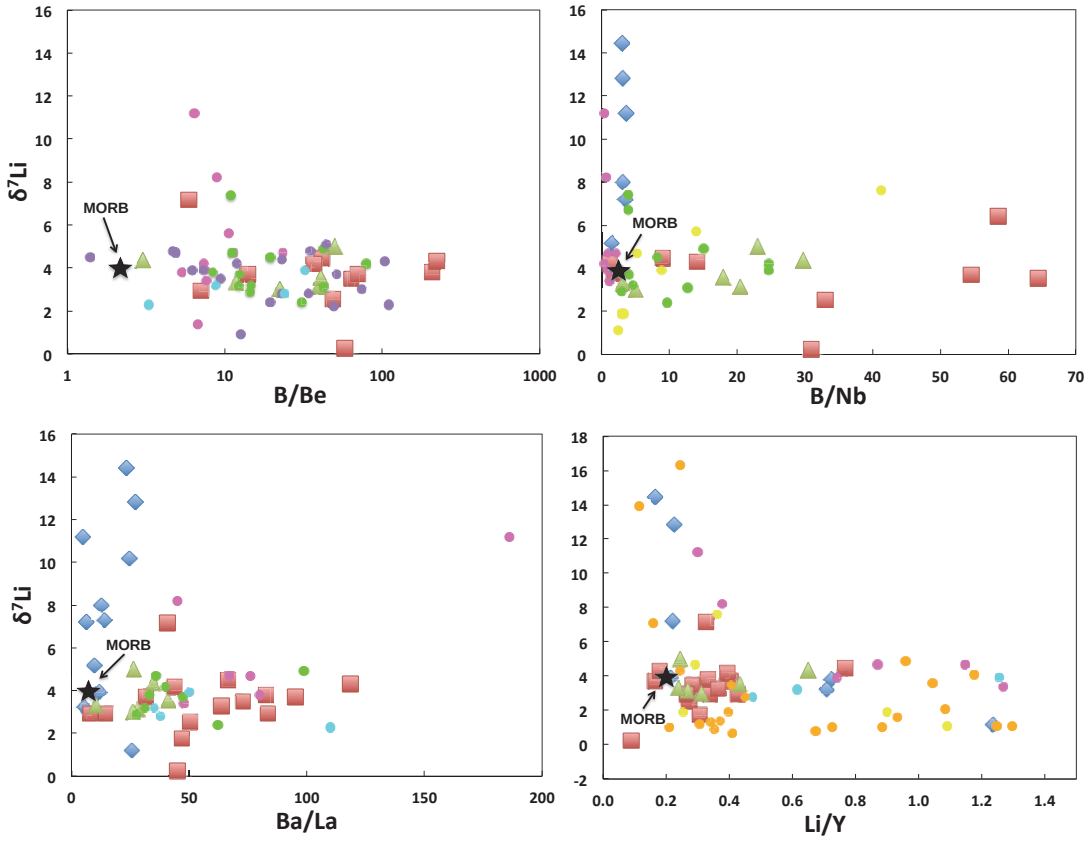

Figure 2.5 δ^7Li isotopic compositions versus traditional tracers of slab fluids: B/Be, Ba/Nb, Ba/La, Li/Y (data from George et al., 2005). There is no published Be data for the sediment in this study. Average MORB (star) is shown along with data for other arcs from the literature. Samples plotted: Arc (red square), back-arc (green triangle), sediment (blue diamond), along with background data from other arcs (Izu, Panama, Kurile, Sunda, Aleutian, Martinique) (see Fig. 2.3 for data sources).

Many studies have utilized U/Th and Th/Ce ratios as tracers of fluid and sediment components in arc lavas (e.g. Turner et al., 1997; Plank and Langmuir, 1998). On Fig. 2.6a we plot δ^7Li against U/Th as a tracer of fluid contributions from the subducting plate. Overall there is a weak positive correlation, but the majority of the lavas lie between likely average compositions of the mantle wedge (DMM) and altered oceanic crust (AOC) which can have a very large range in δ^7Li (Gao et al., 2012). Here the Niuatoputapu lava is displaced from the remaining lavas towards the average volcaniclastic sediment composition. No correlation is observed when the δ^7Li data

from the Tonga-Kermadec lavas is plotted against indices of sediment addition such as Th/Ce (Fig. 2.6b) unlike the findings of Moriguti and Nakamura (1998) or Chan et al. (2002). The back-arc lavas lie at the low U/Th, low Th/Ce end of the data, consistent with lesser overall contributions from the slab (Caulfield et al., 2012a).

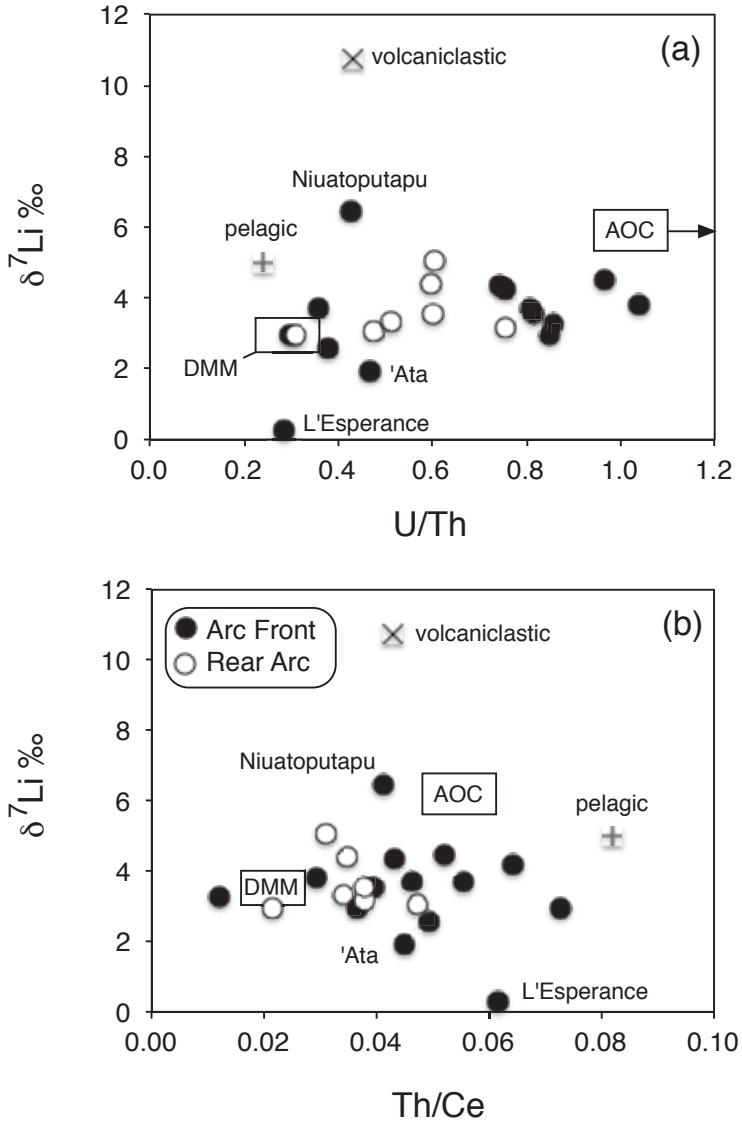

Figure 2.6 Plots of δ^7Li versus U/Th a fluid-sensitive index (a) and Th/Ce a sediment-sensitive index (b). The average compositions of the DSDP Site 204 pelagic and volcaniclastic sediments are also shown along with average estimates for depleted MORB mantle (DMM) and altered oceanic crust (AOC) – data from Elliott et al. (2004), Gao et al. (2012), Kelley et al. (2003), Salters and Stracke (2004).

On Fig. 2.7 we investigate variations between δ^7Li and two other isotope systems that tend to be track sub-arc fluid additions since both B and Sr are fluid mobile (Brenan et al., 1998). There is no correlation between δ^7Li and ^{87}Sr/^{86}Sr though, as in Fig. 4a, both the arc front and back-arc lavas generally fall between DMM and AOC and the average sediment compositions. Although there is less data, we plot δ^7Li versus δ^{11}B on Fig. 5b. Once again, there is no correlation though the diagram does highlight the unusually light B in the ‘Ata sample that may reflect complex mantle wedge circulation caused by the locus of present-day subduction of the Louisville seamounts (Leeman et al., 2017).

The conclusion from Figs. 2.5, 2.6, and 2.7 have to be that there are no trends that unambiguously distinguish between sediment and fluid addition as the main control on the variations in δ^7Li in the Tonga-Kermadec-Lau lavas. It is highly likely that diffusive equilibration with non-subduction modified mantle wedge has erased much of any putative initial subduction-derived signatures (e.g., Elliott et al., 2004; Tang et al., 2014; Penniston-Dorland et al., 2012). Nevertheless, some δ^7Li signals do appear to survive such as that of the Louisville volcaniclastics in the case of the lava from Niuatoputapu. Conversely, the lack of an equivalent signal in similar lavas from neighboring Tafahi testifies to just how fragile they are in the face of diffusive interaction with the wedge.

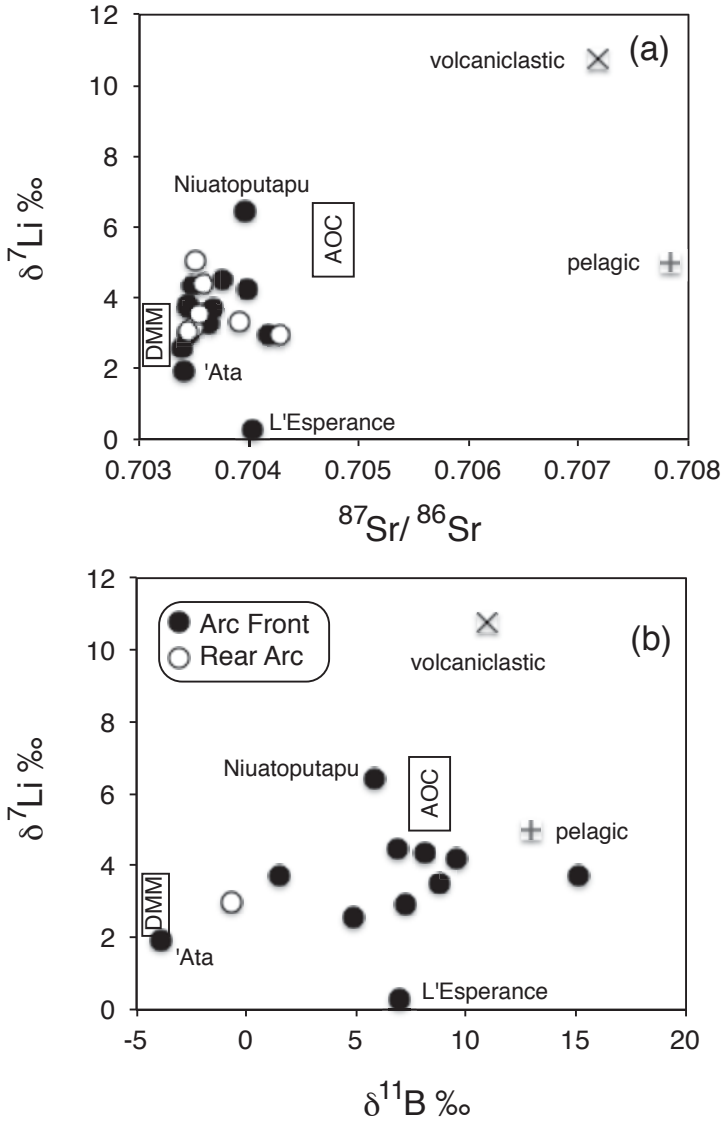

Figure 2.7 Plots of δ^7Li versus (a) ^{87}Sr/^{86}Sr and (b) δ^{11}B. Boron data from Leeman et al. (2017), other symbols and data sources as for Fig. 2.6.

2.5.3 Sediment additions to the mantle wedge

I compare the Tonga-Kermadec lava data with a three-component mixing model between bulk sediment, DMM-1%, and a calculated fluid component from the altered oceanic crust in Figure 2.8 (Ellam & Hawkesworth, 1988; Tomascak et al., 2002; Kelley et al., 2003; Salters & Stracke, 2004; George et al., 2005; Kreinitz et al., 2012). I also plot MORB based on McDonough & Sun (1995) and averaged δ^7Li MORB values from Tomascak et al. (2008). The three end-members in the numerical model (DMM-

1%, fluid, and sediment) were based on calculations presented by George et al. (2005) for the ^{10}Be budget in these lavas. Briefly, the DMM (Salters & Stracke, 2004) component was assumed to have been depleted by 1% batch melt extraction in the back-arc. This composition was calculated using partition coefficients from Blundy & Wood (2003) and assuming a mantle comprising 44% olivine, 41% orthopyroxene, and 14% clinopyroxene. The fluid composition calculated was using the altered oceanic crust composition from ODP Site 801 (Kelley et al., 2003), a Rayleigh distillation process and partition coefficients from Brenan et al. (1995, 1998), Stalder et al. (1998), and Fabrizzio et al. (2013). For estimates of δ^7Li in AOC, there are two reported values from drill cores, one from Brant et al., (2012) and one from Chan et al. (2002b). Both have a large range, spanning -10.9 to +14.5 and +1 to +21, respectively. The heavy δ^7Li from the upper limit of the altered oceanic crust from the East Pacific Rise at +14.5 was used because it was the closest location to the Tonga-Kermadec arc for which data exist (Brant et al., 2012). However, given the large array in δ^7Li reported in Brant et al. (2012), and therefore uncertainty in δ^7Li values, I illustrate how the mixing models change when the parameters for the AOC δ^7Li vary by using the midpoint of the δ^7Li range. I assumed the altered oceanic crust to comprise 28% garnet, 54% clinopyroxene, and 18% amphibole (Kelley et al., 2003). The sediment composition used the average bulk composition from DSDP Site 204 (the average starting composition for the Johnson & Plank (1999) experiments are close to the averages for the sediments used in this study) and sediment melt compositions assumed batch melting and used solid/melt partition coefficients from Johnson & Plank (1999). I assumed a 20% sediment batch melt at 800^{o}C to remain consistent with the model presented by George et al. (2005).

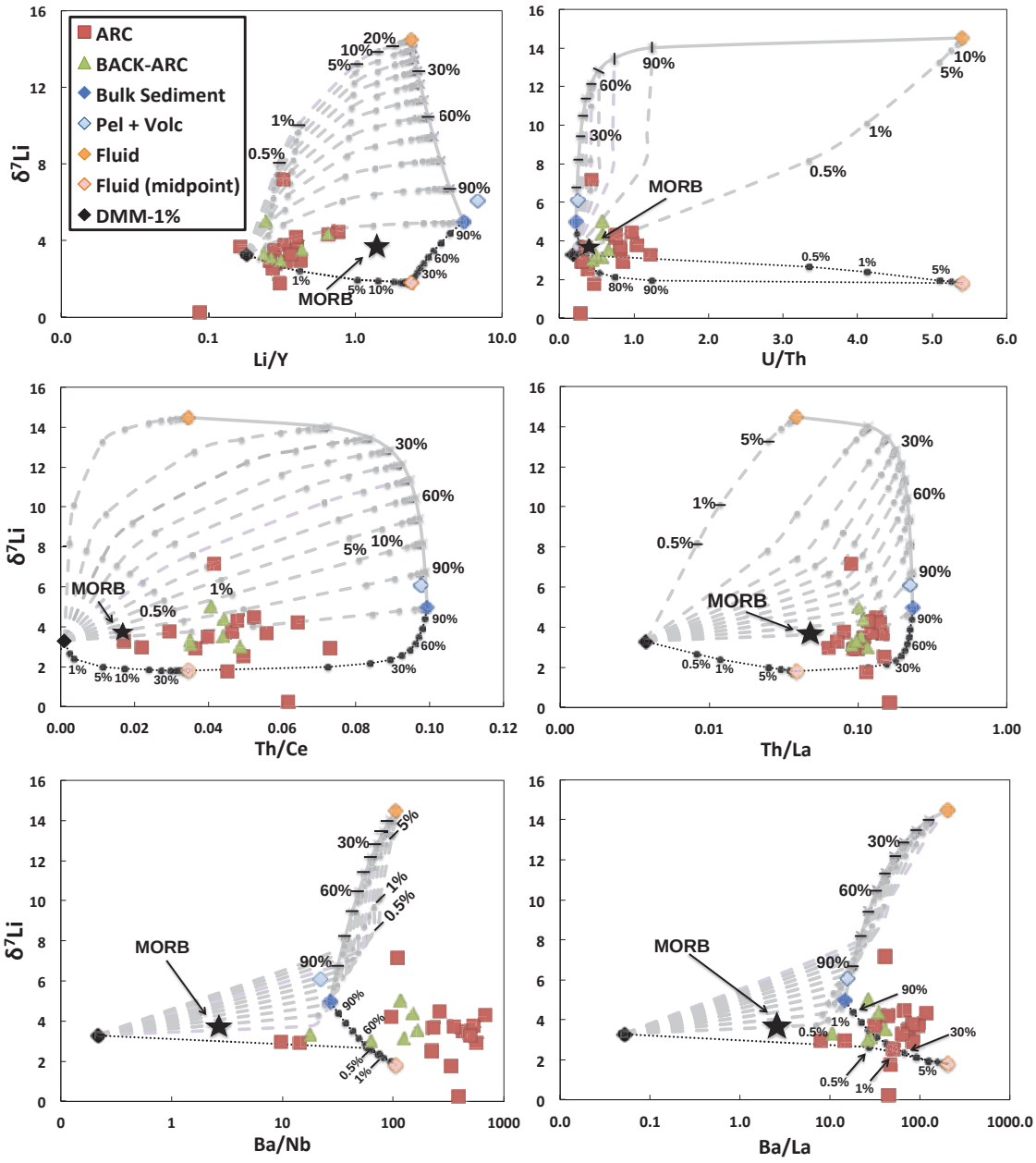

Figure 2.8 Three-component mixing model: bulk sediment melt at 800°C, DMM-1% and a distillation fluid component from the altered oceanic crust (see text for explanation) (Ellam & Hawkesworth, 1988; Tomascak et al., 2002; Salters & Stracke, 2004; Kelley et al., 2003; George et al., 2005; Kreinitz et al., 2012). Average MORB (star) is plotted for reference. The dotted black line extending in the bottom of each model illustrates how the mixing models would change if the parameters for the AOC δ^7Li changed. In this case, we use the midpoint for the large δ^7Li range in AOC reported in Brant et al. (2012), instead of the upper limit as the 'fluid' component.

As shown in Figure 2.8, using the end-member compositions described above, most of the Tonga-Kermadec data fall below the area encompassed by a three-component mixing model. Using the measured pelagic sediment average δ^7Li (+ 5.0) from this study ignores the possible influence of the underlying volcaniclastic sediments. Therefore, I also tested mixing of the weighted sediment, including the volcaniclastics (δ^7Li = + 6.1). Likewise, mixing models using these values with the two-other end-member components (AOC fluid and DMM-1%) does not fully reproduce the lava array on the element ratio plots. This suggests, if the model is correct, the average sediment δ^7Li composition must be lower, or the AOC value is too high (Fig. 2.8) compared to the ones suggested by Chan et al. (2002b, 2005) and Brant et al. (2012).

Plank (2013) showed that both Sunda and Nicaragua arc lavas have an inverse correlation between Y/Li and average weighted δ^7Li (Y/Li is used in lieu of Li/Y so that mixing will form linear arrays). These correlations likely reflect binary mixing between a subducted sediment component and a mantle source (DMM-1%). In Plank's (2013) models, the sediment values reflect the weighted mean for the reported local sediment but are allowed to be up to 3‰ heavier in order to account for fractionation that may occur during fluid loss (Marschall et al., 2007b). For example, isotopic fractionation by clinopyroxene at temperatures greater than 500^{o}C increases δ^7Li by 3‰ (Wunder et al., 2006). This is also consistent with the findings of Marschall et al. (2007b) during repeated experimental dehydration of the subducting oceanic crust. Once the fluid is released from the slab, the residual sediment can be up to 3‰ heavier and Plank (2013) suggests that this composition is likely to be the entire range that is representative of bulk sediment.

Following Plank (2013), I simulate mixing between DMM-1% (Salters & Stracke, 2004) and bulk sediment that has undergone dehydration making it +3‰ heavier (+9.1), plus AOC fluid. Figure 2.9 shows the results of this mixing model. We

see that the Tonga-Kermadec lavas still plot beneath the calculated mixing array, similar to the earlier mixing model presented in this study between DMM-1%, AOC fluid and average bulk sediment component (+6.1), which is shown in Figure 2.8.

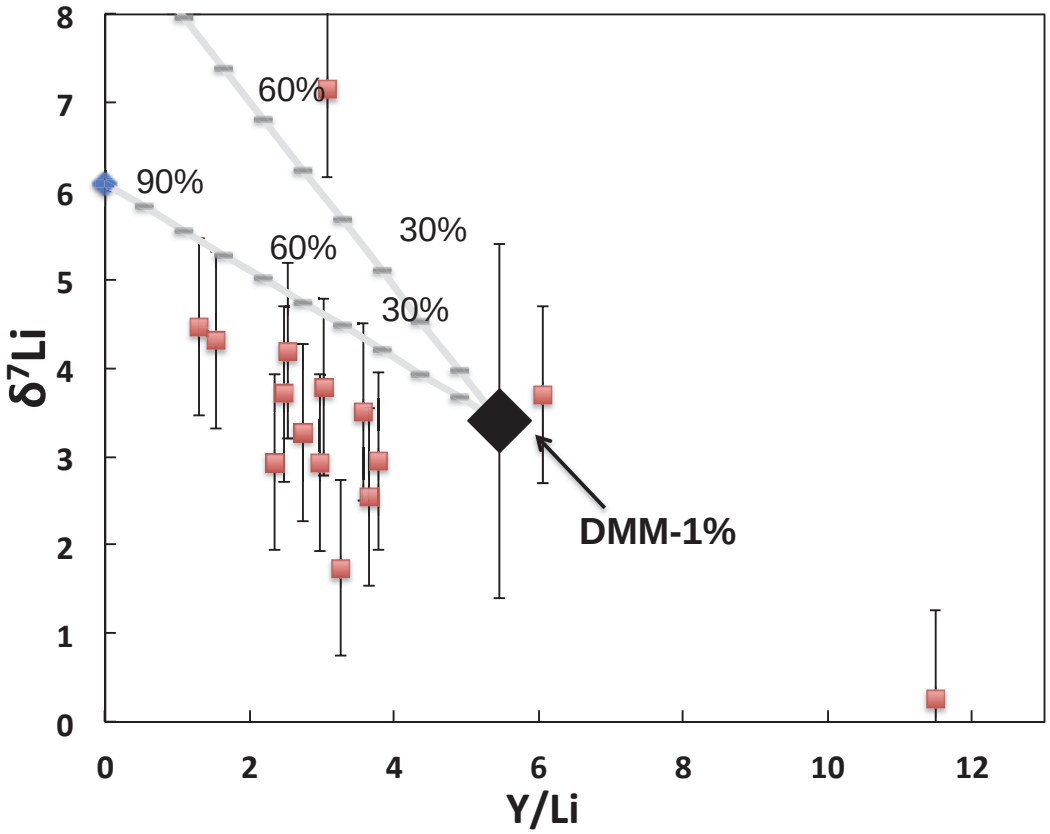

Figure 2.9 Mixing of DMM-1% with local bulk sediments DSDP Site 204. Y/Li, a slab fluid indicator, is used so that mixing follows a straight line (e.g. Plank 2013). The top mixing line represents 3‰ heavier sediment, which accounts for the fractionation that may occur during slab dehydration (Marschall et al., 2007b). The area between the two lines is the mixing field (see text).

Using the calculated sediment averages from this study hides the full range of δ^7Li sediment values that could be involved in the mixing. Therefore, in Figure 2.10, I show the results of a Monte Carlo simulation that allows randomized, two end-member mixing between DMM-1% source ([Li] = 0.7 ppm, [Y] = 4.1 ppm (Salters & Stracke, 2004), δ^7Li = +3.4), and the full range of sediment values for DSDP Site 204 (δ^7Li = +1.2 to +14.4 and their respective [Li]). The δ^7Li value for DMM is an average of the

accepted δ^7Li range of +2 to +6 (Chan et al., 1992, 2002b; Tomascak et al., 2008). Figure 2.10a simulates the addition of the DSDP pelagic sediment compositions alone; they are believed to be the main sediment contributor to the lavas (Turner et al., 1997; George et al., 2005). This results in a smaller and more restricted range for δ^7Li. Figure 2.10b includes the minimum and maximum values for the sediment compositions of the collective units, including the volcaniclastic sediments. Most of the lavas (within error) fall inside the area of binary mixing between DMM and the local sediments in both models shown in Figure 2.10. The Monte Carlo simulation suggests that the lava array can successfully be modeled by the addition of up to 3.5% sediment (Fig. 2.10). Although this simple mixing relationship can account for a large portion of the data, there are still two outliers (Macauley and L'Esperance). I further address the role of fluid in the next section.

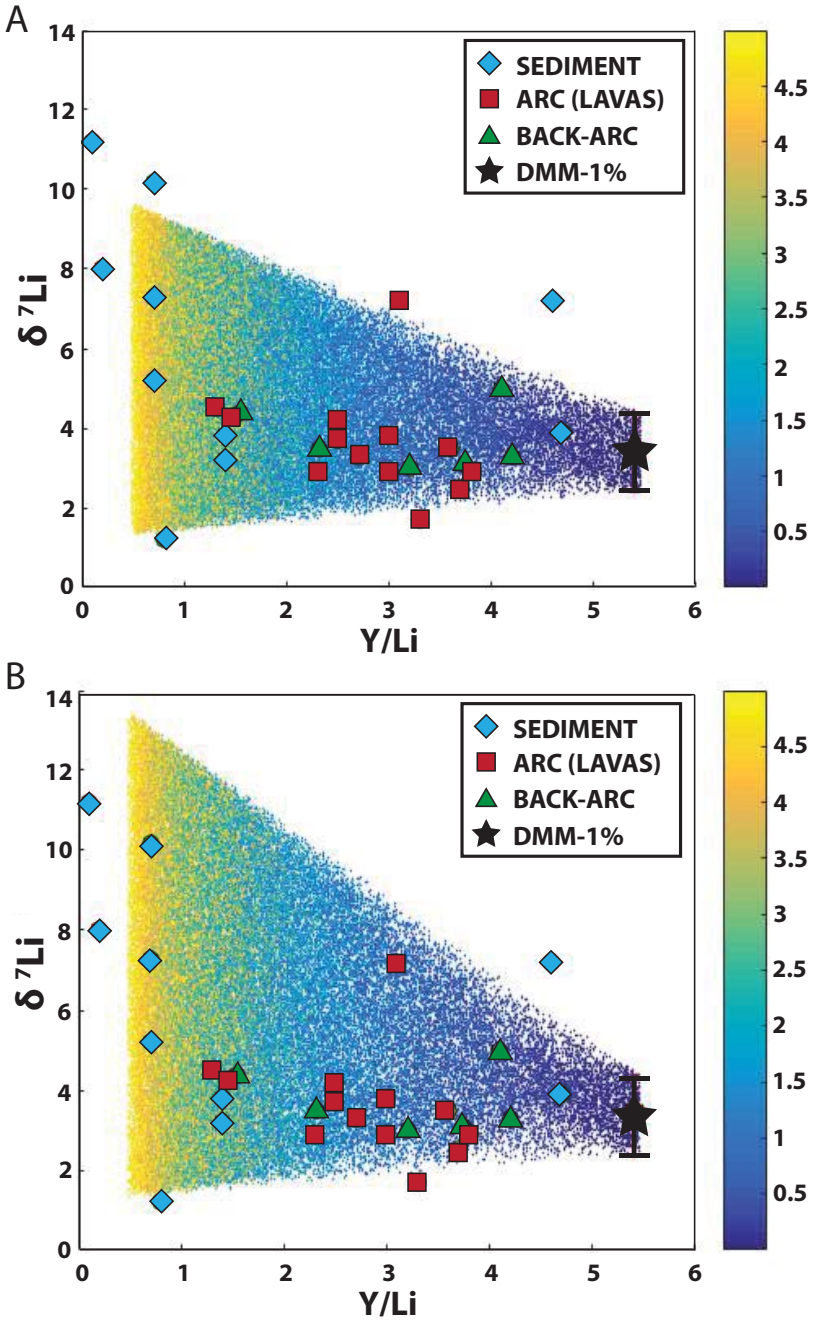

Figure 2.10 Two end-member component mixing model between average DMM-1% (black star) and sediments from DSDP Site 204 (blue diamonds). The gradation of small dots in the background represents random mixing results using a Monte Carlo simulation, and the bar to the right of each panel represents the amount of sediment (%) required to attain that value in the Monte Carlo simulation. Panel A shows mixing with only pelagic sediment component as end-members and Panel B shows mixing using the entire sedimentary core (pelagic + volcaniclastic) for DSDP Site 204. We assumed zero Y from the subducting slab sediment because Y would probably be retained in a garnet component as subduction persists. The lithium isotopes in the Tonga-Kermadec lavas (red squares) can mostly be formed by the addition of less than 3.5% addition of sediments from DSDP Site 204. There are two

outliers (Macauley and L'Esperance) that plot outside of the range shown for Y/Li on these plots (see Table 2.1 for values).

2.5.4 Other possible effects on the Li signal

The majority of the lavas are displaced below the three component-mixing arrays in Figure 2.8. Slightly fewer than half of the lavas from the arc front (7 out of 15) fall closer to the base of the mixing arrays. There are two potential explanations. The first is equilibration of the slab components or arc magmas with the mantle wedge, which would contract the lava compositions towards MORB/DMM-1% on Figure 2.8, thereby greatly reducing the overall range in lithium isotopes. This would mask the effects of Li addition from any fluid/sediment components (cf. George et al., 2005; Plank, 2013) Nevertheless, over time, ongoing sediment and fluid addition would potentially lead to an overall increase in δ^7Li in the mantle wedge. The second explanation, advocated by Tomascak et al. (2002), is that heavy Li released from the subducting slab becomes sequestered into Mg-silicates in the forearc mantle and removed by convection without contributing to the arc lavas. Subsequent additions from the slab to the wedge would be correspondingly enriched in light Li, potentially explaining the displacement of many of the Tonga-Kermadec lavas to low δ^7Li on Figure 2.8. To illustrate this, we can use the midpoint (+ 1.8) from Brant et al. (2012) for the AOC fluid δ^7Li composition. Using this value for AOC fluid, a larger proportion of the data fit within the mixing array in a few ratio plots (Th/Ce; Th/La; Li/Y). This lighter value can explain some of the data, although this is a very light value for AOC fluid and does not satisfy other element ratio plots. In reality, both δ^7Li end members, along with end-member ratios of slab-fluid indicators (e.g. Ba/Nb & Ba/La) might vary and encompass the lava array (Fig. 2.8).

2.5.5 The role of Li in crystal fractionation

There is a possibility of incorporation of low δ^7Li components through interaction with the crust during differentiation. However, due to the small number of samples for each location, the sample set is not ideally suited for this comparison. What can be observed through the data present is that, as a moderately incompatible element, Li concentrations increase with increasing SiO_2 (Fig. 2.3b), but there is no clear correlation between δ^7Li and SiO_2 (Fig. 2.3c). The majority have δ^7Li that ranges from 2.5 to 5.0 ‰ with an average of 3.6 ± 0.7 ‰ that is similar to those reported from other arcs (Bouman et al., 2004; Moriguti and Nakamura, 1998; Tang et al., 2014; Tomascak et al. 2000, 2002) and overlap with the range for MORB. However, there are three notable outliers. For the former two, we replicated the data: Niuatoputapu with δ^7Li = 6.4 and 7.9 ‰, ‘Ata with δ^7Li = 1.6 and 1.9 ‰. However, there was insufficient sample from the L’Esperance sample to undertake a replicate analysis (δ^7Li = 0.3 ‰, see Table 2.1). Thus, it is possible that the range of δ^7Li in this arc may be slightly larger than reported elsewhere.

2.5.6 Subduction geometry

Arc geometry may play a role in how the δ7Li signal is transferred from the slab. For example, a fast convergence rate produces a strong corner flow that may advect away the heavy δ^7Li signal released from the slab (Tomascak et al., 2002). Alternatively, slow convergence rates may promote more direct sampling of subducted sediments due to a hotter slab. For example, the Lesser Antilles has a very slow convergence rate (~2 cm/yr) (Jordan, 1975) and lavas on Martinique exhibit a lithium isotopic signature that is similarly light to the sediments being subducted but they do not show any correlation with other indicators of subduction fluids. The particularly

slow subduction rate may be a factor explaining why a sediment lithium isotopic signature is observed in Martinique yet not in other arcs (Tomascak et al., 2000; 2002). These examples point to a potential role of arc geometry and convergence rate in moderating the lithium isotope signature in erupted lavas. Returning to the Tonga-Kermadec arc, its convergence rate spans a much larger range (up to 20 cm/yr) than many other arcs and may provide a reason why any recycled lithium signal is muted because lithium may have been modified by partitioning into Mg-silicates that are then removed from the budget.

2.5.7 Back-arc lavas from the Fonualei Spreading Center

The lavas from the Fonualei Spreading Center exhibit arc-like geochemical signatures (Caulfield et al., 2012a) yet, like most of the arc front lavas, have δ^7Li (+3.0 to +5.0) that overlap the range of the MORB (+2.0 to +6.0). Conversely, some of the arc front lavas have δ^7Li < 3 which is not observed in the back-arc. This suggests either that there is minimal transfer of Li from the slab beyond the arc front or, alternatively, that the increased slab-to-surface transport distance is sufficient to facilitate full equilibration of the rising magmas with the mantle wedge.

2.6 Conclusions

The analysis of δ^7Li in a sediment profile from DSDP Site 204 provides a more robust constraint on the lithium budget of sediments subducting beneath the Tonga-Kermadec Trench, with weighted averages for δ^7Li [+5.0 (pelagic) and +6.1 (pelagic + volcaniclastic)]. In terms of lithium isotope composition, we do not see a correlation with other slab fluid indicators within the Tonga-Kermadec arc or back-arc lavas. This makes the lithium isotope composition similar to the Kurile, Sunda, Aleutians, and

Lesser Antilles (Martinique) arcs. Only in two arcs, Izu and Central America, have there been clear correlations between slab-derived fluid tracers and lithium isotopes.

The MORB-like lithium isotopic composition of the Tonga-Kermadec lavas suggests that the lithium elemental and isotopic characteristics reflect either, or a combination of, equilibration with the mantle wedge or sequestration and removal of the heavy Li in the system, possibly linked to slab-convergence rate. Bulk sediment mixing modeled for this system does not satisfy a majority of the data for the lavas unless I use a light AOC of +1.8. Using randomized mixing models with the entire range of sediment compositions satisfies most of the lava data and I can quantify the amount of sediment required to reproduce the lithium isotopic signatures of the lavas. With this result, the lavas from the Tonga-Kermadec arc require up to 3.5% sediment addition to reproduce the array observed in the data. Lavas from the Fonualei Spreading Center (δ^7Li = +3.0 to +5.0) show no variation from the widely-accepted lithium isotopic signature range of the MORB (δ^7Li = +2.0 to +6.0), suggesting that there is either little to no lithium transfer from the slab to the back-arc or complete equilibration with the mantle wedge. The fact that δ^7Li in a few arc front lavas (+0.3 to +7.2) fall outside the range of MORB may be the only remnant signature from subducted components. As noted by others, this calls into question the utility of lithium isotopes as straightforward tracers of subducted components in arc lavas.

2.7 References

Acland S. (1996) Magma genesis in the northern Lau Basin, S.W. Pacific. Ph.D. dissertation. University of Durham.

Adam, J., & Green, T. (2006) Trace element partitioning between mica- and amphibole-bearing garnet lherzolite and hydrous basanitic melt: 1. Experimental results and the investigation of controls on partitioning behaviour. *Contributions to Mineralogy and Petrology* 152, 1, 1-17.

Agostini, S., Ryan, J. G., Tonarini, S., & Innocenti, F. (2008) Drying and dying of a subducted slab: coupled Li and B isotope variations in Western Anatolia Cenozoic Volcanism. *Earth and Planetary Science Letters*, *272*(1), 139-147.

Bauer, G.R. (1970) The geology of Tofua Island, Tonga. *Pacific Science* 24, 333-350.

Benton, L.D., Ryan, J.G. & Savov, I.P. (2004) Lithium abundance and isotope systematics of forearc serpentinites, conical seamount, Mariana forearc: Insights into the mechanics of slab-mantle exchange during subduction. *Geochemistry, Geophysics, Geosystems - G3*, 5, *Q08J12*.

Bevis, M., Taylor, F.W., Schutz, B.E., Recy, J. & Isacks, B.L., Helu, S., Singh, R., Kendrick, E., Stowell, J. (1995) Geodetic observations of very rapid convergence and back-arc extension at the Tonga arc. *Nature* 374, 249-251.

Billen, M. I. & Stock, J. (2000) Morphology and origin of the Osbourn Trough. *Journal of Geophysics Research* 105, 13481-13489.

Bloomer, S.H. & Fisher, R.L. (1986) Petrology and geochemistry of igneous rocks from the Tonga trench – A non-accreting plate boundary. *Journal of Geology* 95, 469-495.

Bouman, C., Elliott, T. & Vroon, P.Z. (2004) Lithium inputs to subduction zones. *Chemical Geology* 212, 59-79

Blundy, J. & Wood, B. (2003) Mineral-melt partitioning of uranium, thorium and their daughters. *Reviews in Mineralogy and Geochemistry* 52, 59-123.

Brant, C., Coogan, L.A., Gillis, K.M., Seyfried, W.E., Pester, N.J. & Spence, J. (2012) Lithium and Li-isotopes in young altered upper oceanic crust from the East Pacific Rise. *Geochimica et Cosmochimica Acta* 96, 272-293.

Brenan, J.M., Ryerson, F.J. & Shaw, H.F. (1998) The role of aqueous fluids in the slab-to-mantle transfer of boron, beryllium, and lithium during subduction: experiments and models. *Geochimica et Cosmochimica Acta* 62, 19-20, 3337-3347.

Brenan, J.M., Shaw, H.F., Ryerson, F.J. & Phinney, D.L. (1995) Mineral-aqueous fluid partitioning of trace elements at 900 degrees C and 2.0 GPa: constraints on the trace element chemistry of mantle and deep crustal fluids. *Geochimica et Cosmochimica Acta* 59, 16, 3331-3350.

Brothers, R.N. & Martin, K.R. (1970) The geology of Macauley Island, Kermadec Group. Southwest Pacific. *Bulletin Volcanologique* 34, 330-346.

Brothers, R.N. & Searle, E.J. (1970) The geology of Raoul Island, Kermadec Group, Southwest Pacific. *Bulletin Volcanologique* 34, 7-37.

Burns, R. E., Andrews, J. E., van der Lingen, G. J., Churkin, M., Jr., Galehouse, J. S., Packham, G., Davies, T. A., Kennett, J. P., Dumitrica, P., Edwards, A. R. & Von Herzen, R. P. (1973) Site 204. *Initial Reports of the Deep Sea Drilling Project* 21, 33-56.

Caciagli, N., Brenan, J.M., McDonough, W.F. & Phinney, D. (2011) Mineral-fluid partitioning of lithium and implications for slab-mantle interaction. *Chemical Geology* 280, 3-4, 384-398.

Caulfield, J., Turner, S., Arculus, R., Dale, C., Jenner, F., Pearce, J., Macpherson, C. & Handley, H. (2012a) Mantle flow, volatiles, slab-surface temperatures and melting dynamics in the north Tonga arc–Lau back-arc basin. *Journal of Geophysical Research: Solid Earth* (1978–2012), 117(B11).

Caulfield, J. T., Turner, S. P., Smith, I. E. M., Cooper, L. B., & Jenner, G. A. (2012b) Magma evolution in the primitive, intra-oceanic Tonga arc: petrogenesis of basaltic andesites at Tofua volcano. *Journal of Petrology* 53, 1197-1230.

Chan, L.H., Alt, J.C., Teagle, D.A.H. (2002a) Lithium and lithium isotope profiles through the upper oceanic crust: a study of seawater-basalt exchange at ODP Sites 504B and 896A. *Earth and Planetary Science Letters* 201(1): 187-201.

Chan, L. & Edmond, J.M. (1988) Variation of lithium isotope composition in the marine environment: a preliminary report. *Geochimica et Cosmochimica Acta* 52, 6, 1711-1717.

Chan, L.H., Edmond, J.M., Thompson, G. & Gillis, K. (1992) Lithium isotopic composition of submarine basalts: implications for the lithium cycle in the oceans. *Earth and Planetary Science Letters* 108, 1-3, 151-160.

Chan, L.H., Gieskes, J.M. & You, C.F., Edmond, J.M. (1994) Lithium isotope geochemistry of sediments and hydrothermal fluids of the Guaymas Basin, Gulf of California, *Geochimica et Cosmochimica Acta* 58, 4443-4454.

Chan, L.H., Leeman, W.P. & You, C.F. (2002b) Lithium isotopic composition of Central American Volcanic Arc lavas: Implications for modification of the subarc mantle by slab-derived fluids: Correction. *Chemical Geology* 182, 293-300.

Chan, L.H., Leeman, W.P. & Plank, T. (2006) Lithium isotopic composition of marine sediments. *Geochemistry, Geophysics, Geosystems - G3*, 7, *Q06005*.

Chan, L.H. & Frey, F.A. (2003) Lithium isotope geochemistry of the Hawaiian plume: results from the Hawaii Scientific Drilling Project and Koolau Volcano, *Geochemistry, Geophysics, Geosystems - G3*, 4, 8707.

DeMets, C., R.G. Gordon, D.F. Argus & Stein, S. *(*1994*)* Effect of recent revisions to the geomagnetic reversal time-scale on estimates of current plate motions, *Geophysical Research Letters* 21.20, 2191-2194.

Ellam, R.M & Hawkesworth, C. (1988) Elemental and isotopic variation in subduction related basalts – Evidence for a 3 component model. *Contributions to Mineralogy and Petrology* 98, 72-80.

Elliott, T., Jeffcoate, A. & Bouman, C. (2004) The terrestrial Li isotope cycle: light-weight constraints on mantle convection. *Earth and Planetary Sciences* 220, 231-245.

Ewart, A., Bryan, W.B. & Gill, J. B. (1973) Mineralogy and geochemistry of the younger volcanic islands of Tonga, S.W. Pacific. *Journal of Petrology* 14, 6, 429-465.

Ewart, A. (1976) A petrological study of the younger Tongan andesites and dacites, and the olivine tholeiites of Niua Fo'ou island, S.W. Pacific. *Contributions to Mineralogy and Petrology* 58, 1-21.

Ewart, A., Brothers, R.N. & Mateen, A. (1977) An outline of the geology and geochemistry, and the possible petrogenetic evolution of the volcanic rocks of the Tonga-Kermadec-New Zealand island arc. *Journal of Volcanology Geothermal Research* 2, 205-250.

Ewart, A. & Hawkesworth, C.J. (1987) The Pleistocene-Recent Tongan-Kermadec arc lavas: interpretation of new isotope and rare earth data in terms of a depleted mantle source model. *Journal of Petrology* 28, 295-330.

Ewart A., Bryan W. B., Chappell B.W. & Rudnick R.L. (1994) Regional Geochemistry of the Lau-Tonga arc and backarc systems. *Proceedings of the ODP: Scientific Results* 135, 385-425.

Ewart, A., Collerson, K.D., Regelous, M., Wendt, J.I. & Niu, Y. (1998) Geochemical evolution within the Tonga-Kermadec-Lau arc-back-arc systems: the role of varying mantle wedge composition in space and time. *Journal of Petrology* 39, 3, 331-368.

Fabbrizio, A., Stalder, R., Hametner, K., Günther, D., & Marquardt, K. (2013) Experimental partitioning of halogens and other trace elements between olivine, pyroxenes, amphibole and aqueous fluid at 2 GPa and 900–1,300 C. *Contributions to Mineralogy and Petrology* 166(2), 639-653.

Flesch, G., Anderson, A.R. & Svec, H.J. (1973) A secondary isotopic standard for $^{6}Li/^{7}Li$ determinations. *International Journal of Mass Spectrometry & Ion Physics* 12, 265-272.

Fryer, P., Taylor, B., Langmuir, C.H. & Hochstaedter, A.G. (1990) Petrology and geochemistry of lavas from the Sumisu and Torishima backarc rifts, *Earth and Planetary Science Letters* 100, 1-3, 161-178.

Gao, Y., Vils, F., Cooper, K. M., Banerjee, N., Harris, M., Hoefs, J., Teagle, D. A. H., Casey, J. F., Elliott, T., Laverne, C., Alt, J. C. and Muechlenbachs (2012) Downhole variation of lithium and oxygen isotopic compositions of oceanic crust at East Pacific Rise, ODP Site 1256. *G Geochemistry, Geophysics, Geosystems*, **13**, Q10001.

George, R., Turner, S., Morris, J., Plank, T., Hawkesworth, C.J. & Ryan, J. (2005) Pressure-temperature-time paths of sediment recycling beneath the Tonga-Kermadec arc. *Earth and Planetary Science Letters* 233, 1-2, 195-211.

Gladney, E.S. & Goode, W.E. (1981) Elemental concentrations in eight new United States Geological Survey rock standard: a review. *Geostandards Newsletter* 5, 31-64.

Govindaraju, K. (1994) 1994 compilation of working values and sample descriptions for 383 geostandards. *Geostandards Newsletter* 5, 31-64.

Hawkins, J.W. (1995) The geology of the Lau Basin. In Backarc Basins: Tectonics and Magmatism, 63-138, edited by Brian Taylor, Plenum Press, New York.

Isacks, B.L. & Barazangi, M. (1977) Geometry of Benioff zones: Lateral segmentation and downwards bending of the subducted lithosphere. In: Island Arcs Deep Sea Trenches and Back-Arc Basins. Maurice Ewing Ser. 1, 99-114.

James, R.H., & Palmer, M.R. (2000) The Li isotope composition of international rock standards. *Chemical Geology* 166, 319-326.

Jarrard, R.D. (1986) Relations among subduction parameters. *Reviews of Geophysics* 24, 2, 217-284.

Johnson, M.C. & Plank, T. (1999) Dehydration and melting experiments constrain the fate of subducted sediments. *Geochemistry, Geophysics, Geosystems - G3*, 1, 1007.

Jordan, T.H. (1975) The present-day motions of the Caribbean plate. *Journal of Geophysical Research* 80, 4433-4439.

Kelemen, P.B., Shimizu, N. & Dunn, T. (1993) Relative depletion of niobium in some arc magmas and the continental crust: partitioning of K, Nb, La and Ce during melt/rock reaction in the upper mantle. *Earth and Planetary Science Letters* 120, 3-4, 111-133.

Keller, N.S., Arculus, R.J., Hermann, J. & Richards, S. (2008) Submarine back-arc lava with arc signature: Fonualei Spreading Center, northeast Lau Basin, Tonga. *Journal of Geophysical Research: solid earth*, 113:1-28.

Kelley, K.A., Plank, T., Ludden, J. & Staudigel, H. (2003) Composition of altered oceanic crust at ODP Sites 801 and 1149. *Geochemistry, Geophysics, Geosystems - G3*, 4, 8910.

Krienitz, M.-S., Garbe-Sh*önberg, C.-D., Romer, R.L., Meixner, A., Haase, K.M. & Stroncik, N.A., (2012)* Lithium Isotope Variations in Ocean Island Basalts—Implications for the Development of Mantle Heterogeneity. *Journal of Petrology* 53, 2333-2347.

Langmuir, C.H., Bézos, A., Escrig, S. & Parman, S.W. (2013) Chemical Systematics and Hydrous Melting of the Mantle in Back-Arc Basins, in Back-Arc Spreading Systems: Geological, Biological, Chemical, and Physical Interactions. (eds D. M. Christie, C. R. Fisher, S.-M. Lee and S. Givens), American Geophysical Union, Washington, D. C.

Liu, X.M., Rudnick, R.L., Hier-Majumder, S. & Sirbescu, M.C. (2010) Processes controlling lithium isotopic distribution in contact aureoles: a case study of the Florence County pegmatites, Wisconsin. *Geochemistry, Geophysics, Geosystems - G3*, 11, Q08014.

Liu, X.M., Rudnick, R.L. (2011) Constraints on continental crustal mass loss via chemical weathering using lithium and its isotopes. *Proceedings of the National Academy of Sciences of the United States of America* 108(52): 20873-20880.

Liu, X.M., Rudnick, R.L., McDonough, W.F. & Cummings, M.L. (2013) Influence of chemical weathering on the composition of the continental crust: insights from Li and Nd isotopes in bauxite profiles developed on Columbia River basalts. *Geochimica et Cosmochimica Acta* 115, 73-91.

Liu, X.M., Wanner, C., Rudnick, R.L. & McDonough, W.F. (2015) Processes controlling δ^7Li in rivers illuminated by study of streams and groundwaters draining basalts. *Earth and Planetary Science Letters* 409, 212-224.

Magna, T., Wiechert, U.H. & Halliday, A.N. (2004) Low-blank isotope ratio measurement of small samples of lithium using multiple-collector ICPMS. *International Journal of Mass Spectrometry* 239, 67-76.

Marschall, H.R, Altherr, R. & Rüpke, L. (2007a) Squeezing out the slab – modeling the release of Li, Be and B during progressive high-pressure metamorphism. *Chemical Geology* 239, 323-335.

Marschall, H.R., Pogge von Strandmannn, P.A.E., Seitz, H.M., Elliott, T. & Niu, Y. (2007b) The lithium isotopic composition of orogenic eclogites and deep subducted slabs. *Earth and Planetary Science Letters* 262, 563-580.

McDonough, W.F. & Sun, S.S. (1995) The composition of the Earth. Chemical *Geology* 120, 3-4, 223-253.

Millot, R., Vigier, N., & Gaillardet, J. (2010) Behaviour of lithium and its isotopes during weathering in the Mackenzie Basin, Canada. *Geochimica et Cosmochimica Acta*, *74*(14), 3897-3912.

Minster, J.B. & Jordan, T.H. (1978) Present-day plate motions. *Journal of Geophysical Research: Solid Earth* 83, 5331-5354.

Molnar, P. & Sykes, L.R. (1969) Tectonics of the Caribbean and Middle America Regions from Focal Mechanisms and Seismicity. *Geological Society of America Bulletin* 80, 1639-1684.

Moriguti, T. & Nakamura, E. (1998) Across-arc variation of Li isotopes in lavas and implications for crust/mantle recycling at subduction zones. *Earth and Planetary Science Letters* 163, 167-174.

Morris, J.D., Leeman, W.P. & Tera, F. (1990) The subducted component in island arc lavas: constraints from B-Be isotopes and Be systematics. *Nature* 344, 6261, 31-36.

Morris, J.D., Gosse, J., Brachfeld, S. & Tera, F. (2002) Cosmogenic Be-10 and the solid Earth: studies in geomagnetism, subduction zone processes, and active tectonics. In: Beryllium Mineralogy, Petrology, and Geochemistry, *Reviews in Mineralogy and Geochemistry* 50, 207-270.

Otsuki, K. (1989) Empirical relationships among the convergence rate of plates, rollback rate of trench axis and island-arc tectonics: laws of convergence rate of plates. *Tectonophysics* 159, 1-2, 73-94.

Pearce, J.A., Ernewein, M., Bloomer, S. H., Parson, L. M., Murton, B. J. & Johnson, L.E. (1995) Geochemistry of Lau Basin volcanic rocks: Influence of ridge segmentation and arc proximity, in Volcanism Associated with Extension at Consuming Plate Margins. (ed J. L. Smellie) *Geological Society, London, Special Publications* 81, 53-75.

Pearce, J.A. & Stern, R.J. (2006) Origin of back-arc basin magmas: trace element and isotope perspectives, *Geophysical Monograph* 166, 63-86.

Penniston-Dorland, S.C., Sorensen, S.S., Ash, R.D., & Khadke, S.V. (2010) Lithium isotopes as a tracer of fluids in a subduction zone mélange: Franciscan Complex, CA. *Earth and Planetary Science Letters* 292(1), 181-190.

Penniston-Dorland, S.C., Bebout, G.E., Pogge von Strandmann, P.A., Elliott, T. & Sorensen, S.S. (2012) Lithium and its isotopes as tracers of subduction zone fluids and metasomatic processes: Evidence from the Catalina Schist, California, USA. *Geochimica et Cosmochimica Acta* 77, 530-545.

Plank, T. & Langmuir, C.H. (1998) The chemical composition of subducting sediment and its consequences for the crust and mantle. *Chemical Geology* 145, 325-394.

Plank, T. (2013) The Chemical Composition of Subducting Sediments. In: Holland H.D. and Turekian K.K. (eds.) *Treatise on Geochemistry*, Second Edition, vol. 4, 607-629.

Protti, M., Guendel, F. & McNally, K. (1995) Correlation between the age of the subducting Cocos Plate and the geometry of the Wadati-Benioff zone under Nicaragua and Costa Rica. *Special Paper, Geological Society of America* 295, 309-326.

Regelous, M., Collerson, K.D., Ewart, A. & Wendt, J.I. (1997) Trace element transport rates in subduction zones: evidence from Th, Sr and Pb isotope data for Tonga-Kermadec Arc lavas. *Earth and Planetary Science Letters* 150, 3-4, 291-302.

Regelous, M., Gamble, J.A. & Turner, S.P. (2010) Mechanism and timing of Pb transport from subducted oceanic crust and sediment to the mantle source of arc lavas. *Chemical Geology* 273, 1, 46-54.

Rudnick, R.L., Tomascak, P.B., Heather, B.N. & Gardner, L.R. (2004) Extreme lithium isotopic fractionation during continental weathering revealed in saprolites from South Carolina. *Chemical Geology* 212, 45-57.

Ryan, J.G. & Langmuir, C.H. (1987) The systematics of lithium abundance in young volcanic rocks. *Geochimica et Cosmochimica Acta* 51, 1727-1741.

Salters, V.J.M. & Stracke, A. (2004) Composition of the depleted mantle. *Geochemistry, Geophysics, Geosystems - G3*, 5, *Q05B07*.

Stalder, R., Foley, S.F., Brey, G.P., & Horn, I. (1998) Mineral-aqueous fluid partitioning of trace elements at 900–1200 C and 3.0–5.7 GPa: new experimental data for garnet, clinopyroxene, and rutile, and implications for mantle metasomatism. *Geochimica et Cosmochimica Acta, 62*(10), 1781-1801.

Stoffers, P., Worthington, T.J., Schwarz-Schampera, U., Hannington, M.D., Massoth, G.J., Hekinian, R., Schmidt, M., Lundsten, L.J., Evans, L.J., Vaiomo'unga, R. & Kerby, T. (2006), Submarine volcanoes and high-temperature hydrothermal venting on the Tonga arc, southwest Pacific, *Geology* 34, 453–456.

Sutherland, R. & Hollis, C. (2001) Cretaceous demise of the Moa plate and strike-slip motion at the Gondwana margin. *Geology* 29, 279-282.

Syracuse, E.M. & Abers, G.A. (2006) Global compilation of variations in slab depth beneath arc volcanoes and implications. *Geochemistry, Geophysics, Geosystems - G3*, 7, *Q05017*.

Tang, M., Rudnick, R.L., Chauvel, C. (2014) Sedimentary input to the source of Lesser Antilles lavas: A Li perspective. *Geochimica et Cosmochimica Acta* 144, 43-58.

Teng, F.Z., McDonough, W.F., Rudnick. R.L., Walker, R.J.& Sirbescu, M.L.C. (2006) Lithium isotopic systematics of granites and pegmatites from the Black Hills, South Dakota. *American Mineralogist* 91, 1488-1498.

Shihong, T., Zengqian, H., Aina, S., Kejun, H., Wenjie, H., Zhenzhen, L., Yue, Z., Yanguang, G., Yanhe, L., Dan, Y. and Zhusen, Y. (2012) Separation and Precise Measurement of Lithium Isotopes in Three Reference Materials Using Multi Collector-Inductively Coupled Plasma Mass Spectrometry. *Acta Geologica Sinica* 86: 1297–1305.

Tomascak, P.B., Ryan, J.G. & Defant, M.J. (2000) Lithium isotope evidence for light element decoupling in the Panama subarc mantle. *Geology* 28, 507-510.

Tomascak, P.B., Widom, E., Benton, L.D., Goldstein, S.L. & Ryan, J.G. (2002) The control of lithium budgets in island arcs. *Earth and Planetary Science Letters* 196, 227-238.

Tomascak, P.B., Langmuir, C.H., le Roux, P.J. & Shirey, S.B. (2008) Lithium isotopes in global mid-ocean ridge basalts. *Geochimica et Cosmochimica Acta* 72, 6, 1626-1637.

Turner, S. & Hawkesworth, C. (1997) Constraints on flux rates and mantle dynamics beneath island arcs from Tonga-Kermadec lava geochemistry. *Nature* 389, 568-573.

Turner, S., Hawkesworth, C., Rogers, N., Bartlett, J., Worthington, T., Hergt, J., Pearce, J. & Smith, I. (1997) ^{238}U-^{230}Th disequilibria, magma petrogenesis, and flux rates beneath the depleted Tonga-Kermadec island arc. *Geochimica et Cosmochimica Acta* 61, 22, 4855-4884.

Turner, S., Handler, M., Bindeman, I. & Suzuki, K. (2009) New insights into the origin of O-Hf-Os isotope signatures in arc lavas from Tonga-Kermadec. *Chemical Geology* 266, 3, 196-202.

Verney-Carron, A., Vigier, N., & Millot, R. (2011) Experimental determination of the role of diffusion on Li isotope fractionation during basaltic glass weathering. *Geochimica et Cosmochimica Acta*, *75*(12), 3452-3468.

Vils, F., Tonarini, S., Kalt, A. & Seitz, H.-M. (2009) Boron, lithium and strontium isotopes as tracers of seawater-serpentinite interaction at Mid-Atlantic ridge, ODP Leg 209. *Earth and Planetary Science Letters* 286, 414-425.

Wendt, J.I., Regelous, M., Collerson, K.D., & Ewart, A. (1997) Evidence for a contribution from two mantle plumes to island-arc lavas from northern Tonga. *Geology*, *25*(7), 611-614.

Wright, I.C., Worthington, T.J. & Gamble, J.A. (2006) New multibeam mapping and geochemistry of the 30–35 S sector, and overview, of southern Kermadec arc volcanism. *Journal of Volcanology and Geothermal Research* 149, 263-296.

Wunder, B., Meixner, A., Romer, R.L. & Heinrich, W. (2006) Temperature-dependent isotopic fractionation of lithium between clinopyroxene and high-pressure fluids. *Contributions to Mineralogy and Petrology* 151, 112-120.

You, C.F., Castillo, P.R., Gieskes, J.M., Chan, L.H. & Spivac A.J. (1996) Trace element behavior in hydrothermal experiments: Implications for fluid processes at shallow depths in subduction zones. *Earth and Planetary Science Letters* 140, 41-52.

Zack, T., Tomascak, P.B., Rudnick, R.L., Dalpé, C. & McDonough, W.F. (2003) Extremely light Li in orogenic eclogites: the role of isotope fractionation during dehydration in subducted oceanic crust. *Earth and Planetary Science Letters* 208, 279-290.

3 Volatile Contents Reveal Mid-Ocean Basalt Tapping an Ocean Island Magma Source

Abstract

The North Fiji Basin (NFB) and the connected Lau Basin are located in a complex area of volcanism. The NFB is a back-arc basin (BAB) that is a result of an extinct subduction zone, which incorporates the complicated geodynamics of two rotating landmasses: Fiji and Vanuatu island arc. Collectively this makes the spreading centers of the NFB the highest producing spreading centers on record. Here we present volatile concentrations, and major and trace element data for a triple junction spreading center in the NFB to show their unique relative enrichment in water when compared to other mid-ocean ridge basalts (MORB) around the world. The samples from the NFB exhibit a combination of major MORB-like chemical signatures along with high water content similar to ocean island basalts (OIB). This observation in geochemistry is unlike any other studied MORB or back-arc basin because it is not attributed to a subduction-

related signature. Our results employ volatile elements (carbon dioxide and water) and their constraints, both combined with trace element ratios to indicate a potential wet plume source for the observed enrichment in the North Fiji Basin.

3.1 Introduction

Volatile elements play a fundamental role in magmatic processes including, but not limited to, melting (Asimow & Langmuir, 2003), fractional crystallization (Huppert et al., 1982), and degassing (Métrich & Wallace, 2008). Volatile elements are incompatible elements that prefer to partition into the liquid when melting occurs. They differ from standard lithophile elements as they prefer to be in the vapor phase and are dependent on pressure to remain in a dissolved state. Lithophile elements, in contrast, have traditionally been used to compare the fertility of a melt within mid-ocean ridges establishing certain elemental affinities (e.g. LREE/HREE ratios) for deeper mantle signatures (e.g. plumes) (Weaver, 1991; Halliday et al., 1995). Several studies have improved our ability to constrain the volatile content of the mantle (Hirth & Kohlstedt, 1996; Saal et al., 2002; Eiler, 2003). However, there is still work to be done to fully characterize and understand the reservoirs that occupy the upper mantle.

Lavas from the Samoan volcanoes span a broad range in H_2O (0.63–1.50 wt.%) and CO_2 (6–233 ppm) contents. The water contents of Samoan lavas exceed the range of MORB (<0.7 wt.%) but do not exceed arc lavas (<8 wt.%) (e.g. Grove et al., 2002). OIB water content is comparable to back-arc basin lavas (Newman et al., 2000). However, other geochemical characteristics differentiate OIBs, particularly in Samoa, to the depleted mantle MORB (DMM) found at back-arc basins. These include highly radiogenic $^{87}Sr/^{86}Sr$ (up to 0.789), low $^{143}Nd/^{144}Nd$ (down to 0.5125), and lavas highly enriched with trace element (Wright & White, 1987; Farley et al., 1992). This distinct

geochemical signature in the Samoan OIB makes up what is commonly known as 'Enriched Mantle 2' (EM2). The origin of EM2 was initially interpreted as subducted oceanic crust and terrigenous sediment that was recycled into the mantle (Weaver, 1991). More recently, Workman et al. (2004) modified the interpretation by highlighting the incorrect Pb isotope compositions, smooth trace element patterns, and low $^{187}Os/^{188}Os$, high $^{3}He/^{4}He$ (>8 Ra), to buttress their hypothesis of an ancient (2.5 Ga) metasomatized oceanic lithosphere subducting and being stored in the deep mantle before recycling into the Samoan plume.

It is well documented that the Samoan plume has infiltrated into the Lau Basin through an opening in the Pacific plate that originates at the northern termination of the Tonga-Kermadec arc (e.g. Giardini & Woodhouse, 1986; Volpe et al., 1988; Turner & Hawkesworth, 1998; Price et al., 2014). Evidence from lavas in the Lau Basin exhibit elevated helium and strontium isotopes and decreased neodymium isotopic data; these findings have been used to suggest the presence of OIB material within the Lau Basin (Macpherson et al., 1998; Shaw et al., 2004). However, as noted by Turner and Hawkesworth (1998), it does not affect the arc front lavas. Slightly further westward (~1,000 km), in the North Fiji Basin, a lack of abundant data limits our ability to trace how far the Samoan plume extends into the North Fiji Basin. Price et al. (2014) employ the use of Sr, Nd, and Pb isotopic compositions to illustrate the extent to which the Samoan plume extends south-west into the neighboring Lau and North Fiji basins. They argue that toroidal flow around the Tonga slab that is a result of rapid rollback leads to advected plume material beneath both basins. However, it is uncertain how far south the plume material extends.

Here we reveal upper mantle heterogeneities in the North Fiji Basin (NFB); these unusual magmas are volatile-rich and have an ocean island basalt (OIB) signature within a back-arc setting. We report an in-depth geochemical study of the Northeast Fiji

Triple Junction (NEFTJ), by using a combination of geochemical data: volatile element concentrations, major and trace element concentrations, and isotope signatures. The new data suggest that the presence of the Samoan plume spans over 1400 km, to at least as far as the Northeast Fiji Triple Junction, in the North Fiji Basin.

3.2 Geological background and sample description

3.2.1 Geologic Setting

The North Fiji Basin (NFB) is surrounded by the former Vitiaz subduction zone to the north and the New Hebrides Trench to the south and extends into the Hunter Fracture Zone. The NFB is a triangular depression that has resulted from two stages: 1) the clockwise rotation of the Vanuatu island arc and the counter-clockwise rotation of Fiji, which belongs to the remnant Lau-Colville Ridge, and 2) a synchronized opening of the Lau Basin (Gill & Gorton, 1975; Falvey, 1978; James & Falvey, 1978; Malahoff et al., 1982b; Huchon et al., 1994; Musgrave & Firth, 1999; Hall, 2002). The Vanuatu island arc and Fiji began rotating between 5.5–9 Ma (Gill & Gorton, 1975) while Malahoff et al. (1982a) constrain it to have commenced between 7–8 Ma. Within this dynamic tectonic setting, there has been complex magmatism with varying geochemical signatures.

The NFB has not been as thoroughly geochemically fingerprinted as the neighboring Lau Basin. However, three distinctive sources have previously been identified and studied in the NFB: 1) Back-arc basin basalt (BABB; defined by Sinton & Fryer, 1987) magma type that is enriched in incompatible elements (K, Rb, Zr, Ba), relative to N-MORB, 2) Highly depleted N-MORB lavas that have evolved by crystal fractionation involving principally olivine and plagioclase, which samples are believed to be from the old North Fiji Basin crust (Price et al., 1990), and 3) Transitional basalts,

towards E-MORB, that are alkali and incompatible element enriched, relative to N-MORB (Sinton et al., 1994; Eissen et al., 1994). The above magma types are chronologically ordered (oldest – youngest), and as such record the history of the basin. The history of the NFB mirrors that of the Lau Basin, which begins as BABB magma, where the subducting slab fingerprints onto the magmas. The magma type then changes to a depleted MORB-type, and in the case of the North Fiji and Lau Basins, evolves to a transitional magma that is affected by diverse mantle sources. In addition, any analyses of volatile elements that have been carried out in the NFB have reported <1.5 wt.% H_2O in the South Pandora Ridge, in the northern part of the NFB, waning to <0.2 wt.% H_2O in the lavas to the center of the NFB, nearest to the Northeast Fiji Triple Junction (Aggrey et al., 1988). Previous studies of the lavas closest to the NEFTJ have been characterized as N-MORB, on H_2O and trace elements (Aggrey et al., 1988; Sinton et al., 1994).

Samples from the NFB that have been extensively analyzed for major and trace elements and isotopic compositions show that the NFB lavas (particularly in the South Pandora Ridge) have high $^{87}Sr/^{86}Sr$ (up to 0.7037), low $^{143}Nd/^{144}Nd$ (down to 0.51283), and $^{176}Hf/^{177}Hf$ (down to 0.28303) relative to MORB (Sinton et al., 1994; Price et al., 2014). Additionally, trace element ratios (Ba/Sm, Nb/Zr, La_N/Sm_N, La_N/Lu_N) as a function of $^{143}Nd/^{144}Nd$ highlight how the South Pandora Ridge in the NFB plot near or in the field for Samoan lavas. However, the two samples analyzed closest to our field of study for this paper show no such correlations in the above trace element ratios. The only relationship that is observed by Price et al. (2014), for the sample nearest to the Northeast Fiji Triple Junction, in a Ba/Nb ratio as a function of $^{87}Sr/^{86}Sr$ figure, whereby it plots in the space between MORB and Samoan lavas.

3.2.2 Previous studies of the North Fiji Basin and nearby Lau Basin

Lavas erupted in back-arc basins globally are characterized by having geochemically depleted signatures (e.g. McCulloch & Gamble, 1991; Langmuir et al., 2006; Pearce & Stern, 2006). However, the Lau Basin is unusual in that it samples several isotopically distinct hotspot components. First, the Samoan hotspot has been credited with influencing the geochemistry of Lau Basin lavas, where distinctive high-$^{87}Sr/^{86}Sr$ and high-$^{3}He/^{4}He$ signatures—associated with the Samoan plume—have been identified in the Rochambeau Rifts in the northern Lau Basin (e.g., Lytle et al., 2012; Lupton et al., 2009; Poreda & Craig, 1992) (Fig. 4.1). The Samoan hotspot track, constructed on the >100 Ma Pacific lithosphere, extends west of the Samoan hotspot (Fig. 4.1). The hotspot track runs parallel to (and slightly north of) the Vitiaz Lineament, a bathymetric low that defines the boundary between the old, thick Pacific lithosphere and the young, thin lithosphere of the Lau and North Fiji Basins. Price et al. (2014) suggest that there is a keel of under-plated Samoan plume residue, attached to the base of the lithosphere, present along the length of the Samoan hotspot, including the portion of the hotspot that lies north of the Lau and North Fiji Basins. Price et al. (2014) argued that rollback of the subducting Pacific Plate, from 4 Ma to the present, has induced a long-lived toroidal flow field around the northern edge of the subducting Tonga slab: under-plated Samoan plume material is entrained in the toroidal flow field and advected southward into the Lau and North Fiji Basins (Price et al., 2014), thus explaining the Samoan plume signatures—including high $^{3}He/^{4}He$ and enriched $^{87}Sr/^{86}Sr$—in the Lau and North Fiji Basins up to 1400 km west of the Samoan hotspot.

3.2.3 Sample Description

The lavas analyzed in this study were collected from the 2012 Northern Lau Transit Expedition of the R/V Southern Surveyor (cruise name: ss2012_v02). The locations of the samples are indicated in Figure 3.1 and expressed in Table 3.1. Fifteen basaltic submarine dredges were collected on the expeditions. The samples are divided into three regions: Caldera, S arm, and NE arm. The samples used in this study consist of very fresh, unaltered glass, suggesting that they are very young (Johnson & Sinton, 1990).

Table 3.1 Sample information and chemical data for the lavas in this study. NLTD: (39 to 50) are 'Fiji-Caldera' samples, (44 to 46) are 'S. arm' samples, (38 & 48) are 'NE arm' samples. There is a 1σ uncertainty for volatile concentrations.

Sample	NLTD-39-5	NLTD-40-1	NLTD-41-8	NLTD-42-1	NLTD-43-1	NLTD-49-1	NLTD-50-1	NLTD-50-2	NLTD-50-3	NLTD-44-1	NLTD-45-1	NLTD-45-2	NLTD-46-1	NLTD-47-1	NLTD-47-2	NLTD-47-3	NLTD-47-4	NLTD-47-5	NLTD-48-1
Latitude	-16.94	-17.31	-16.95	-16.98	-16.98	-16.95	-16.96	-16.96	-16.96	-17.31	-17.19	-17.19	-17.07	-16.85	-16.85	-16.85	-16.85	-16.85	-16.88
Longitude	173.93	173.80	173.92	173.92	173.91	173.92	173.94	173.94	173.94	173.80	173.85	173.85	173.89	173.96	173.96	173.96	173.96	173.96	173.92
Depth min (m)	2010	2010	1980	1942	1937	1988	1890	1890	1890	2645	2455	2455	2210	2325	2325	2325	2325	2325	2141
Depth max (m)	2029	2031	2001	1969	1985	1998	2010	2010	2010	2689	2459	2459	2220	2431	2431	2431	2431	2431	2209
Major elements (wt %)																			
SiO_2	50.0	47.7	49.3	50.1	50.2	50.0	50.3	49.6	49.6	50.1	48.6	50.4	50.1	50.4	50.1	50.4	50.5	50.7	49.0
TiO_2	1.2	2.3	2.8	2.2	1.2	1.4	1.3	1.7	1.7	1.5	1.9	1.0	1.5	1.6	1.6	1.4	1.6	1.5	2.1
Al_2O_3	15.2	18.0	15.8	15.7	14.9	15.3	15.4	16.0	16.1	15.0	17.6	15.1	15.2	14.7	14.7	14.8	14.7	14.7	17.7
FeO	9.3	7.7	9.0	9.0	9.7	9.8	9.4	8.7	8.7	10.4	8.1	9.7	10.3	10.6	10.5	10.3	10.5	10.4	7.3
MnO	0.17	0.14	0.18	0.17	0.18	0.16	0.17	0.17	0.16	0.19	0.13	0.18	0.18	0.20	0.20	0.16	0.21	0.21	0.14
MgO	8.0	7.6	5.9	6.3	7.9	7.8	8.1	7.9	8.0	7.4	7.6	8.0	7.7	7.2	7.2	7.2	7.2	7.2	7.4
CaO	12.2	10.6	10.2	11.1	12.6	12.3	12.4	11.7	11.7	12.1	11.2	13.1	12.0	12.1	12.1	12.1	12.2	12.1	11.0
Na_2O	2.7	3.2	3.6	3.4	2.7	2.9	2.7	2.8	2.8	2.7	2.9	2.5	2.7	3.0	2.9	3.0	3.0	3.0	3.2
K_2O	0.22	0.87	1.13	0.80	0.09	0.11	0.12	0.44	0.45	0.14	0.69	0.08	0.12	0.14	0.13	0.13	0.14	0.14	0.91
P_2O_5	0.15	0.42	0.49	0.39	0.11	0.13	0.10	0.23	0.24	0.13	0.31	0.08	0.14	0.14	0.13	0.13	0.15	0.14	0.43
Total	99.2	98.5	98.3	99.1	99.6	99.8	100.2	99.3	99.4	99.7	99.1	100.1	100.0	100.1	99.6	99.7	100.1	99.9	99.2
Mg#	60.3	64.0	53.7	55.6	59.1	58.5	60.6	61.9	62.3	56.1	62.6	59.7	57.1	54.7	55.2	55.5	54.8	55.3	64.3
Trace elements (ppm)																			
Li	4.8	4.7	6.2	5.6	5.4	4.7	5.0	5.0	5.1	4.9	5.1	5.1	5.2	5.7	5.3	6.0	5.2	5.7	4.6
Be	0.4	1.0	1.4	1.1	0.3	0.5	0.3	0.7	0.6	0.4	0.9	0.3	0.5	0.5	0.5	0.5	0.5	0.5	1.1
Na (BCR)	2.9	3.4	3.7	3.5	2.9	3.0	2.8	2.9	2.9	2.8	3.1	2.6	2.8	3.1	3.1	3.0	3.1	3.1	3.3
Na	2.7	3.2	3.6	3.4	2.7	2.9	2.7	2.9	2.8	2.7	3.0	2.5	2.8	3.0	3.0	3.0	3.0	3.1	3.2
Mg (BCR)	8.1	7.8	6.0	6.4	8.1	8.1	8.2	8.1	8.2	7.5	7.8	8.2	7.8	7.2	7.3	7.2	7.3	7.2	7.5
Mg	7.7	7.3	5.7	6.2	7.6	7.9	8.1	8.1	8.1	7.1	7.4	7.9	7.7	7.1	7.1	7.1	7.1	7.2	7.2
Al (612)	14.3	17.0	14.7	14.6	13.9	14.9	15.2	15.9	15.6	13.9	16.5	14.4	14.8	14.3	14.2	14.3	14.2	14.3	16.7
Al (BCR)	15.2	18.5	15.8	15.7	15.2	15.2	15.3	15.9	15.7	15.0	17.2	14.9	14.9	14.5	14.6	14.4	14.5	14.4	17.3
P	596.7	1780.6	2148.1	1702.7	430.3	531.7	471.0	956.7	949.9	589.6	1363.3	357.1	609.9	600.1	590.0	593.2	598.4	603.2	1807.2
P (BCR)	617.9	1857.3	2192.9	1717.6	445.6	545.3	480.4	965.4	969.3	603.0	1442.4	369.6	614.7	608.8	611.5	599.1	611.2	605.7	1882.2
K (BCR)	1848.0	7745.7	9774.9	6777.4	827.1	938.4	975.4	3823.3	3758.0	1217.2	5975.4	736.2	919.4	1139.6	1144.4	1132.6	1156.7	1150.2	7896.9
Ca	11.9	10.3	9.9	10.9	12.3	12.4	12.4	11.6	11.6	11.9	11.1	13.0	12.1	12.1	12.0	12.2	12.1	12.1	10.8
Ca (BCR)	12.2	10.6	10.2	11.1	12.6	12.3	12.4	11.7	11.7	12.1	11.2	13.1	12.0	12.1	12.1	12.1	12.2	12.1	11.0
Sc	40.7	25.3	34.0	37.6	43.1	44.5	43.7	38.8	37.3	41.9	30.9	44.8	43.9	45.8	45.1	45.3	45.4	45.8	30.5
Ti	7446.1	12950.8	15322.0	12491.5	6582.9	8029.9	7277.6	9666.3	9554.2	8663.3	11195.4	6168.3	8901.9	8624.7	8568.7	8718.0	8586.2	8607.0	11701.3
V	270.6	211.5	294.4	289.7	273.1	287.4	278.7	262.5	259.4	311.6	234.6	276.6	315.3	311.2	309.5	311.3	312.1	314.8	221.3
Cr	235.2	167.3	88.9	110.5	160.2	324.7	301.5	310.4	310.4	309.9	232.8	327.7	283.8	137.1	140.8	137.8	142.2	145.0	227.3
Mn	1388.0	1056.6	1321.3	1345.9	1444.6	1498.3	1424.7	1313.8	1292.6	1526.3	1159.3	1448.2	1542.6	1576.2	1561.4	1566.9	1566.6	1579.1	1086.4
Mn (BCR)	1459.2	1118.3	1368.2	1377.6	1522.1	1510.3	1435.6	1313.1	1300.9	1585.5	1214.9	1489.3	1559.9	1596.5	1618.9	1594.5	1611.9	1603.3	1125.2
Co	44.7	36.9	34.6	37.0	46.6	46.2	45.8	42.6	42.4	44.4	38.3	46.4	46.7	46.3	45.7	46.0	46.4	46.5	35.8
Ni	74.4	127.8	33.6	45.5	49.7	76.1	77.4	96.8	97.5	65.7	108.0	58.7	67.9	48.3	47.5	47.4	48.8	47.9	98.7
Cu	90.3	47.7	57.5	72.4	102.6	99.5	93.8	80.3	81.2	90.9	64.2	115.7	88.3	102.4	102.7	103.9	103.3	104.6	68.7

Sample	NLTD-39-5	NLTD-40-1	NLTD-41-8	NLTD-42-1	NLTD-43-1	NLTD-49-1	NLTD-50-1	NLTD-50-2	NLTD-50-3	NLTD-44-1	NLTD-45-1	NLTD-45-2	NLTD-46-1	NLTD-47-1	NLTD-47-2	NLTD-47-3	NLTD-47-4	NLTD-47-5	NLTD-48-1
Zn	95.1	84.7	100.9	96.4	94.2	95.4	92.2	90.1	88.7	108.1	83.0	92.0	107.3	104.7	101.5	104.5	102.7	105.3	74.6
Ga	16.8	19.8	20.3	19.1	16.5	17.5	17.1	17.9	17.7	17.8	18.8	16.7	17.8	17.9	17.8	18.1	18.3	18.1	19.0
As	0.2	0.5	0.7	0.5	0.1	0.1	0.2	0.3	0.3	0.2	0.4	0.1	0.2	0.1	0.2	0.1	0.2	0.2	0.6
Se	0.3	0.3	0.4	0.4	0.3	0.3	0.3	0.3	0.3	0.3	0.3	0.3	0.4	0.3	0.3	0.4	0.4	0.3	0.3
Rb	4.6	21.3	28.5	20.5	1.7	2.0	2.3	10.5	10.0	2.7	16.9	1.6	1.9	2.4	2.3	2.4	2.4	2.5	24.0
Sr	130.7	348.2	273.7	218.2	107.3	125.3	125.2	224.2	218.3	116.8	277.2	94.3	122.4	129.9	129.1	128.9	129.8	130.6	271.1
Y	23.2	22.3	30.4	29.7	22.9	26.9	25.0	25.5	24.2	28.8	22.7	23.5	32.2	29.2	28.9	29.2	28.9	29.4	24.1
Zr	71.4	154.0	195.1	162.0	59.0	77.1	65.0	106.8	106.4	85.9	128.5	55.3	92.6	85.1	84.7	86.0	84.1	85.4	160.9
Nb	6.1	31.6	39.8	27.7	2.3	2.6	3.0	13.2	12.6	3.5	24.4	2.2	2.7	3.4	3.4	3.5	3.5	3.4	32.4
Mo	0.38	1.53	1.96	1.43	0.22	0.25	0.25	0.72	0.72	0.30	1.18	0.21	0.27	0.31	0.30	0.30	0.30	0.31	1.67
Ag	0.03	0.02	0.02	0.02	0.03	0.03	0.03	0.02	0.03	0.03	0.02	0.04	0.03	0.03	0.03	0.03	0.03	0.03	0.02
Cd	0.14	0.13	0.17	0.16	0.15	0.15	0.14	0.13	0.13	0.16	0.13	0.15	0.15	0.17	0.16	0.16	0.16	0.17	0.13
In	0.07	0.07	0.08	0.08	0.07	0.07	0.07	0.07	0.07	0.08	0.07	0.07	0.08	0.08	0.08	0.08	0.08	0.08	0.06
Sn	1.6	2.4	2.7	2.4	1.4	1.6	1.5	1.9	2.0	1.8	2.2	1.5	1.9	1.9	1.9	1.8	1.8	1.8	2.4
Sb	0.02	0.05	0.06	0.05	0.01	0.02	0.02	0.03	0.03	0.01	0.04	0.01	0.01	0.01	0.01	0.01	0.01	0.01	0.05
Cs	0.05	0.22	0.31	0.23	0.02	0.02	0.03	0.10	0.11	0.03	0.18	0.02	0.02	0.03	0.03	0.02	0.03	0.02	0.26
Ba	49.9	246.0	297.9	207.4	19.0	20.1	24.5	109.8	105.1	27.0	195.7	17.4	19.0	25.8	25.3	25.7	26.0	25.9	245.2
La	4.6	19.0	23.8	17.3	2.5	3.1	3.1	9.3	8.9	3.6	15.1	2.4	3.5	3.7	3.7	3.7	3.7	3.7	19.7
Ce	11.6	39.4	48.9	36.3	7.5	9.2	8.5	20.7	20.3	10.7	31.8	6.9	10.7	10.7	10.5	10.8	10.7	10.7	40.0
Pr	1.7	4.9	6.1	4.6	1.2	1.5	1.4	3.0	2.8	1.7	4.0	1.1	1.8	1.7	1.7	1.7	1.7	1.8	4.9
Nd	8.5	21.5	26.5	20.2	6.7	8.6	7.9	14.0	13.5	9.3	17.7	6.4	10.1	9.5	9.5	9.5	9.4	9.4	21.4
Sm	2.8	5.3	6.5	5.3	2.5	3.1	2.7	3.8	3.8	3.3	4.6	2.4	3.5	3.3	3.3	3.4	3.3	3.3	5.1
Eu	1.1	1.8	2.2	1.8	1.0	1.2	1.1	1.5	1.4	1.2	1.6	0.9	1.3	1.3	1.3	1.3	1.3	1.3	1.8
Gd	3.6	5.2	6.5	5.8	3.3	4.2	3.7	4.1	4.4	4.4	4.7	3.2	4.5	4.2	4.4	4.4	4.1	4.2	4.9
Tb	0.6	0.8	1.0	0.9	0.6	0.7	0.7	0.8	0.7	0.8	0.7	0.6	0.8	0.8	0.8	0.8	0.8	0.8	0.8
Dy	4.0	4.4	5.9	5.6	4.0	4.8	4.4	4.7	4.5	5.0	4.5	4.0	5.7	5.3	5.1	5.1	5.1	5.3	4.7
Ho	0.9	0.8	1.2	1.1	0.9	1.0	1.0	1.0	0.9	1.1	0.9	0.9	1.2	1.1	1.1	1.1	1.1	1.1	0.9
Er	2.6	2.2	3.2	3.1	2.6	3.0	2.8	2.7	2.7	3.2	2.4	2.6	3.5	3.3	3.3	3.3	3.2	3.2	2.5
Tm	0.4	0.3	0.4	0.4	0.4	0.4	0.4	0.4	0.4	0.5	0.3	0.4	0.5	0.5	0.5	0.5	0.4	0.5	0.3
Yb	2.5	2.0	2.9	3.1	2.5	3.0	2.7	2.5	2.4	3.3	2.2	2.7	3.4	3.2	3.1	3.2	3.1	3.1	2.3
Lu	0.4	0.3	0.4	0.4	0.4	0.4	0.4	0.4	0.3	0.5	0.3	0.4	0.5	0.5	0.5	0.5	0.5	0.5	0.3
Hf	1.8	3.6	4.8	3.9	1.7	2.1	1.9	2.9	2.8	2.3	3.1	1.6	2.5	2.4	2.3	2.3	2.4	2.3	3.8
Ta	0.3	1.7	2.2	1.5	0.1	0.2	0.2	0.8	0.7	0.2	1.3	0.1	0.2	0.2	0.2	0.2	0.2	0.2	1.8
W	0.09	0.45	0.58	0.41	0.03	0.03	0.04	0.17	0.16	0.04	0.35	0.03	0.03	0.04	0.04	0.04	0.04	0.04	0.50
Re	0.0010	0.0005	0.0009	0.0010	0.0006	0.0010	0.0007	0.0008	0.0009	0.0015	0.0003	0.0010	0.0011	0.0009	0.0009	0.0010	0.0021	0.0007	0.0005
Pt	0.0004	0.0002	0.0006	0.0010	0.0003	0.0003	0.0006	0.0005		0.0005	0.0004	0.0001	0.0003	0.0005	0.0004	0.0004	0.0007	0.0003	0.0007
Au	0.0005	0.0009	0.0019	0.0016				0.0005	0.0007	0.0005	0.0007	0.0003	0.0008	0.0007	0.0005	0.0012	0.0004	0.0007	0.0018
Tl	0.011	0.027	0.040	0.030	0.008	0.008	0.009	0.017	0.018	0.011	0.026	0.008	0.013	0.013	0.012	0.012	0.013	0.015	0.035
Pb	0.6	1.5	1.8	1.4	0.4	0.5	0.4	0.9	0.9	0.5	1.2	0.4	0.5	0.5	0.5	0.5	0.6	0.5	1.5
Bi	0.0080	0.0086	0.0098	0.0084	0.0089	0.0066	0.0079	0.0086	0.0081	0.0088	0.0072	0.0087	0.0081	0.0093	0.0086	0.0085	0.0082	0.0082	0.0088
Th	0.5	2.5	3.3	2.3	0.2	0.2	0.2	1.1	1.0	0.3	1.9	0.2	0.2	0.3	0.3	0.3	0.3	0.3	2.7
U	0.12	0.59	0.81	0.57	0.05	0.06	0.06	0.26	0.26	0.07	0.48	0.05	0.06	0.07	0.08	0.08	0.08	0.08	0.69

Sample	NLTD-39-5	NLTD-40-1	NLTD-41-8	NLTD-42-1	NLTD-43-1	NLTD-49-1	NLTD-50-1	NLTD-50-2	NLTD-50-3	NLTD-44-1	NLTD-45-1	NLTD-45-2	NLTD-46-1	NLTD-47-1	NLTD-47-2	NLTD-47-3	NLTD-47-4	NLTD-47-5	NLTD-48-1
/olatile elements																			
H_2O [wt %]	0.25	0.84	0.96	0.76	0.18	0.23	0.19	0.48	0.48	0.25	0.67	0.16	0.25						0.74
+/-	0.00	0.00	0.00	0.00	0.00	0.00	0.00	0.00	0.00	0.00	0.00	0.00	0.00						0.00
CO_2 [ppm]	265.2	125.9	165.8	181.3	318.1	200.3	163.3	359.8	391.2	140.8	94.7	113.1	226.1						80.4
+/-	2.2	0.6	1.1	1.3	1.3	0.8	0.9	2.3	1.1	1.1	0.6	0.6	0.9						0.6
F [ppm]	165.4	523.8	625.4	444.2	118.1	145.4	135.1	294.8	295.8	167.6	427.6	107.0	167.6						471.8
+/-	0.6	1.6	1.7	1.9	0.3	0.6	0.6	0.9	1.2	0.3	1.8	0.5	0.7						1.9
P [ppm]	612.4	1910.5	2301.4	1802.8	433.7	545.7	477.2	1020.2	1014.6	602.2	1497.2	357.8	616.7						1959.6
+/-	1.9	4.3	4.3	2.8	1.0	1.0	1.4	2.6	2.3	1.0	3.1	1.7	1.2						3.0
S [ppm]	1088.1	826.6	1102.9	1119.3	1162.8	1203.2	1109.1	1033.9	1046.1	1264.3	940.0	1159.4	1283.6						819.8
+/-	3.0	2.6	3.5	6.9	2.4	3.6	3.2	2.9	4.2	4.6	2.5	4.9	4.8						2.4
Cl [ppm]	54.3	258.3	321.9	298.2	51.4	129.6	43.5	116.5	101.7	42.8	206.3	71.0	135.1						280.4
+/-	0.1	0.8	0.9	1.1	0.2	0.8	0.3	0.4	0.6	0.2	1.3	0.4	0.7						1.4
$^{87}Sr/^{86}Sr$	0.7031			0.7036	0.7029	0.7029	0.7030	0.7035	0.7035	0.7030	0.7036	0.7029	0.7028		0.7029	0.7029			0.7037
$^{143}Nd/^{144}Nd$	0.5130	0.5129	0.5129	0.5129	0.5131	0.5131	0.5132	0.5130	0.5130	0.5132	0.5129	0.5131	0.5131		0.5131	0.5131			0.5129

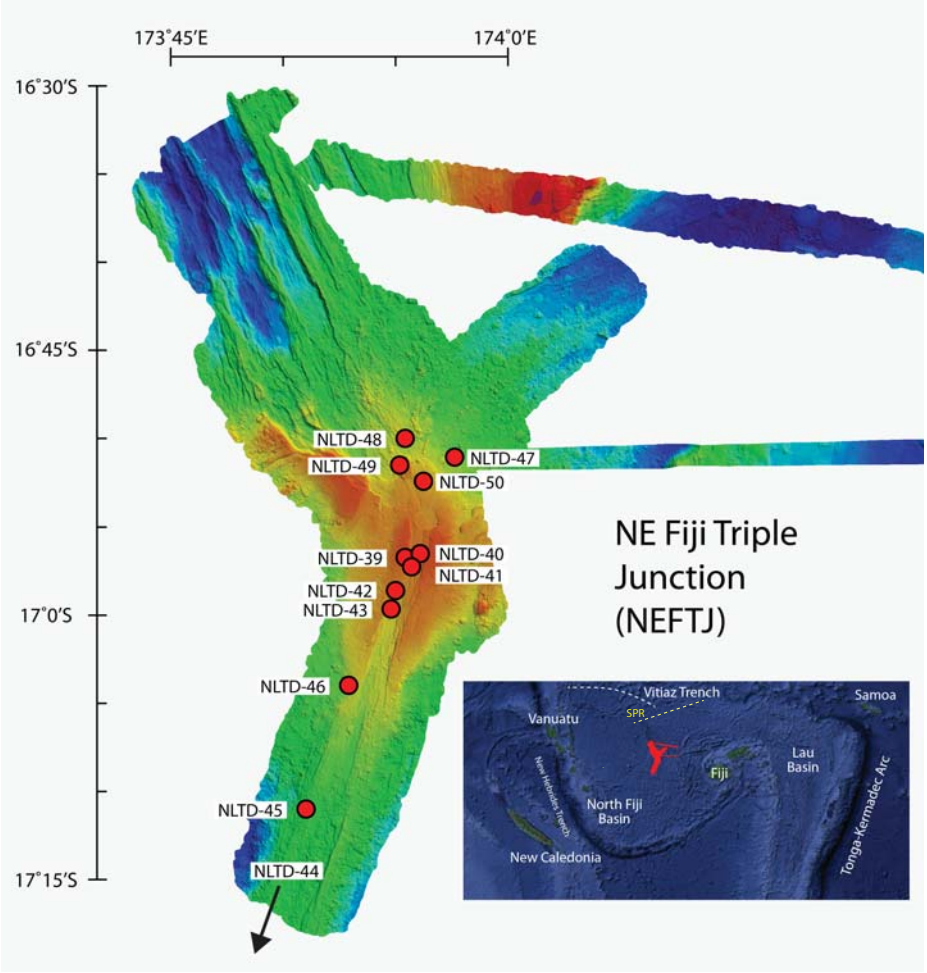

Figure 3.1 Bathymetric map for the NEFTJ, indicating sample locations with a map (inset) showing the major tectonic features of the North Fiji Basin and Lau Basin. The white dotted line in the inset map shows the approximate location of the extinct Vitiaz arc and the yellow dotted line shows the location of the South Pandora Ridge (SPR), both are located to the north of the NEFTJ (red). The seafloor bathymetry was mapped with a multibeam echo sounder Kongsberg Simrad EM300 that sends 30 kHz frequency signals beneath the vessel. These signals produce a fan arc of 135 beams with a 1° by 1° range. The colors represented in the bathymetric map are indicative of depth. Depth ranges from ~2700 m (blue) to ~1800 m (red). The red dots show the samples for this study, with one further sample to the south located off the map.

3.2.3.1 Dredges in the Caldera

Nine samples from seven different dredge locations were recovered around the caldera of the NE Fiji Triple Junction. Dredge 39 sampled a mound in the caldera

yielding fresh glassy pillow basalts except for one larger pillow fragment that contained low to moderate brown alteration. The basalts contain large (1–3 mm) phenocrysts of plagioclase and olivine. Similarly, Dredge 40 sampled a deeper mound nearby. The yield included hydrothermal breccias covered in Fe-oxyhydroxides and aphyric basalts with moderate to high alteration in which the glasses graduated in colors, from black to brown. Dredges 41–43 were sampled from an area named 'Clapham Junction' located in the southern part of the caldera. While Dredge 41 samples a lava field, 42 and 43 sampled the central ridge within the rift to the south of the caldera rim. Dredges 41 and 42 were similar in yield, containing glassy aphyric pillow basalts with thickly chilled margins and low to moderate alteration. Dredge 43 appears slightly more evolved than glasses from the same area, containing plagioclase-phyric (<5 mm) glassy pillow basalts. Dredges 49 and 50 sampled from the western floor and southeastern wall of the caldera. Dredge 49 contained aphyric glassy basalt and Dredge 50 returned a large quantity of glass that contained low to no weathering and minimal olivine phenocrysts (3 mm).

3.2.3.2 Dredges in the S arm

The S arm region of the NE Fiji Triple junction contains three of the dredge sites analyzed in this study. Dredge 44 was made on lava plain in the southern section of the south arm. This dredge was the furthest south we sampled in the NEFTJ. The rock types in this dredge varied from weathered aphyric lava to strongly plagioclase-phyric (<10mm) glassy pillow basalts with atypical olivine phenocrysts. There was light to moderate Fe-alteration within the rocks and minimal Mn cover. Dredge 45 sampled from the lava plain in the middle of the South arm containing plagioclase-olivine-phyric glassy pillow basalts. There was low to moderate weathering with the glassy rind having a dull luster. Several of the rocks collected in this dredge appeared to be more

primitive than the plagioclase-rich ones. We have analyzed both in this study. Dredge 46, located in the northern section of the S arm, samples a ridge. The rocks are low to moderately altered pillow basalts.

3.2.3.3 Dredges in the NE arm

Samples were recovered from two dredge locations in the NE arm. Dredge 47 was made on the ridge in the southern section of the northeast arm. The yield was low containing minimal pillow glass fragments with 1-mm Mn crust. We analyzed five samples from the glass fragments recovered in Dredge 47. Dredge 48 was made from an N-S striking ridge in the southern section of the northeast arm. The yield was composed of pillow basalts with low to moderately altered glass rinds and containing plagioclase (1–2 mm) and olivine phenocrysts.

3.3 Analytical techniques

We measured the volatile content of 15 samples from deeply (~1,900m to 3,000m) erupted pillow basalts in the North Fiji Basin (see Fig. 3.1). Multiple quenched fresh glass chips from the rims of each sample were hand-picked to remove any visible alteration products. Larger pieces were put through a hydraulic press, crushed to a smaller mountable size and hand-picked. Several glass chips were mounted in an epoxy disc for geochemical analysis.

3.3.1 Major element analyses

Following sample mounting, the bulk compositional data and high-resolution backscattered electron (BSE) images for polished sections were obtained using the FEI NOVA NanoSEM 600 scanning electron microscope (SEM), which employs a field emission electron source, at the Smithsonian Institution. The SEM operated at 15 keV

with a sample current of 2-3nA. The SEM is equipped with a Thermo-Noran energy dispersive X-ray analytical system, and data are stored and processed using Thermo-Scientific Noran System Six software. The System Six software allows for full-spectrum imaging, in which complete energy-dispersive spectrum is collected and stored for each pixel within a map. The bulk composition of each frame (corrected for overlap) was determined by summing the compositions for all pixels, summing the frame compositions, and normalizing the totals to 100%. The software allows extraction of data from irregularly shaped areas so that unwanted pixels (e.g., epoxy and cracks) can be eliminated. Spectra were quantified using Gaussian spectrum fitting and Phi-Rho-Z matrix correction. For this study, two check standards were used, USGS reference materials for basaltic glasses: VG-2 (Juan de Fuca Ridge) and VG-A99 (Hawaii). Both were analyzed as unknowns at the beginning and end of each analytical session and again after every nine samples. Each sample was analyzed for major elements three times; the averages are reported in Table 3.1.

3.3.2 Trace element analyses

Trace element concentrations of the NEFTJ were measured at the Research School of Earth Sciences (RSES), Australian National University (ANU), using a 7500S Agilent ICP-MS, coupled to a HelEx laser-ablation system. A full description of the trace element analyses by laser-ablation ICP-MS is given in the study by Jenner & O'Neill (2012). Basaltic reference material BCR-2G (USGS) was run as an unknown with NIST SRM 612 for external calibration (preferred values from Norman et al. (2004)) in the same analytical session as the NEFTJ samples. The parameters of the ICP-MS are: RF power = 1350 W; ablation cell gas flow = 0.3 L min^1 He + 0.02 L min^1 H_2; auxiliary gas flow = 1.0 L min^1Ar; laser energy = 50 55 mJ, linked to an ANU HelEX laser-ablation system, which employs a 193-nm wavelength EXCIMER laser

(110 (ArF) COMPex, Lambda Physik). The ablation diameter used was 86 μm and a laser repetition rate of 5 Hz, with a 187 μm spot for a few elements with low abundances. Data were acquired with 20 or 30 s of background measurement, followed by between 30 and 40 s of sample ablation (with longer count times for elements with low abundances). The ICP-MS was calibrated to low oxide production rates (ThO^+/Th^+ typically <0.4%, measured using NIST SRM 612) and this rate was monitored throughout each analytical session. The analysis was undertaken after >30 min after each sample change to ensure background counts, and oxide production rates during data collection were minimal. This method of analyzing trace elements with LA-ICP-MS has a long-term (over a minimum of 3 years) RSD (relative standard deviation) as determined by replicate measurements of standards (NIST SRM 612 and BCR-2G) of ≤ 2–4%.

3.3.3 Volatile element analyses

Volatile elements and halogens were analyzed on a Cameca nanoSIMS (secondary ion mass spectrometer) 50L at the Carnegie Institute for Science Department of Terrestrial Magnetism (DTM), following methods outlined by Hauri et al. (2002). The propagated uncertainties (1σ) of the final values take into account the uncertainty in the blank measurement and the uncertainty on the slope of the DTM calibration line. Glass fragments were mounted in epoxy in Al-metal disks and polished. The mounts were dried in an oven at 70°C for several days followed by coating in gold (top and sides). The mounts were stored in the oven at 70°C between ion probe analytical sessions to minimize water adsorption from the laboratory air.

The samples and standards outgas in an airlock attached to the ion microprobe sample chamber, and again when inserted into the sample chamber. Measurements are taken at pressure $<5\times10^{-9}$ Torr, sample current 5-10nA, 10 kV, tuned with an imaged

field of view of 150 μm diameter on the sample surface, using a large contrast aperture at the crossover (400 μm). A 100 μm diameter field aperture is inserted into the image plane, and entrance and exit slits are then closed to achieve a mass resolution of 2400. The 100 μm field aperture limits the ion optical field of view to an area of 10 μm in diameter and gives access to only those ions originating from the central 10 μm of the crater. The total time for analysis is 10 min per spot: 5 min pre-sputter period followed by the collection of five sets of ratios. The standard used in this study is the San Carlos olivine (Mathez & Delaney, 1981; Mackwell & Kohlstedt, 1990).

3.3.4 Sr and Nd chemical separation and mass spectrometry

All Sr, and Nd isotopic measurements in this study were done on 200 to 450 mg of fresh volcanic glass (for NLTD lavas). Different methods of sample leaching, dissolution, column separation and mass spectrometric analysis were used when analyzing the NLTD samples (Fall 2012-Spring 2013). These methods are described below.

All samples were acid leached prior to digestion at the Ecole Normale Supérieure in Lyon (ENS Lyon). The NLTD glasses were leached using the protocol of Blichert-Toft and Albarède (2009), which consists of leaching the glasses with 2 ml 6M HCl for 20 minutes at 120° C, followed by 10 minutes of sonication, then another 10 minutes at 120° C, followed by 5 minutes of sonication and finally 5 more minutes at 120° C; the HCl is pipetted off and the samples rinsed twice in milliQ H_2O.

Following leaching and rinsing, all samples were dissolved in a 3:1 mixture of concentrated double-distilled HF and HNO_3 followed by evaporation to dryness after digestion for 48 hours at 130° C. Chromatography of the samples in this study were done by leaching the attacked samples for 48 hours with concentrated double-distilled HF following the methods outlined in Blichert-Toft et al. (1997). The CaMg-fluoride

precipitates resulting from the HF leaching step, which contained the Sr and Nd, were redissolved in 6M HCl after first fuming them with double-distilled $HClO_4$ to decompose the fluorides.

For the NLTD samples, the fraction hosting Sr and Nd following dissolution and leaching out of the Hf at ENS Lyon was transported to Boston University (BU) where Sr and Nd for these samples were recovered from the clean wash off the Pb columns using 0.7M HBr. Strontium and Nd for the NLTD samples were separated using ion-exchange chromatography at BU: Sr was separated using Eichrom Sr-spec resin, and Nd was separated using a two-step protocol involving Eichrom TRU resin followed by Eichrom LN-Spec resin (following methods in Price et al., 2014).

For all samples, Hf, Pb, Sr, and Nd were separated from the same sample dissolutions, thereby minimizing sample consumption and avoiding potential sample heterogeneity that could otherwise lead to unwanted isotopic variations. The total procedural blanks for Hf, Pb, Sr and Nd of the NLTD samples are < 20 pg, < 30 pg, < 80 pg and < 35 pg, respectively (Price et al. (2014) and J. Blichert-Toft routine blank measurements). The blanks are all negligible relative to the amount of sample of Sr and Nd that were analyzed.

Neptune MC-ICP-MS measured strontium and Nd isotopic compositions for the NLTD samples at the Woods Hole Oceanographic Institution (WHOI); the column chemistry and mass spectrometry for the NLTD samples were carried out during the same analytical sessions as the sample unknowns (and unleached USGS reference materials) analyzed in Price et al. (2014). Details on the measurement and standard normalization protocols are as follows:

Strontium. For samples measured by MC-ICP-MS, intensities were measured on masses 82 through 88 and corrections for isobaric interferences on masses 87 (Rb), 84 (Kr) and 86 (Kr) was made offline following the procedures outlined in Jackson and

Hart (2006). Isotopic ratios of Sr were corrected for instrumental mass bias relative to $^{86}Sr/^{88}Sr$ of 0.1194 using an exponential law. Measured $^{87}Sr/^{86}Sr$ ratios of the samples were corrected for the offset between the measured and preferred $^{87}Sr/^{86}Sr$ values (0.710240; Jackson and Hart, 2006) for SRM 987. The external precision of the $^{87}Sr/^{86}Sr$ measurements is estimated to be 15–25 ppm (2σ) (Hart and Blusztajn, 2006).

Neodymium. For samples measured by MC-ICP-MS on the Thermo-Finnigan Neptune at WHOI, Nd isotopic compositions were corrected for instrumental mass fractionation relative to $^{146}Nd/^{144}Nd$ of 0.7219 using an exponential law. The JNdi-1 and La Jolla Nd standards were run during each analytical session. The $^{143}Nd/^{144}Nd$ values for JNDi-1 were adapted to the La Jolla $^{143}Nd/^{144}Nd$ value using a conversion factor of 1.000503 (Tanaka et al., 2000). When this preferred JNdi-1 value (0.512104; Jackson and Carlson, 2012) is adapted to the La Jolla $^{143}Nd/^{144}Nd$ using a ratio of 1.000530 (Tanaka et al. 2000), the preferred La Jolla value is 0.511847. The La Jolla and La Jolla-renormalized JNdi-1 $^{143}Nd/^{144}Nd$ measurements were averaged to give a final La Jolla average for the analytical session; measured sample $^{143}Nd/^{144}Nd$ ratios were corrected for the offset between measured and preferred (0.511847) La Jolla $^{143}Nd/^{144}Nd$ values (White and Patchett, 1984). The external precision of the $^{143}Nd/^{144}Nd$ measurements at WHOI is estimated to be 15–25 ppm (2σ) (Hart and Blusztajn, 2006).

3.4 Results

3.4.1 Major Element Geochemistry

A summary of the sample descriptions and chemical data is provided in Table 3.1. The North Fiji Basin lavas are a combination of alkalic and tholeiitic lavas, with SiO_2 from 47.7 to 50.6 wt.% and total alkalis (Na_2O+K_2O) from 2.5 to 4.7 wt.% (Figure 3.2). The caldera samples span across the alkali tholeiite division. The NE arm samples

are all alkali, and the samples from the S arm plot mostly in the tholeiitic field with only one sample plotting at the boundary. The lavas have similar major element compositions to averaged primitive normal MORB (Melson et al., 2002), except K_2O and P_2O_5 that fall below our data. However, these are still within range for observed normal MORB.

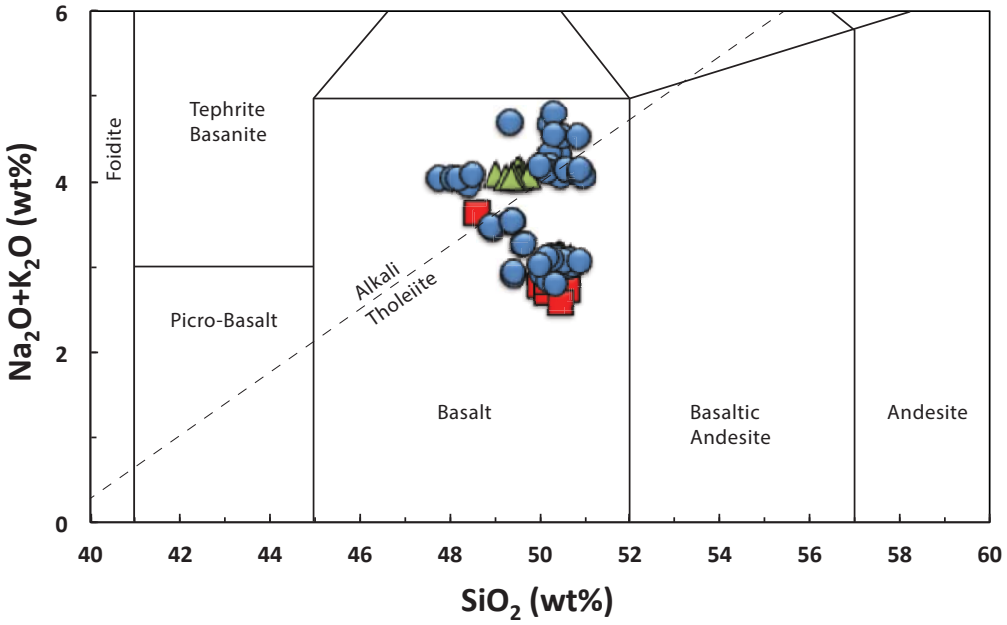

Figure 3.2 Total alkali versus silica plot summarizing the classifications of the rocks used in this study. The boundary for the alkaline and subalkaline/tholeiitic rocks is from Macdonald and Katsura (1964). The symbols are divided by their respective areas and remain the same for all subsequent plots. Circles represent the NEFTJ – Caldera (53 samples from 7 dredges were analyzed for majors), squares represent NEFTJ – S arm (9 samples from 3 dredges), and triangles represent NEFTJ – NE arm (14 samples from 2 dredges).

3.4.2 Water and carbon dioxide in lavas

For a back-arc basin so far removed from a subduction zone, the lavas in the NFB exhibit a surprisingly large range of volatile elements: H_2O (0.16–0.9 wt.%) and CO_2 (80–359 ppm) (Fig. 3.3). The NFB lavas have volatile levels that exceed the range of MORB (< 0.7 wt.% H_2O) (Fig. 3.3) and are similar to the OIB arrays of the Galapagos and Samoan hotspots.

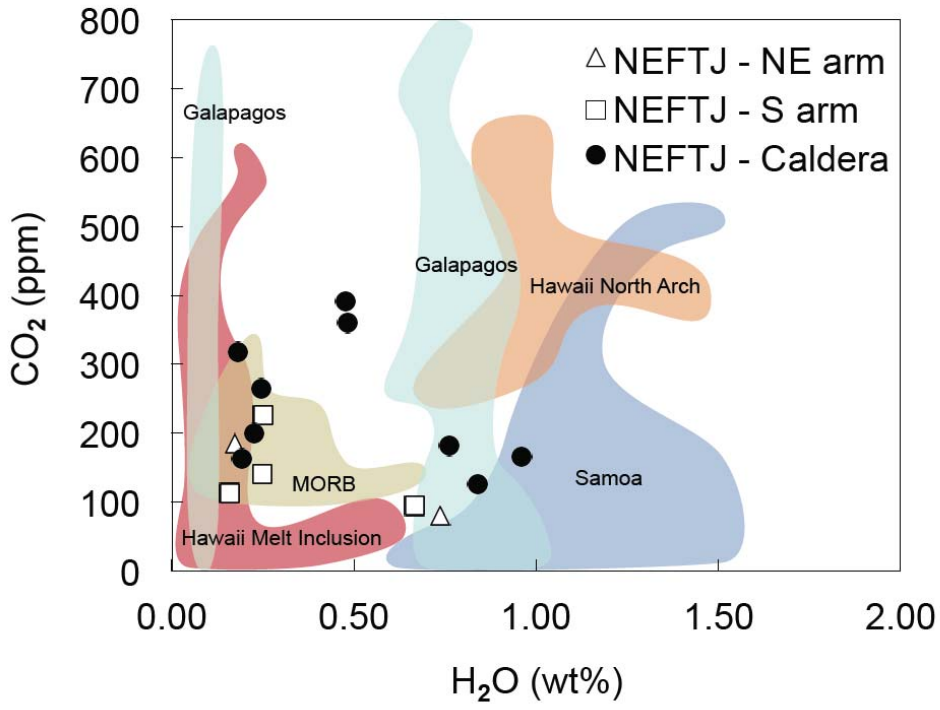

Figure 3.3 Carbon dioxide content versus water, comparing studies of volatiles in magmas within other settings (Hawaii North Arch – Dixon et al., 1997; Hawaii Melt Inclusion – Hauri, 2002; MORB – le Roux, 2006; Samoa – Workman et al., 2006; Galapagos – Koleszar et al., 2009). The samples from this study are categorized into three groups: Northeast Fiji Triple Junction Northeast arm (NEFTJ – NE arm), Northeast Fiji Triple Junction South arm (NEFTJ – S arm), Fiji – Caldera (located in the center of the NEFTJ).

Dissolved volatile elements in magmas exsolve by the formation of bubbles as the pressure exerted on the magma decreases. When vapor saturation pressure is equal to the hydrostatic pressure and magma ascent is slow, degassing can occur, but, when ascent is much faster, vapor saturation pressures increase because the magma does not have enough time to degas (Dixon & Stolper, 1995). It is evident that some of these samples lie on the '1:1 line' between the depth of sample collection and the vapor saturation pressure (Fig. 3.4b). However, the majority of the samples are oversaturated in H_2O and CO_2 vapor. Additionally, there is a minimal distribution of vesicles within these rocks (0–5 vol.%), where, if the lavas had been fully exsolved, the vesicles would

have been ubiquitous. In Figure 3.4a, the variation of CO_2 with no change in H_2O displays open-system degassing in the magmas; however, an increase in H_2O at lower pressures suggests incomplete degassing of these saturated magmas upon quenching.

The solubility of CO_2 is much lower than H_2O in basaltic magmas (Javoy & Pineau, 1991; Dixon et al., 1995; Shishkina et al., 2010). Considering the similarities in incompatibility between CO_2 and Nb (Saal et al., 2002; Cartigny et al., 2008), a correlation between CO_2 and Nb would be expected if the magmas were undegassed. The CO_2/Nb ratio is expected to be between 200 and 400 for undegassed melts; however, the NFB has CO_2/Nb ratios of <136. There is a lack of correlation between CO_2/Nb when plotted against MgO (not shown), and the lavas overlap with the MORB field. With low CO_2/Nb values, open-system degassing for the NEFTJ lavas predominantly consists of CO_2 in a vapor. Open-system degassing follows the decreasing CO_2 trend indicated in Figure 3.4a and, at lower pressures, water becomes the dominant vapor phase. While the carbon dioxide vapor phase, shows a larger distribution relative to water in many of the NFB lavas (Fig. 3.4a), as the degassing follows the open-system decompression path there is no decrease in water. Thus, water loss (if any) has most likely not been significant and is, therefore, considered negligible.

The lavas above the 1:1 line in Figure 3.4b have experienced incomplete degassing as they quenched rapidly. The dredge depth used in this plot is an average of the minimum and maximum dredge depths, meaning that the lavas, which traversed tens to hundreds of meters, could have been collected at any point in that range. The average dredge depth used may not be accurate for each sample and could explain why the NEFTJ (S arm and NE arm) samples are at or below the 1:1 saturation line. The least degassed samples are from the shallower (~1990 m deep) dredged caldera lavas and the most degassed are the deeper (~2200 – 2600 m deep) dredged S arm and NE arm lavas.

However, all of the lavas have sufficiently high saturation pressures that any loss of water by degassing is insignificant.

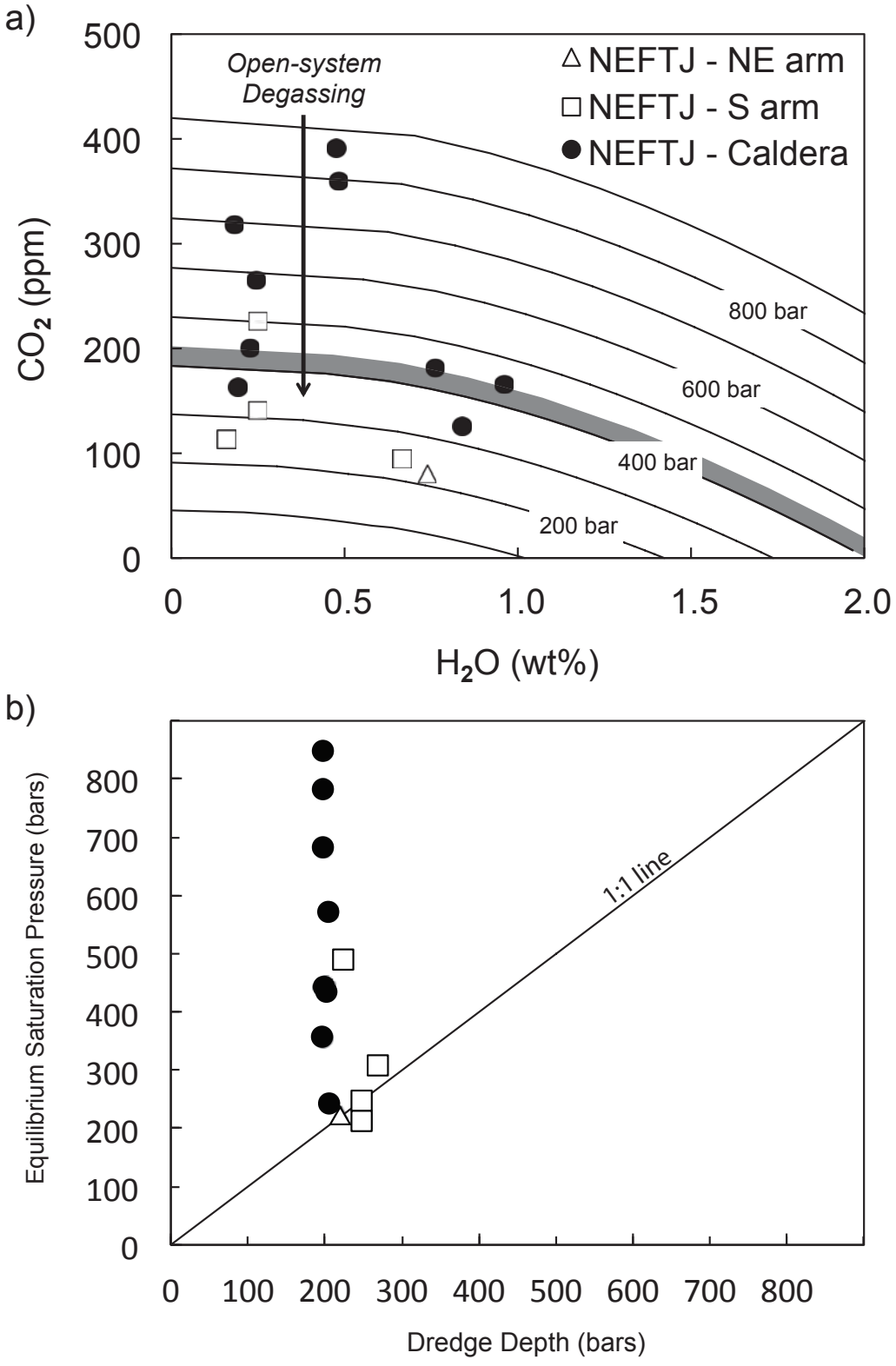

Figure 3.4 Panel (a) Carbon dioxide content versus water is plotted with curves of constant pressure, for the isobars (solid lines) and open system degassing

trends reported in Dixon & Stolper (1995) and Newman & Lowenstern (2002). The grey area represents the vapor saturation pressure for which the lavas in this study erupted. Panel (b) Relationship between depth at which the lavas in this study were collected and the calculated vapor saturation pressure (after Dixon, 1997) for mixed volatile (H_2O-CO_2) system. Given the use of a dredge in collecting samples there is a difference in dredge depth from start to finish (expressed as the error bars). The '1:1 line' represents the threshold between saturated or oversaturated (those that plot on or above the '1:1 line') and undersaturated (those that plot below the '1:1 line') lavas at any given depth of eruption. The range in depth of collection for the samples is ~1,900m to ~3,000m. The majority of the 'Fiji – Caldera' samples are saturated for their depth of eruption versus the flanks of the triple junction which do not exhibit as large a range in saturation (NEFTJ – NE arm & NEFTJ – S arm).

3.4.3 Trace Element Geochemistry

The lavas analyzed in this study display a broad range of trace element abundances. We illustrate these variations in primitive mantle-normalized plots (spider-grams) (Figure 3.5). At maximum, the abundances for the lavas vary by nearly an order of magnitude for incompatible elements. The shapes of the spider-grams fall into two broadly similar patterns, where approximately half of the samples have higher concentrations of incompatible elements about the rest of the samples. The two broad patterns were observed in all three regions of the NEFTJ, and no systematic difference between them appeared to display. However, we continued to separate them by the three regions for consistency.

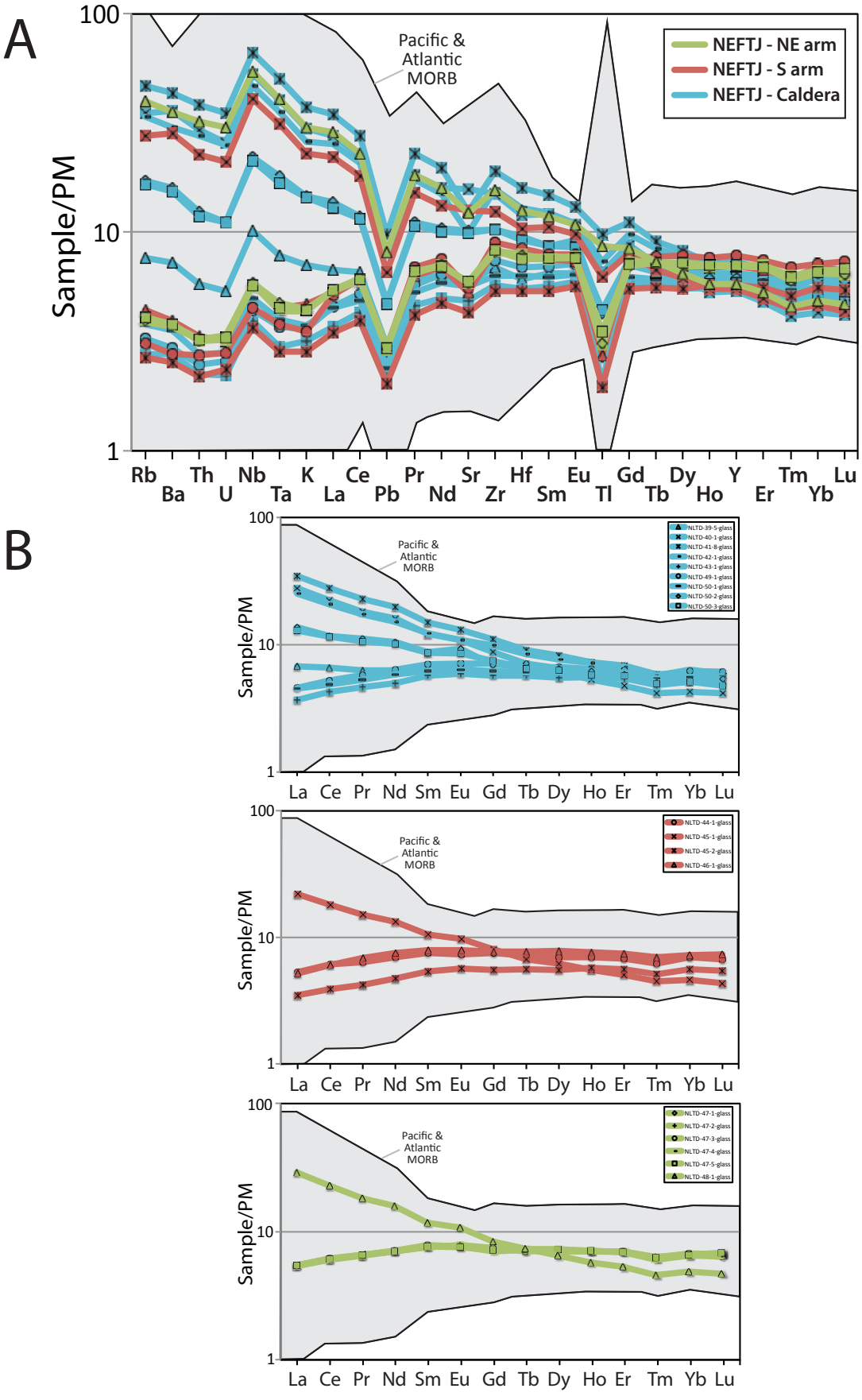

Figure 3.5 (A) Primitive mantle-normalized trace element patterns in this study showing fourteen glasses from the NEFTJ compared to a span of Pacific and

Atlantic MORB. The spider-gram shows two compositionally distinct magmas located in the NEFTJ. (B) Primitive mantle-normalized trace element patterns for the lavas analyzed in this study (NEFTJ) compared to MORB. Previously published MORB data from Jenner & O'Neill (2012) are compared with fourteen glasses from this study.

The glasses analyzed in this study have all evolved past clinopyroxene saturation. This is evident in the presence of olivine and clinopyroxene in the hand samples in addition to the low Mg numbers calculated as:

Molar percent = 100 x MgO/[MgO+FeO]

and which span from 54 to 64. La/Sm and Gd/Yb ratios for glasses plot vertically when compared against MgO, partially overlapping the MORB field (Fig. 3.6c-d). This suggests that the fractionation of olivine, clinopyroxene, and in some cases plagioclase has had little to no impact on incompatible element ratios. Therefore, the use of these incompatible trace element ratios as a tool to evaluate primary melts is suitable.

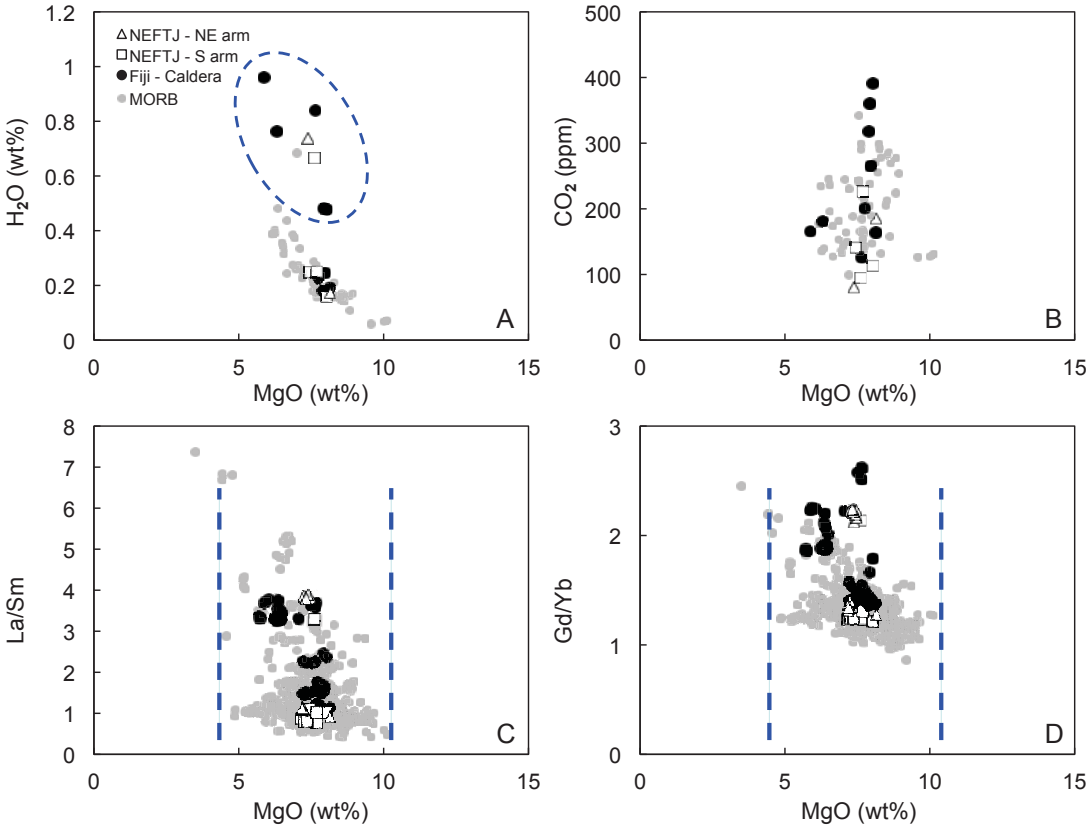

Figure 3.6 MgO compared to (A) water, (B) carbon dioxide, (C) La/Sm, and (D) Gd/Yb ratios in lavas from the North Fiji Basin. In addition to new data from this study, previously published values from MORB are also shown (Melson et al., 2002; le Roux et al., 2006; Jenner & O'Neill, 2012). Symbols for the new data from the lavas in this study are the same as in Figure 3.2, in addition to the symbol for mid-ocean ridge basalt (MORB).

La/Sm is used as a proxy for source enrichment. Sr isotope values are presented and discussed in depth in the following chapter, although the trends they exhibit are also significant to this chapter. The La/Sm values for the lavas in this study range from 1.1 to 3.8 and steep positive correlation with $^{87}Sr/^{86}Sr$. Gd/Yb also correlate with $^{87}Sr/^{86}Sr$, spanning from 1.2 to 2.4. The Gd/Yb trend is horizontal for the lavas with lower $^{87}Sr/^{86}Sr$ values (0.7028 to 0.7031) and a slightly positive trend for the lavas with higher $^{87}Sr/^{86}Sr$ (0.7034 to 0.7036). The steepness of the rare earth element slopes suggests melting of material that fractionates light from heavy rare earth elements, such as melting within the garnet lherzolite stability zone, for very steep slopes, or for lesser

slopes, melting within spinel lherzolite stability zone (Hauri et al., 1994; Salters et al., 2002). Conversely, N-MORB taps a depleted mantle that has undergone polybaric mixing and fractionation to create a homogeneous source with a flat rare earth element pattern; La/Sm and Gd/Yb are both around 1 (Hofmann, 1988). In the following sections, we attempt to distinguish the primary geochemical signals that enable us to understand the sources that have contributed to the composition and evolution of the mantle beneath the NFB.

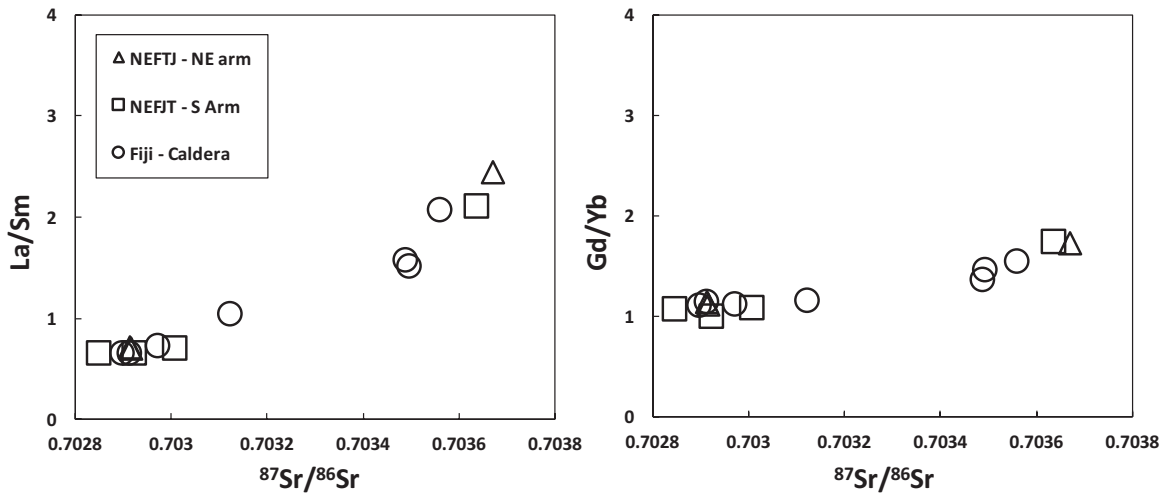

Figure 3.7 $^{87}Sr/^{86}Sr$ compared to (left) La/Sm, (right) Gd/Yb ratios in lavas from the North Fiji Basin. The symbols are the same for both graphs.

3.5 Discussion

3.5.1 Implications for magmatic source(s)

Although the North Fiji Basin is situated in a back-arc basin, plate reconstructions have shown that the subducting slab is <1400 km to the east (Price et al., 2014). The NFB is a result of rollback of slabs from subduction zones to the east and west (Musgrave and Firth, 1999; Hall, 2002), but is not subject to flux from active subduction at the Vitiaz trench. The Vitiaz slab has ceased subducting and instead has continued to roll back, resulting in a horizontal slab beneath the NFB (Auzende et al.,

1995; Musgrave and Firth, 1999). The substantial distance from the active trench coupled with stagnant tectonics of the area precludes the NFB lavas from having slab inputs; this is evident from trace element patterns which show the lack of enrichment in fluid mobile elements (i.e. U, Th, and Pb) but a relative enrichment in L-REE relative to N-MORB, observed as steep slopes in Figure 3.5. For comparison, the Mariana Trough and Lau back-arc basin, which are two of the most comprehensively studied and geochemically well-characterized (with the inclusion of volatile elements) back-arc basins, have gradational major and trace element compositions that span from island arc type to geochemically depleted (N-type) MORB (Pearce et al., 1994; Ewart et al., 1998; Newman et al., 2000). A decrease in carbon dioxide, as the lavas degas, along with other inherited trace element signatures from the subducting slab such as U, Th, and Pb enrichments, are recognized to be an effect of proximity to the active arc (Volpe et al., 1990; Gribble et al., 1996; Newman et al., 2000). While we do observe some similarities in the enrichment of water and carbon dioxide, we cannot discern all the geochemical characteristics indicative of a subduction zone influence. This suggests that the enrichment of measured volatile elements and light rare earth elements stem from an enriched deeper source. This is in contrast to back-arc basin magmas erupting in the Eastern Manus Basin and associated with the Mariana and Tonga arc.

The basalts from the NFB show no variation in MgO when compared to CO_2 and trace element discrimination ratios (Fig. 3.6). The lavas show enrichment in water relative to MORB within the same range of MgO (Fig. 3.6a, in blue dotted line). While the lavas often plot within MORB fields, the MgO values are too low to be directly derived from the mantle. We also observe a slight positive trend between CaO and MgO, indicating some fractional crystallization. However, the La/Sm array within a localized MgO range suggests that La/Sm ratios in the lavas have not been affected by fractional crystallization. Thus, these ratios can be used to link source variations.

Geochemically, H_2O behaves similarly to light rare earth elements (LREE) (Michael, 1995). H_2O is traditionally paired with Ce, given its well-studied and restricted range in MORB, OIB, and arc lavas (Stolper & Newman, 1994; Michael, 1995; Dixon & Clague, 2001; Dixon et al., 2002; Simons et al., 2002; Workman et al., 2006; Ruscitto et al., 2012). We observe a positive correlation in the NFB lavas between H_2O and Ce, suggesting no water loss (Fig. 3.8b). In addition to a positive correlation, the lavas have a similar slope to MORB that plots in a field adjacent to the NFB lavas. We also note that the range for the NFB lavas extends further than that of MORB, towards a more enriched OIB-like source. There is a lack of correlation between H_2O/Ce ratios and MgO, except an apparent elevated H_2O/Ce range relative to MORB.

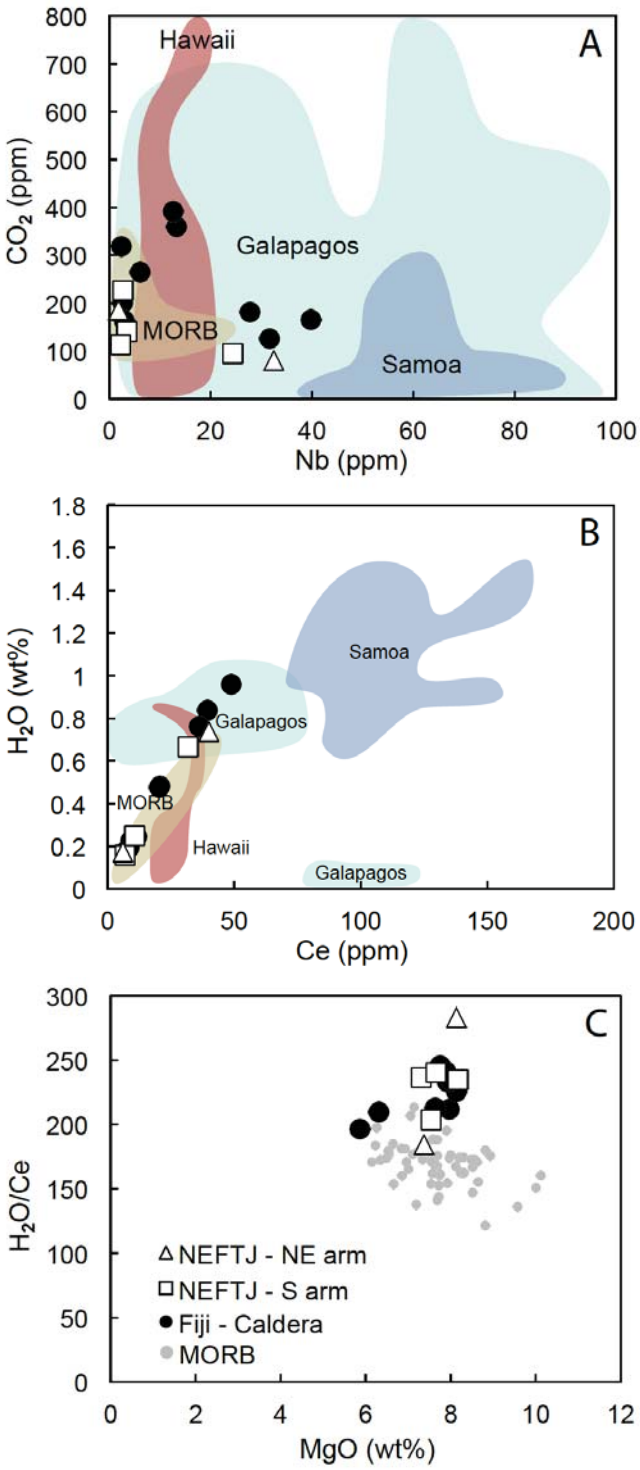

Figure 3.8 Panels show variations in (A) carbon dioxide and Nb, (B) water and Ce, (C) H_2O/Ce and MgO in lavas from the North Fiji Basin. The lavas in this study are compared to previously published values from the ocean island basalts (OIB) and mid-ocean ridge basalts (MORB): Hawaii Melt Inclusion (Hauri, 2002), MORB (le Roux et al., 2006), Samoa (Workman et al., 2006), Galapagos (Koleszar et al., 2009). Circles represent the NEFTJ – Caldera (53 samples from 7 dredges were analyzed for majors), squares represent NEFTJ

– S arm (9 samples from 3 dredges), and triangles represent NEFTJ – NE arm (14 samples from 2 dredges).

As indicators of source enrichment, H_2O/Ce display a near horizontal linear array when plotted against La/Sm and a positive correlation with Gd/Yb (Fig. 3.9a-b). H_2O is more incompatible than Ce, with the result that, as the source becomes more enriched in incompatible elements, the H_2O/Ce ratio also increases (Michael, 1995). Moreover, when compared to MORB, the NFB lavas are all enriched in H_2O/Ce. La/Sm values in the NFB lavas range from 0.9 to 3.8 while Gd/Yb values range from 1.2 to 2.5. The NFB lavas overlap the MORB range for both La/Sm (~1.1) and Gd/Yb (~1.3) (le Roux et al., 2006), although they extend beyond the MORB array. High La/Sm and Gd/Yb ratios (>1) are indicators of deeper melting within the stability field of garnet lherzolite (Hauri et al., 1994).

Enrichment of these combined ratios (La/Sm and Gd/Yb) with no measurable enrichment in fluid mobile elements challenges the concept of adding a hydrous component to the melt through the dehydration of a subduction zone slab. By coupling these element ratios with water, it is evident that a plume (less depleted) source is responsible for the enriched geochemical signatures we observed. This is consistent with recorded observations near the plate boundary much further to the north, where the Samoan plume is infiltrating the mantle as a result of tectonic forces in the area (Price et al., 2014).

CO_2/Nb, when plotted against La/Sm and Gd/Yb (Fig. 3.9c-d), displays two trends: a vertical and a negative correlation. These trends can readily be explained by allowing two compositionally different magmas to degas. At one extreme, depleted samples at high degrees of partial melting will have a low initial CO_2 and, as a result, will only lose a fraction of it by degassing. Conversely, an enriched sample with low

degrees of partial melt and high initial CO_2 will lose most of the initial CO_2 upon degassing (Javoy et al., 1978). While both lavas have similar CO_2, their trace elements vary vastly, resulting in the two trends observed in Figure 3.9c-d. If the samples had not degassed, a trend between CO_2 and Nb would be evident, but does not occur (Fig. 3.8a).

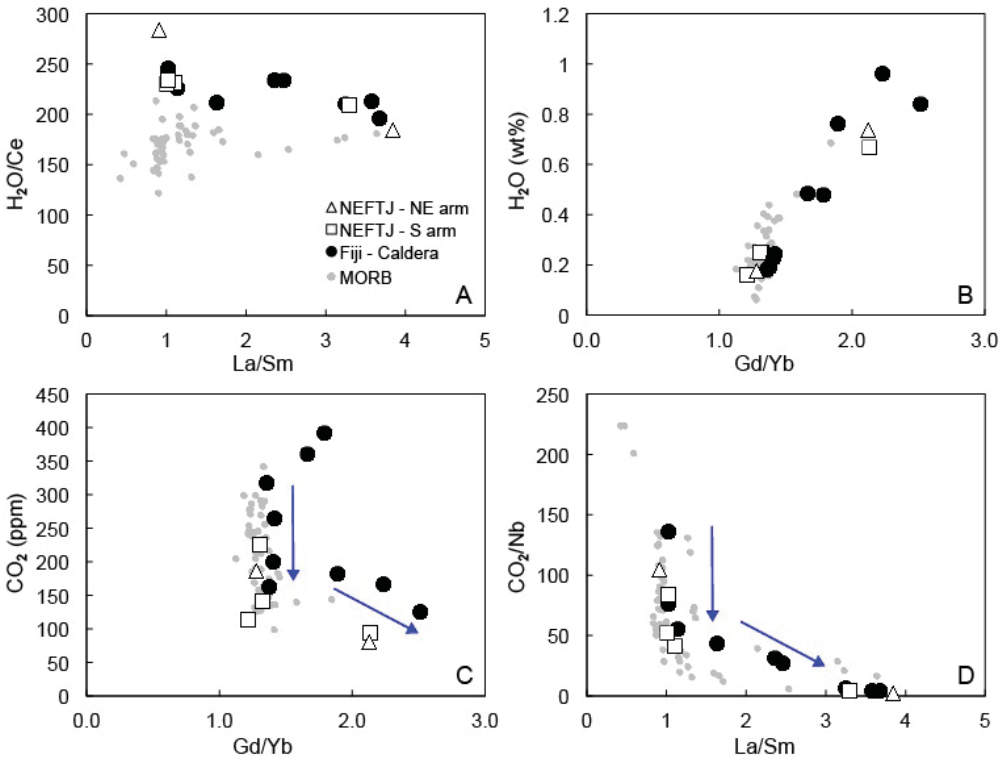

Figure 3.9 Panels show variations in (A) H_2O/Ce and La/Sm, (B) H_2O and Gd/Yb, (C) CO_2 and Gd/Yb, and (D) CO_2/Nb and La/Sm for lavas from the North Fiji Basin and mid-ocean ridge basalts (MORB) (le Roux et al., 2006). Circles represent the NEFTJ – Caldera (53 samples from 7 dredges were analyzed for majors), squares represent NEFTJ – S arm (9 samples from 3 dredges), and triangles represent NEFTJ – NE arm (14 samples from 2 dredges). Water data plot higher than the MORB field, while carbon dioxide data plots within the MORB field. The arrows in panels (C) & (D)] indicate the degassing paths of two compositionally distinct lavas (refer to text).

Continental crust is depleted and exhibits a negative Nb anomaly (Hofmann, 1997). Conversely, a positive Nb anomaly usually signifies the melting of an enriched source. Figure 3.5 illustrates extended trace element abundance spider-grams for the NEFTJ. The spider-gram establishes trends for two compositionally distinct magmas.

The first, a steep slope showing enrichment in High Field Strength Elements (HFSE), Large Ion Lithophile Elements (LILE), and a negative Sr anomaly which represents plagioclase fractionation. The second, a shallower slope in the opposite direction, indicates melting of a depleted source with depletion in HFSE's and LILE's. Both compositionally distinct magmas retain positive Nb anomalies and negative Pb, Sr, and Tl anomalies that are not characteristic of a slab source (Hofmann, 1997). Additionally, a condensed REE spider-gram (Figure 3.5) exhibits the same patterns seen in the extended REE spider-gram. The NEFTJ lavas display a REE pattern that is congruent with MORB data from Jenner & O'Neill (2012).

3.5.2 Mantle Melting Models

We show two stage-melting models in Figure 3.10 for three compositions: Spinel – Spinel, Garnet – Garnet, and Spinel – Garnet. The original primitive mantle composition was taken from Palme & O'Neill (2014). The transition between spinel lherzolite and garnet lherzolite occurs between 18–27 kbar dependent on temperature (Klemme & O'Neill, 2000); we used the initial garnet lherzolite source mineral proportions from Davis et al. (2009). The primitive mantle was melted by various degrees (1–20%) using partition coefficients from the published literature (Table 3.2 and 3.3) to show how the slope decreases with an increase in the fraction of melting. We used a batch melting equation where the composition of the liquid (melt) is calculated:

$$C_L/C_0 = 1 / [D_0 + F(1 - P)]$$

(from Shaw, 1970; in Rollinson, 1993). The composition of a trace element in the melt (C_L) is determined as a function of the original composition (C_0), where D_0 in the equation is the bulk distribution coefficient at onset of melting, F is the weight fraction of melt produced (melt/[melt+rock]), and P is the bulk distribution coefficient of minerals making up the melt. The second stage melting uses the same previous batch

melting equation and partition coefficients. However, we modified both the primitive mantle trace element composition to be representative of the residual mantle and the initial lherzolite source mineral proportions, from the original Davis et al. (2009) lherzolite to a different value (Ol: 55%, Opx: 24%, Cpx: 18%, Gt: 5%), to simulate the depletion observed in Figure 3.5.

Table 3.2 Values in trace element modeling, peridotite melting, magma/mantle interaction. References for each value are located at the bottom of the Table.

	D ol/liq	D opx/liq	D cpx/liq	D gar/liq	D sp/liq
olivine	1				
orthopyroxene		1			
clinopyroxene			1		
garnet				1	
spinel					1
rutile					
Ba	1.0E-09 [a]	0.00001 [a]	0.00068 [f]	0.0001 [a]	0 [a]
Th	1.0E-09 [a]	0.00001 [a]	0.016 [g]	0 [a]	
U	1.0E-09 [a]	0.00001 [a]	0.003 [h]	0.005 [j]	0 [a]
K	1.0E-09 [b]	0.00001 [b]	0.0072 [b,f]	0.00001 [b]	0.01 [a]
Nb	0.001 [b]	0.0029 [b]	0.0072 [b,f]	0.013 [b]	0.01 [b]
La	0.000007 [b]	0.001 [b]	0.0536 [b,f]	0.001 [b]	0.0006 [b,m]
Ce	0.00001 [b]	0.003 [b]	0.0858 [b,f]	0.008 [b]	0.0006 [b,m]
Pb	0.00001 [a]	0.003 [a]	0.072 [b,f]	0.0005 [k]	0 [a]
Pr	0.00004 [a]	0.006 [a]	0.13 [a]	0.033 [a]	0.0006 [b,m]
Sr	0.00001 [b]	0.003 [b]	0.1283 [b,f]	0.007 [b]	0 [a]
Nd	0.00007 [b]	0.009 [b]	0.1873 [b,f]	0.057 [l]	0.0006 [b,m]
Zr	0.004 [b]	0.04 [b]	0.1234 [b,f]	0.5 [b]	0.07 [b]
Hf	0.004 [a]	0.04 [a]	0.256 [b,f]	0.5 [b]	0.07 [b]
Sm	0.0007 [b]	0.02 [b]	291 [b,f]	0.217 [l]	0.0006 [b,m]
Eu	0.00095 [b]	0.03 [b]	0.33 [b,f]	0.45 [l]	0.0006 [b,m]
Gd	0.0012 [a]	0.04 [a]	0.37 [a]	0.9 [a]	0.0006 [a]
Tb	0.0026 [a]	0.05 [a]	0.41 [a]	1.5 [a]	0.006 [a]
Ti	0.015 [b,c]	0.15 [b,c]	0.4 [b,c,f]	0.6 [b]	0.15 [b]
Dy	0.004 [b]	0.06 [b]	0.442 [b,f]	2 [l]	0.0015 [b,m]
Ho	0.007 [a]	0.065 [a]	0.43 [a]	2.8 [a]	0.0023 [a]
Er	0.009 [b]	0.09 [b]	0.43 [i]	3.5 [l]	0.003 [b,m]
Yb	0.023 [b]	0.1 [b]	0.43 [b,f]	7 [l]	0.0045 [b,m]
Lu	0.03 [a]	0.12 [a]	0.433 [b,f]	9 [l]	0.0053 [b,m]
Y	0.023 [a]	0.1 [a]	0.467 [b,f]	7 [a]	0.0045 [a]
Co	2 [a]	2 [a]	2 [a]	1 [a]	2 [a]
Ni	10 [d]	3.5 [e]	3 [e]	5 [e]	10 [e]

	References for the values
a	Kelemen et al., 2003
b	Kelemen et al., 1993
c	Kelemen et al., 1990
d	Value based on Arndt, 1977; Hart & Davis, 1978; Kinzler et al., 1990
e	olivine/liquid from references in d, plus mineral/olivine from Bodinier et al., 1987; Kelemen et al., 1998
f	Hart & Dunn, 1993
g	Value based on LaTourrette & Burnett 1992 and Hauri et al., 1994
h	Beattie, 1993
i	Adjusted from value in Hart & Dunn (1993) to give smooth REE pattern for garnet peridotite and eclogite melting
j	Value based on LaTourrette & Burnett, 1992; Beattie, 1993; Hauri et al., 1994
k	Value based on Beattie, 1993; Hauri et al., 1994; Salters et al., 2002
l	Shimizu & Kushiro, 1975
m	Stosch, 1982
n	Value from Philpotts & Schnetzler, 1970a,b; Schnetzler & Philpotts, 1970
o	Interpolated based on garnet D pattern in Kelemen et al. (1993) and K, La values
p	Irving & Frey, 1978
q	Green et al., 1989
r	Jenner et al., 1993
s	Nicholls & Harris, 1980
t	Ti is a major element during partial melting with residual rutile, and its concentration is controlled by phase equilibrium rather than partitioning. However, Ti value is interpolated based on garnet and cpx D patterns in refs. a,b,f, then adjusted to fit observation by Rapp et al. (1999), that Ti is not fractioated from REE during rutile saturated partial melting of eclogite
u	Luhr & Carmichael, 1984
v	Larsen, 1979
w	Dostal et al., 1983
x	Fujimaki et al., 1984
y	Hart & Brooks, 1974
z	Green & Pearson, 1987
aa	Foley et al., 2000

Table 3.3 Values in trace element modeling, eclogite melting, magma/mantle interaction. References for each value are the same as Table 3.2.

	D gar/liq	D cpx/liq	D rutile/liq
olivine			
orthopyroxene			
clinopyroxene		1	
garnet	1		
spinel			
rutile			1
Ba	0.02 [n]	0.02 [n,u]	0 [a]
Th	0.001 [a]	0.03 [v,w]	0 [a]
U	0.005 [a]	0.04 [v,w]	0 [a]
K	0.02 [n]	0.02 [n]	0 [a]
Nb	0.05 [o]	0.02 [v]	30 [z,aa]
La	0.08 [p]	0.04 [x]	0 [a]
Ce	0.2 [n,p]	0.08 [x]	0 [a]
Pb	0.005 [a]	0.1 [v]	0 [a]
Pr	0.4 [a]	0.14 [a]	0 [a]
Sr	0.03 [n,q,r]	0.07 [n,w,y]	0 [a]
Nd	0.8 [n,p]	0.2 [x]	0 [a]
Zr	5 [q]	0.3 [v,x]	40 [a]
Hf	5 [p]	0.3 [u,x]	40 [a]
Sm	5 [n,p,q,s]	0.4 [x]	0 [a]
Eu	7 [n,p]	0.45 [n,v,w,x]	0 [a]
Gd	10 [n,p]	0.6 [x]	0 [a]
Tb	14 [n,p]	0.65 [a]	0 [a]
Ti	12 [t]	0.6 [t]	100 [t,aa]
Dy	16 [n,s]	0.7 [n,x]	0 [a]
Ho	18 [p.s]	0.7 [a]	0 [a]
Er	20 [n]	0.7 [x]	0 [a]
Yb	25 [n,p,s]	0.7 [n,v,w,x]	0 [a]
Lu	30 [n,p]	0.7 [n,v,w,x]	0 [a]
Y	25 [q]	0.8 [v]	0 [a]
Co	2 [p]	1 [w]	0 [a]
Ni	1 [a]	1 [a]	0 [a]

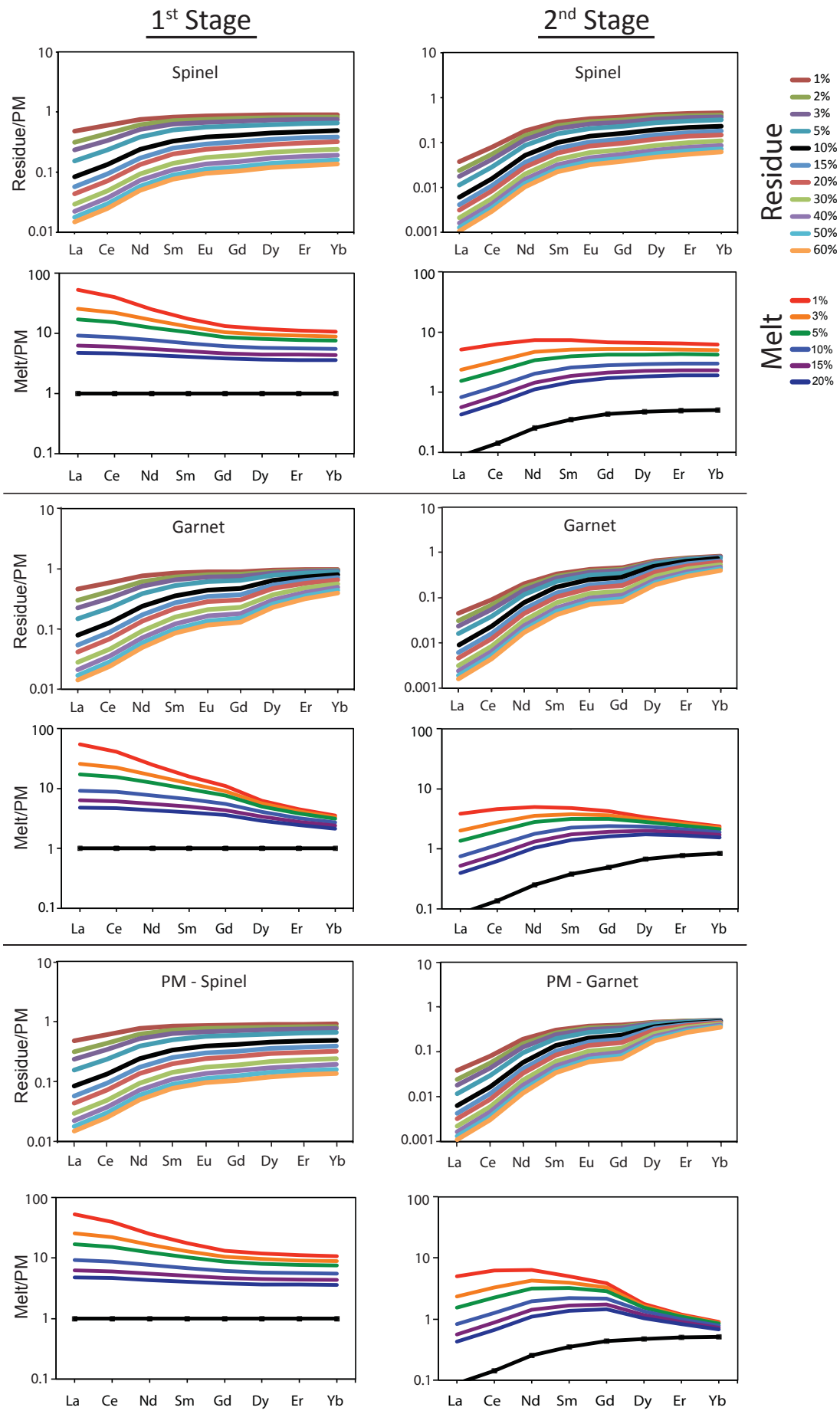
1st Stage
2nd Stage
Spinel
Spinel
Garnet
Garnet
PM - Spinel
PM - Garnet
Residue/PM
Melt/PM
La Ce Nd Sm Eu Gd Dy Er Yb
Residue
1%
2%
3%
5%
10%
15%
20%
30%
40%
50%
60%
Melt
1%
3%
5%
10%
15%
20%

Figure 3.10 Two-stage mantle melting models for Spinel – Spinel, Garnet – Garnet, Spinel – Garnet stability zones. The partition coefficients used in the models are found in Tables 3.2 and 3.3 along with their respective sources. The black line in the melt plots is the starting composition before melting.

The residual mantle (residue) was modeled using the batch melting equation where the composition of the solid (residue) is calculated:

$$C_S/C_0 = [1/(1 - F)] \times [(1 - PF/D_0)^{1/P}]$$

(from Shaw, 1970; in Rollinson, 1993). The trace element composition of the solid (or residue) (C_S) is determined as a function of the original composition (C_0), D_0 is the bulk partition coefficient at onset melting of the residual solid, and P is the bulk distribution coefficient of the minerals that make up the melt.

We show that with a two-stage melting model of a garnet-bearing lherzolite we can produce the REE signatures observed in the NEFTJ (Fig. 3.11). By melting low degrees (~1%) of an initial lherzolite that has 4% garnet we can reproduce the first steep enriched trend seen in Figure 3.5. In addition, the second stage melting of the residual mantle requires higher degrees of partial melting (>10%) in order exhibit the steepness of the originally depleted REE pattern. While our model includes 5% garnet in the second-stage melt of the residual mantle, the composition of the second-stage melt is indistinguishable between garnet and spinel lherzolite (Figure 3.11) because of the strong overlapping signature from garnet. Conversely, the first stage melting between spinel and garnet contain strong opposing signatures. Garnet progresses away from the source with a positive slope at ~45% angle where it is a factor of fractionation between La/Sm and Gd/Yb, while spinel progresses away from the source at a nearly vertical angle and is predominantly controlled by the fractionation of La/Sm. The Gd/Yb trend (Figure 3.11) of the natural samples matches the model by having garnet in the source. However, the composition of the second stage melt remains ambiguous in the models.

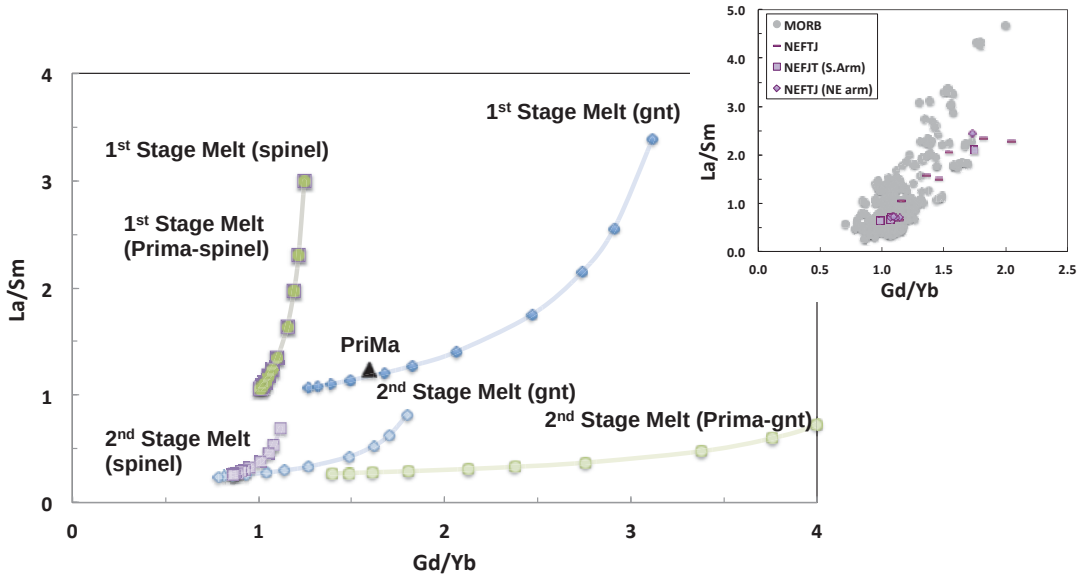

Figure 3.11 Two-Stage melting models from a Primitive Mantle source (Palme & O'Neill, 2014) for spinel and garnet lherzolites. The three models are coordinated by symbols: spinel to garnet (circle), spinel to spinel (square), garnet to garnet (diamond). Trace element Kd's used in the models are presented in Table 3.2. The inset graph demonstrates a positive trend for the lavas in the study (NEFTJ), with a MORB background, that our models attempted to recreate with two-stage melting.

H_2O correlates just as well with the degree of melting (Figure 3.12) and provides strong evidence that garnet is not the mineral that is controlling the volatile elements in the NEFTJ. The volatile elements must, therefore, be hosted in other silicate minerals. In addition, a plot (Figure 3.13) showing the relationship between Nd and Sr isotopic compositions reveals that there is mixing between a MORB composition and the Samoan plume as the lavas plot in the isotopic space between these two end-members (Workman et al., 2004, 2006; Jackson et al., 2007, 2010; Gale et al., 2013).

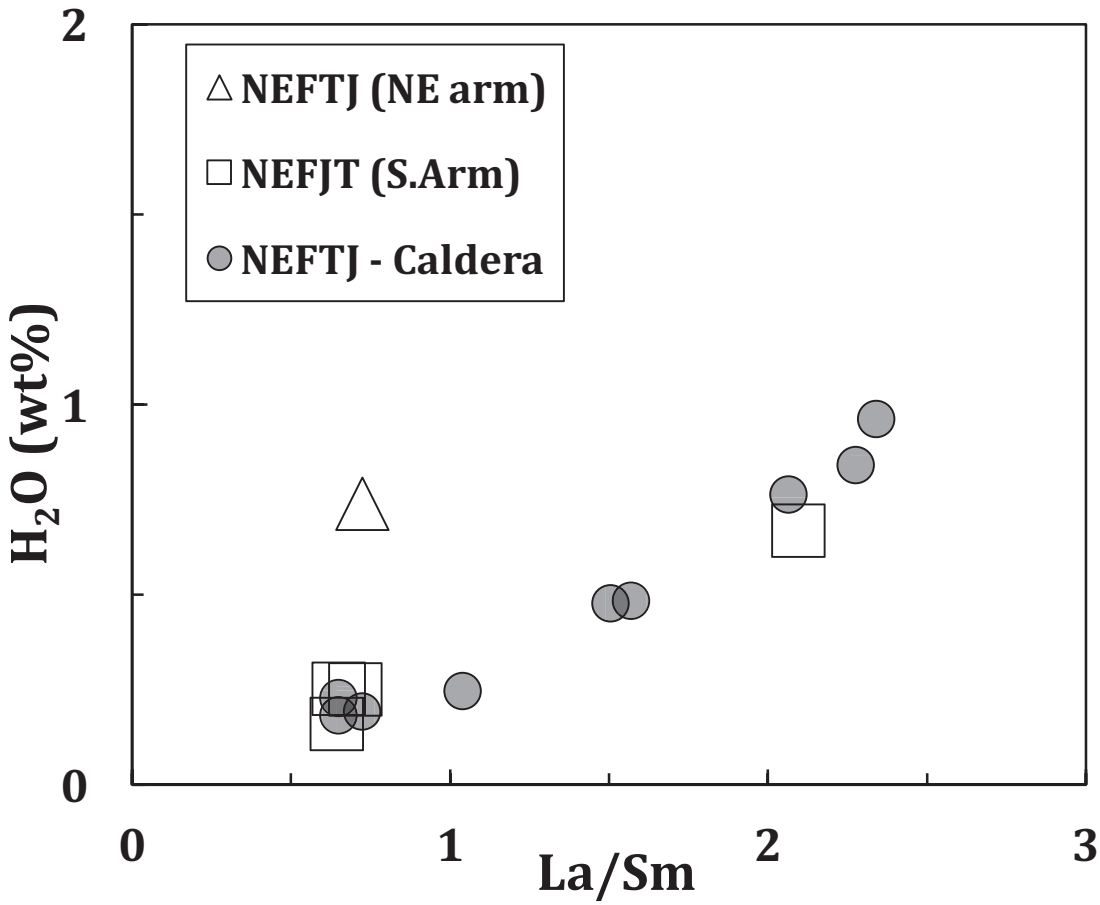

Figure 3.12 La/Sm ratio as a function of H_2O. This shows that there is a mixture of N-MORB type (La/Sm <1) with a more enriched source (La/Sm >1). With the exception of an outlier, the NEFTJ (NE arm), the data trends towards an increase in H_2O concentration as the magma source is enriched.

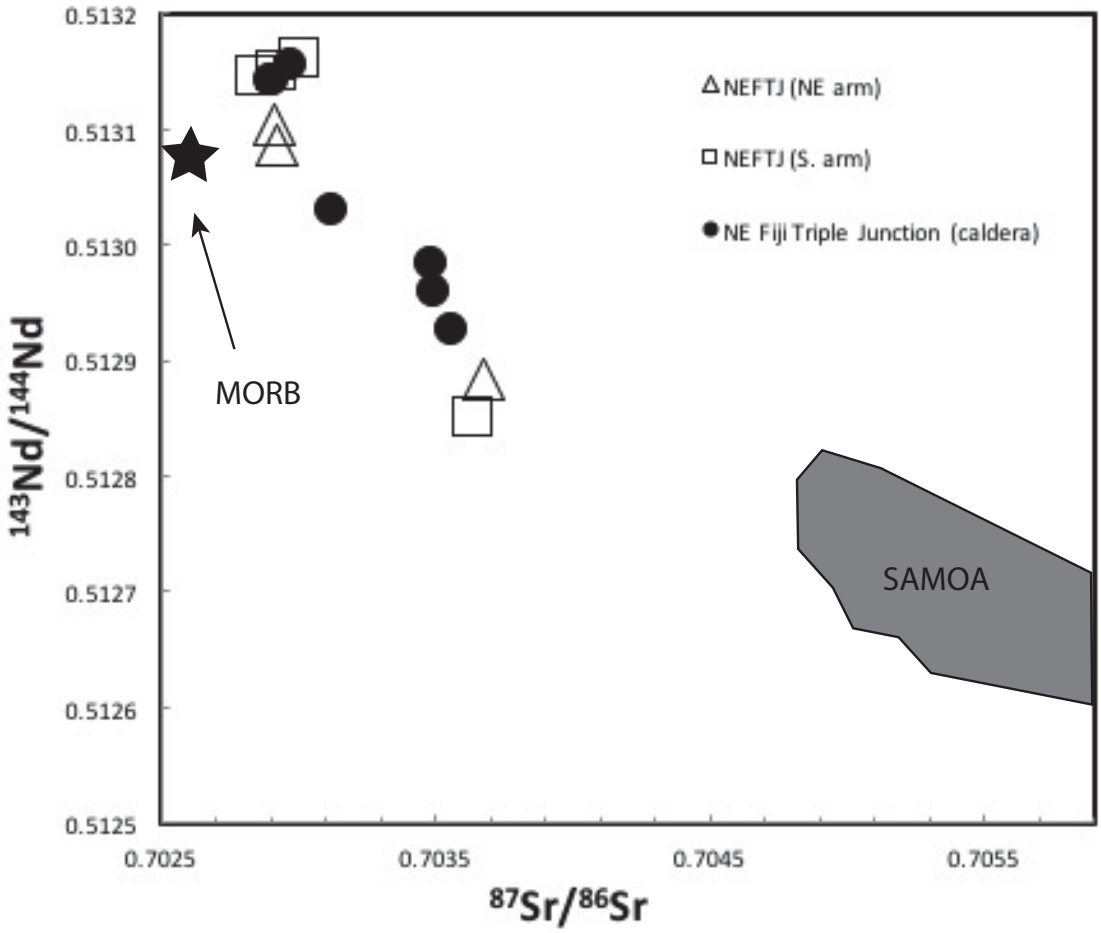

Figure 3.13 Plot showing Nd and Sr isotopic compositions for the lavas from the NEFTJ along with data for MORB and Samoa (Workman et al., 2004, 2006; Jackson et al., 2007, 2010; Gale et al., 2013).

We argue that, with the evidence presented through the major element, trace element, and volatile analyses, the observed intrusion of the Samoan plume beneath the Australian plate is permeating as far south as the NEFTJ (Fig. 3.14), through a toroidal flow or finger-like structures (Turner and Hawkesworth, 1998; Price et al., 2014). The Samoan plume melts low degrees of deep, heterogeneously mixed, mantle within a garnet-bearing stability field to produce an enriched melt with a depleted residue. The second melting of this residue requires a high degree of melting, as shown through our models, such as a spreading center, to produce the adequate depleted signature observed in the NEFTJ. This two-stage melting is consistent with our trace element modeling and

our conclusion that a depleted mantle enriched with Samoan plume melt generates the geochemical signatures for the lavas erupting at the NEFTJ.

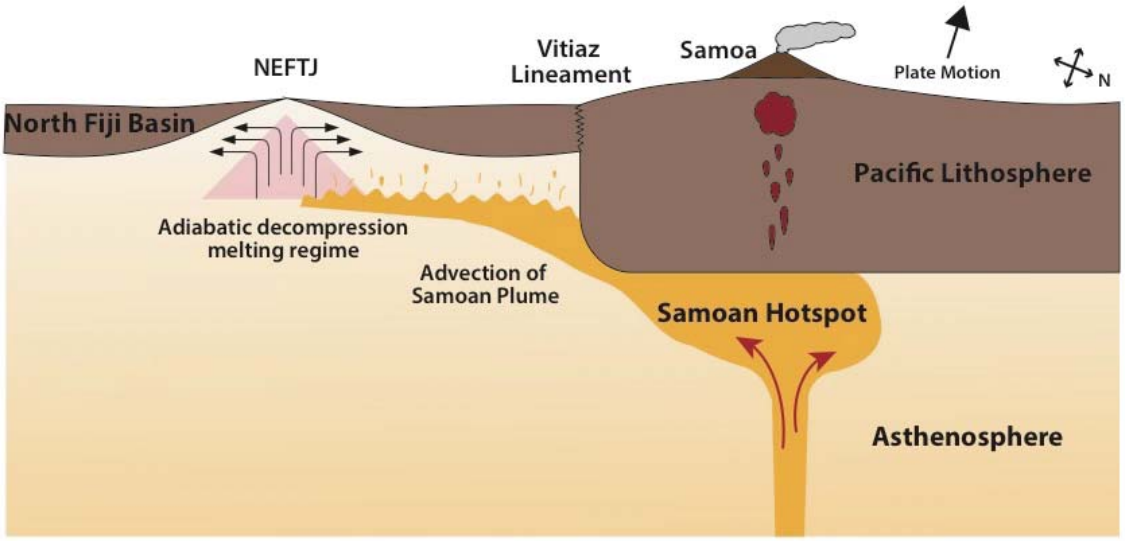

Figure 3.14 Schematic of the Samoan hotspot infiltrating the North Fiji Basin in the Australian Plate. Adiabatic upwelling of a depleted mantle MORB leads to a hotspot fingerprinting its geochemical signature upon many of the lavas that would otherwise have a depleted signature within both the North Fiji and Lau Basins. This fingerprint is recognizable through the use of isotope, trace, and volatile elements.

3.6 Conclusions

Here we provide data for major, trace, and volatile element values for a region of the North Fiji Basin not studied before. Based on these data, we have found that the lavas from the NFB (triple junction) have degassed upon eruption, affecting only the carbon dioxide in the lavas. Moreover, we discovered that the water content of these lavas exceeds that of MORB, along with enrichment in REEs (La/Sm and Gd/Yb) relative to MORB. We explain these geochemical signatures as a result of a mixture of melts from variable sources in the mantle. These sources are MORB mixing with an

enriched plume (OIB) source in the field of garnet lherzolite stability, followed by advection and adiabatic decompression melting within the spreading center. The discovery of these magma signatures beneath the NFB is important in understanding the heterogeneities of volatile elements in the mantle, in addition to linking deeper mantle and subsurface crustal processes.

3.7 References

Aggrey, K. E., Muenow, D. W., & Sinton, J. M. (1988) Volatile abundances in submarine glasses from the North Fiji and Lau back-arc basins. *Geochimica et Cosmochimica Acta*, *52*(10), 2501-2506.

Arndt, N. T. (1977) Partitioning of nickel between olivine and ultrabasic and basic komatiite liquids. *Carnegie Institution of Washington Yearbook*, 76, 553-557.

Asimow, P. D., & Langmuir, C. H. (2003) The importance of water to oceanic mantle melting regimes. *Nature*, 421(6925), 815-820.

Aubaud, C., Hirschmann, M. M., Withers, A. C., & Hervig, R. L. (2008) Hydrogen partitioning between melt, clinopyroxene, and garnet at 3 GPa in a hydrous MORB with 6 wt.% H2O. *Contributions to Mineralogy and Petrology*, 156(5), 607-625.

Auzende, J. M., Pelletier, B., & Eissen, J. P. (1995) The North Fiji Basin geology, structure, and geodynamic evolution. In: *Backarc Basins* (pp. 139-175). Springer US.

Beattie, P. (1993) Uranium–thorium disequilibria and partitioning on melting of garnet peridotite. *Nature*, 363, 63-65.

Blichert-Toft, J. & Albarède, F., (1997) The Lu-Hf isotope geochemistry of chondrites and the evolution of the mantle-crust system. *Earth Planet. Sci. Lett.* 148, 243-258.

Blichert-Toft, J., & Albarède, F. (2009) Mixing of isotopic heterogeneities in the Mauna Kea plume conduit. *Earth and Planetary Science Letters*, 282(1), 190-200.

Blundy, J. D., Robinson, J. A. C., & Wood, B. J. (1998) Heavy REE are compatible in clinopyroxene on the spinel lherzolite solidus. *Earth and Planetary Science Letters*, 160(3), 493-504.

Bodinier, J. L., Dupuy, C., Dostal, J., & Merlet, C. (1987) Distribution of trace transition elements in olivine and pyroxenes from ultramafic xenoliths: Application of microprobe analysis. *American Mineralogist*, 72(9-10), 902-913.

Cartigny, P., Pineau, F., Aubaud, C., & Javoy, M. (2008) Towards a consistent mantle carbon flux estimate: Insights from volatile systematics (H 2 O/Ce, δD, CO 2/Nb) in the North Atlantic mantle (14 N and 34 N). *Earth and Planetary Science Letters*, *265*(3), 672-685.

Davis, F. A., Tangeman, J. A., Tenner, T. J., & Hirschmann, M. M. (2009) The composition of KLB-1 peridotite. *American Mineralogist*, 94(1), 176-180.

Dixon, J. E., Stolper, E. M., & Holloway, J. R. (1995) An experimental study of water and carbon dioxide solubilities in mid-ocean ridge basaltic liquids. Part I: calibration and solubility models. *Journal of Petrology*, 36(6), 1607-1631.

Dixon, J. E. & Stolper, E. M. (1995) An experimental study of water and carbon dioxide solubilities in mid-ocean ridge basaltic liquids. Part II: applications to degassing. *Journal of Petrology*, 36(6), 1633-1646.

Dixon, J. E. (1997) Degassing of alkalic basalts. *American Mineralogist*, 82, 368-378.

Dixon, J. E., & Clague, D. A. (2001) Volatiles in basaltic glasses from Loihi Seamount, Hawaii: Evidence for a relatively dry plume component. *Journal of Petrology*, 42(3), 627-654.

Dixon, J. E., Leist, L., Langmuir, C., & Schilling, J. G. (2002) Recycled dehydrated lithosphere observed in plume-influenced mid-ocean-ridge basalt. *Nature*, 420(6914), 385-389.

Dostal, J., Dupuy, C., Carron, J. P., De Kerneizon, M. L. G., & Maury, R. C. (1983) Partition coefficients of trace elements: application to volcanic rocks of St. Vincent, West Indies. *Geochimica et Cosmochimica Acta*, 47(3), 525-533.

Eiler, J. (2003) Inside the subduction factory. Washington DC American Geophysical Union Geophysical Monograph Series, 138.

Eissen, J. P., Nohara, M., Cotten, J., & Hirose, K. (1994) North Fiji Basin basalts and their magma sources: Part I. Incompatible element constraints. *Marine Geology*, 116(1), 153-178.

Ewart, A., Collerson, K. D., Regelous, M., Wendt, J. I., & Niu, Y. (1998) Geochemical evolution within the Tonga-Kermadec-Lau arc-back-arc systems: the role of varying mantle wedge composition in space and time. *Journal of Petrology*, 39(3), 331-368.

Falvey, D. A. (1978) Analysis of palaeomagnetic data from the New Hebrides. *Bulletin - Australian Society of Exploration Geophysicists*, 9(3), 117-123.

Farley, K. A., Natland, J. H., & Craig, H. (1992) Binary mixing of enriched and undegassed (primitive?) mantle components (He, Sr, Nd, Pb) in Samoan lavas. *Earth and Planetary Science Letters*, 111(1), 183-199.

Foley, S. F., Barth, M. G., & Jenner, G. A. (2000) Rutile/melt partition coefficients for trace elements and an assessment of the influence of rutile on the trace element characteristics of subduction zone magmas. *Geochimica et Cosmochimica Acta*, 64(5), 933-938.

Fujimaki, H., Tatsumoto, M., & Aoki, K. I. (1984) Partition coefficients of Hf, Zr, and REE between phenocrysts and groundmasses. In *Lunar and Planetary Science Conference Proceedings* (Vol. 14, pp. B662-B672).

Gaetani, G. A., Kent, A. J., Grove, T. L., Hutcheon, I. D., & Stolper, E. M. (2003) Mineral/melt partitioning of trace elements during hydrous peridotite partial melting. *Contributions to Mineralogy and Petrology*, 145(4), 391-405.

Gale, A., Dalton, C. A., Langmuir, C. H., Su, Y., & Schilling, J. G. (2013) The mean composition of ocean ridge basalts. *Geochemistry, Geophysics, Geosystems*, 14(3), 489-518.

Giardini, D., & Woodhouse, J. H. (1986) Horizontal shear flow in the mantle beneath the Tonga arc. *Nature*, 319, 551-555.

Gill, J. B. & Gorton, M. P. (1975) A proposed geological and geochemical history of Eastern Melanesia. *The Western Pacific: Island Arcs, Marginal Seas and Geochemistry*, P.T. Coleman, ed., University of Western Australia Press, Perth, W.A., 543-566.

Green, T. H., & Pearson, N. J. (1987) An experimental study of Nb and Ta partitioning between Ti-rich minerals and silicate liquids at high pressure and temperature. *Geochimica et Cosmochimica Acta*, 51(1), 55-62.

Green, T. H., Sie, S. H., Ryan, C. G., & Cousens, D. R. (1989) Proton microprobe-determined partitioning of Nb, Ta, Zr, Sr and Y between garnet, clinopyroxene and basaltic magma at high pressure and temperature. *Chemical Geology*, 74(3-4), 201-216.

Gribble, R. F., Stern, R. J., Bloomer, S. H., Stüben, D., O'Hearn, T., & Newman, S. (1996) MORB mantle and subduction components interact to generate basalts in the southern Mariana Trough back-arc basin. *Geochimica et Cosmochimica Acta*, 60(12), 2153-2166.

Grove, T., Parman, S., Bowring, S., Price, R., & Baker, M. (2002) The role of an H2O-rich fluid component in the generation of primitive basaltic andesites and andesites from the Mt. Shasta region, N California. *Contributions to Mineralogy and Petrology*, 142(4), 375-396.

Hall, R. (2002) Cenozoic geological and plate tectonic evolution of SE Asia and the SW Pacific: computer-based reconstructions, model and animations. *Journal of Asian Earth Sciences*, 20(4), 353-431.

Halliday, A. N., Lee, D. C., Tommasini, S., Davies, G. R., Paslick, C. R., Fitton, J. G., & James, D. E. (1995) Incompatible trace elements in OIB and MORB and source enrichment in the sub-oceanic mantle. *Earth and Planetary Science Letters*, 133(3), 379-395.

Hart, S., & Blusztajn, J. (2006) Age and geochemistry of the mafic sills, ODP site 1276, Newfoundland margin. *Chemical Geology* 235:222–237. doi: 10.1016/j.chemgeo.2006.07.001

Hart, S. E., & Brooks, C. (1974) Clinopyroxene-matrix partitioning of K, Rb, Cs, Sr and Ba. *Geochimica et Cosmochimica Acta*, 38(12), 1799-1806.

Hart, S. R., & Davis, K. E. (1978) Nickel partitioning between olivine and silicate melt. *Earth and Planetary Science Letters*, 40(2), 203-219.

Hart, S. R., & Dunn, T. (1993) Experimental cpx/melt partitioning of 24 trace elements. *Contributions to Mineralogy and Petrology*, 113(1), 1-8.

Hauri, E. H., Wagner, T. P., & Grove, T. L. (1994) Experimental and natural partitioning of Th, U, Pb and other trace elements between garnet, clinopyroxene and basaltic melts. *Chemical Geology*, 117(1), 149-166.

Hauri, E. (2002) SIMS analysis of volatiles in silicate glasses, 2: isotopes and abundances in Hawaiian melt inclusions. *Chemical Geology*, 183(1), 115-141.

Hauri, E., Wang, J., Dixon, J. E., King, P. L., Mandeville, C., & Newman, S. (2002) SIMS analysis of volatiles in silicate glasses: 1. Calibration, matrix effects and comparisons with FTIR. *Chemical Geology*, 183(1), 99-114.

Hirth, G., & Kohlstedt, D. L. (1996) Water in the oceanic upper mantle: implications for rheology, melt *extraction and the evolution of the lithosphere. Earth and Planetary Science Letters, 144*(1), 93-108.

Hofmann, A. W. (1988) Chemical differentiation of the Earth: the relationship between mantle, continental crust, and oceanic crust. *Earth and Planetary Science Letters*, 90(3), 297-314.

Hofmann, A. W. (1997) Mantle geochemistry: the message from oceanic volcanism. *Nature*, 385(6613), 219-229.

Huchon, P., Gracia, E., Ruellan, E., Joshima, M., & Auzende, J. (1994) Kinematics of active spreading in the central North Fiji Basin (Southwest Pacific). *Marine Geology,* 116(1-2), 69-87.

Huppert, H. E., Sparks, R. S. J., & Turner, J. S. (1982) Effects of volatiles on mixing in calc-alkaline magma systems. *Nature*, 297(5867), 554-557.

Irving, A. J., & Frey, F. A. (1978) Distribution of trace elements between garnet megacrysts and host volcanic liquids of kimberlitic to rhyolitic composition. *Geochimica et Cosmochimica Acta*, 42(6), 771-787.

Jackson, M.G., & Carlson, R.W. (2012) Homogeneous superchondritic 142Nd/144Nd in the mid-ocean ridge basalt and ocean island basalt mantle. *Geochemistry, Geophysics, Geosystems*, 13(6).

Jackson, M.G., & Hart, S. (2006) Strontium isotopes in melt inclusions from Samoan basalts: Implications for heterogeneity in the Samoan plume. *Earth and Planetary Science Letters* 245:260–277. doi: 10.1016/j.epsl.2006.02.040

Jackson, M. G., Hart, S. R., Koppers, A. A., Staudigel, H., Konter, J., Blusztajn, J., Kurz, M., & Russell, J. A. (2007) The return of subducted continental crust in Samoan lavas. *Nature*, 448(7154), 684-687.

Jackson, M. G., Hart, S. R., Konter, J. G., Koppers, A. A., Staudigel, H., Kurz, M. D., Blusztajn, J., & Sinton, J. M. (2010) Samoan hot spot track on a "hot spot highway": Implications for mantle plumes and a deep Samoan mantle source. *Geochemistry, Geophysics, Geosystems*, 11(12).

James, A. & Falvey, D.A. (1978) Analysis of palaeomagnetic data from Viti Levu, Fiji. *Bulletin - Australian Society of Exploration Geophysicists,* 9(3), 115-117.

Javoy, M., Pineau, F., & Iiyama, I. (1978) Experimental determination of the isotopic fractionation between gaseous CO2 and carbon dissolved in tholeiitic magma. *Contributions to Mineralogy and Petrology*, 67(1), 35-39.

Javoy, M., & Pineau, F. (1991) The volatiles record of a "popping" rock from the Mid-Atlantic Ridge at 14 N: chemical and isotopic composition of gas trapped in the vesicles. *Earth and Planetary Science Letters*, 107(3), 598-611.

Jenner, G. A., Foley, S. F., Jackson, S. E., Green, T. H., Fryer, B. J., & Longerich, H. P. (1993) Determination of partition coefficients for trace elements in high pressure-temperature experimental run products by laser ablation microprobe-inductively coupled plasma-mass spectrometry (LAM-ICP-MS). *Geochimica et Cosmochimica Acta*, 57(23-24), 5099-5103.

Jenner, F. E., & O'Neill, H. S. C. (2012) Analysis of 60 elements in 616 ocean floor basaltic glasses. *Geochemistry, Geophysics, Geosystems*, 13(2).

Johnson, K. T., & Sinton, J. M. (1990) Petrology, tectonic setting, and the formation of back-arc basin basalts in the North Fiji Basin. *Geol. Jahrb. Reihe D*, 92, 517-545.

Kelemen, P. B., Joyce, D. B., Webster, J. D., & Holloway, J. R. (1990) Reaction between ultramafic rock and fractionating basaltic magma II. Experimental investigation of reaction between olivine tholeiite and harzburgite at 1150–1050 C and 5 kb. *Journal of Petrology*, 31(1), 99-134.

Kelemen, P. B., Hart, S. R., & Bernstein, S. (1998) Silica enrichment in the continental upper mantle via melt/rock reaction. *Earth and Planetary Science Letters*, 164(1), 387-406.

Kelemen, P. B., Shimizu, N., & Dunn, T. (1993) Relative depletion of niobium in some arc magmas and the continental crust: partitioning of K, Nb, La and Ce during melt/rock reaction in the upper mantle. *Earth and Planetary Science Letters*, 120(3-4), 111-134.

Kelemen, P. B., Yogodzinski, G. M., & Scholl, D. W. (2003) Along-Strike Variation in the Aleutian Island Arc: Genesis of High Mg# Andesite and Implications for Continental Crust. *Inside the subduction factory*, 223-276.

Kinzler, R. J., Grove, T. L., & Recca, S. I. (1990) An experimental study on the effect of temperature and melt composition on the partitioning of nickel between olivine and silicate melt. *Geochimica et Cosmochimica Acta*, 54(5), 1255-1265.

Koleszar, A. M., Saal, A. E., Hauri, E. H., Nagle, A. N., Liang, Y., & Kurz, M. D. (2009) The volatile contents of the Galapagos plume; evidence for H 2 O and F open system behavior in melt inclusions. *Earth and Planetary Science Letters*, 287(3), 442-452.

Langmuir, C. H., A. Bezos, S. Escrig, & S. W. Parman (2006) Chemical systematics and hydrous melting of the mantle in back-arc basins, Back-Arc Spreading Systems: Geological, Biological, Chemical, and Physical Interactions, Geophys. Monogr., edited by D. M. Christie, et al., vol. 166, 87 pp., AGU, Washington, D. C.

Larsen, L. M. (1979) Distribution of REE and other trace elements between phenocrysts and peralkaline undersaturated magmas, exemplified by rocks from the Gardar igneous province, south Greenland. *Lithos*, 12(4), 303-315.

LaTourrette, T. Z., & Burnett, D. S. (1992) Experimental determination of U and Th partitioning between clinopyroxene and natural and synthetic basaltic liquid. *Earth and Planetary Science Letters*, 110(1-4), 227-244.

le Roux, P. J., Shirey, S. B., Hauri, E. H., Perfit, M. R., & Bender, J. F. (2006) The effects of variable sources, processes and contaminants on the composition of

northern EPR MORB (8–10 N and 12–14 N): Evidence from volatiles (H 2 O, CO 2, S) and halogens (F, Cl). *Earth and Planetary Science Letters*, 251(3), 209-231.

Luhr, J., & Carmichael, I. S. E. (1984) Volatiles and trace element partitioning in the El Chichon trachyandesite, *EOS,* 65, 299.

Lupton, J. E., Arculus, R. J., Greene, R. R., Evans, L. J., & Goddard, C. I. (2009) Helium isotope variations in seafloor basalts from the Northwest Lau Back-arc Basin: Mapping the influence of the Samoan hotspot. *Geophysical Research Letters*. doi: 10.1029/2009GL039468

Lytle, M. L., Kelley, K. A., Hauri, E. H., Gill, J. B., Papia, D., & Arculus, R. (2012) Tracing mantle sources and Samoan influence in the northwestern Lau back-arc basin. *Geochemistry Geophysics Geosystems* 13:Q10019 doi: 10.1029/2012GC004233

Macdonald, G. A., & Katsura, T. (1964) Chemical composition of Hawaiian lavas. *Journal of petrology*, 5(1), 82-133.

Mackwell, S. J., & Kohlstedt, D. L. (1990) Diffusion of hydrogen in olivine: implications for water in the mantle. *Journal of Geophysical Research: Solid Earth*, 95(B4), 5079-5088.

Macpherson, C. G., Hilton, D. R., Sinton, J. M., Poreda, R. J., & Craig, H. *(*1998*) H*igh $^{3}He/^{4}He$ ratios in the Manus backarc basin: Implications for mantle mixing and the origin of plumes in the western Pacific Ocean, *Geology, 26(*11*),* 1007–1010.

Malahoff, A., Feden, R. H., & Fleming, H. S. (1982a) Magnetic anomalies and tectonic fabric of marginal basins north of New Zealand. *Journal of Geophysical Research,* 87, 4109-4125.

Malahoff, A., Hammond, S. R., Naughton, J. J., Keeling, D. L., & Richmond, R. N. (1982b) Geophysical evidence for post-Miocene rotation of the island of Viti Levu, Fiji, and its relationship to the tectonic development of the North Fiji Basin. *Earth and Planetary Science Letters,* 57(2), 398-414.

Mathez, E. A., & Delaney, J. R. (1981) The nature and distribution of carbon in submarine basalts and peridotite nodules. *Earth and Planetary Science Letters*, 56, 217-232.

McCulloch, M.T., & Gamble, J.A. (1991) Geochemical and geodynamical constraints on subduction zone magmatism. *Earth and Planetary Science Letters*, *102*(3), 358-374.

McDade, P., Blundy, J. D., & Wood, B. J. (2003) Trace element partitioning on the Tinaquillo Lherzolite solidus at 1.5 GPa. *Physics of the Earth and Planetary Interiors*, 139(1), 129-147.

Melson, W. G., O'Hearn, T., & Jarosewich, E. (2002) A data brief on the Smithsonian abyssal volcanic glass data file. *Geochemistry, Geophysics, Geosystems*, 3(4).

Métrich, N., & Wallace, P. J. (2008) Volatile abundances in basaltic magmas and their degassing paths tracked by melt inclusions. *Reviews in mineralogy and geochemistry*, 69(1), 363-402.

Michael, P. (1995) Regionally distinctive sources of depleted MORB: evidence from trace elements and H 2 O. *Earth and Planetary Science Letters*, 131(3), 301-320.

Musgrave, R. J., & Firth, J. V. (1999) Magnitude and timing of New Hebrides Arc rotation: paleomagnetic evidence from Nendo, Solomon Islands. *Journal of Geophysical Research: Solid Earth (1978–2012)*, 104(B2), 2841-2853.

Newman, S., Stolper, E., & Stern, R. (2000) H_2O and CO_2 in magmas from the Mariana arc and back arc systems. *Geochemistry, Geophysics, Geosystems*, 1(5), doi:10.1029/1999GC000027

Newman, S. & Lowenstern, J. B. (2002) VolatileCalc: a silicate melt–H_2O–CO_2 solution model written in Visual Basic for Excel. *Computers & Geosciences*, 28(5), 597-604.

Nicholls, I. A., & Harris, K. L. (1980) Experimental rare earth element partition coefficients for garnet, clinopyroxene and amphibole coexisting with andesitic and basaltic liquids. *Geochimica et Cosmochimica Acta*, 44(2), 287-308.

Norman, M. D., Pearson, N. J., Sharma, A., & Griffin, W. L. (1996) Quantitative analysis of trace elements in geological materials by laser ablation ICPMS: instrumental operating conditions and calibration values of NIST glasses. *Geostandards Newsletter*, 20(2), 247-261.

Palme, H. & O'Neill, H. St.C. (2014) Geochemical estimates of mantle compostion. In: Holland H.D. and Turekian K.K. (eds.) *Treatise on Geochemistry*, Second Edition, vol. 3, pp. 1-39.

Pearce, J. A., Ernewein, M., Bloomer, S. H., Parson, L. M., Murton, B. J., & Johnson, L. E. (1994) Geochemistry of Lau Basin volcanic rocks: influence of ridge segmentation and arc proximity. *Geological Society, London, Special Publications*, 81(1), 53-75.

Pearce, J. A., & Stern, R.J . (2006) Origin of back-arc basin magmas: Trace element and isotope perspectives. In: Chemical Systematics and Hydrous Melting of the Mantle in Back-Arc Basins, edited by D.M. Christie et al., pp 63–86, AGU, Washington, D. C.

Philpotts, J. A., & Schnetzler, C. C. (1970a) Phenocryst-matrix partition coefficients for K, Rb, Sr and Ba, with applications to anorthosite and basalt genesis. *Geochimica et Cosmochimica Acta*, 34(3), 307-322.

Philpotts, J. A., & Schnetzler, C. C. (1970b) Potassium, rubidium, strontium, barium, and rare-earth concentrations in lunar rocks and separated phases. *Science*, 167(3918), 493-495.

Poreda, R. J., & Craig, H. (1992) He and Sr isotopes in the Lau Basin mantle: depleted and primitive mantle components. *Earth and Planetary Science Letters* 113:487–493.

Price, A. A., Jackson, M. G., Blichert-Toft, J., Hall, P. S., Sinton, J. M., Kurz, M. D., & Blusztajn, J. (2014) Evidence for a broadly distributed Samoan-plume signature in the northern Lau and North Fiji Basins. *Geochemistry, Geophysics, Geosystems*, 15(4), 986-1008.

Price, R. C., Johnson, L. E., & Crawford, A. J. (1990). Basalts of the North Fiji Basin: the generation of back arc basin magmas by mixing of depleted and enriched mantle sources. *Contributions to Mineralogy and Petrology*, 105(1), 106-121.

Rapp, R. P., Shimizu, N., Norman, M. D., & Applegate, G. S. (1999) Reaction between slab-derived melts and peridotite in the mantle wedge: experimental constraints at 3.8 GPa. *Chemical Geology*, 160(4), 335-356.

Rollinson, H. R. (1993) *Using geochemical data: evaluation, presentation, interpretation*. Longman Scientific & Technical, Harlow, 103-170.

Ruscitto, D. M., Wallace, P. J., Cooper, L. B., & Plank, T. (2012) Global variations in H2O/Ce: 2. Relationships to arc magma geochemistry and volatile fluxes. *Geochemistry, Geophysics, Geosystems*, 13(3).

Saal, A. E., Hauri, E. H., Langmuir, C. H., & Perfit, M. R. (2002) Vapor undersaturation in primitive mid-ocean ridge basalt and the volatile content of the Earth's upper mantle. *Nature,* 419(6906), 451-455.

Salters, V. J., Longhi, J. E., & Bizimis, M. (2002) Near mantle solidus trace element partitioning at pressures up to 3.4 GPa. *Geochemistry, Geophysics, Geosystems*, 3(7), 1-23.

Schnetzler, C. C., & Philpotts, J. A. (1970) Partition coefficients of rare-earth elements between igneous matrix material and rock-forming mineral phenocrysts—II. *Geochimica et Cosmochimica Acta*, 34(3), 331-340.

Shaw, D. M. (1970) Trace element fractionation during anatexis. *Geochimica et Cosmochimica Acta*, *34*(2), 237-243.

Shaw, A. M., Hilton, D. R., Macpherson, C. G., Sinton, J. M. (2004) The CO2-He-Ar-H2O systematics of the Manus back-arc basin: Resolving source composition from degassing and contamination effects. Geochimica Et Cosmochimica Acta. 68:1837-1856.

Shimizu, N., & Kushiro, I. (1975) The partitioning of rare earth elements between garnet and liquid at high pressures: preliminary experiments. *Geophysical Research Letters*, 2(10), 413-416.

Shishkina, T. A., Botcharnikov, R. E., Holtz, F., Almeev, R. R., & Portnyagin, M. V. (2010) Solubility of H 2 O-and CO 2-bearing fluids in tholeiitic basalts at pressures up to 500MPa. *Chemical Geology*, 277(1), 115-125.

Simons, K., Dixon, J., Schilling, J. G., Kingsley, R., & Poreda, R. (2002) Volatiles in basaltic glasses from the Easter-Salas y Gomez Seamount Chain and Easter Microplate: Implications for geochemical cycling of volatile elements. *Geochemistry, Geophysics, Geosystems*, 3(7), 1-29.

Sinton, J. M., & Fryer, P. (1987) Mariana Trough lavas from 18 N: Implications for the origin of back arc basin basalts. *Journal of Geophysical Research: Solid Earth*, 92(B12), 12782-12802.

Sinton, J. M., Price, R. C., Johnson, K. T., Staudigel, H., & Zindler, A. (1994) Petrology and geochemistry of submarine lavas from the Lau and North Fiji back-arc basins. In *Basin formation, ridge crest processes, and metallogenesis in the North Fiji Basin* (pp. 119-135). Springer Berlin Heidelberg.

Stolper, E., & Newman, S. (1994) The role of water in the petrogenesis of Mariana trough magmas. *Earth and Planetary Science Letters*, 121(3), 293-325.

Stosch, H. G. (1982) Rare earth element partitioning between minerals from anhydrous spinel peridotite xenoliths. *Geochimica et Cosmochimica Acta*, 46(5), 793-811.

Tanaka, T., Togashi, S., Kamioka, H., Amakawa, H., Kagami, H., Hamamoto, T., Yuhara, M., Orihashi, Y, Yoneda, S., Shimizu, H., Kunimaru, T., Takahashi, K., Yanagi, T., Nakano, T., Fujimaki, H., Shinjo, R., Asahara, Y., Tanimizu, M. & Dragusanu, C. (2000) JNdi-1: a neodymium isotopic reference in consistency with LaJolla neodymium. *Chemical Geology*, *168*(3-4), 279-281.

Turner, S., & Hawkesworth, C. (1998) Using geochemistry to map mantle flow beneath the Lau Basin. *Geology*, 26(11), 1019-1022.

Volpe, A. M., Macdougall, J. D., & Hawkins, J. W. (1988) Lau Basin basalts (LBB): trace element and Sr Nd isotopic evidence for heterogeneity in backarc basin mantle. *Earth and Planetary Science Letters*, 90(2), 174-186.

Volpe, A. M., Macdougall, J. D., Lugmair, G. W., Hawkins, J. W., & Lonsdale, P. (1990) Fine-scale isotopic variation in Mariana Trough basalts: Evidence for heterogeneity and a recycled component in backarc basin mantle. *Earth and Planetary Science Letters*, 100(1), 251-264.

Weaver, B. L. (1991) The origin of ocean island basalt end-member compositions: trace element and isotopic constraints. *Earth and Planetary Science Letters*, 104(2), 381-397.

White, W.M., & Patchett, J. (1984) Hf-Nd-Sr isotopes and incompatible element abundances in island arcs: implications for magma origins and crust-mantle evolution. *Earth and Planetary Science Letters* 67:167–185.

Workman, R. K., Hart, S. R., Jackson, M., Regelous, M., Farley, K. A., Blusztajn, J., Kurz, M., & Staudigel, H. (2004) Recycled metasomatized lithosphere as the origin of the Enriched Mantle II (EM2) end-member: Evidence from the Samoan Volcanic Chain. *Geochemistry, Geophysics, Geosystems*, 5(4).

Workman, R. K., Hauri, E., Hart, S. R., Wang, J., & Blusztajn, J. (2006) Volatile and trace elements in basaltic glasses from Samoa: Implications for water distribution in the mantle. *Earth and Planetary Science Letters*, 241(3), 932-951.

Wright, E., & White, W. M. (1987) The origin of Samoa: new evidence from Sr, Nd, and Pb isotopes. *Earth and Planetary Science Letters*, 81(2), 151-162.

4 Geodynamic Implications for Zonal and Meridional Isotopic Patterns Across the northern Lau and North Fiji Basins

Author's Preface

The following chapter is a published journal article in Geochemistry, Geophysics, Geosystems, volume 18, issue 3, p 1013-1042 (March 2017). The distribution of work is highlighted in a table 'List of Contributions/Contributors – Division of Labor in co-authored articles' (page iv). I contributed to the concept and design of the project. The planning and implementation of the project, where I contributed in how the project was going to be executed, analysis and interpretation of the data, and writing of the article. The written portion went through various iterations in which the people listed in the table contributed. Chapter 3 and Chapter 4 are

complementary, and as such, Allison Price (who had the overall responsibility for the project in Chapter 4) had similar input into Chapter 3 (where I had the overall responsibility).

Pages 119-174 of this thesis have been removed as they contain published material under copyright. Removed contents published as:

Price, A. A., Jackson, M. G., Blichert-Toft, J., Kurz, M. D., Gill, J., Blusztajn, J., Jenner, F., Brens, R., and Arculus, R. (2017), Geodynamic implications for zonal and meridional isotopic patterns across the northern Lau and North Fiji Basins, Geochemistry, Geophysics, Geosystems, vol. 18, no. 3, pp. 1013– 1042, doi.org/10.1002/2016GC006651.

5 An experimental approach to understanding the genesis of silicic arc magmas: A case study from the Late volcano in the Tonga-Kermadec arc

Abstract

Late volcano is located slightly north of the center of the Tonga-Kermadec island arc. The lavas present on the volcano form the beginning of a trend towards more geochemically evolved arc magmas observed in the neighboring volcanoes. Basaltic andesite is the dominant type of rock on this volcano, although minor andesitic flows have also been observed. The phenocryst assemblages of the basaltic andesite lavas from Late are commonly plagioclase ± clinopyroxene ± orthopyroxene. We present new

analytical and experimental data to constrain the depth and pressures at which the geochemically evolved arc magmas from Late volcano were formed. Data suggest that crystal fractionation was the dominant process and this study also identifies the most likely fractionating assemblage. Phase relations from the natural samples were determined for a basaltic andesite (55.39 wt% SiO_2). The mineral phase assemblages and the interstitial matrix of the natural basaltic andesites were reproduced experimentally under H_2O-saturated conditions for all pressures greater than 1atm. The phenocryst assemblages in the experiments at high pressures are dominantly garnet ± clinopyroxene ± plagioclase (and varying proportions of glass). All of the experiments performed at 1atm are anhydrous, with phenocryst assemblages that are commonly clinopyroxene ± plagioclase ± ilmenite (and glass). Pyroxene thermobarometry suggests crystallization at 1020-1070 ^{o}C and depth that, by analogy to neighboring volcanoes, is between 0.8-1.8 kbar.

5.1 Introduction

Intra-oceanic arc lavas allow us to peer into processes that are occurring deep within the Earth but cannot access otherwise. Unlike many continental arcs, the lavas that are regularly generated at intra-oceanic arcs have not evolved so strongly and therefore represent a more reliable link to mantle processes. However, when an arc product does not prescribe to the expectations of mafic lavas production, it becomes a matter of much debate resulting in numerous models to explain this result (Wade et al., 2005; Smith et al., 2006, 2010; Brophy, 2008; Reubi & Blundy, 2009). In particular, arguments have focused on the role of fractional crystallization of basaltic magmas in contrast to partial melting of lower crustal amphibolites with or without magma-mixing (Petford & Gallagher, 2001; Dufek & Bergantz, 2005; Annen et al., 2006). However,

fractional crystallization of basalt and partial melting of lower crustal amphibolites can be indistinguishable in major element and trace element characteristics of felsic lavas (Brophy, 2008). Therefore, understanding how evolved magmas are produced in an intra-oceanic arc is the crucial first step in understanding complex subduction zone processes.

Most previous studies of the Tonga-Kermadec arc have focused on along-arc characterization (e.g., Ewart et al., 1973; Ewart & Hawkesworth, 1987; Gamble et al., 1993; Turner et al., 1997, 2000, 2009; Turner & Hawkesworth, 1997; Ewart et al., 1998; George et al., 2005; Hergt & Woodhead, 2007; Castillo et al., 2009) with specific studies in this region mostly focusing on either the Taupo volcanic zone and the Kermadec arc (e.g., Gamble et al, 1997; Smith et al., 2003, 2006, 2009; Haase et al., 2006, 2011, 2014; Cameron et al., 2010; Shane & Wright, 2011; Timm et al., 2011; Price et al., 2012). Recently, two studies analyzed Late's neighboring volcanic islands, Tofua and Fonualei (Caulfield et al., 2012; Turner et al., 2012). Tofua has predominantly erupted basaltic andesite lavas, with minor dacitic lavas, whereas the eruptive products of Fonualei have mainly been dacitic for the last 165 years, with basaltic andesite and andesitic basal flows recorded as underlying the current dacitic flows. The petrogenetic model proposed for these two volcanic islands based on combining linear least-square models with mineralogy and major and trace element chemistry, is consistent with the general model proposed by Ewart et al. (1973) which suggests that the genesis of evolved lavas in the Tongan arc is due to low-pressure fractional crystallization of the parental magmas. Therefore, these two islands can be combined with data from Late allow us to form an evolutionary geochemical array for these more evolved lavas in the Tonga-Kermadec island arc.

In this chapter, we report experimental results on a natural basaltic andesite to yield preliminary constraints for an evolved lava within an island arc (Tonga-

Kermadec) that is better known for some of the most primitive lavas found in oceanic island arcs. This principal aim of the study was to recreate the temperature and pressure constraints, reported by previous work, in which these rocks are formed and to reproduce the phase assemblage observed in the natural sample. Our experiments aim to build on the theoretical work of these earlier researchers, although, as discussed in this chapter, some unforeseen limitations to this study restricted our ability to produce a comprehensive result. However, we will explore the interpretations we can make with the experiment results and data.

5.1.1 Geological setting

The Tonga-Kermadec island arc stretches from northeast of New Zealand to southwest of Samoa. The arc has formed from subduction of the Pacific plate beneath the Australian plate with an interruption in volcanism where the Louisville ridge subducts midway along the arc. This cessation in volcanism delineates the Tongan portion (to the north) and Kermadec portion (to the south) of the Tonga-Kermadec island arc.

Late island is located slightly north of the center of the Tonga Arc on the Tofua ridge at around 18.81^{o}S (Fig. 5.1). Late island comprises a small subaerial component within the context of a broader submarine volcano. The volcano rises 1500 m from the sea floor with a well-defined subaerial, conical volcanic peak reaching 540 m above sea level. The island is 6 km in diameter and circular with a 400-m wide and 150-m deep summit crater near its center. Small cinder cones occur to the southwest and on the northern flanks of the summit. There are two other craters on the island that are presumed to be explosion or collapse craters, one of which is filled with a saltwater lake. Late has had only two eruptions in recorded history, in 1790 and 1854, both of which have produced basaltic andesite and andesite lavas. The surface of the top part of

the central cone is covered with glassy spatter material and blocks. The majority of the lavas described by Bryan et al. (1972) are basaltic andesite with a younger andesitic flow generated from one of the northern cinder cones.

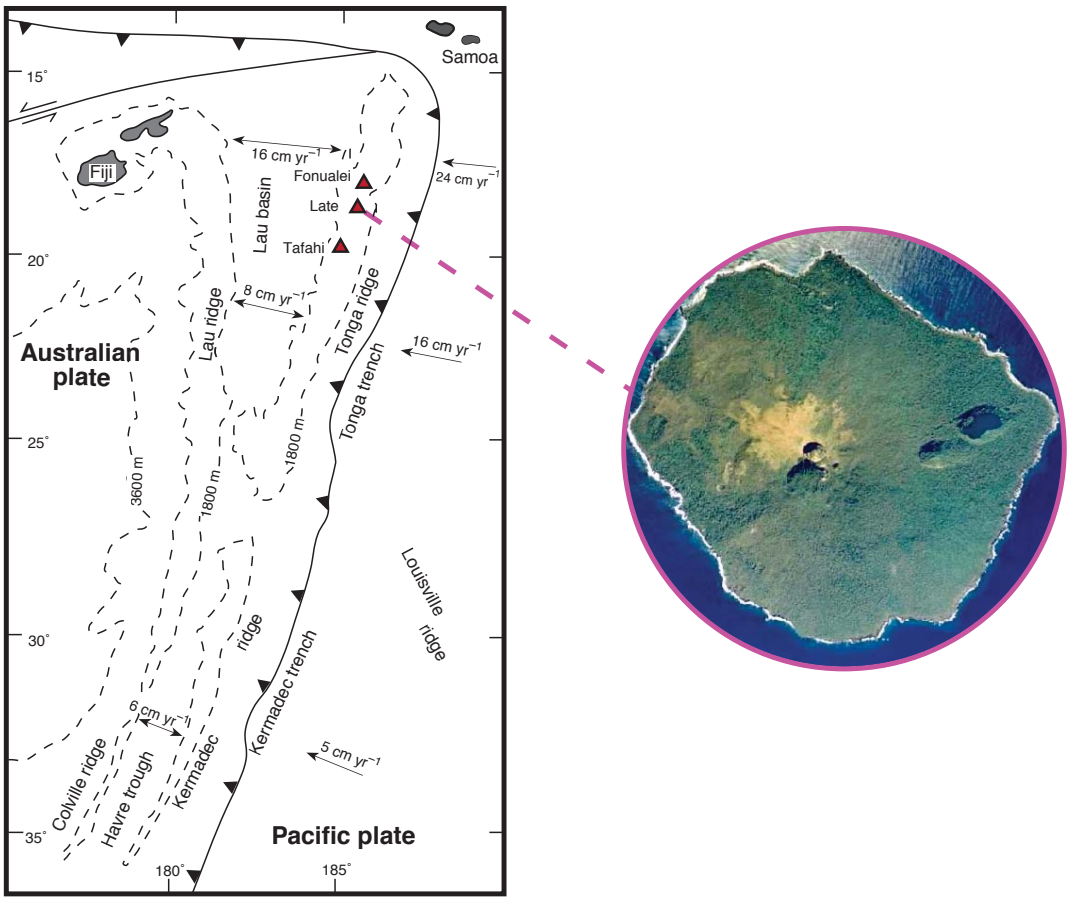

Figure 5.1 Map of the Tonga-Kermadec arc showing the boundary between the Australian plate and the Pacific plate. The map shows bathymetry of features on the Australian plate, such as the Lau ridge and the Tonga ridge. The boundary along the Australian plate and Pacific plate is convergent, with a decrease in relative plate motion from north to south. The back-arc, Lau basin, is opening in a 'V' shape as a result of slab rollback (Bevis et al., 1995). The red triangles in the map represent the three volcanoes discussed in this study (Late, Fonualei, and Tafahi). The photograph is of Late volcano (right panel), the volcano that forms the basis of this study (from Smithsonian Institution).

5.1.2 Geochemical and petrological context of Late

The lavas from Late volcano, along with two neighboring volcanic islands, Tofua (to the south) and Fonualei (to the north), have allowed researchers to study and

illustrate magmatic evolution within one of the most primitive intra-oceanic arcs. Late, Tofua and Fonualei form an array representing geochemical evolution (with increasing SiO_2), progressing from basalt to basaltic andesite and ultimately to dacitic lavas (Fig. 5.2). The lavas erupted on Late, and the neighboring islands of Tofua and Fonualei are low-K tholeiites (Ewart et al., 1973, 1977; Ewart 1977). The lavas from the Tongan arc are inferred to have originated from highly depleted mantle wedge peridotite. The mantle wedge beneath the Tongan arc is believed to be refractory with depletion in high-field strength elements (HFSE) relative to light rare earth elements (LREE) attributed to varying degrees of back-arc melt extraction (Ewart & Hawkesworth, 1987; Woodhead et al., 1993; Ewart et al., 1994; Caulfield et al., 2008; Cooper et al., 2010). In addition to the geochemical signatures derived from the depleted mantle wedge, other signatures influencing the overall chemistry of the Tongan lavas have been detected, particularly a fluid flux from the altered oceanic crust and melts of sedimentary rocks. The altered oceanic crust fluid, which is derived from dehydration of the subducting oceanic crust, is indicated in lavas by high ratios of large-ion lithophile elements (LILE)/HFSE that decrease southward along the arc (Regelous et al., 1997, 2010; Turner et al., 1997). The addition of sediment melts in the Tonga-Kermadec arc has been identified using a variety of trace element and isotopic signatures, particularly through the most unambiguous tracer, ^{10}Be, which can be used to narrow down the sediment flux to 0.25-1% (Plank & Langmuir, 1993; Turner et al., 1997; George et al., 2005).

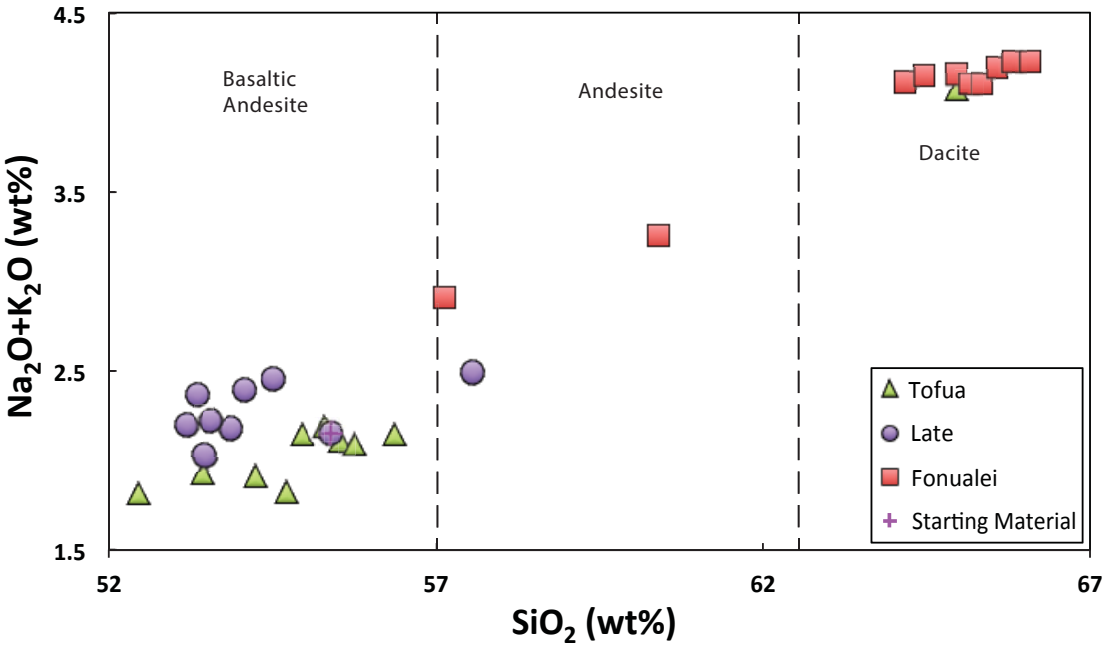

Figure 5.2 Classification of select Tongan volcanism (adapted from Turner et al., 2012), plotted on a total alkali versus silica (TAS) for sampled Tofua, Fonualei, and Late lavas (Ewart, 1973; Caulfield et al., 2012; Turner et al., 2012). The cross hairs represent the starting material used in this study. The TAS diagram illustrates a gradation in silica content towards a more evolved composition in what otherwise would be a primitive end-member intra-oceanic arc.

The phenocryst assemblages of the basaltic andesite lavas (53-55 wt% SiO_2) from Late are commonly plagioclase ± clinopyroxene ± orthopyroxene (Fig. 5.3). The groundmass material is primarily quenched glass with plagioclase and coarse microcrystals of clinopyroxene. The plagioclase phenocryst compositions for Late are all bytownite, ranging in anorthite (84.3–87.8 wt%), albite (11.8–15.4 wt%), and orthoclase (0.3–0.5 wt%) proportions with subsidiary augite and pigeonite (Ewart et al., 1973).

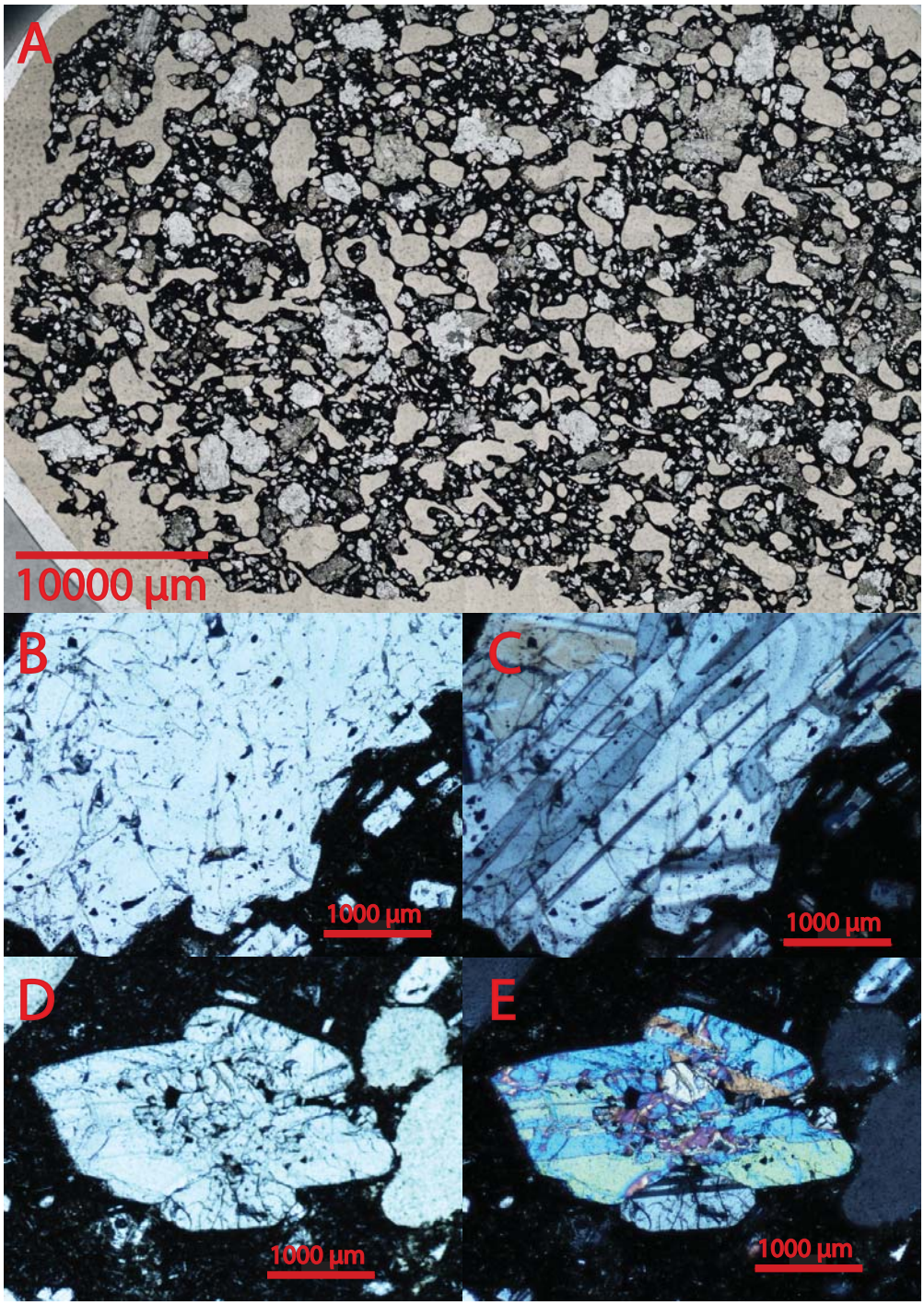

Figure 5.3 Petrographic images of natural basaltic andesite samples from Late. Since only a powder sample exists for the sample used in this study (Late-1), the thin section of Late-2 (pictured above), which is similar in composition and mineralogy to Late-1 (Ewart et al., 1973), is used by proxy as a petrographic guide to the powdered sampled. Panel (A) shows a macroscopic view of the thin section that has been impregnated by epoxy because of a high proportion of vesicles. Panel (B) demonstrates a large colorless plagioclase phenocryst surrounded by a fine grain matrix of glass, plagioclase, and clinopyroxene microlites in plane polarized light while panel (C) shows the same phenocryst through cross-polarized light with polysynthetic twinning in first order grey

and white. Panel (D) displays a large colorless clinopyroxene phenocryst in the center of the image surrounded by a fine-grained matrix of glass, plagioclase, and clinopyroxene microlites. Panel (E) exhibits the same clinopyroxene phenocryst in cross-polarized light, displaying higher birefringence and second order interference colors.

5.2 Experimental and analytical methods

5.2.1 Starting material and experimental details

The starting material (L1) used in our high- and atmospheric-pressure experiments was a naturally occurring basaltic andesite from Late. Both this sample and volcanic island material have been extensively studied and geochemically characterized (Ewart, 1973). This sample also represents the first stage of magmatic evolution that culminates in dacitic eruptions on neighboring volcanoes (Tofua and Fonualei) along the Tonga-Kermadec arc.

The material selected for our phase-equilibria experiments is porphyritic lava from the Late volcano, with a phenocryst assemblage composed of plagioclase, augite, and pigeonite. The matrix (volumetrically ~73%) is predominantly glass with microcrystalline plagioclase and clinopyroxene. The bulk rock composition of the starting material reported in previous studies (Ewart et al., 1973) was determined by electron microprobe analyses of the glass (Table 5.1) in the Geophysical Laboratory at the Carnegie Institution of Washington.

Water content of 5 wt% was added to the capsule once the rock powder was inserted (capsule details are explained in the next section). This water content was derived from Carmichael (2002), which analyzed the conditions in which a hydrous andesitic magma with no trace of hydrous bearing minerals could form. This is further explored in the discussion section of this chapter.

The rock fragments were cleaned in an ultrasonic bath and initially ground using a tungsten carbide ball mill. This powder was then melted at 900 ^{o}C using a 1atm furnace where the sample was fused in the air in a platinum crucible and quenched by dropping into a water bath. The sample was crushed and ground in ethanol using an agate mortar and pestle to achieve a fine grain size (~10μm). This powder was further dried in an oven at 120 ^{o}C. A minimum of two cycles of melting and grinding was performed to improve chemical homogeneity. At each interval, a cut of the powder was analyzed with a petrographic microscope to confirm a crystal-absent glass.

Table 5.1 Composition (wt%) of starting material L1 (basaltic andesite) used in this study

	L1
	This Study
SiO_2	55.39
TiO_2	0.57
Al_2O_3	17.64
Cr_2O_3	-
FeO*	7.52
MnO	0.19
MgO	4.23
CaO	11.00
Na_2O	1.75
K_2O	0.40
P_2O_5	0.08
NiO	-
F	-
Total	98.77
Mg#	52.70
CIPW (wt%)	
Qz	12.34
Co	-
Or	2.36
Ab	14.98
An	39.55
Lc	-
Ne	-
Di	12.55
Hy	15.70
Ol	-
Mt	1.23
Il	1.10
Hm	-
Ap	0.19

*Total Fe as FeO

5.2.2 High-pressure experiments

Phase-equilibria experiments were performed at a range of pressures (2.5–25 kbar) and temperatures (900–1242 ^{o}C) using a piston-in technique in a half-inch (1.27

cm) Boyd-England (1960) type end-loaded, solid-medium piston cylinder apparatus at Macquarie University. The furnace assemblies (1.27 cm in diameter) were composed of talc-pyrex outer sleeves and crushable air-fired boron-nitride components (Fig. 5.4). Oxygen fugacity within the furnace assembly lies between the Ni-NiO and magnetite-wüstite buffers (Green, 1976). A friction correction of 10% was applied to the measured pressures (Akella, 1973). The precision in pressure measurements is estimated to be within 0.5 kbar of the designated value. Temperatures were measured with a Pt-$Pt_{90}Rh_{10}$ thermocouple and were automatically controlled by a Leeds & Northrup Electromax V single-loop controller. The temperature was maintained within ±2 ^{o}C of the initial set value. Run durations are presented in Table 5.2, ranging from 1–28 h in the high-pressure experiments ≥5 kbar and up to 144 h at lower pressures (2.5 kbar). Experiments were quenched by manually turning off the single-loop controller while maintaining the designated run pressure.

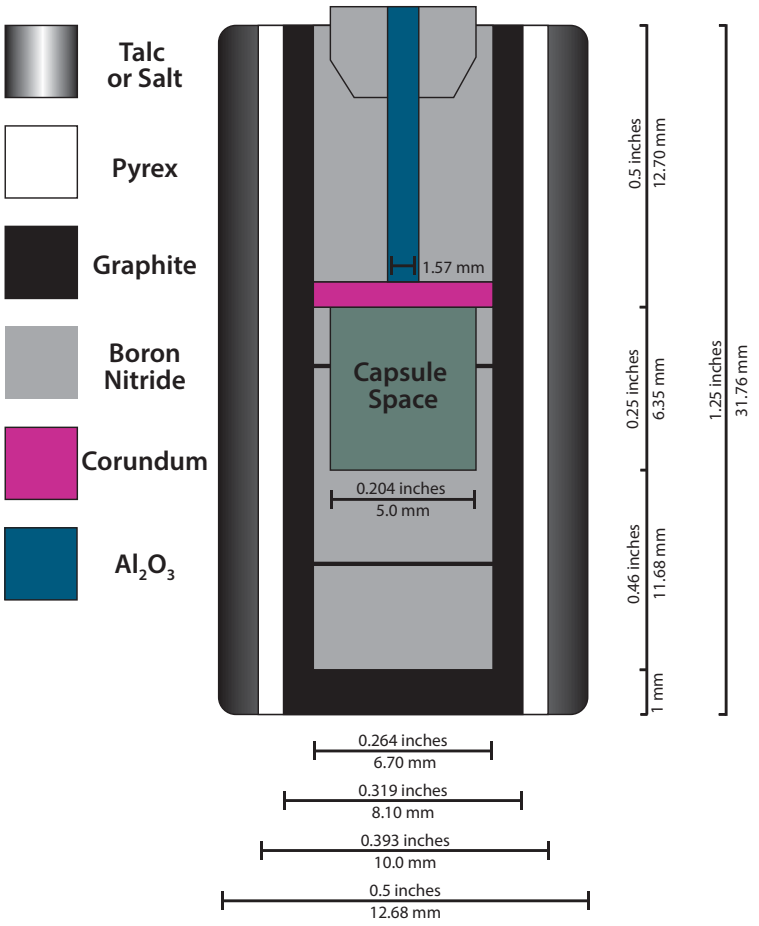

Figure 5.4 Cross section of piston cylinder assembly used in experiments.

Experiments were conducted on 20 mg starting mixtures encased in welded $Ag_{70}Pd_{30}$, Cr-Al, or Pt-PtRh capsules (Table 5.2). A micro-syringe, attached to a manually operated height adjustable lever, was used to add water to the capsule. The capsule was weighed at each interval where material was either added or removed to track any potential loss of components.

After the experiments, the capsule was cleaned and weighed. To check potential water loss, the capsule was pierced and placed in the oven at 120 ^{o}C for a minimum of one hour before re-weighing. The capsules were sectioned longitudinally with a small diamond saw, mounted in epoxy, and polished for optical inspection and microprobe analysis.

Table 5.2 Experimental conditions and run products (determined by SEM)

Run no.	%H2O	P (kbar)	T (° C)	Time (hrs)	∆ log fO_2 (NiNiO)	capsule	Assemblage [a]
B16-12	0	1E-03	1242	21	0.85	-	L
B02-12	0	1E-03	1196	115	0.74	-	L + pl
B26-12	0	1E-03	1177	88	0.7	-	L + pl
B17-12	0	1E-03	1158	63	0.65	-	L + pl
B22-12	0	1E-03	1139	91	0.61	-	L + pl
B29-12	0	1E-03	1120	67	0.56	-	L + cpx + pl
B26-14	0	1E-03	1117	67	0.55	-	L + cpx + pl
B29-14	0	1E-03	1099	59	0.5	-	L + cpx + pl + il
B01-14	0	1E-03	1080	68	0.45	-	L + cpx + pl + il
2005	5	2.5 [b]	900	144		Ag-Pd	L + cpx + pl
2007	5	2.5 [b]	950	24		Ag-Pd	+ cpx + opx + pl + mt
2008	5	2.5 [b]	1000	2		Ag-Pd	L + cpx + pl + il
2009	5	2.5 [b]	1000	91		Ag-Pd	L + cpx + opx + pl
2010	5	2.5 [b]	900	94		Ag-Pd	+ cpx + opx + pl + mt
2021	5	5.5	900	82		Ag-Pd	L + cpx + opx
2023	5	5	850	75		Ag-Pd	L + cpx + opx + pl
Mount 2 - 15	5	20	1100	7		Cr-Al	L + cpx + pl
Mount 2 - 27	5	10	1020	5		Cr-Al	L + cpx
Mount 2 - 28	5	15	1060	6		Cr-Al	L + gt + cpx
Mount 2 - 29	5	25	1140	5		Cr-Al (melted)	L + cpx
Mount 2 - 31	5	10	980	10		Cr-Al	L + cpx
Mount 2 - 32	5	10	940	12		Cr-Al	L + gt + cpx
Mount 2 - 33	5	25	1100	4		Cr-Al	L + gt + cpx

Run no.	%H2O	P (kbar)	T (° C)	Time (hrs)	∆ log fO_2 (NiNiO)	capsule	Assemblage [a]
Mount 2 - 34	5	5	980	10		failed	L + cpx
Mount 2 - 35	5	20	940	10.5		Cr-Al	L + gt + cpx
Mount 2 - 36	5	5	1020	8		Cr-Al	L
Mount 2 - 37	5	20	1040	6		Cr-Al	L + gt + cpx
Mount 10 - 39	5	25	1000	9		Cr-Al	L + gt + cpx
Mount 10 - 40	5	10	900	28		Cr-Al	L + gt + cpx
Mount 10 - 41	5	25	1160	1		Pt-PtRh	L + gt + cpx
Mount 10 - 42	5	20	1140	1.5		Pt-PtRh	L + gt + cpx
Mount 10 - 43	5	25	1200	1		Pt-PtRh	L + gt + cpx
Mount 10 - 44A	5	*no info*	*no info*	-		-	indiscernible
Mount 10 - 47	5	5	900	26		Pt-PtRh	L + cpx + pl
Mount 10 - 48	5	25	1220	1		Pt-PtRh	L + cpx
Mount 10 - 50	5	25	940	20		Cr-Al	L + gt + cpx
Mount 10 - 60	5	15	900	27		Cr-Al	L + gt + cpx
Mount 10 - 62	2	10	980	9.5		Cr-Al	L + gt + cpx + pl

[a] L-liquid; gt-garnet; cpx-clinopyroxene; opx-orthopyroxene; pl-plagioclase; il-ilmenite; mt-magnetite

[b] 2.5kb pressures attempted and quenched however piston cylinder fluctuated in pressure. Therefore, our results for 2.5kb are not reliable.

5.2.3 One-atmosphere experiments

One-atmosphere (1-atm) experiments were performed at the Australian National University, Canberra. The sample was mixed with polyethylene oxide reagent to form a thin paste which was mounted onto 3-5mm diameter palladium wire loops. No issues arose with potential Fe loss using the Pd wire loops. The wire loops loaded with the sample were lowered into vertical muffle tube furnaces where the samples were converted into a silicate glass. Oxygen fugacity was controlled by an upward flow of $CO:CO_2$ gas mixture (10,000 SCCM CO_2 to 100 SCCM CO) into the furnace by Tylan F2800 mass flow controllers. Oxygen fugacity was buffered at NiNiO and calculated as outlined in O'Neill and Mavrogenes (2002), with uncertainties estimated to be ±0.05 log units. The calculated oxygen fugacity for the samples is reported in Table 5.2.

Two samples were run adjacent to each other at each temperature interval. The experiments were loaded into an already partly-heated furnace (~600 ^{o}C) to prevent the samples, which were closely spaced on the wire loops, from sticking to each other. Once loaded, the CO and CO_2 gases were switched on, and the temperature was gradually increased by 6 ^{o}C at one-minute intervals. The temperature inside the furnace was measured by two type B ($Pt_{94}Rh_6$ - $Pt_{70}Rh_{30}$) thermocouples and was set 10-15 ^{o}C higher (monitored by Eurotherm controllers) to correct for the placement of the thermocouple in the furnace. All samples except one were run over 48 hrs. The samples were quenched by releasing the wire loops into a water bath.

5.2.4 Mineral identification and chemistry

Minerals and matrix glasses in the experiments were identified using a Zeiss EVO MA15 scanning electron microscope with Oxford Instruments Aztec Synergy

EDS/EBSD, followed by chemical analyses on a Cameca SX-100 electron microprobe at Macquarie University. Glass analyses were obtained using 15-keV accelerating voltage, 15-nA beam current, and a defocused beam with the largest possible spot size for any given area (30μm). The conditions for mineral analyses were modified to attain a focused spot size of 1μm and an operating current of 20-nA. Counting times were 10s for peaks and 5s on the background on each side of the peak, and Na and K were analyzed first in each measurement to minimize alkali volatilization. Corrections to the raw data were made using the ZAF correction procedure of Bence and Albee (1968) using the PAP program (Pouchou and Pichoir, 1984).

5.3 Experimental results

5.3.1 Run products

Experimental conditions and phase assemblages are presented in Table 5.2. Phases present include quenched glass, garnet, clinopyroxene, orthopyroxene, plagioclase, and accessory Ti-magnetite. Where present, garnet crystals populate large areas given their relatively large crystal size (Fig. 5.5a-d). All of the experiments nucleated crystals, except for the experiments with conditions at [1-atm, 1242 ^{o}C] and [5 kbar, 1020 ^{o}C], these are above the liquidus. Figure 5.6 illustrates the phases present in the experiments. The garnet nucleated at higher temperatures and pressures (e.g., [25 kbar, 1200 ^{o}C], [20 kbar, 1150 ^{o}C], [15 kbar, 1060 ^{o}C], [10 kbar, 940 ^{o}C], [10 kbar, 900 ^{o}C]). Clinopyroxene was present in all the runs at 5 kbar and higher, while plagioclase was only observed in one high-pressure sample [5 kbar, 900 ^{o}C]. However, Figure 5.5b shows the presence of plagioclase at high-pressure [10 kbar, 980 ^{o}C], but this sample had only 2 wt% H_2O and therefore is not included in the phase diagram presented.

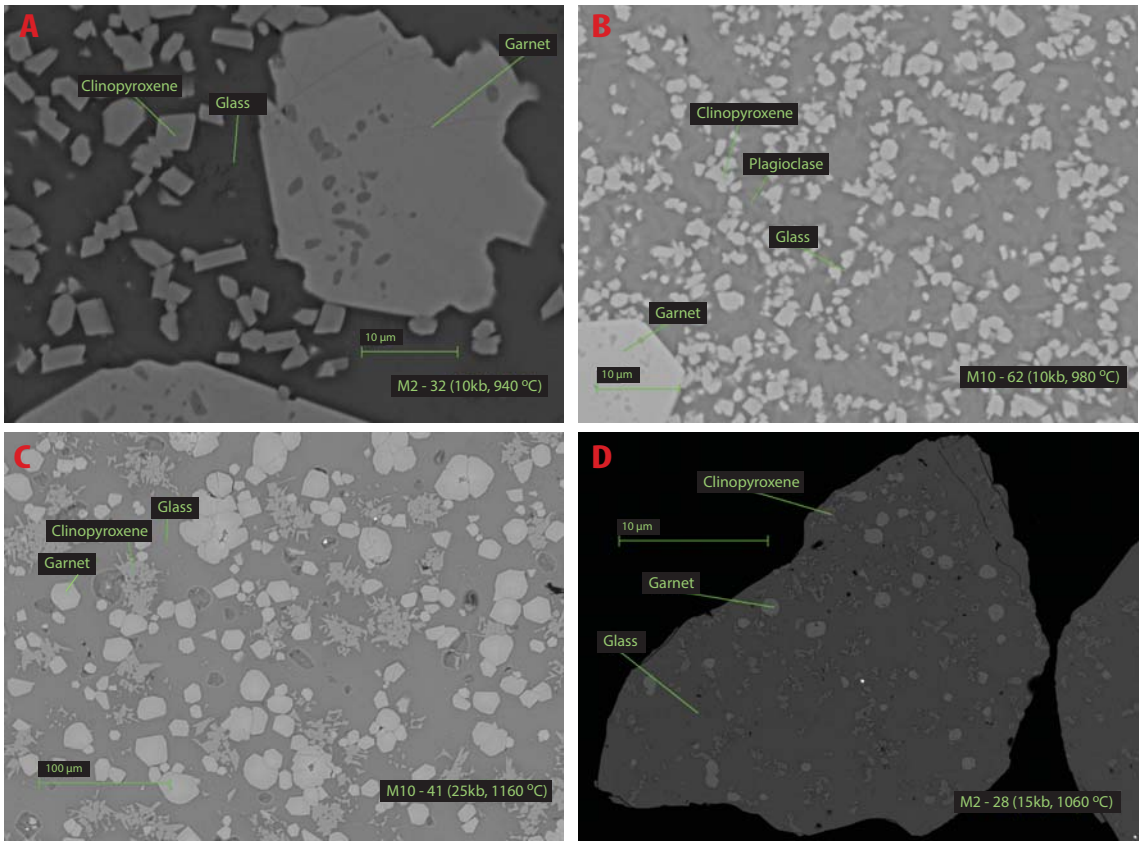

Figure 5.5 Backscattered electron images of mineral assemblages at various P-T conditions. (A) 10 kbar, 940 °C, 5 wt% H_2O; (B) 10 kbar, 980 °C, 2wt% H_2O; (C) 25 kbar, 1160 °C, 5wt% H_2O; (D) 15 kbar, 1060 °C, 5wt% H_2O. Crystal phases present are large crystals of garnet relative to the smaller clinopyroxene and plagioclase crystals. The groundmass is predominantly glass with microcrystals of plagioclase and clinopyroxene. Panel (b) represents the only sample that nucleated all three the minerals (garnet, clinopyroxene, plagioclase). However, Panel (b) not only being near the cotectic, only had 2 wt% H_2O, which appears to have allowed the conditions for large phenocrysts to nucleate.

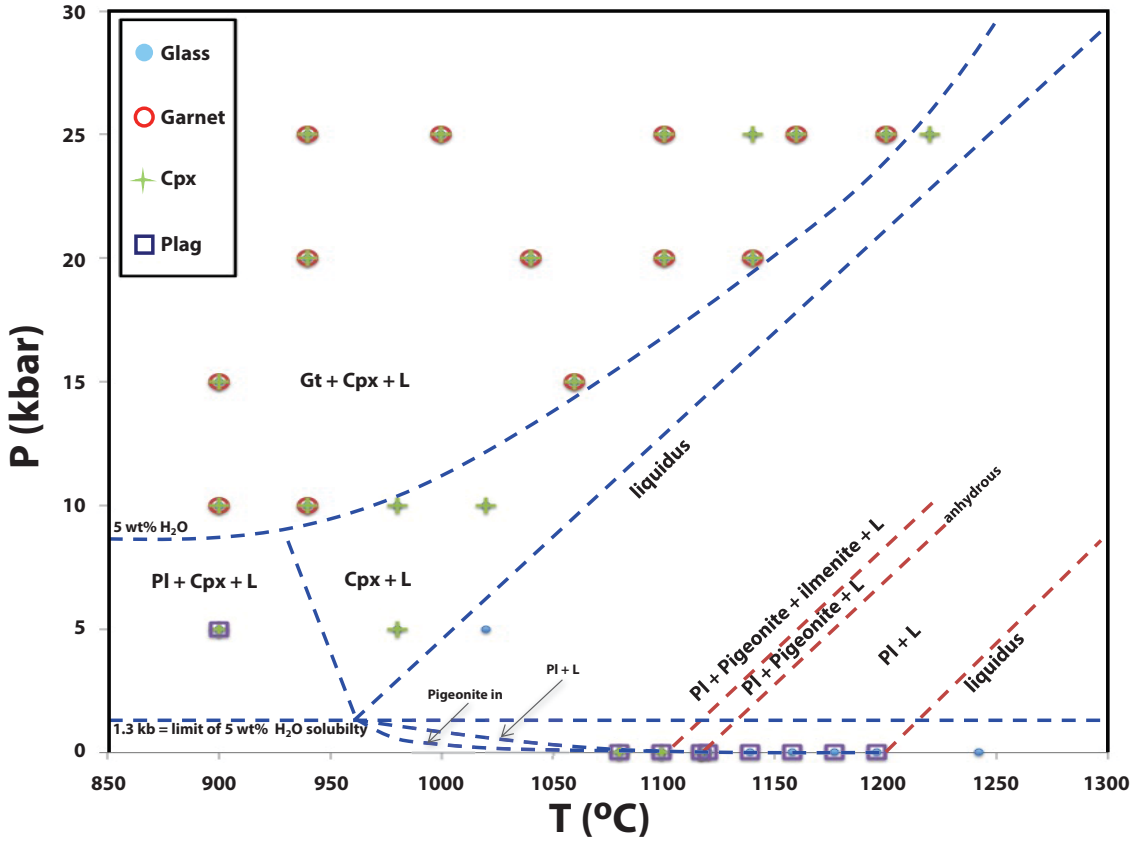

Figure 5.6 Stability fields for garnet, clinopyroxene, and plagioclase in the temperature range for magma generation within intra-oceanic arcs with the addition of 5 wt% H_2O or no addition of H_2O (anhydrous). The limit of 5 wt% H_2O solubility is 1.3 kbar for water saturation of andesite (Eggler, 1972). The phase diagram shows that at higher pressures: (1) garnet stability at 10kbar increases with decreasing temperatures, (2) clinopyroxene is represented throughout all the phase boundaries, (3) plagioclase enters at low pressure and low temperatures. While the anhydrous one-atmosphere experiments show that the melting temperatures for plagioclase and clinopyroxene increase.

Several runs were vesicular, ([5 kbar, 1020 ^{o}C] above the liquidus), [5 kbar, 980 ^{o}C], [5 kbar, 900 ^{o}C]) which was in the lower pressure and temperature range of the piston cylinder runs. The experiment at [5 kbar, 980 ^{o}C] contained numerous micro-crystals that had a signature similar to garnet with high aluminum relative to magnesium. The experiment at [25 kbar, 1220 ^{o}C] had low amounts of microcrystals

and no observed phenocrysts, suggesting that the run was slightly above the garnet-stability region.

One experiment was performed with 2 wt% H_2O. This sample was crystal-rich, and there was a low glass yield. This run contains mostly glass, plagioclase, and clinopyroxene crystals. It is close to the garnet-in boundary because the garnet crystals were smaller than the garnet in any of the other samples. This suggests that water may have affected nucleation by increasing the number of nucleation sites.

The 1-atm experiments each yielded two experiments at each set temperature. Both beads in the experiments were prepared and handled the same way. The experiments ([1-atm, 1242 ^{o}C], [1-atm, 1196 ^{o}C], [1-atm, 1177 ^{o}C]) were near the liquidus which made it difficult to discern crystal nucleation. Moreover, these samples were heavily fractured through the quenching process, making it difficult to distinguish crystals from fractures, particularly at the smaller scale. I etched these samples to expose the crystals in the samples. Etching the samples revealed that [1-atm, 1242 ^{o}C] was above the liquidus and [1-atm, 1196 ^{o}C] and [1-atm, 1177 ^{o}C] were close to the liquidus. However, the latter two contained microcrystals of plagioclase.

The lower temperature 1-atm runs [1120 ^{o}C], [1117 ^{o}C], [1099 ^{o}C], and [1180 ^{o}C] all contain larger crystals of plagioclase, glass, and small crystals of clinopyroxene. This is because, for plagioclase, the number of nuclei is small and the growth rate is high, resulting in larger phenocrysts. The accessory mineral found in the 1-atm runs is ilmenite, which nucleated at the lowest temperatures (below 1099 ^{o}C) run for experiments [1-atm, 1099 ^{o}C] and [1-atm, 1080 ^{o}C]. The run products in the 2.5 kbar range were a combination of glass, plagioclase, clinopyroxene, orthopyroxene, and either ilmenite or magnetite as accessory phases.

5.3.2 Mineral chemistry

For each experimental run, the individual phases (listed in Table 5.2) were analyzed and reported in Tables 5.3 through 5.6. Ewart et al. (1973) found two types of pyroxene compositions in the natural rocks, augite (cpx) and hypersthene (opx). Clinopyroxene compositions for the experiments are $Wo_{12-48} - En_{20-55} - Fs_{12-35}$. The pyroxenes that nucleated in our experiments varied slightly in composition (Fig. 5.7a). Most of the pyroxenes were augite; however, in two experiments diopside and hedenbergite formed. Moreover, I averaged three analyses for the experimental run at [5 kbar, 900 ^{o}C] which is included in the tables, yet we note that the chemical analyses for that sample showed crossing grain boundaries and did not return an accurate analysis of the clinopyroxene in this sample. Plagioclase phenocrysts in the natural sample are extremely calcic bytownite ($An_{84–89}$) that plot near the anorthite-bytownite boundary (Ewart et al., 1973). The plagioclase phenocrysts in the experiments are less calcic than the natural sample but still plot in the bytownite region (Fig. 5.7b). Plagioclase compositions are $An_{72-78} - Ab_{21-26} - Or_{0.5-1.8}$.

Table 5.3 Melt compositions (wt%)

Run no.	B16-12	B02-12	B26-12	B17-12	B22-12	B29-12	B26-14	B29-14	B01-14	M10-47	M10-62	M10-60	M10-50	M10-43
P (kbar)	1 atm	1 atm	1 atm	1 atm	1 atm	1 atm	1 atm	1 atm	1 atm	5	10	15	25	25
T (^{o}C)	1242	1196	1177	1158	1139	1120	1117	1099	1080	900	980	900	940	1200
N[a]	31	26	12	18	17	21	20	29	12	2	2	1	4	1
SiO_2	54.04	54.49	54.93	54.86	54.60	54.80	55.89	58.49	58.54	49.63	55.43	38.91	43.84	54.64
TiO_2	0.59	0.64	0.70	0.74	0.79	0.76	0.78	0.60	0.79	0.45	0.42	1.17	1.13	0.56
Al_2O_3	16.89	15.84	13.97	13.33	12.47	16.12	15.68	16.58	15.34	16.63	21.08	20.67	18.53	16.27
Cr_2O_3	0.01	0.01	0.02	0.02	0.02	0.01	0.04	0.04	0.05	-	-	-	-	-
FeO*	9.60	9.84	11.06	11.73	12.67	10.48	9.74	7.20	9.16	11.53	5.82	20.24	16.55	6.42
MnO	0.18	0.21	0.21	0.23	0.27	0.18	0.21	0.19	0.22	0.25	0.13	0.38		0.18
MgO	4.20	4.52	5.19	5.36	5.72	3.31	3.58	2.95	3.56	6.28	1.91	6.57	5.62	4.59
CaO	10.94	10.62	10.09	9.83	9.80	10.72	10.68	10.44	9.58	13.04	10.84	12.49	13.52	13.73
Na_2O	1.97	1.95	1.82	1.81	1.63	2.06	1.84	1.89	1.67	1.04	2.56	-	0.90	1.45
K_2O	0.50	0.65	0.56	0.58	0.56	0.62	0.60	0.71	0.51	0.32	0.49	-	0.47	0.45
P_2O_5	0.09	0.10	0.11	0.11	0.12	0.12	0.14	0.14	0.17	0.09	0.11	0.17	0.15	0.13
H_2O	0	0	0	0	0	0	0	0	0	5	2	5	5	5
NiO	0.03	0.02	0.03	0.02	0.01	0.02	-	-	-	-	-	-	-	-
Total[b]	99.01	98.87	98.66	98.60	98.65	99.18	99.18	99.23	99.59	99.26	98.79	100.60	100.71	98.42
Mg#	46.43	47.64	48.18	47.51	47.21	38.49	42.13	44.76	43.50	51.90	39.40	39.14	40.22	58.61
CIPW (wt%)														
Qz	8.64	9.05	10.32	10.19	10.19	10.16	12.85	17.24	18.40	2.50	10.90	-	-	11.09
Co	-	-	-	-	-	-	-	-	-	-	-	-	-	-
Or	2.95	3.90	3.37	3.49	3.37	3.66	3.55	4.20	3.01	1.89	2.95	-	2.72	2.72
Ab	16.84	16.67	15.57	15.48	13.96	17.52	15.65	16.08	14.22	8.88	21.92	-	7.53	12.44
An	36.09	32.87	28.64	26.88	25.37	33.19	33.04	34.94	32.97	39.99	45.07	55.94	44.52	37.12
Lc	-	-	-	-	-	-	-	-	-	-	-	-	-	-
Ne	-	-	-	-	-	-	-	-	-	-	-	-	-	-
Di	15.13	16.46	17.81	18.21	19.26	16.57	16.33	13.68	11.40	20.36	7.29	3.73	17.40	25.64
Hy	17.45	18.00	20.89	22.15	23.98	15.45	15.17	11.22	16.61	23.44	9.87	5.05	2.63	8.57
Ol	-	-	-	-	-	-	-	-	-			29.47	20.11	
Mt	1.57	1.59	1.80	1.91	2.07	1.70	1.58	1.17	1.48	1.87	0.94	3.23	2.62	1.04
Il	1.14	1.23	1.35	1.42	1.52	1.46	1.50	1.14	1.50	0.85	0.80	2.20	2.11	1.08
Hm	-	-	-	-	-	-	-	-	-	-	-	-	-	-
Ap	0.21	0.23	0.25	0.25	0.28	0.28	0.32	0.32	0.39	0.21	0.25	0.39	0.35	0.30

*Total Fe as FeO

[a] Number of spots analyzed

[b] All usable data from EPMA

Table 5.4 Clinopyroxene compositions (wt%)

Run no.	B26-14	B29-14	B01-14	M10-47	M10-40	M10-42	M10-50	M10-39	M10-41	M10-48
P (kbar)	1 atm	1 atm	1 atm	5	10	20	25	25	25	25
T (^{o}C)	1117	1099	1080	900	900	1140	940	1000	1060	1220
N[a]	4	9	8	3	2	2	3	2	2	1
SiO_2	51.67	51.94	50.55	51.75	50.25	50.80	44.70	52.25	45.47	52.48
TiO_2	0.26	0.52	0.41	0.38	0.52	0.24	1.00	0.24	0.61	0.63
Al_2O_3	8.25	7.53	3.07	21.67	7.31	8.05	17.47	1.53	13.72	17.31
Cr_2O_3	0.06	0.09	-	-	0.05	-	-	-	-	-
FeO*	13.80	13.73	15.29	8.15	11.48	6.54	15.49	20.80	13.21	8.06
MnO	0.33	0.48	0.49	0.14	0.19	0.19	0.46	0.52	0.36	0.27
MgO	15.04	13.08	17.24	3.11	10.59	12.70	6.12	18.90	9.78	6.43
CaO	8.21	11.70	13.26	10.53	18.72	21.29	13.95	5.74	16.74	11.55
Na_2O	0.96	0.76	0.16	1.72	0.81	0.81	1.25	0.19	1.26	1.75
K_2O	0.19	0.35	0.03	0.40	0.12	-	0.39	0.64	-	0.5
P_2O_5	0.03	0.16	-	0.11	-	0.09	0.18	-	-	-
H_2O	0	0	0	5	5	5	5	5	5	5
NiO	0.06	-	-	0.06	-	-	-	-	-	-
Total[b]	98.80	100.34	100.50	97.96	100.04	100.71	101.01	100.81	101.15	98.98
Mg#	68.34	65.36	69.07	43.05	64.63	79.37	43.90	64.29	59.46	61.25
				Compositions (recalculated to 100 wt%)						
Wo	20.6	28.8	27.0	11.9[c]	44.1	41.2	48.3	49.6	43.1	40.4
En	52.4	44.8	48.8	54.5[c]	34.7	33.5	40.1	20.4	33.4	24.6
Fs	27.0	26.4	24.3	33.6[c]	21.1	25.4	11.6	30.0	23.5	35.0

*Total Fe as FeO

[a] Number of spots analyzed

[b] All usable data from EPMA

Table 5.5 Plagioclase compositions (wt%)

Run no.	B16-12	B02-12	B26-12	B17-12	B22-12	B29-12	B26-14	B29-14	B01-14
P (kbar)	1 atm	1 atm	1 atm	1 atm	1 atm	1 atm	1 atm	1 atm	1 atm
T (^{o}C)	1242	1196	1196	1158	1139	1120	1117	1099	1080
N[a]	12	3	3	19	14	6	8	8	4
SiO_2	50.44	49.54	49.67	49.98	51.04	50.90	51.51	53.10	53.42
TiO_2	0.05	0.04	0.03	0.08	0.04	0.07	0.11	0.13	0.17
Al_2O_3	28.51	29.58	29.33	28.99	28.54	27.49	26.98	26.05	26.07
Cr_2O_3	-	-	-	0.01	-	-	-	-	-
FeO*	1.33	0.92	1.08	1.99	1.61	1.94	2.56	2.68	3.08
MnO	-	-	-	0.03	0.02	-	0.09	-	0.09
MgO	0.43	0.26	0.31	0.69	0.47	0.56	1.17	0.64	0.66
CaO	15.18	15.77	15.71	14.82	14.89	14.70	14.69	13.97	13.46
Na_2O	2.64	2.38	2.48	2.92	2.81	2.66	2.37	2.69	2.69
K_2O	0.11	0.10	0.09	0.15	0.11	0.15	0.17	0.21	0.28
P_2O_5	0.04	-	-	0.02	0.02	-	-	0.05	-
H_2O	0	0	0	0	0	0	0	0	0
NiO	-	-	-	0.01	0.03	-	-	-	-
Total[b]	98.73	98.59	98.70	99.68	99.55	98.47	99.65	99.50	99.93
				Compositions (recalculated to 100 wt%)					
An	75.6	78.1	77.4	73.1	74.1	74.6	76.6	73.2	72.1
Ab	23.8	21.3	22.1	26.1	25.3	24.4	22.4	25.5	26.1
Or	0.7	0.6	0.5	0.9	0.7	0.9	1.1	1.3	1.8

*Total Fe as FeO

[a] Number of spots analyzed

[b] All usable data from EPMA

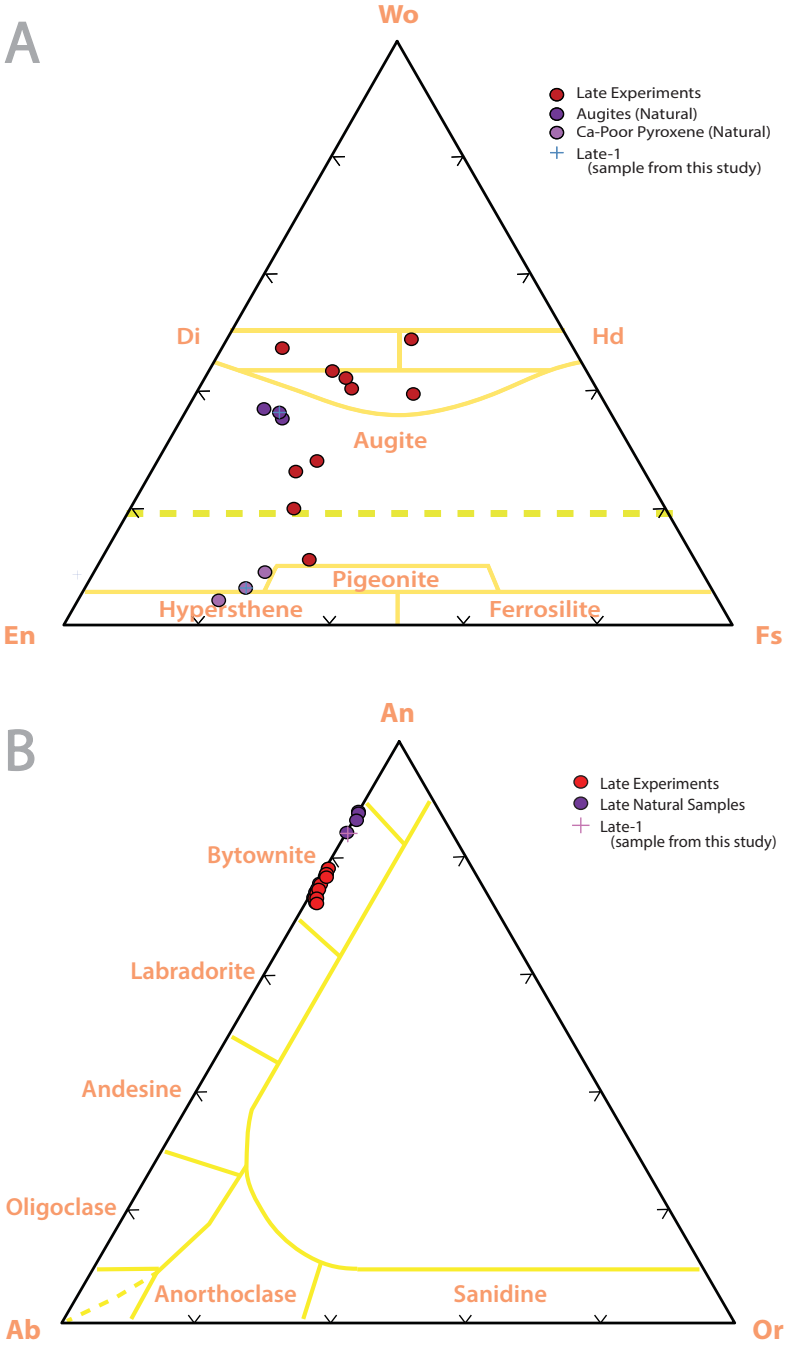

Figure 5.7 (A) Pyroxene compositions in mole percent for a range of natural and experimental run products from Late volcano. The dotted line denotes the boundary between clinopyroxene and orthopyroxene. Wo, Di, Hd, En, and Fs denote pyroxene end-members: wollastonite, diopside, hedenbergite, enstatite, and ferrosillite. (B) Plagioclase compositions in mole percent for a range of plagioclase phenocrysts analyzed in the natural and experimental run

products from Late. The ternary diagram illustrates the variation in plagioclase between Anorthite-Albite-Orthoclase (An-Ab-Or).

5.3.3 Phase relations of L1

To understand fully the stability fields for the phases present in the experiments, the experimental results (Table 5.1) were used to construct a P-T phase diagram (Fig. 5.6), which depicts the stability fields for garnet, clinopyroxene, and plagioclase. The phase diagram contains the experiments conducted with 5 wt% H_2O at ≥5 kbar and anhydrous 1-atm experiments within the temperature range for magma generation within intra-oceanic arcs. According to Eggler (1972), the maximum pressure for saturation with 5 wt% H_2O in andesites is 1.3 kbar. The P-T phase diagram illustrates that garnet stability increases at lower pressures as the temperature of the magma decreases (i.e., at higher temperatures garnet is confined to higher pressures). Clinopyroxene was found in all of the hydrated experiments, and it was the only observed phase found at the liquidus. Plagioclase enters at 5 kbar and 900 ^{o}C in the P-T diagram.

The anhydrous 1-atm experiments have a liquidus that is shifted to slightly above 1200 ^{o}C. At 1196 ^{o}C plagioclase appears and at 1120 ^{o}C clinopyroxene (pigeonite) enter (Fig. 5.6). An accessory phase mineral (Ti-ilmenite) is observed at 1099 ^{o}C. Two duplicate beads, with the same starting material, were each hanging on the 1-atm experiment loop. The run products for both were often similar regarding phases present, except for sample B26-14 (at 1117 ^{o}C), which had crystals form in only one of the beads; however, the run was replicated at the same temperature (sample B26-12).

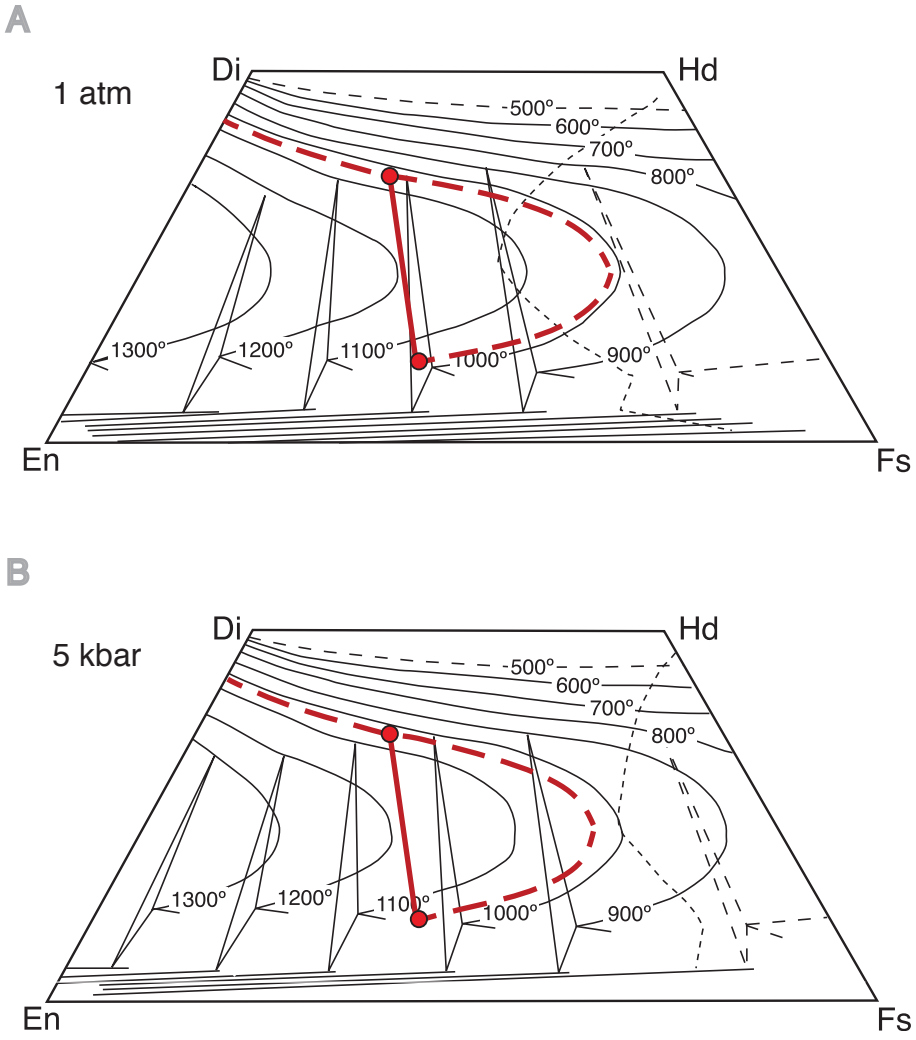

Figure 5.8 Quadrilateral diagram adapted from Lindsley and Andersen (1983) showing compositions of natural coexisting clinopyroxenes and orthopyroxenes within the Late-1 lavas (Ewart et al., 1973). Di, Hd, En, and Fs denote pyroxene end-members: diopside, hedenbergite, enstatite, and ferrosilite. The pyroxenes plot slightly above the 1000 °C temperature curve.

5.3.4 Attainment of Equilibrium

Previous studies show that the duration for which the experiments ran was sufficient to achieve equilibrium in melts and mineral assemblages (Green, 1972; Green, 1976; Nicholls & Harris, 1980). Above 1100 °C, the time required to produce equilibrium is 1-4 h, below 1100 °C needed greater than 6-12 h, and below 950 °C

greater than 12 h is sufficient. Additionally, the equilibrium between the phases and the melt is indicated by the homogeneity of the mineral phases.

5.3.5 Use of limited data

Only limited data could be collected due to issues with the analytical facilities. This meant that not all of the run products and phases were able to be analysed for major elements. The successful experiments were analyzed for mineral phases and scanned for back-scattered electron images. In some cases, such as samples M10-47 and M10-60, the analyses overlapped a microcrystal resulting in a mixture of glass and mineral, these analyses have been excluded. Furthermore, variability in Fe is observed as a direct result of a small number of analyses, FeO totals increase as the number of analysis decrease. This probably also has to do with minimal overlapping in microcrystals. However, the lack of further analysis does not allow for a conclusive result. As an outcome of the limited data, the foundation of this study became to positively identify the phases in its experiments and their interpretation concerning the depth of crystallization beneath Late.

5.4 Discussion

5.4.1 Island-arc magmas: evidence for hot, wet, and shallow melt generation

Ewart et al. (1973) inferred that the crystallization of Tongan magmas had occurred at ≤2 kbar in pressure. This inference was made using experimental and mineralogical constraints of high alumina basalt in water saturated conditions (Yoder & Tilley, 1962), and the olivine tholeiite water in undersaturated conditions (Holloway &

Burnham, 1972). Ewart (1976) also estimated temperatures for the crystallization of the Tongan basaltic andesites, using various geothermometers to calculate the temperature of the Tongan basaltic andesites, resulting in estimates for: (1) pyroxene equilibration (990-1150 ^{o}C), (2) initial eruptive quenching (1008-1124 ^{o}C), and (3) plagioclase liquidus temperatures at 1 bar (1210-1277 ^{o}C).

Naturally coexisting augite and pigeonite pyroxenes in the sample from Late (L1) were used to constrain the estimated temperature of crystallization following the method used by Lindsley and Andersen (1983) (Fig. 5.8). The projection on Figure 5.8a is on a 1-atm quadrilateral and generates a temperature of ~1020 ^{o}C. If we use the 5 kbar quadrilateral (Fig. 5.8b), it produces a higher temperature of ~1075 ^{o}C. This figure is consistent with the calculated values attained by other studies (Ewart et al., 1973; Ewart, 1976; Caulfield et al., 2012; Turner et al., 2012). Ewart et al. (1973) inferred through the use of linear least-squares models, mineralogy, and major and trace element chemistry, which more evolved lavas from the Tongan arc are the product of fractional crystallization of basalt andesite magmas at low pressure (≤2 kbar). Ewart (1976) further refined the model by combining temperature estimates with experimental data to infer crystallization in water-saturated conditions at pressures <2 kbar. Recent studies of Tofua and Fonualei have utilized geothermometry to constrain the temperatures of the evolved lavas on the respective islands to 950-1200 ^{o}C for Tofua, and a smaller range of 1000-1100 ^{o}C for Fonualei (Caulfield et al., 2012; Turner et al., 2012).

Water and carbon dioxide (H_2O and CO_2) contents for lavas from Tofua have been reported by Cooper (2009) as yielding a maximum H_2O content of 4.16 wt% and a maximum CO_2 content of 350 ppm. Using the H_2O-CO_2-melt solution model (VolatileCalc) of Newman and Lowenstern (2002), saturation curves were calculated by Cooper (2009) to show that a degassing trend occurred between the pressures of 0.5-2 kbar. Caulfield et al. (2012) elaborated by highlighting the incremental changes of water

at a consistent carbon dioxide range, inferring magmatic ponding. This is supported by Spilliaert et al. (2006) who concluded, from melt inclusion data, deep CO_2 flushing followed by dehydration of the magma. Thus, magma was being stored at a shallow depth (<5 km) and the predominance of crystallization, occurring as the magma ascends, is driven by the loss of volatile elements.

A comparison of the Late lavas to Paricutin andesites (located in Mexico; Eggler, 1972) shows that saturation with 5 wt% H_2O occurs up to ~1.5 kbar. The Paricutin andesites are similar to the Late basaltic andesites except for being less calcic and more alkali and silica-rich. The liquidus of Late occurs at a lower temperature than at Paricutin (~1050^{o}C at 5 kbar increasing to 1205^{o}C at 1-atm) (Eggler, 1972). Moreover, Ewart et al. (1977) postulated that the absence of amphibole and olivine and the preponderance of highly calcic plagioclase in the lavas meant that the magmas had less water and were only water saturated at pressures <0.5 kbar. Therefore, if the lavas from Late have similar water contents to the neighboring volcanoes, then it supports the models featuring shallow crustal fractional crystallization suggested by both Caulfield et al. (2012) and Turner et al. (2012).

5.4.2 Partial melting of amphibole versus fractional crystallization

Amphibole is notably absent from the lavas from Late and the neighboring volcanoes that erupted evolved lavas to the north (Fonualei) and the south (Tofua). However, given the number of publications addressing the role of fractional crystallization and amphibole in generating silicic magmas in intra-oceanic arcs (Wade et al., 2005; Smith et al., 2006, 2010; Brophy, 2008, 2009; Reubi & Blundy, 2009, Caulfield et al., 2012; Turner et al., 2012), this section will explore this topic in the light of the experimental data from Late.

Davidson et al. (2012) explored a means by which to differentiate mineral control (amphibole and clinopyroxene versus garnet) and sediment melting on REE partitioning, by employing Dy/Dy*. The equation is calculated as:

$$Dy/Dy^* = Dy_N / La_N^{4/13} Yb_N^{9/13}$$

(Davidson et al. 2012) where Dy_N, La_N, and Yb_N are the chondrite-normalized values of Dy, La, and Yb, respectively. The normalization constants I use are from Nakamura (1974). Using Dy/Dy*, as a representative middle rare earth element, and Dy/Yb allows discrimination of amphibole and clinopyroxene from garnet fractionation by measuring the concavity of the REE pattern. The effects of minerals such as olivine, clinopyroxene, amphibole, garnet, and plagioclase on the REE patterns are expressed in Dy/Dy*-Dy/Yb, illustrated in Figure 5.9; however, Davidson et al. (2012) argued that olivine and plagioclase do not present significant effects on the concavity of the REE pattern and that clinopyroxene, amphibole, and garnet were the primary minerals accountable as the controls. Amphibole (and to a lesser extent clinopyroxene) have the most significant effect on both Dy/Dy* and Dy/Yb, which leads to a positive slope "step-down" feature away from the MORB field. A garnet influence (batch partial melting and fractional crystallization) only affects Dy/Yb, displayed on the Dy/Dy*-Dy/Yb figure as a horizontal array away from the MORB field and in the opposite direction to amphibole and clinopyroxene. Both trends are distinguishable features of the control these three minerals have on the REE pattern. Figure 5.9 illustrates general arc characteristics of depleted and enriched lavas derived from variably enriched MORB sources. Moreover, Figure 5.9 demonstrates the "step-down" feature ubiquitous in arcs which Davidson et al. (2012) suggest is controlled by amphibole or clinopyroxene fractionation. The lavas from Late plot in a similar step-down manner as the lavas from other arcs around the world. This trend supported the hypothesis made by Davidson et al. (2007, 2012) that amphibole has an important influence on the

formation of these lavas. However, given that there is no amphibole present in the natural samples these studies could not preclude the role that clinopyroxene may play in controlling arc differentiation trends.

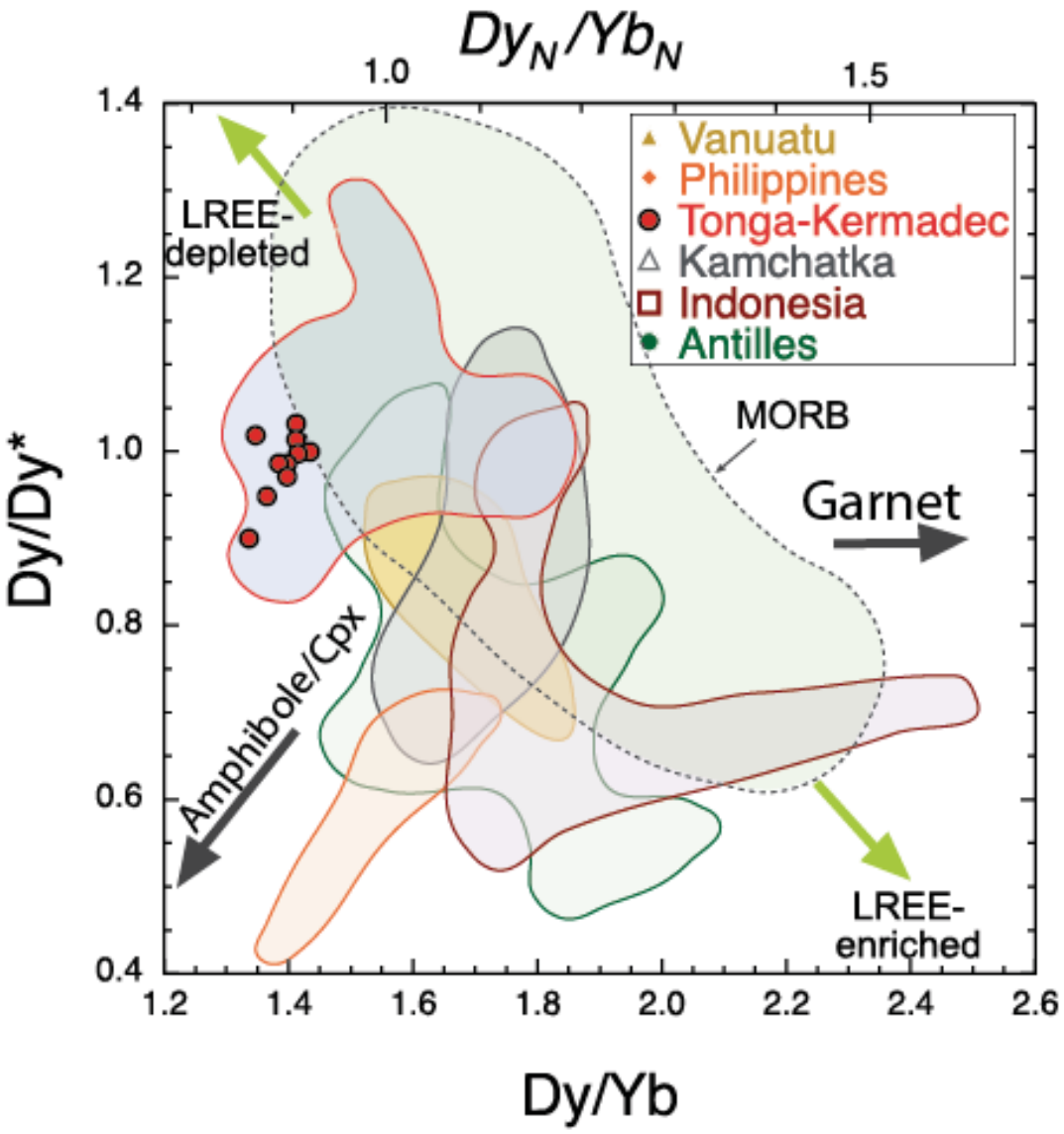

Figure 5.9 Variation of Dy/Dy* and Dy/Yb (from Davidson et al., 2012), showing general differences among arcs. Dy/Dy*, a representative middle rare earth element, and DY/Yb allows discrimination of amphibole and clinopyroxene from garnet fractionation by measuring the concavity of the REE pattern. The lavas from Late (red symbols) plot within the Tonga-Kermadec field in a 'step-down' feature which suggests fractionation from amphibole and/or clinopyroxene. The fields show variable degrees of source LREE depletion and LREE enrichment. However, amphibole remains absent from all studies and investigations in the Tongan arc and Late volcano.

Studies have highlighted several factors that delineate the presence of amphibole in intermediate magmas: the source region, the stability of amphibole in water-undersaturated melts, and the amount of water affecting the temperature of the partial melt (Eggler, 1972; Foden and Green, 1992; Ghiroso, 1999). A study of the possible ascent path for an andesitic magma from the Colima volcano (Carmichael, 2002) in Mexico addressed the conditions in which a hydrous magma with no trace of hydrous-bearing minerals could form. The fate in the direction of magma ascent is dependent on the temperature and initial water content of the magma. Water-undersaturated (< 6 wt% H_2O) magmas at temperatures above 950^oC ascend, losing water, through the liquidus, circumventing the amphibole stability field, to a P-T region where anhydrous minerals precipitate (olivine, pyroxene, and plagioclase) (Carmichael, 2002). Therefore, the Late magmas are constrained by conditions where they are either too hot to crystallize amphibole or when the temperatures become suitable for amphibole nucleation, water will have already been lost from the magma through fractional crystallization processes, further preventing amphibole crystallization. None of the experiments from Late produced amphibole, suggesting that water remained undersaturated in the experiments; however, it is possible that the water content of the experiments is either lower or higher than natural conditions, particularly because water for Late has been taken by proxy from neighboring volcanoes (Cooper, 2010). Additionally, higher calcic plagioclase crystallizes at lower temperatures as a cause of higher water contents, which is observed in the plagioclase from the natural sample (Fig. 5.7b). Conversely, the experiments produced less calcic plagioclase which suggests that the water content in the experiments was lower than in the natural sample.

Both fractional crystallization and partial melting of lower crustal amphibolite can lead to similar major and trace element characteristics in felsic magmas; however, constraints have been proposed to highlight the presence of amphibole. A decrease in

Dy/Yb ratios as the magma evolves (Fig. 5.10a) has been suggested to be a clear indicator of the presence of amphibole as the fractionating phase (Davidson et al., 2007). However, the Late lavas plot on a horizontal array (with a slope for the linear trendline of -0.0308) indicating that amphibole is not present in the fractionation of their magmas. Furthermore, models proposed by Brophy (2008) to discriminate between the effects of fractional crystallization and amphibolite partial melting require lavas that are influenced by amphibolite melting to display a horizontal or negative array. By contrast, the Late lavas (Fig. 5.10bc) demonstrate a positive array as they follow the shallow crustal (low-P) fractionation trend.

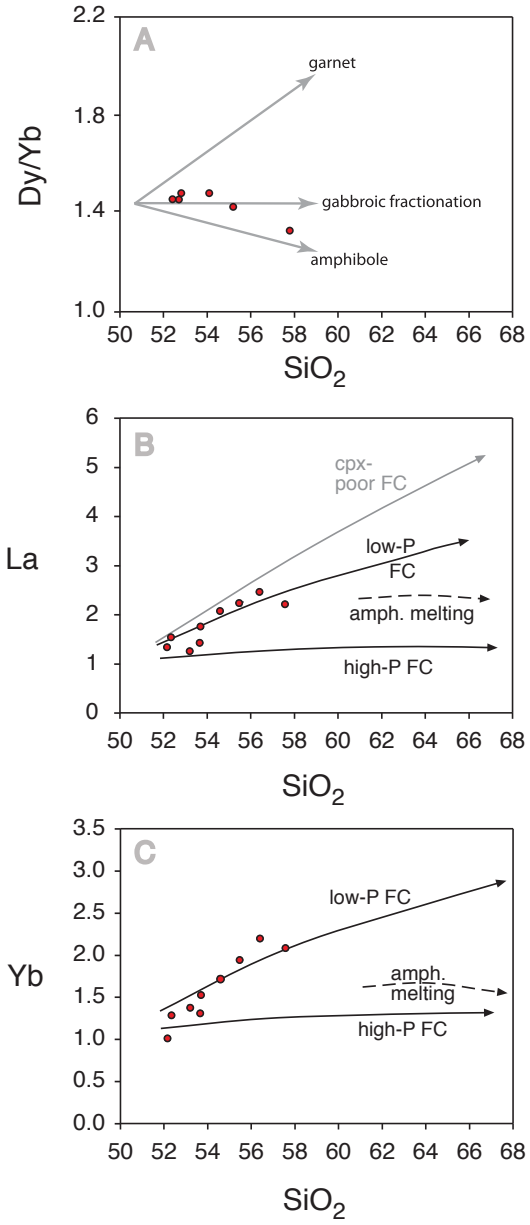

Figure 5.10 Variation of Dy/Yb, La, and Yb vs SiO_2 for the Late volcanic rocks (red symbols) along with vectors calculated by (A) Davidson et al. (2007) for fractionation in heavy rare earth elements by garnet, gabbroic fractionation, or amphibole (B & C) and by Brophy (2008) for low-P and high-P crustal fractional crystallization or amphibolite partial melting. (A) Late volcanic samples plot flat along the gabbroic fractionation vector and (B) follow the low-P (lower crustal) fractional crystallization trend.

Models produced by Ewart et al. (1973), Caulfield et al. (2012), and Turner et al. (2012) have shown that the magmas from the Tongan arc have undergone low-pressure

fractional crystallization from mafic parental magmas. Furthermore, a recent study (Adam et al., 2016) on the phase equilibria of the crystal phases present (plagioclase, orthopyroxene, and diopside) plots bulk rock data from the Tonga-Kermadec arc on a $CaAl_2O_4$-silica-forsterite projection (Fig. 5.11). Adam et al. (2016) demonstrate magma evolution by fractional crystallization that is driven by water loss from magmas as they ascend to shallow (low pressure) depths. The phase equilibria in conjunction with the barometry for phenocrysts (0.8-1.8 kbar) in the Tongan lavas (Ewart et al., 1973; Caulfield et al., 2012) show that the melts fractionated along at the same low-pressure cotectic.

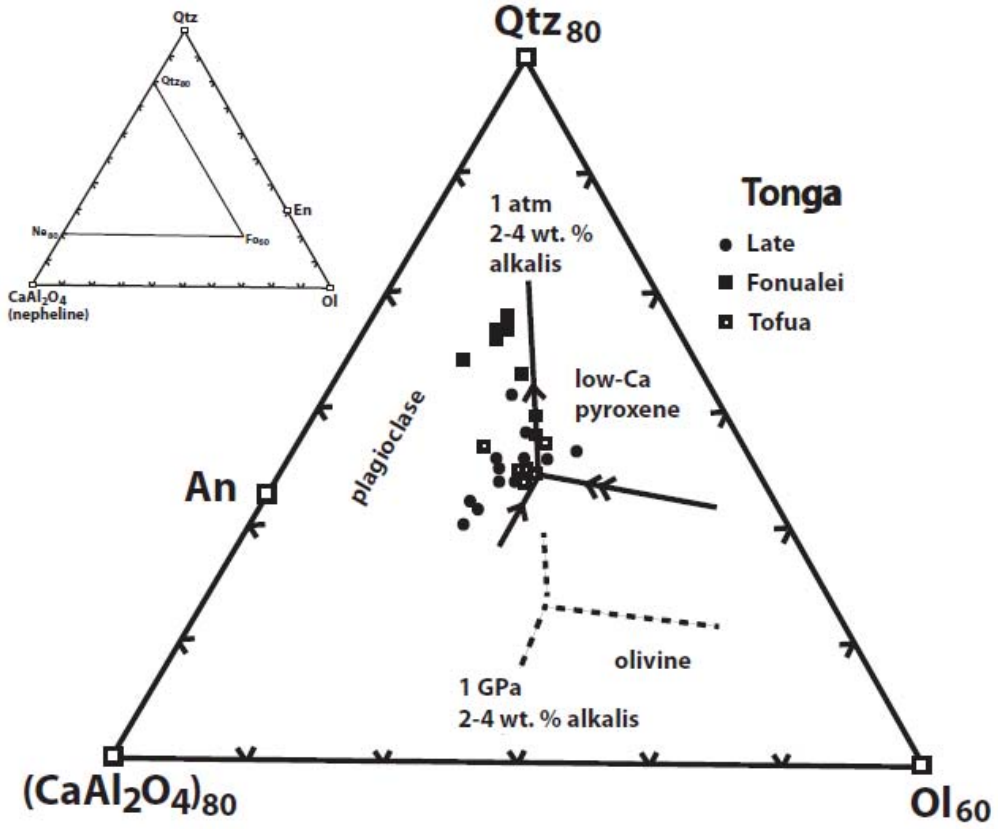

Figure 5.11 Compositional data for Tongan volcanic rocks projected within the $CaAl_2O_4$-silica-forsterite system, together with diopside-saturated liquidus relations for matching low-alkali melts (from Adam et al., 2016). Data for Late volcanic rocks: Ewart et al. (1973). Data for liquidus relations: Baker &

Eggler (1987), Moore & Carmichael (1988), Draper and Johnson (1992), Grove et al., (2003).

The available phase equilibria experiments for the Late volcano suffice to nullify an origin by high-pressure crystallization or a partial melting origin. The absence of amphibole in the Late samples and in reported observations along the arc (Baker et al., 1971; Bryan et al., 1972; Ewart et al., 1973, 1977; Ewart & Hawkesworth, 1987; Caulfield et al., 2012; Turner et al. 2012), along with the evidence presented in this section, supports the assertion made in other studies that amphibole does not play a role in the fractionation of these magmas (Ewart et al., 1973; Caulfield et al., 2012; Turner et al., 2012).

5.4.3 Future work

The conclusions made in this study support current models. The limitations of the experimental apparatus mean that we could not reach the low pressures necessary to produce a definitive result at the low pressures inferred by geochemical modeling. Further work in constraining P-T conditions for evolved lavas in the Tonga-Kermadec arc will need to conduct successful experiments that can reliably maintain pressures of <2.5 kbar. Utilizing a rapid-quench TZM apparatus is the way to accurately generate experiments at those lower (<2.5 kbar) pressures. These apparatuses are currently being constructed at the Australia National University, with completion not expected until late next year.

5.5 Conclusions

The Late volcanic rocks are neither the most primitive nor the most fractionated rocks in the Tonga-Kermadec arc. However, when compared to the neighboring

volcanoes, together they form an array that spans from primitive to more evolved rocks. The experiments performed on Late-1 provide us with a unique window into the evolution of these intra-oceanic arc magmas. The experiments conducted in this study support the previous studies which negate the existence of amphibole (and subsequently a derivation by partial melting of lower crustal amphibolite). Furthermore, the experiments in this study show that the P-T stability field for Late is in a shallower crust. The magmatic evolution of Late has been one of fractional crystallization propelled by water loss from magmas as they ascend to shallow (low pressure) depths. The phase equilibria in conjunction with the barometry for phenocrysts (0.8-1.8 kbar) in the Tongan lavas show that the melts equilibrated at the same low-pressure cotectic through fractional crystallization.

5.6 References

Akella, J. (1973) Friction measurement in solid-media, high-pressure apparatus. *Carnegie Inst. Yearbook*, *73*, 606-609.

Annen, C., Blundy, J. D., & Sparks, R. S. J. (2005) The genesis of intermediate and silicic magmas in deep crustal hot zones. *Journal of Petrology*, *47*(3), 505-539.

Baker, P. E., Harris, P. G., & Reay, A. (1971) The geology of Tofua island, Tonga. *Royal Society New Zealand Bulletin*, *8*, 67-79.

Bence, A. E., & Albee, A. L. (1968) Empirical correction factors for the electron microanalysis of silicates and oxides. *The Journal of Geology*, *76*(4), 382-403.

Bevis, M., Taylor, F.W., Schutz, B.E., Recy, J. & Isacks, B.L., Helu, S., Singh, R., Kendrick, E., Stowell, J. (1995) Geodetic observations of very rapid convergence and back-arc extension at the Tonga arc. *Nature* 374, 249-251.

Boyd, F. R., & England, J. L. (1960) Apparatus for phase-equilibrium measurements at pressures up to 50 kilobars and temperatures up to 1750° C. *Journal of Geophysical Research*, *65*(2), 741-748.

Brophy, J. G. (2008) A study of rare earth element (REE)–SiO_2 variations in felsic liquids generated by basalt fractionation and amphibolite melting: a potential test for discriminating between the two different processes. *Contributions to Mineralogy and Petrology*, *156*(3), 337-357.

Brophy, J. G. (2009) Decompression and H_2O exsolution driven crystallization and fractionation: development of a new model for low-pressure fractional crystallization in calc-alkaline magmatic systems. *Contributions to Mineralogy and Petrology*, *157*(6), 797.

Bryan, W. B., Stice, G. D., & Ewart, A. (1972) Geology, petrography, and geochemistry of the volcanic islands of Tonga. *Journal of geophysical research*, *77*(8), 1566-1585.

Cameron, E., Gamble, J., Price, R., Smith, I., McIntosh, W., & Gardner, M. (2010) The petrology, geochronology and geochemistry of Hauhungatahi volcano, SW Taupo Volcanic Zone. *Journal of Volcanology and Geothermal Research*, *190*(1), 179-191.

Carmichael, I. S. (2002) The andesite aqueduct: perspectives on the evolution of intermediate magmatism in west-central (105-99 W) Mexico. *Contributions to Mineralogy and Petrology*, *143*(6), 641-663.

Castillo, P. R., Lonsdale, P. F., Moran, C. L., & Hawkins, J. W. (2009) Geochemistry of mid-Cretaceous Pacific crust being subducted along the Tonga–Kermadec Trench: Implications for the generation of arc lavas. *Lithos*, *112*(1), 87-102.

Caulfield, J. T., Turner, S. P., Dosseto, A., Pearson, N. J., & Beier, C. (2008). Source depletion and extent of melting in the Tongan sub-arc mantle. *Earth and Planetary Science Letters*, *273*(3), 279-288.

Caulfield, J. T., Turner, S. P., Smith, I. E. M., Cooper, L. B., & Jenner, G. A. (2012). Magma evolution in the primitive, intra-oceanic Tonga arc: petrogenesis of basaltic andesites at Tofua volcano. *Journal of Petrology*, *53*(6), 1197-1230.

Cooper, L. B. (2010) Volatiles in Tonga Arc magmas and their role in unraveling subduction zone processes. PhD thesis, Boston University.

Cooper, L. B., Plank, T., Arculus, R. J., Hauri, E. H., Hall, P. S., & Parman, S. W. (2010) High-Ca boninites from the active Tonga Arc. *Journal of Geophysical Research: Solid Earth*, *115*(B10).

Davidson, J., Turner, S., Handley, H., Macpherson, C., & Dosseto, A. (2007) Amphibole “sponge” in arc crust?. *Geology*, *35*(9), 787-790.

Davidson, J., Turner, S., & Plank, T. (2012) Dy/Dy*: variations arising from mantle sources and petrogenetic processes. *Journal of Petrology*, *54*(3), 525-537.

Dufek, J., & Bergantz, G. W. (2005) Lower crustal magma genesis and preservation: a stochastic framework for the evaluation of basalt–crust interaction. *Journal of Petrology*, *46*(11), 2167-2195.

Eggler, D. H. (1972) Water-saturated and undersaturated melting relations in a Paricutin andesite and an estimate of water content in the natural magma. *Contributions to Mineralogy and Petrology*, *34*(4), 261-271.

Ewart, A. (1976) A petrological study of the younger Tongan andesites and dacites, and the olivine tholeiites of Niua Fo'ou Island, SW Pacific. *Contributions to Mineralogy and Petrology*, *58*(1), 1-21.

Ewart, A., Brothers, R. N., & Mateen, A. (1977) An outline of the geology and geochemistry, and the possible petrogenetic evolution of the volcanic rocks of the Tonga-Kermadec-New Zealand island arc. *Journal of volcanology and geothermal research*, *2*(3), 205-250.

Ewart, A., Bryan, W. B., Chappell, B. W., & Rudnick, R. L. (1994). Regional geochemistry of the Lau-Tonga arc and backarc systems. In *Proceedings of the Ocean Drilling Program. Scientific Results* (Vol. 135, pp. 385-425). Ocean Drilling Program.

Ewart, A., Bryan, W. B., & Gill, J. B. (1973) Mineralogy and geochemistry of the younger volcanic islands of Tonga, SW Pacific. *Journal of Petrology*, *14*(3), 429-465.

Ewart, A., & Hawkesworth, C. J. (1987) The Pleistocene-Recent Tonga-Kermadec arc lavas: interpretation of new isotopic and rare earth data in terms of a depleted mantle source model. *Journal of petrology*, *28*(3), 495-530.

Gamble, J. A., Smith, I. E. M., McCulloch, M. T., Graham, I. J., & Kokelaar, B. P. (1993) The geochemistry and petrogenesis of basalts from the Taupo Volcanic Zone and Kermadec Island Arc, SW Pacific. *Journal of volcanology and geothermal research*, *54*(3-4), 265-290.

Gamble, J. A., Christie, R. H. K., Wright, I. C., & Wysoczanski, R. J. (1997) Primitive K-rich magmas from Clarke volcano, southern Kermadec arc: A paradox in the K-depth relationship. *Canadian Mineralogist* 35, 195-211.

Ghiorso, M. S. (1999) On the stability relations of hydrous minerals in water-undersaturated magmas. *American Mineralogist*, *84*(10), 1506-1511.

George, R., Turner, S., Morris, J., Plank, T., Hawkesworth, C., & Ryan, J. (2005) Pressure–temperature–time paths of sediment recycling beneath the Tonga–Kermadec arc. *Earth and Planetary Science Letters*, *233*(1), 195-211.

Green, T. H. (1972) Crystallization of calc-alkaline andesite under controlled high-pressure hydrous conditions. *Contributions to Mineralogy and Petrology*, *34*(2), 150-166.

Green, D. H. (1976) Experimental testing of "equilibrium" partial melting of peridotite under water-saturated, high-pressure conditions. *The Canadian Mineralogist*, *14*(3), 255-268.

Foden, J. D., & Green, D. H. (1992) Possible role of amphibole in the origin of andesite: some experimental and natural evidence. *Contributions to Mineralogy and Petrology*, *109*(4), 479-493.

Haase, K. M., Stroncik, N., Garbe-Schönberg, D., & Stoffers, P. (2006) Formation of island arc dacite magmas by extreme crystal fractionation: an example from

Brothers Seamount, Kermadec island arc (SW Pacific). *Journal of Volcanology and Geothermal Research*, *152*(3), 316-330.

Haase, K. M., Krumm, S., Regelous, M., & Joachimski, M. (2011) Oxygen isotope evidence for the formation of silicic Kermadec island arc and Havre–Lau backarc magmas by fractional crystallisation. *Earth and Planetary Science Letters*, *309*(3), 348-355.

Haase, K. M., Lima, S., Krumm, S., & Garbe-Schönberg, D. (2014) The magmatic evolution of young island arc crust observed in gabbroic to tonalitic xenoliths from Raoul Island, Kermadec Island Arc. *Lithos*, *210*, 199-208.

Hergt, J. M., & Woodhead, J. D. (2007) A critical evaluation of recent models for Lau–Tonga arc–backarc basin magmatic evolution. *Chemical Geology*, *245*(1), 9-44.

Holloway, J. R., & Burnham, C. W. (1972) Melting relations of basalt with equilibrium water pressure less than total pressure. *Journal of Petrology*, *13*(1), 1-29.

Lindsley, D. H., & Andersen, D.J. (1983) A two-pyroxene thermometer. *Journal of Geophysical Research: Solid Earth*, *88*(S02).

Nakamura, N. (1974) Determination of REE, Ba, Fe, Mg, Na and K in carbonaceous and ordinary chondrites. *Geochimica et Cosmochimica Acta*, *38*(5), 757-775.

Newman, S., & Lowenstern, J. B. (2002) VolatileCalc: a silicate melt–H_2O–CO_2 solution model written in Visual Basic for Excel. *Computers & Geosciences*, *28*(5), 597-604.

Nicholls, I. A., & Harris, K. L. (1980) Experimental rare earth element partition coefficients for garnet, clinopyroxene and amphibole coexisting with andesitic and basaltic liquids. *Geochimica et Cosmochimica Acta*, *44*(2), 287-308.

O'Neill, H. S. C., & Mavrogenes, J. A. (2002) The sulfide capacity and the sulfur content at sulfide saturation of silicate melts at 1400 C and 1 bar. *Journal of Petrology*, *43*(6), 1049-1087.

Petford, N., & Gallagher, K. (2001) Partial melting of mafic (amphibolitic) lower crust by periodic influx of basaltic magma. *Earth and Planetary Science Letters*, *193*(3-4), 483-499.

Pouchou, J. L., & Pichoir, F. (1984) A New Model for Quantitative X-Ray Microanalysis. I.--Application to the Analysis of Homogeneous Samples. *Rech. Aerosp.*, (3), 167-192.

Price, R. C., Gamble, J. A., Smith, I. E., Maas, R., Waight, T., Stewart, R. B., & Woodhead, J. (2012) The anatomy of an Andesite volcano: a time–stratigraphic study of andesite petrogenesis and crustal evolution at Ruapehu Volcano, New Zealand. *Journal of Petrology*, *53*(10), 2139-2189.

Regelous, M., Collerson, K. D., Ewart, A., & Wendt, J. I. (1997) Trace element transport rates in subduction zones: evidence from Th, Sr and Pb isotope data for Tonga-Kermadec arc lavas. *Earth and Planetary Science Letters*, *150*(3), 291-302.

Regelous, M., Gamble, J. A., & Turner, S. P. (2010) Mechanism and timing of Pb transport from subducted oceanic crust and sediment to the mantle source of arc lavas. *Chemical Geology*, *273*(1), 46-54.

Reubi, O., & Blundy, J. (2009) A dearth of intermediate melts at subduction zone volcanoes and the petrogenesis of arc andesites. *Nature*, *461*(7268), 1269.

Shane, P., & Wright, I. C. (2011) Late Quaternary tephra layers around Raoul and Macauley Islands, Kermadec Arc: implications for volcanic sources, explosive volcanism and tephrochronology. *Journal of Quaternary Science*, *26*(4), 422-432.

Smith, I. E., Stewart, R. B., & Price, R. C. (2003) The petrology of a large intra-oceanic silicic eruption: the Sandy Bay Tephra, Kermadec Arc, Southwest Pacific. *Journal of Volcanology and Geothermal Research*, *124*(3), 173-194.

Smith, I. E., Worthington, T. J., Price, R. C., Stewart, R. B., & Maas, R. (2006) Petrogenesis of dacite in an oceanic subduction environment: Raoul Island, Kermadec arc. *Journal of Volcanology and Geothermal Research*, *156*(3), 252-265.

Smith, I. E., Price, R. C., Stewart, R. B., & Worthington, T. J. (2009) An assessment of the mantle and slab components in the magmas of an oceanic arc volcano: Raoul Volcano, Kermadec arc. *Journal of Volcanology and Geothermal Research*, *184*(3), 437-450.

Smith, I. E., Stewart, R. B., Price, R. C., & Worthington, T. J. (2010) Are arc-type rocks the products of magma crystallisation? Observations from a simple oceanic arc volcano: Raoul Island, Kermadec Arc, SW Pacific. *Journal of Volcanology and Geothermal Research*, *190*(1), 219-234.

Spilliaert, N., Allard, P., Métrich, N., & Sobolev, A. V. (2006) Melt inclusion record of the conditions of ascent, degassing, and extrusion of volatile-rich alkali basalt during the powerful 2002 flank eruption of Mount Etna (Italy). *Journal of Geophysical Research: Solid Earth*, *111*(B4).

Timm, C., Graham, I. J., de Ronde, C. E., Leybourne, M. I., & Woodhead, J. (2011) Geochemical evolution of Monowai volcanic center: New insights into the northern Kermadec arc subduction system, SW Pacific. *Geochemistry, Geophysics, Geosystems*, *12*(8).

Turner, S., Bourdon, B., Hawkesworth, C., & Evans, P. (2000) 226 Ra–230 Th evidence for multiple dehydration events, rapid melt ascent and the time scales of differentiation beneath the Tonga–Kermadec island arc. *Earth and Planetary Science Letters*, *179*(3), 581-593.

Turner, S., Caulfield, J., Rushmer, T., Turner, M., Cronin, S., Smith, I., & Handley, H. (2012) Magma evolution in the primitive, intra-oceanic Tonga arc: rapid petrogenesis of dacites at Fonualei volcano. *Journal of petrology*, *53*(6), 1231-1253.

Turner, S., Handler, M., Bindeman, I., & Suzuki, K. (2009) New insights into the origin of O–Hf–Os isotope signatures in arc lavas from Tonga–Kermadec. *Chemical Geology*, *266*(3), 187-193.

Turner, S., & Hawkesworth, C. (1997) Constraints on flux rates and mantle dynamics beneath island arcs from Tonga-Kermadec lava geochemistry. *Nature*, *389*(6651), 568.

Turner, S., Hawkesworth, C., Rogers, N., Bartlett, J., Worthington, T., Hergt, J., Pearce, J., & Smith, I. (1997) 238 U-230 Th disequilibria, magma petrogenesis, and flux rates beneath the depleted Tonga-Kermadec island arc. *Geochimica et Cosmochimica Acta*, *61*(22), 4855-4884.

Wade, J. A., Plank, T., Stern, R. J., Tollstrup, D. L., Gill, J. B., O'Leary, J. C., Eiler, J. M., Moore, R. B., Woodhead, J. D., Trusdell, F., Fischer, T. P. & Hilton, D. R. (2005) The May 2003 eruption of Anatahan volcano, Mariana Islands: Geochemical evolution of a silicic island-arc volcano. *Journal of Volcanology and Geothermal Research*, *146*(1), 139-170.

Woodhead, J., Eggins, S., & Gamble, J. (1993) High field strength and transition element systematics in island arc and back-arc basin basalts: evidence for multi-phase melt extraction and a depleted mantle wedge. *Earth and Planetary Science Letters*, *114*(4), 491-504.

Yoder Jr, H. S., & Tilley, C. E. (1962) Origin of basalt magmas: an experimental study of natural and synthetic rock systems. *Journal of Petrology*, *3*(3), 342-532.

6 Conclusion

The research presented in this thesis looks at numerous factors that affect the output of volcanic rocks in subduction zones. Chapter 2 begins with an analysis of lithium isotopes and how they are transferred from input to output in the Tonga-Kermadec arc. Chapter 3 employs trace and volatile elements to understand the geochemical reservoirs that occupy the upper mantle to explain heterogeneities in the North Fiji basin. Chapter 4 aims to constrain the nature of the various geochemical plume signatures to constrain the origin of the geochemical signals in the Lau and North Fiji basin by mapping mantle flow patterns through the use of various geochemical tools. In Chapter 5, I return to the arc front to constrain the depth and temperature in which the evolved lavas from Late volcano formed. This final chapter provides a summary of the ideas presented in this thesis and reflects on the current understanding of Tongan volcanics and the scope for further work.

6.1 Summary of lithium isotopes

I have undertaken a reconnaissance study of Li isotopes in the oceanic Tonga-Kermadec arc and Lau back-arc as well as the sediment profile at DSDP Site 204. Like many arc lavas, the range in δ^7Li appears to have been muted by diffusive equilibration

with ambient mantle. Nevertheless, lava from Niuatoputapu Island appears to carry a signature from the subducting Louisville volcaniclastic sediments. Lavas from ‘Ata and L’Esperance Islands have unusually low δ^7Li of unknown origin. The remaining arc front and back-arc lavas show results of δ^7Li = 3.6 ± 0.7 ‰. Modelled δ^7Li – Y/Li relationships require 1-3% bulk sediment addition to explain the range in observed ratios. This is an order of magnitude higher than required by Th-Nd-Be isotope systematics, suggesting an important role for fluid addition of Li from both the subducting sediments and altered oceanic crust beneath this arc – back-arc system.

6.2 Summary of volatile content beneath the North Fiji basin

The samples from the NFB exhibit a combination of major MORB-like chemical signatures along with high water content similar to ocean island basalts (OIB). This observation in geochemistry is unlike any other studied MORB or back-arc basin because it is not attributed to a subduction-related signature. Our results employ volatile elements (carbon dioxide and water) and their constraints, both combined with trace element ratios, to indicate a potential wet plume source for the observed enrichment in the North Fiji Basin. I have found that the lavas from the NFB (triple junction) have degassed upon eruption, affecting only the carbon dioxide in the lavas. Moreover, I discovered that the water content of these lavas exceeds that of MORB and displays enrichment in REEs (La/Sm and Gd/Yb) relative to MORB. These geochemical signatures result from a mixture of melts from variable sources in the mantle. These sources are MORB mixed with an enriched plume (OIB) source in the field of garnet lherzolite stability, followed by advection and adiabatic decompression melting within the spreading center.

6.3 Summary of shallow mantle flow beneath the Lau and North Fiji basins

Firstly, we find that strong zonal and meridional geochemical patterns exist within the region which can be explained by the incorporation of three different Pacific hotspots via different processes over the past 4 Ma. Secondly, we found that the incorporation of under-plated Samoan mantle material via toroidal flow around the subducting Pacific Plate is a process that has probably occurred over the past ~4 Ma. Stronger Samoan geochemical signatures are seen in the eastern Lau Basin compared to the northern North Fiji Basin as the younger, hotter, and less viscous Samoan under-plated material located in the east is more easily entrained than the older, colder, more viscous under-plated Samoan material to the north of the North Fiji Basin to the west. Thirdly, the weaker signals of geochemical enrichment observed in the western regions of the back-arc basins compared to the eastern regions may be due to longer periods of mixing with depleted ambient back-arc basin mantle, which will serve to more severely attenuate entrained Samoan hotspot signatures in the west. Fourthly, a plate reconstruction suggests that, although the subduction of the Rarotonga Hotspot track by ~2 Ma can help to explain strong $^{87}Sr/^{86}Sr$ in lavas in the Lau Basin, only Samoan under-plated material can account for the enriched geochemical signatures in the North Fiji Basin. Fifthly, we also found that the most radiogenic Sr (EM) and Pb (HIMU) isotopic compositions in the Lau and North Fiji Basin lavas are limited to the northeastern Lau Basin and are likely to be related to the recent initiation of subduction of the Rurutu and Rarotonga hotspot tracks beneath the northeast Lau Basin, as well as enhanced entrainment of younger, hotter, under-plated Samoan plume material. Lastly, we found that north-south gradients in both the Lau and North Fiji Basins are most enriched in the northern portions of the basin and become more depleted southward.

6.4 Summary of origin of silicic volcanism in Tonga

The experiments conducted in this study support previous studies which negate the existence of amphibole (and subsequently a derivation by partial melting of lower crustal amphibolite). Furthermore, the experiments in this study also show that the P-T stability field for Late is in a shallower crust. The magmatic evolution of Late has been one of fractional crystallization propelled by water loss from magmas as they ascend to shallow (low pressure) depths. The phase equilibria in conjunction with the barometry for phenocrysts (0.8-1.8 kbar) in the Tongan lavas show that the melts equilibrated at the same low-pressure cotectic through fractional crystallization.

7 APPENDICES

A. CSIRO Research Voyage (ss2012_v02): Northern Lau Transit Expedition (NoLauTE)

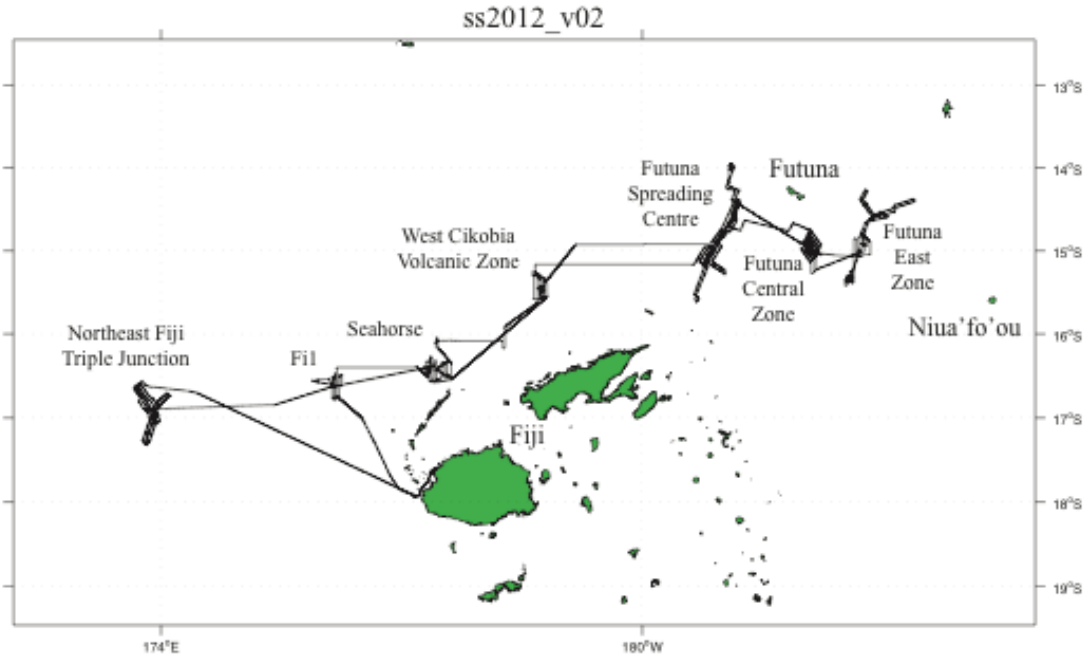

Figure 1 Voyage Track

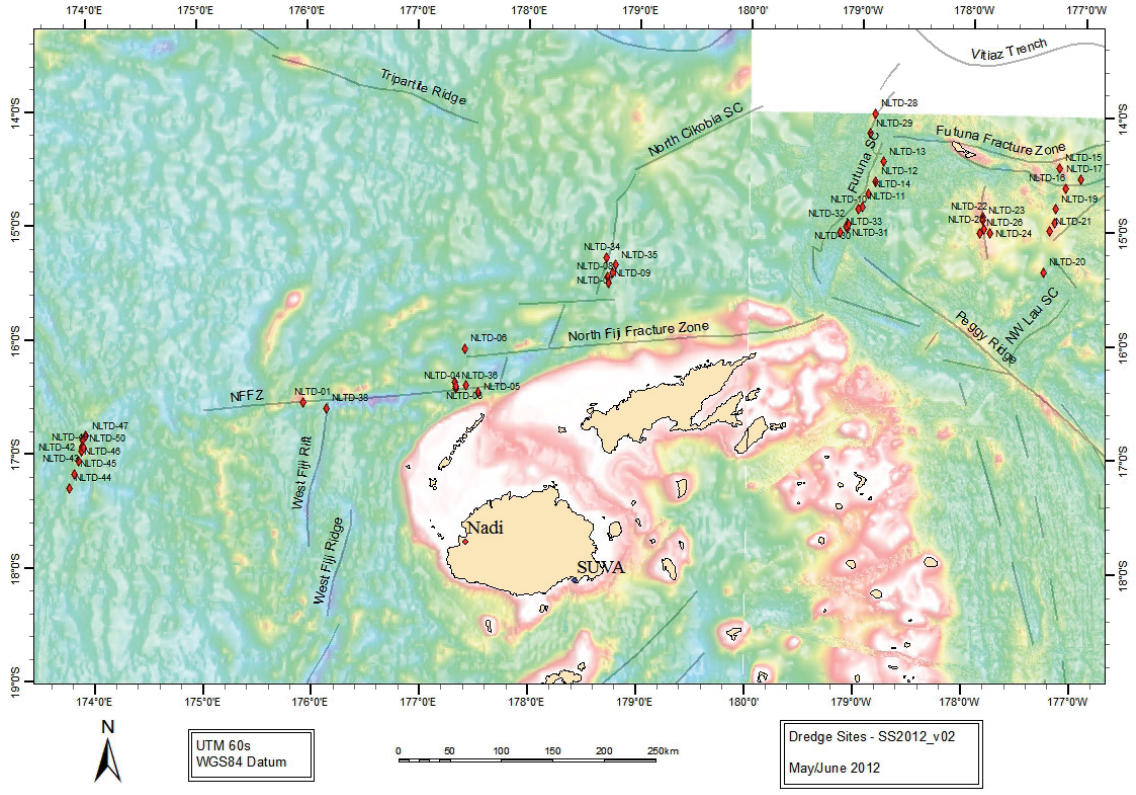

Figure 2 Location of dredges

Table 1 Dredge locations and sample description

Dredge #	Amount of buckets	Description (macro)	Bucket tracking #	Family sample #	Lat/Long (start)	Lat/Long (end)	Location desc.	Date of dredge	Depth range (min-max) meters	Depth (min)	Depth (max)
1	1	*assortment of sedimentary rocks (mudstones & s.s.) - heavy Mn coating, likely old fijian crustal basement*	1	NONE	-16 34.163/+175 56.528	-16 34.351/+175 56.788	**Balmoral Ridge**Crest (west of N. end of Viwa Rift) - sampled summit	13/05/2012	800-834	1740	1835
2	2	*vesicular glass with light - moderate Mn coatings on pillow lavas*	2,3	NLTD 02-4	-16 23.959/+177 19.870	-16 24.000/+177 20.15	**Seahorse Ridge 3**- sampled ridge crest in the extensional relay zone between Yasawa and Yadua Troughs, Fi2 target area	14/05/2012	1740-1835	1767	1901
3	2	*highly altered, vesicular basalt; very few pumice pieces*	4,5	NLTD 03-6	-16 27.27/+177 20.257	-16 27.357/+177 20.580	**Seahorse Ridge 3**- sampled southern tumescence In the ERZ between Yasawa & Yadua Troughs, Fi2 target area	14/05/2012	1767-1901	1720	1805
4	4	*glass exhibiting alternating colors of grey & black (band-like); highly vesicular glass with very light amount of alteration; vesicular aphyric basalt with chilled margins-pillow fragments*	6-9	NLTD 04-2	-16 25.777/+177 25.835	-16 25.749/+177 26.111	**Seahorse Ridge 4**- sampled crest in the ERZ between Yasawa and Yadua Troughs (north of Fiji), Fi2 target area	15/05/2012	1720-1805	1608	1750
5	1	*vesicular pieces of aphyric basalt with altered coatings of Mn; amount of vesicles vary both in size and distribution of the basalt samples; aggregated cumulated of 1/2-2cm pieces of weathered basalt; minimal glass also located in samples*	10	NLTD 05-2	-16 29.259/+177 32.327	-16 29.425/+177 32.704	**Seahorse Ridge 6**- sampled ridge crest in the ERZ between Yasawa and Yadua Troughs, Fi2 target area	15/05/2012	1608-1750		
6	1	*predominantly Fe-stained altered rock (fine grained lava); pumice; multiple chips of Mn-Fe coated rock chips*	11	NONE	-16 06.502/+177 25.220	-16 06.172/+177 25.363	**Central Hill**- sampled from southern summit of Central Hill	15/05/2012	1756-1786	1702	1765
7	3	*assorted aphyric basalt (altered & fresh) pillow fragments and lava tubules; basaltic glass with moderate-heavy coatings of Mn*	12-14	NLTD 07-12	-15 25.518/+178 45.193	-15 25.82/+178 45.92	**West Cikobia(WCVZ)** - sampled from northern summit flank of prominent edifice in West Cikobia Volcanic Zone	16/05/2012	1702-1765	1851	1871
8	1	*heavily altered pillow basalts with a covering of heavily altered glass; minor vesicles*	15	NLTD 08-1	-15 27.562/+178 42.521	-15 27.794/+178 42.851	**West Cikobia (WCVZ)**- sampled main ridge of West Cikobia VZ	17/05/2012	1851-1871	1903	1909
9	1	*large pillows with heavy alteration; assorted bag of mostly glassy pieces with Mn coatings; no vesicles*	16	NLTD 09-1	-15 31.650/+178 43.987	-15 31.310/+178 43.664	**West Cikobia (WCVZ)**- sampled from large donut edifice in WCVZ	17/05/2012	1903-1909	1965	2015
10	1	*lightly altered vesicular glass; basaltic pillow fragments with microphyric plagioclase & olivines (not as much olivine relative to plagioclase)*	17	NLTD 10-2	-14 50.707/+179 01.290	-14 50.688/+179 01.210	**Futuna spreading center (ZC1)**- sampled from central rift in northern ZC1 (zona central 1), Futuna spreading center	18/05/2012	1965-2015	1720	1750
11	1	*basalt with chill margins (glass) & light Mn coatings; no vesicles; sparsely olivine and plagioclase microphyric*	18	NLTD 11-1	-14 48.996/+178 58.789	-14 49.141/+178 58.782	**Futuna spreading center (ZC1)**- sampled from 'pancake with a cherry on top' (volcanic edifice) east of central rift in northern part of ZC1	19/05/2012	1720-1750	1879	1890
12	1	*thin layering of glass covering vesicular basalt pillows with light - moderate amounts of alteration; oldish-looking; excellent examples of gas bubbles <0.5 mm radial to cores; (possible olivines or plag)*	19	NLTD 12-2	-14 35.679/+178 52.313	-14 35.681/+178 51.977	**Futuna spreading center (ZC2)**- sampled from rifted pancake (volcanic edific), on rift axis, in the northern part of ZC2	19/05/2012	1879-1890	2040	2054
13	1	*fresh glassy rinded pillow basalt fragments with minimal amount of vesicles & light alteration*	20	NLTD 13-2	-14 25.442/+178 48.050	-14 25.415/+178 47.740	**Futuna spreading center (ZC3)**- sampled from subdued edifice on rift axis in the northern part of ZC3	19/05/2012	2040-2054	1843	1900
14	1	*glassy basalt with phenocrysts of plagioclase; minimal amount of vesicles and alteration*	21	NLTD 14-1	-14 42.456/+178 55.836	-14 42.484/+178 55.644	**Futuna spreading center (ZC2)**- sampled from subdued edifice on rift axis in the central part of ZC2	19/05/2012	1843-1900	711	780
15	1	*biogenic sediments (corals/worms/shells) trapped in a highly altered basalt flow fragments; very little glass visible*	22	NLTD 15-1	-14 26.535/+177 12.41	-14 26.726/+177 12.685	**East Futuna**- sampled from the SW crater wall in the north zone of the East Futuna Area	21/05/2012	711-780	1071	1128
16	1	*moderately vesicular (spherical bubbles) deep brown-black glass coated pillow fragments; very sparse plagioclase microphenocrysts (<1mm)*	23	NLTD 16-1	-14 36.977/+177 09.114	-14 37.203/+177 09.414	**East Futuna**- sampled from the main culmination of East Futuna area	21/05/2012	1071-1128	1842	1935
17	2	*v. fresh glassy pillows with a large distribution of plagioclase phenocrysts (<1cm) and sparse amount of olivines (<5mm); very lightly altered edges of rock*	24,25	NLTD 17-1	-14 32.131/+177 01.260	-14 32.342/+177 01.074	**East Futuna** - sampled from the NE rift of the E. Futuna area	21/05/2012	1842-1935	1349	1379
18	2	*massive pillow basalts with minor vesicles; very highly altered; sparsely distributed microphyric plagioclase*	26,27	NLTD 18-1 & 18-3	-14 55.429/+177 14.854	-14 55.526/+177 14.736	**Sula sula Caldera**- sampled from the central mound of caldera, E. Futuna area	22/05/2012	1349-1379	1601	1630
19	2	*thin layering of glass covering boulders-cobbles of basalt with variable amount of light - moderate alteration; minimal vesicles; sparsely microphyric plagioclase basalt*	28,29	NLTD 19-16	-14 47.900/+177 14.616	-14 48.310/+177 14.451	**Ridge north of Sula Sula Caldera**- sampled from ridge north of 'Sula sula caldera', E. Futuna area	22/05/2012	1601-1630	760	867
20	1	*pumice; volcanic ash (fine grained); old basement of highly altered rock (possibly cut by glacier (?)); volcaniclastic & biogenic sediments (corals)*	30	NONE	-15 21.690/+177 26.417	-15 21.80/+177 26.71	**South Futuna**- sampled from NW flank of the SW ridge of the major S. Futuna edifice	23/05/2012	760-867	1072	1197
21	1	*aphyric basalt with glass; highly vesicular glass; moderately Mn-altered pillows with minor vesicles*	31	NLTD 21-1	-15 00.143/+177 17.287	-15 00.266/+177 17.136	**SW of Sula sula Caldera (EFVZ)**- sampled from a line of volcanic mounds, SW of Sula sula Caldera, East Futuna Volcanic Zone (EFVZ)	23/05/2012	1072-1197	690	744
22	1	*very vesicular basalt with glass ; minor alteration of Mn coating; phenocrysts of olivine (<3mm)*	32	NLTD 22-14	-14 53.146/+177 53.777	-14 53.400/+177 53.582	**Northern end 'Squid' (CFVZ)**- sampled North end of 'Squid' structure, Central Futunal Volcanic Zone	24/05/2012	690-744	708	750
23	2	*minimal glass; very vesicular; vesicle sizes vary (<2cm); moderate alteration of Mn coating over basalt; very few olivine micro-phenocrysts (<1mm)*	33,34	NLTD 23-12	-14 54.923/+177 53.862	-14 55.278/+177 53.639	**South end 'Squid' (CFVZ)**- sampled from south end of 'Squid' structure, Central Futuna Volcanic Zone	24/05/2012	708-750	1095	1230
24	1	*1/4 bucket of gravel sized ash aggregates; very vesicular glass; 2 blocks of aphyric basalt recovered; very minimal alteration; 1 piece of pumice*	35	NLTD 24-1	-15 01.744/+177 49.708	-15 02.030/+177 49.561	**South Futuna**- sampled from cone in eastern sector of South Futuna Zone	25/05/2012	1095-1230	579	590

Dredge #	Amount of buckets	Description (macro)	Bucket tracking #	Family sample #	Lat/Long (start)	Lat/Long (end)	Location desc.	Date of dredge	Depth range (min-max) meters	Depth (min)	Depth (max)
25	1	olivine phenocrysts (<1/2cm); many shell fragments; few samples look like sub aerial ash deposits; all very altered in a thick (5mm) Mn crust	36	NONE	-14 59.789/+177 53.038	-14 59.99/+177 53.111	**South Futuna** - sampled from western flank of large edifice in central sector of S. Futuna zone	25/05/2012	579-590	992	1006
26	2	few pieces of pumice; aphyric basalt with very few phenocrysts of olivine; Mn alteration (~2mm thick)	37,38	NLTD 26-7	-15 01.589/+177 55.001	-15 01.862/+177 54.848	**South Futuna** - sampled from a chain of edifices in the west central sector of the S. Futuna zone	25/05/2012	992-1006		-
27	0	***ABORTED*** *- French visa expired*	-	-	-14 56.29'S/+177 56.02'W	-14 56.44'S/+177 55.95'W	**ABORTED - South Futuna** sample from a rubbly ridge in the west cen sector of the S. Futuna zone	25/05/2012	-	790	860
28	2	pillow lava basalt with olivine; micro-phenocrysts; vesicular with moderate alteration; nc fresh-looking (altered) glass pieces	39,40	NLTD 28-20	-14 00.008/+178 52.621	-14 00.167/+178 52.599	**Futuna spreading center** sampled from northern ridge crest, North Zone, Futuna spreading center	26/05/2012	790-860	1568	1674
29	1	moderately altered Mn-coated (~1 mm thick) glass rind covered pillow lava fragments; 'hyaloclastilic' welded material in layered blocks; sparse olivine microphenocrysts; slight vesicular	41	NLTD 29-18	-14 10.218/+178 55.213	-14 10.428/+178 55.099	**Futuna spreading center (FSC)** sampled ridge crest, Zone Relais, FSC	26/05/2012	1568-1674	2060	2080
30	4	moderately fresh black glass coated pillow fragments; sparsely plagioclase & (d. green) c microphyric; moderately vesicular	42-45	NLTD 30-24 & 30-38	15 00.389/+179 06.890	-15 00.511/+179 06.806	**South Futuna (SFSC)** - sampled from 'cool' looking 'pancake' without fracture, Southern FSC	27/05/2012	2060-2080	2104	2172
31	2	fresh black glass rinded (light-mod alteration) pillow fragments; olivine & plagioclase microphyric; moderately vesicular	46,47	NLTD 31-11	-14 59.267/+179 07.856	-14 59.430/+179 07.723	**South Futuna (SFSC)** sampled linear rubbly ridge, SFSC	27/05/2012	2104-2172	1983	2007
32	1	fresh glass (light alteration - a few mod altered pieces) and pillow lava fragments with predominantly plagioclase <4mm (& minor olivine) phenocrysts ***NOTE:*** broken dredge) black glass, sparsely vesicular, sparsely plagioclase-olivine phyric pillow basalt; phenocry <5mm; olivine is d. green - not very primitive; olivine contains spinel microinclusions; gat	48	NLTD 32-1	-14 58.387/+179 06.888	-14 58.552/+179 06.747	**South Futuna (SFSC)** sampled from a dome on rubbly ridge, SFSC (***NOTE:*** *bottom of dredge ripped off - only recovered samples in pip*	28/05/2012	1983-2007	2157	2235
33	2	microclasts in one glass chip; also cpx microphenocrysts	49,50	NLTD 33-7	-15 02.807/+179 10.956	-15 02.910/+179 10.777	**S. end of Futuna spreading center (SFSC)** sampled from a dome on a rubbly ridge, SFSC	28/05/2012	2157-2235	2260	2266
34	1	pumice; 1 ash covered deposit; very minimal glass all fine-grained; moderately altered	51	NLTD 34-3	-15 17.521/+178 42.185	-15 17.704/+178 42.335	**West Cikobia Volcanic Zone (WCVZ)** sampled in the *northern* part of WCVZ	29/05/2012	2260-2266	1979	2107
35	3	young glass covering aphyric pillow basalt; light aleration Mn coatings; minimally vesicular	52-54	NLTD 35-3	-15 21.356/+178 47.334	-15 21.645/+178 47.597	**West Cikobia (WCVZ)** sampled in *northeast* part of WCVZ	29/05/2012	1979-2107	1780	1824
36	1	highly altered aphyric basalt; vesicular; ash covered; 1/4 bucket of ash in a heavy mud suspension; biogenic sediments; very little glass; strong H2S smell when breaking open samples (***NOTE:*** *Family sample only split amongst Ali,Fran&Raul due to size constraints)*	55	NLTD 36-7	-16 25.795/+177 20.380	-16 26.017/+177 20.556	**Seahorse Ridge 3** sampled from Ridge 3 of seahorse area, in betwee previous 2 dredges on this ridge **ABORTED - Seahorse Ridge 3** sample from northern end of Ridge 3 of	30/05/2012	1780-1824		-
37	0	***ABORTED*** *- Tension reading issues*	-	-	-16 23.55'S/+177 19.92'E	-16 23.66'S/+177 20.00'E	Seahorse Area, close to NLTD-2	30/05/2012	-	2993	3020
38	1	*low yield from dredge; relatively homogenous plagioclase rich (<1cm) basalts/glass*	56	NLTD 38-1	-16 37.324/+176 09.741	-16 37.716/+176 09.572	**Fi1** - sampled from rubbly ridge in central Fi1	31/05/2012	2993-3020	2010	2029
39	5	fresh black glass bearing basalt with large phenocrysts of plagioclase and olivine; light - moderate alteration on the larger pillow fragment (1 piece)	57-61	NLTD 39-5	-16 56.693/+173 55.748	-16 56.913/+173 55.926	**Fiji Triple Junction (northeast)** sampled from mound in Caldera, northeast Fiji Triple Junction	01/06/12	2010-2029	2010	2031
40	3	Covered in Fe-oxy-hydroxides; must be close to hydrothermal vent system; hydrotherma breccia (glass frags mixing with surrounding mud); variation in gradation of glass colors; aphyric basalt with minimal vesicles with mod-high alteration	62-64	NLTD 40-1	-16 56.339/+173 55.589	-16 56.461/+173 55.733	**Fiji Triple Junction (northeast)** sampled from low mound in Caldera, northeast Fiji Triple Junction	01/06/12	2010-2031	1980	2001
41	5	*glassy aphyric basalts; thickly chilled margins; minimal vesicles; low-mod alteration*	65-69	NLTD 41-8	-16 57.014/+173 55.364	-16 57.162/+173 55.506	**Clapham Junction** sampled from lava field in southern part of calder northeast Fiji Triple Junction	01/06/12	1980-2001	1942	1969
42	2	glassy aphyric pillow basalts; minimal vesicles; mod (red) alteration; **green 'staining' in places	70,71	NLTD 42-1	-16 58.669/+173 54.922	-16 58.854/+173 54.970	**Clapham Junction** sampled from central ridge in rift near southern ri of caldera, northeast Fiji Triple Junction	01/06/12	1942-1969	1937	1985
43	1	*low yield from dredge; plagioclase-phyric (<5mm); non-vesicular black/gray glass coverir pillow basalt; appears slightly more evolved than previous glasses (from same area); app older than caldera samples*	72	NLTD 43-1	-16 59.020/+173 54.830	-16 59.095/+173 55.006	**Clapham Junction** sampled fom overlapping rift eastwards of NLTD-4 forming the central ridge in rift near southern rim of caldera, northe Fiji Triple Junction	02/06/12	1937-1985	2645	2689
44	1	*rock types vary from 'old-looking', weathered aphyric TOs strongly plagioclase (<10mm)- phyric flakes; varying degrees of plagioclase crystal sizes (<10mm) in an aphyric host gla light -moderatedly altered (Fe-alteration within rock) (Mn covering on some piece); little vesicles; 1 olivine phenocryst seen in the plag-phyric material*	73	NLTD 44-1	-17 18.302/+173 47.783	-17 18.502/+173 48.073	**NE Fiji Triple Junction (south arm)** sampled from lava plain in souther section of south arm, northeast Fiji Triple Junction	02/06/12	2645-2689	2455	2459
45	1	*variably (light-mod) altered & dull shine to glass; plagioclase-olivine-phyric glass rinded ((***NOTE:*** *family 1 is copiously plagioclase-phyric; family 2 looks more primitive than fan*	74	NLTD 45-1 & 45-2	-17 11.114/+173 51.106	-17 11.201/+173 51.205	**NE Clapham Junction** sampled from lava plain in middle section of South Arm, northeast Fiji Triple Junction	02/06/12	2455-2459	2210	2220
46	2	*dark black pillow basalts; variable shine; copious glass chips in mud bucket; lightly- mod altered*	75,76	NLTD 46-1	-17 04.070/+173 53.122	-17 04.241/+173 53.226	**NE Fiji Triple Junction (south arm)** sampled from a ridge in northern section of south arm, northeast Fiji Triple Junction	02/06/12	2210-2220	2325	2431
47	1	*low yield from dredge; minimal glass in mud bucket with Mn crust (enough to fill 1/2 a s bag total) (Fran received every family sub-sample)*	77	NLTD 47- (1Ron) (2&3Ali) (4Ken) (5Raul)	-16 50.929/+173 57.452	-16 51.097/+173 57.672	**NE Fiji Triple Junction (northeast arm)** sampled from a ridge in southe section of northeast arm, Northeast Fiji Triple Junction	03/06/12	2325-2431	2141	2209
48	2	*light-mod altered glass rinded pillow basalts, feldspar-olivine-phyric (mostly)-light/no & (very few)-moderately alterated shiny glass lava tube & flows; aphyr*	78,79	NLTD 48-1	-16 52.937/+173 55.370	-16 53.002/+173 55.499	**NE Fiji Triple Junction (northeast arm)** sampled from a N-S striking ridge in southern section of northeast arm, Northeast Fiji Triple Junction	03/06/12	2141-2209	1988	1998
49	2	*vesicles; 1 feldspar observed*	80,81	NLTD 49-1	-16 56.770/+173 55.189	-16 56.912/+173 55.444	**NE Fiji Triple Junction** sampled from the western floor of the caldera northeast Fiji Triple Junction	03/06/12	1988-1998	1890	2010
50	10	*copious amounts of fresh glass; very light - no alteration; (hydrothermal?)-sulfide miner present; minimal olivine present (1 phenocryst [~3mm] observed - which Fran has '50-10*	82-91	NLTD 50-1; 50-2; 5 3	-16 57.323/+173 56.100	-16 57.511/+173 56.437	**NE Fiji Triple Junction** sampled from the southeastern walll of the caldera, northeast Fiji Triple Junction	03/06/12	1890-2010		

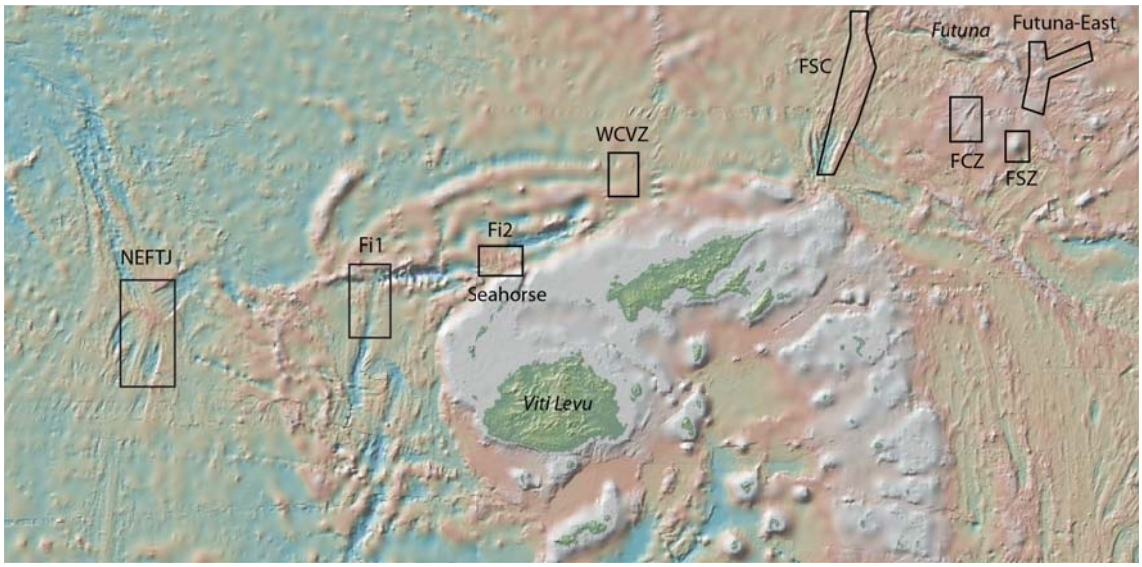

Figure 3 Schematic outline of the individual areas mapped with the Kongsberg EM300 30kHz multibeam sonar during ss2012_v02 (NoLauTe). Abbreviations: NEFT, *Northeast Fiji Triple Junction*; Fi1, *Fiji One*; Fi2, *Fiji Two (Seahorse)*; WCVZ, *West Cikobia Volcanic Zone*; FSC, *Futuna Spreading Center*; FCZ, *Futuna Central Zone*; FSZ, *Futuna South Zone*.

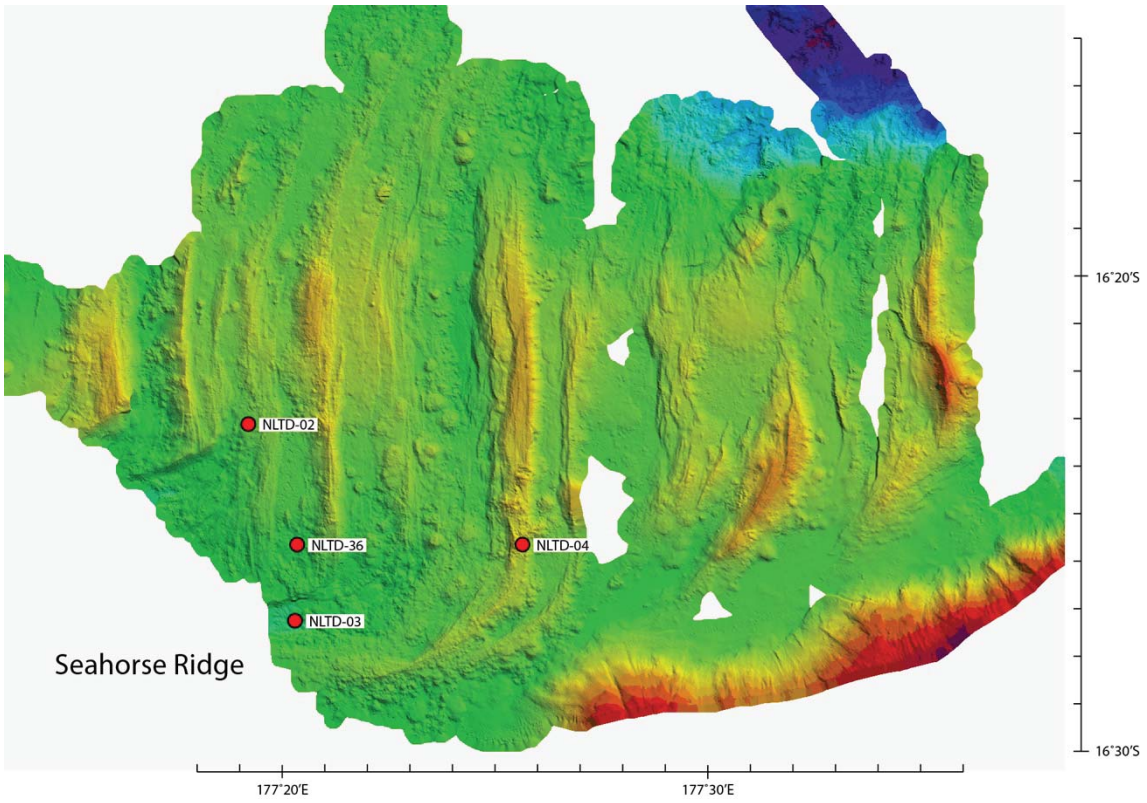
NLTD-02
NLTD-36
NLTD-04
NLTD-03
Seahorse Ridge
16°20'S
16°30'S
177°20'E
177°30'E

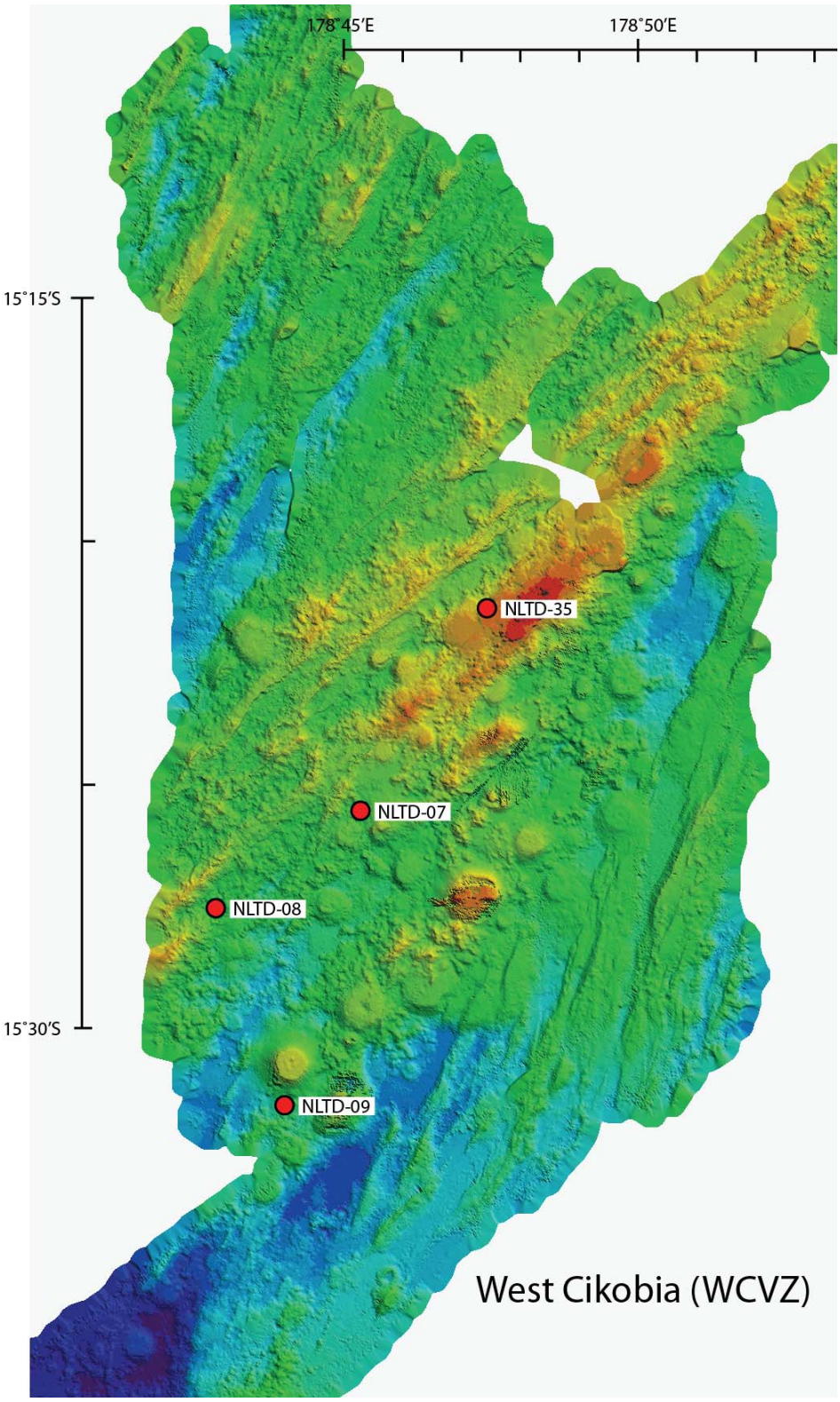
178°45'E
178°50'E
15°15'S
15°30'S
NLTD-35
NLTD-07
NLTD-08
NLTD-09
West Cikobia (WCVZ)

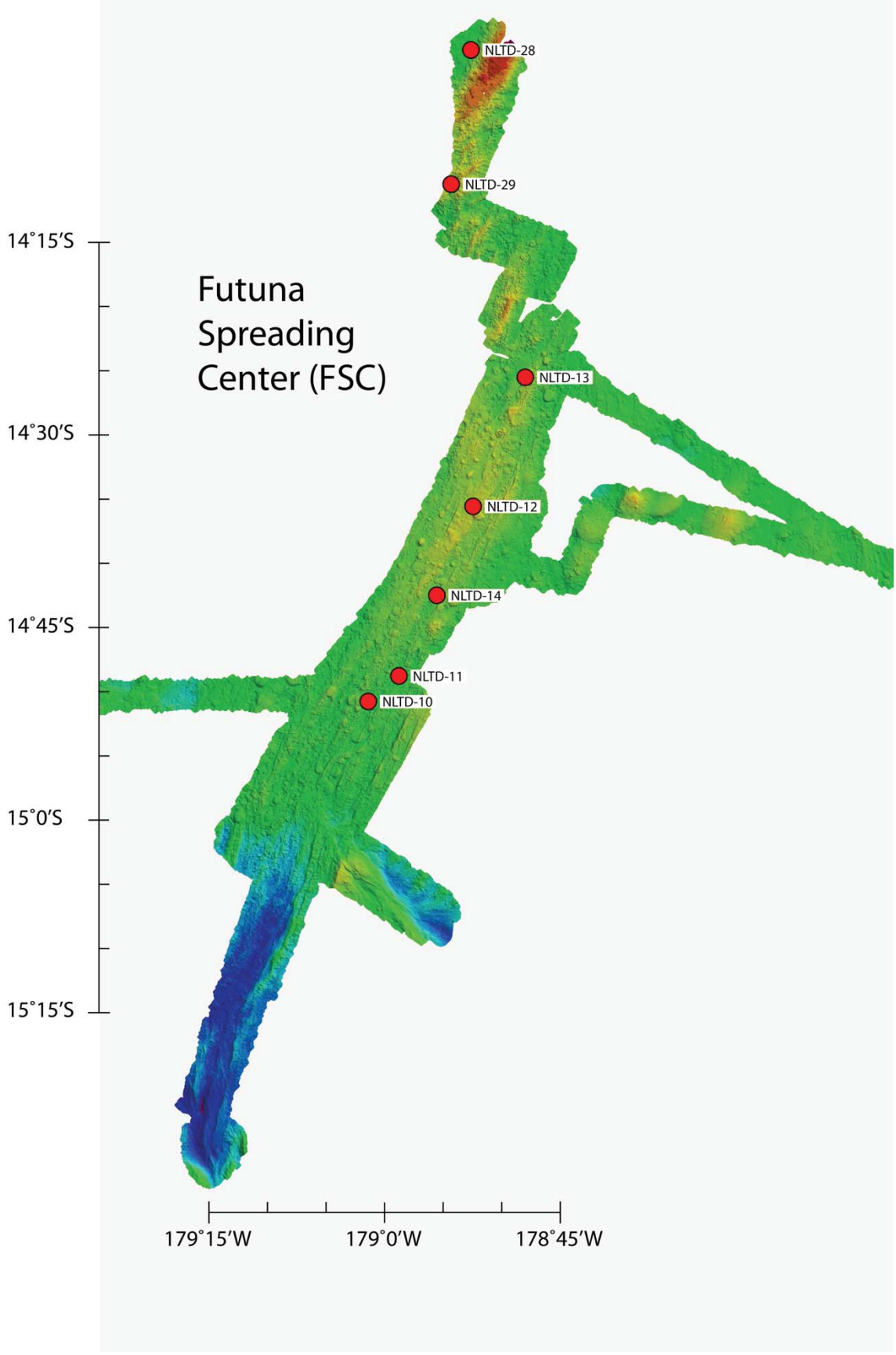
NLTD-28
NLTD-29
Futuna
Spreading
Center (FSC)
NLTD-13
NLTD-12
NLTD-14
NLTD-11
NLTD-10
14°15′S
14°30′S
14°45′S
15°0′S
15°15′S
179°15′W
179°0′W
178°45′W

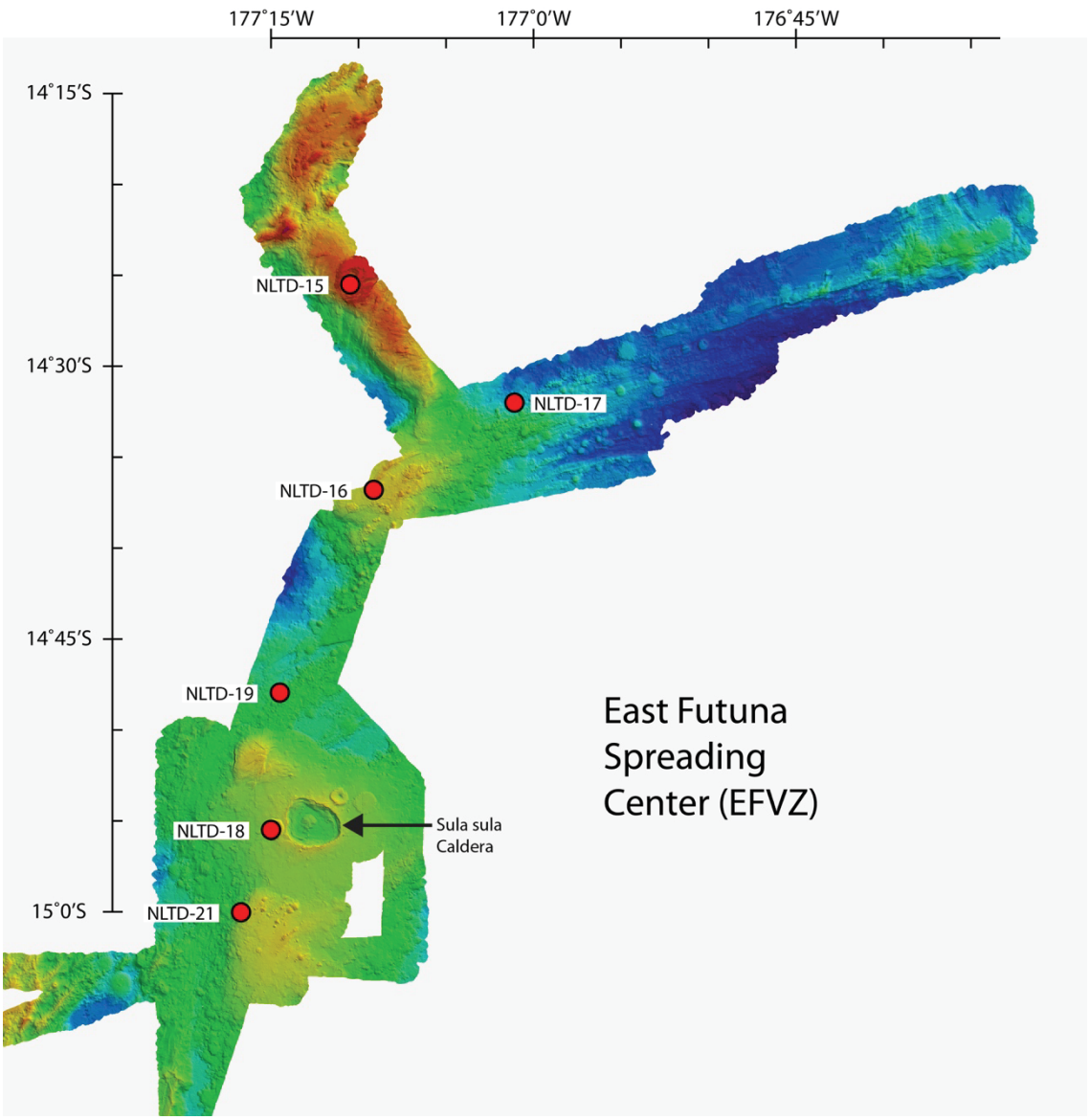
177°15'W
177°0'W
176°45'W
14°15'S
14°30'S
14°45'S
15°0'S
NLTD-15
NLTD-17
NLTD-16
NLTD-19
NLTD-18
NLTD-21
Sula sula
Caldera
East Futuna
Spreading
Center (EFVZ)

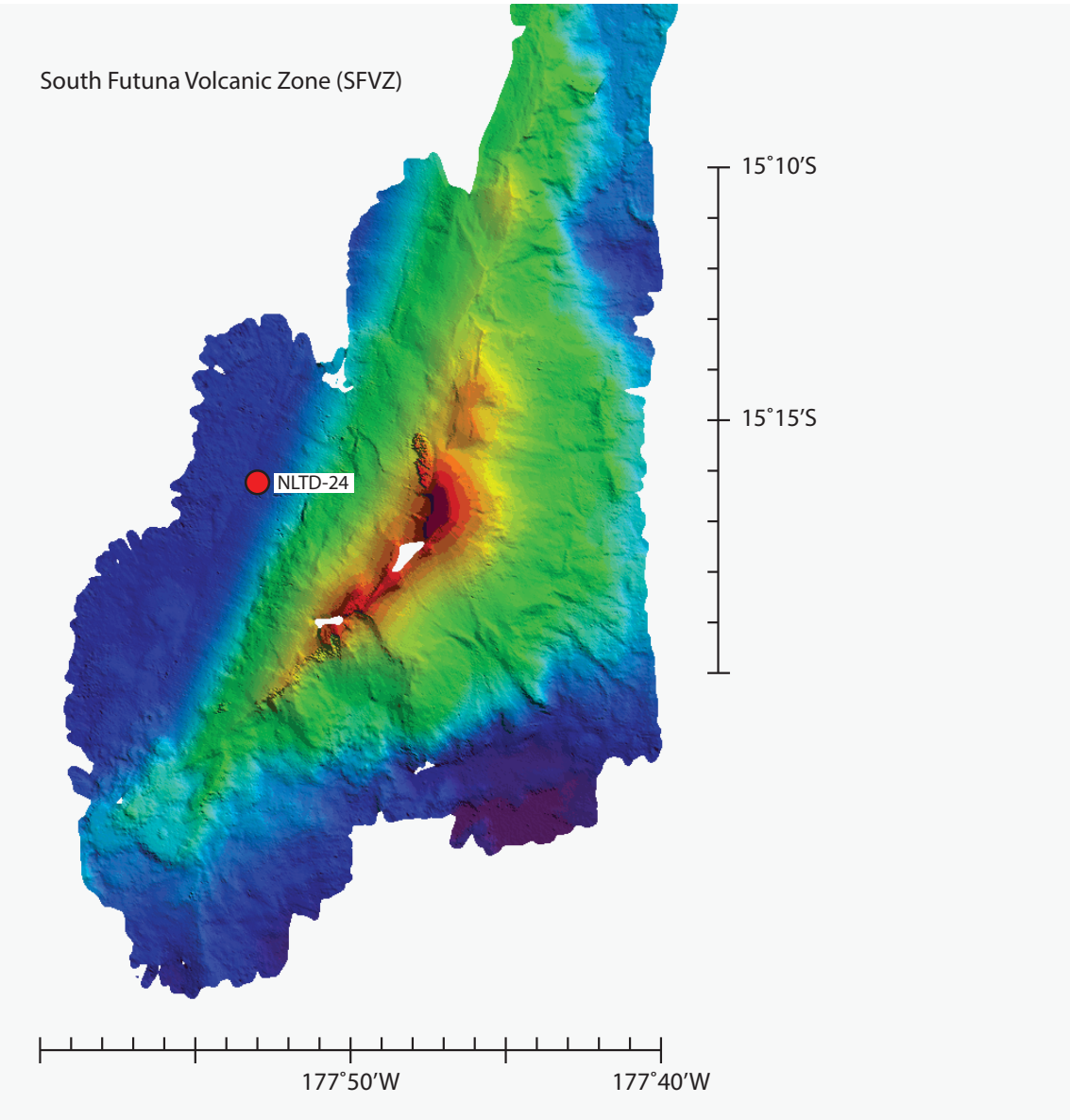
South Futuna Volcanic Zone (SFVZ)
15˚10'S
15˚15'S
NLTD-24
177˚50'W
177˚40'W

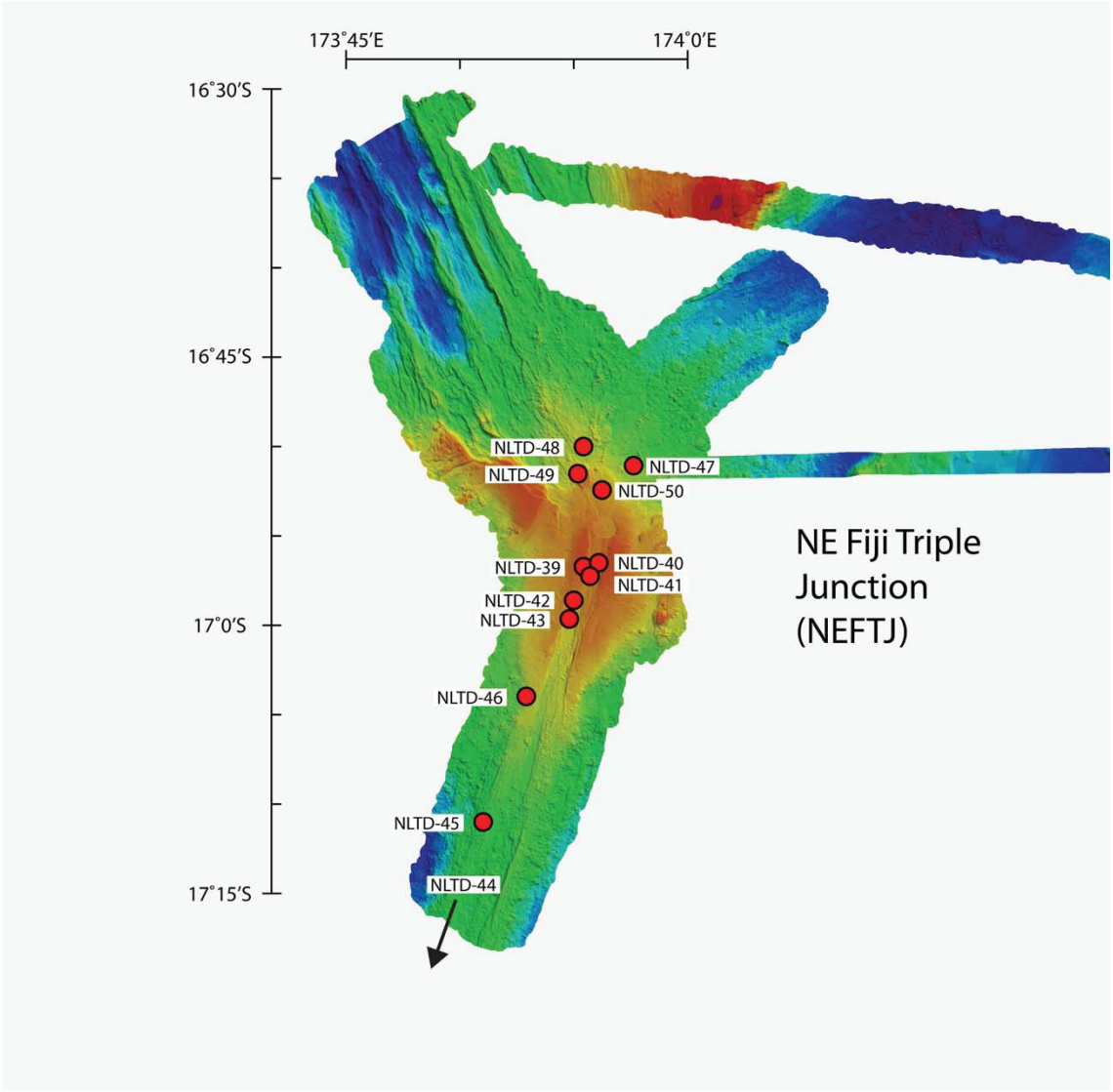
173°45′E
174°0′E
16°30′S
16°45′S
17°0′S
17°15′S
NLTD-48
NLTD-49
NLTD-47
NLTD-50
NLTD-39
NLTD-40
NLTD-41
NLTD-42
NLTD-43
NLTD-46
NLTD-45
NLTD-44
NE Fiji Triple Junction (NEFTJ)

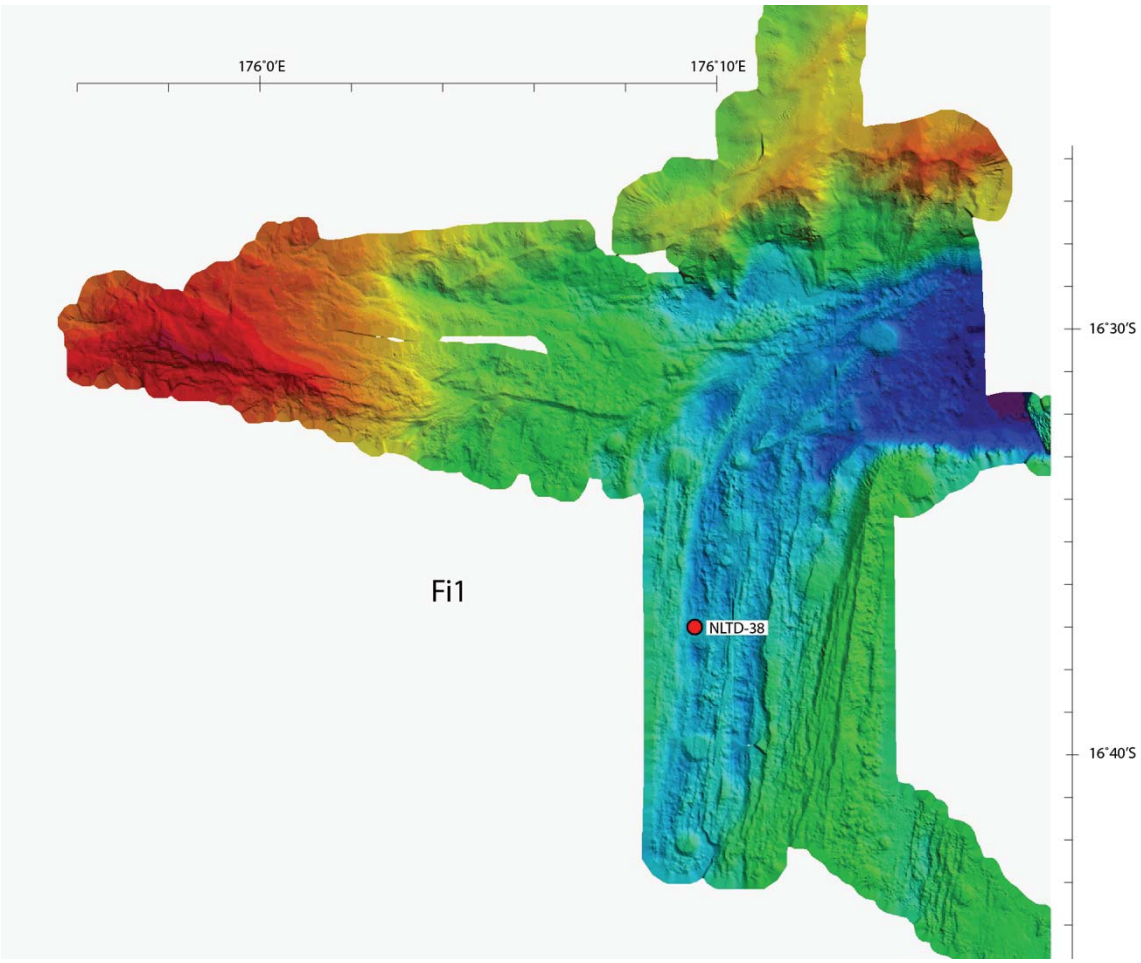

Figure 4 Bathymetric (swath) maps of the field areas samples in the northern Lau and North Fiji basins. The seafloor bathymetry was mapped with a multibeam echo sounder Kongsberg Simrad EM300 that sends 30 kHz frequency signals beneath the vessel. These signals produce a fan arc of 135 beams with a 1° by 1° range. The colors represented in the bathymetric map are indicative of depth. Depth ranges from ~2700 m (blue) to ~1800 m (red). The red dots show the samples collected and analyzed for this thesis; some samples are located off the maps.

Table 2 Major, trace, and volatile element data for the samples dredged from the Lau and North Fiji Basin

	Seahorse Ridge 3			Seahorse 4	Central Hill	West Cikobia (WCVZ)				Futuna Spreading Center						
	NLTD-02-4-glass	NLTD-03-6-glass	NLTD-36-7-glass	NLTD-04-2-glass	NLTD-06-1-glass	NLTD-07-12	NLTD-08-1-	NLTD-09-1	NLTD-35-3-glass	NLTD-10-2-	NLTD-11-1	NLTD-12-2	NLTD-13-2	NLTD-14-1-	NLTD-28-2	NLTD-29-1
SiO_2 wt%	59.55	51.85	56.04	58.30	58.13	49.92	48.24	50.17	49.60	51.08	47.63	50.68	49.70	50.75	50.52	46.88
TiO_2 wt%	1.24	2.05	1.72	1.50	1.53	1.80	1.28	1.66	1.53	1.46	1.63	1.33	1.39	1.53	1.23	2.01
Al_2O_3 wt%	15.00	14.50	13.97	13.80	13.88	15.60	16.39	15.12	15.50	14.91	16.19	15.35	16.11	14.84	15.47	15.48
FeO wt%	7.69	11.62	11.74	11.52	11.71	9.62	10.02	10.42	10.05	9.63	9.43	9.07	9.45	9.88	9.68	10.93
MnO wt%	0.14	0.21	0.21	0.22	0.24	0.18	0.19	0.16	0.21	0.16	0.18	0.16	0.17	0.17	0.17	0.19
MgO wt%	3.17	4.46	2.30	1.91	1.95	7.46	8.63	7.44	8.19	7.35	7.61	7.79	8.54	7.29	8.42	6.76
CaO wt%	6.87	9.05	6.27	6.03	5.99	10.45	12.28	12.03	11.62	11.85	13.16	12.71	11.66	11.99	10.61	12.33
Na_2O wt%	4.04	3.45	4.07	4.14	4.15	2.84	2.37	2.17	2.33	2.39	2.67	2.36	2.40	2.37	2.40	3.04
K_2O wt%	0.49	0.54	0.63	0.53	0.53	0.62	0.13	0.26	0.29	0.32	0.56	0.24	0.28	0.34	0.23	0.59
P_2O_5 wt%	0.22	0.44	0.45	0.57	0.57	0.23	0.10	0.13	0.16	0.16	0.19	0.12	0.11	0.13	0.11	0.23
Total	98.41	98.16	97.40	98.52	98.67	98.71	99.63	99.56	99.47	99.32	99.24	99.81	99.80	99.29	98.83	98.45
Mg#	42.36	40.60	25.87	22.77	22.89	58.03	60.55	56.00	59.22	57.63	59.01	60.49	61.70	56.79	60.78	52.44
Li	11.56	12.97	18.52	19.67	19.77	5.69	4.69	5.70	5.00	4.95	4.29	4.41	4.22	4.90	4.56	4.97
Be	0.89	1.00	1.27	1.31	1.36	0.84	0.34	0.45	0.52	0.54	0.76	0.47	0.50	0.58	0.41	0.94
Na (BCR)	4.65	3.65	4.57	4.75	4.45	2.79	2.29	2.31	2.48	2.56	2.73	2.52	2.49	2.53	2.52	3.18
Na	4.28	3.65	4.27	4.48	4.43	2.72	2.20	2.26	2.33	2.52	2.66	2.41	2.41	2.47	2.43	3.06
Mg (BCR)	3.34	4.54	2.35	1.97	1.91	7.63	8.84	7.82	8.46	7.34	7.67	8.03	8.69	7.31	8.59	7.00
Mg	3.02	4.46	2.19	1.83	1.89	7.39	8.46	7.60	8.02	7.18	7.44	7.65	8.35	7.11	8.30	6.75
Al 612	14.12	14.75	12.96	12.89	13.30	14.74	15.33	14.11	14.46	14.07	15.25	14.21	15.08	14.10	14.85	15.12
Al (BCR)	14.85	14.24	14.04	13.54	13.52	15.42	16.21	14.86	15.50	14.76	15.88	14.85	15.82	14.65	15.24	15.90
P	999.89	1867.15	2095.97	2470.10	2427.75	1028.17	394.09	598.79	677.11	681.51	884.18	460.14	510.79	655.45	393.72	904.74
P (BCR)	1128.08	1941.08	2206.01	2693.99	2522.19	1073.13	415.86	622.24	701.04	705.39	921.11	489.02	539.86	682.52	412.02	948.35
K (BCR)	4456.38	4372.98	5469.25	4744.29	4422.18	5180.25	889.92	2269.24	2445.91	2824.48	4816.27	2096.07	2370.21	2967.22	1932.34	5129.92
Ca	6.85	9.22	6.00	5.93	6.08	10.56	12.18	12.02	11.33	11.88	13.30	12.42	11.55	12.20	10.54	12.28
Ca (BCR)	6.87	9.05	6.27	6.03	5.99	10.45	12.28	12.03	11.62	11.85	13.16	12.71	11.66	11.99	10.61	12.33
Sc	19.93	33.28	23.57	21.37	22.69	35.75	43.42	43.32	41.13	42.07	35.80	40.04	33.07	41.65	29.36	36.75
Ti	7036.88	11161.28	9878.72	8616.94	8770.75	10045.60	7083.40	8649.12	8705.05	8111.51	9074.62	7004.99	7500.28	8258.56	6977.67	11870.10
V	160.37	369.49	108.70	41.15	41.83	287.26	307.40	358.58	334.33	307.38	272.00	259.23	251.29	296.60	216.52	318.63
Cr	47.87	26.49	5.32	7.43	7.58	306.87	323.38	346.41	330.44	297.43	261.31	135.79	378.20	229.02	378.04	194.03
Mn	1086.72	1703.26	1722.41	1805.60	1845.75	1394.44	1456.70	1544.10	1471.76	1444.57	1296.00	1363.44	1309.49	1443.01	1319.45	1472.55
Mn (BCR)	1195.15	1723.90	1838.40	1919.26	1851.02	1428.28	1518.49	1586.40	1540.58	1475.18	1335.03	1427.22	1356.61	1478.59	1362.61	1527.09
Co	23.58	37.23	22.44	18.26	18.25	42.57	49.71	46.22	46.40	43.06	45.12	44.86	47.87	44.80	47.87	46.33
Ni	22.41	19.54	4.44	3.13	3.10	130.81	160.81	106.34	127.79	79.31	97.51	58.74	170.52	59.99	165.10	84.62

	Seahorse Ridge 3			Seahorse 4	Central Hill	West Cikobia (WCVZ)				Futuna Spreading Center						
	NLTD-02-4-glass	NLTD-03-6-glass	NLTD-36-7-glass	NLTD-04-2-glass	NLTD-06-1-glass	NLTD-07-12	NLTD-08-1-	NLTD-09-1	NLTD-35-3-glass	NLTD-10-2-	NLTD-11-1	NLTD-12-2	NLTD-13-2	NLTD-14-1-	NLTD-28-2	NLTD-29-1
Cu	39.95	84.10	28.60	19.71	19.66	78.44	121.27	100.02	92.42	93.97	114.25	105.40	94.56	104.69	84.74	136.07
Zn	95.16	146.55	175.35	200.18	197.29	107.69	100.56	110.66	104.06	99.05	89.98	82.16	98.44	96.75	102.50	109.58
Ga	19.37	20.63	22.45	23.94	24.40	17.92	17.12	17.60	17.05	16.97	17.17	15.66	17.92	16.83	17.16	20.09
As	0.32	0.66	0.50	0.51	0.52	0.36	0.12	0.20	0.22	0.22	0.32	0.15	0.19	0.23	0.16	0.37
Se	0.25	0.37	0.43	0.47	0.47	0.38	0.36	0.41	0.34	0.33	0.35	0.30	0.29	0.37	0.24	0.47
Rb	10.80	7.52	13.87	12.68	12.82	20.92	3.12	10.63	10.23	8.51	13.99	5.45	5.18	8.14	4.51	11.94
Sr	132.97	283.04	114.80	97.95	103.97	156.88	83.09	98.52	114.69	131.53	271.56	151.65	168.68	162.67	160.38	293.51
Y	36.42	39.74	75.70	83.93	89.78	29.50	25.15	28.59	26.92	24.60	17.48	18.35	17.99	22.03	15.77	21.68
Zr	188.43	182.95	292.03	295.84	313.46	126.02	60.66	78.53	83.62	83.18	94.38	62.20	65.15	81.74	51.51	117.79
Nb	5.21	14.12	8.56	9.13	9.61	20.30	3.35	10.76	11.67	8.54	18.35	4.89	5.64	9.53	5.50	17.45
Mo	0.99	0.72	0.93	1.06	1.07	0.76	0.20	0.34	0.36	0.49	0.86	0.34	0.45	0.54	0.40	0.91
Ag	0.04	0.04	0.03	0.03	0.03	0.03	0.04	0.03	0.03	0.03	0.04	0.03	0.03	0.03	0.03	0.05
Cd	0.13	0.19	0.22	0.26	0.27	0.15	0.13	0.15	0.14	0.14	0.13	0.13	0.13	0.14	0.13	0.16
In	0.07	0.10	0.13	0.15	0.15	0.08	0.07	0.08	0.07	0.07	0.06	0.06	0.06	0.07	0.06	0.08
Sn	2.08	2.20	3.14	3.62	3.66	2.28	1.70	1.90	1.60	2.00	2.02	1.84	1.91	1.88	1.72	2.12
Sb	0.06	0.04	0.06	0.06	0.05	0.03	0.01	0.02	0.02	0.02	0.03	0.01	0.02	0.02	0.01	0.03
Cs	0.23	0.15	0.26	0.22	0.22	0.22	0.03	0.10	0.10	0.09	0.18	0.06	0.06	0.10	0.06	0.16
Ba	81.48	121.74	112.33	91.76	93.81	192.11	28.80	105.39	105.23	78.00	135.68	50.76	47.43	81.23	44.63	117.24
La	10.26	15.14	13.68	13.55	13.95	13.30	2.84	7.92	7.93	6.36	11.19	3.94	4.44	6.98	3.70	10.90
Ce	24.40	33.56	34.84	37.52	37.90	28.71	7.97	17.27	17.47	15.41	24.28	10.35	11.00	16.29	8.87	24.56
Pr	3.10	4.53	5.18	5.60	5.88	3.56	1.24	2.26	2.36	2.12	3.01	1.50	1.55	2.15	1.31	3.24
Nd	14.80	20.69	27.16	29.25	30.89	15.81	6.84	10.48	10.96	10.32	13.11	7.52	7.74	10.06	6.33	14.88
Sm	4.76	5.51	8.70	9.88	10.37	4.42	2.56	3.30	3.33	3.23	3.40	2.36	2.49	3.00	1.98	3.90
Eu	1.43	1.89	2.63	2.92	3.14	1.46	0.97	1.18	1.22	1.16	1.22	0.95	0.94	1.06	0.83	1.45
Gd	6.07	6.51	11.35	12.93	13.83	5.38	3.68	4.42	4.15	4.04	3.65	2.97	3.28	3.62	2.52	4.22
Tb	0.95	1.12	1.93	2.20	2.34	0.81	0.61	0.74	0.73	0.65	0.54	0.48	0.50	0.61	0.47	0.68
Dy	6.31	7.08	12.86	14.55	15.56	5.38	4.23	5.08	4.67	4.39	3.40	3.36	3.41	4.05	2.91	4.28
Ho	1.35	1.54	2.85	3.19	3.47	1.13	0.96	1.09	1.05	0.94	0.69	0.70	0.70	0.84	0.62	0.89
Er	3.95	4.47	8.42	9.41	10.11	3.25	2.78	3.22	2.97	2.81	1.85	2.11	2.01	2.43	1.75	2.34
Tm	0.58	0.65	1.20	1.34	1.46	0.47	0.40	0.45	0.42	0.39	0.26	0.29	0.28	0.34	0.24	0.32
Yb	4.46	4.42	8.39	9.56	10.14	3.29	3.05	3.32	2.97	2.79	1.79	2.15	1.94	2.49	1.56	2.08
Lu	0.61	0.64	1.24	1.38	1.48	0.48	0.45	0.48	0.44	0.40	0.25	0.30	0.29	0.35	0.23	0.30
Hf	4.42	4.38	7.72	7.90	8.34	3.10	1.69	2.19	2.33	2.19	2.30	1.57	1.74	2.09	1.38	2.95
Ta	0.37	0.75	0.56	0.55	0.58	1.11	0.20	0.61	0.63	0.51	1.07	0.29	0.35	0.57	0.32	1.10
W	0.197	0.195	0.217	0.206	0.209	0.324	0.048	0.193	0.185	0.116	0.206	0.056	0.069	0.126	0.058	0.172
Re	0.0009	0.0016	0.0006	0.0005	0.0002	0.0012	0.0013	0.0019	0.0018	0.0009	0.0012	0.0007	0.0012	0.0014	0.0005	0.0014
Pt	0.0014	0.0013	0.0008	0.0013	0.0007	0.0020	0.0036	0.0020	0.0011	0.0008	0.0030	0.0004	0.0006	0.0006	0.0008	0.0005
Au	0.0010	0.0019	0.0014	0.0011	0.0011	0.0019	0.0024	0.0016	0.0011	0.0020	0.0029	0.0004	0.0006	0.0014	0.0008	0.0009
Tl	0.0505	0.0636	0.0729	0.0673	0.0686	0.0341	0.0063	0.0171	0.0150	0.0169	0.0242	0.0119	0.0138	0.0182	0.0106	0.0302
Pb	2.14	1.98	2.37	2.24	2.28	1.35	0.33	0.75	0.74	0.77	1.12	0.56	0.64	0.83	0.48	1.27
Bi	0.0270	0.0274	0.0271	0.0257	0.0259	0.0084	0.0061	0.0092	0.0099	0.0081	0.0108	0.0101	0.0097	0.0095	0.0080	0.0161
Th	1.5993	1.1743	1.7197	1.4208	1.5306	1.8773	0.2861	1.1837	1.1123	0.7134	1.3151	0.3377	0.4263	0.7638	0.3457	1.1715
U	0.6471	0.4487	0.5506	0.4899	0.4884	0.3946	0.0641	0.2273	0.2127	0.1787	0.3363	0.0916	0.1189	0.1874	0.1096	0.3174

	Seahorse Ridge 3			Seahorse 4	Central Hill	West Cikobia (WCVZ)				Futuna Spreading Center						
	NLTD-02-4-glass	NLTD-03-6-glass	NLTD-36-7-glass	NLTD-04-2-glass	NLTD-06-1-glass	NLTD-07-12	NLTD-08-1-	NLTD-09-1	NLTD-35-3-glass	NLTD-10-2-	NLTD-11-1	NLTD-12-2	NLTD-13-2	NLTD-14-1-	NLTD-28-2	NLTD-29-1
CO_2	3.56	4.75	2.66	7.84	6.73	81.48	100.35	89.81	111.46	93.49	98.07	106.38	142.88	83.14	28.96	160.47
+/-	0.25	0.40	0.28	0.22	1.03	0.71	0.67	0.53	1.09	0.83	1.00	0.89	1.14	0.96	0.58	1.36
H_2O	1.21	1.41	1.29	1.36	1.30	0.64	0.19	0.34	0.34	0.44	0.71	0.35	0.37	0.48	0.37	0.81
+/-	0.00	0.01	0.00	0.01	0.04	0.0029	0.00	0.00	0.00	0.00	0.00	0.00	0.00	0.00	0.00	0.00
F	273.61	476.22	578.10	718.17	710.85	467.36	136.57	259.07	262.89	265.66	365.29	197.89	187.18	264.93	149.66	375.93
+/-	0.81	1.68	1.21	2.44	2.65	1.37	0.41	0.52	1.05	0.54	0.53	0.46	0.39	0.32	0.85	2.08
P	1044.69	2170.23	2216.98	2737.15	2710.87	1094.78	409.14	620.96	688.50	705.96	948.05	476.25	527.97	667.94	408.78	1005.78
+/-	1.65	4.79	5.03	4.17	8.28	2.46	1.04	1.43	1.42	1.27	1.94	1.05	1.62	1.26	1.45	3.22
S	77.63	338.37	666.31	634.77	630.62	1070.50	994.61	1187.23	1054.19	1030.34	1082.04	1025.88	1117.79	1145.80	882.32	1635.93
+/-	0.28	0.95	1.97	1.90	1.66	2.89	2.94	3.37	3.25	1.89	2.05	1.95	3.49	2.99	2.50	4.60
Cl	2242.58	1014.07	1867.05	1806.13	1754.64	229.14	49.01	108.34	92.29	138.55	376.46	61.32	76.68	140.99	206.01	364.15
+/-	16.06	6.54	4.66	10.59	2.24	1.10	0.33	0.38	0.41	0.46	1.34	0.22	0.38	0.59	0.49	0.94

	East Futuna		Sula sula caldera (EFVZ)					Central Futuna Volcanic Zone (CFVZ)			South Futuna (SFVZ)						
	NLTD-15-1	NLTD-16-1	NLTD-17-1	NLTD-18-1-1	NLTD-18-3-1	NLTD-19-16	NLTD-21-1-glass	NLTD-22-14	NLTD-23-7-1	NLTD-23-12-glass	NLTD-24-1	NLTD-26-7	NLTD-30-24	NLTD-30-38	NLTD-31-11	NLTD-32-1	NLTD-33-6-glass
SiO_2 wt%	49.66	51.01	47.87	48.51	52.83	50.55	66.59	49.10	48.02	47.99	49.26	48.87	50.48	50.36	50.34	50.49	50.61
TiO_2 wt%	1.80	1.91	1.47	1.01	2.12	2.23	0.75	1.59	1.69	1.76	1.94	1.80	1.61	1.57	1.60	1.51	1.59
Al_2O_3 wt%	14.83	15.89	17.69	16.66	14.34	14.88	13.27	16.23	16.49	16.31	16.37	16.51	14.59	14.85	14.62	14.81	14.59
FeO wt%	10.77	8.56	9.53	9.17	11.46	11.30	7.30	9.52	10.45	10.53	8.71	8.82	10.48	10.36	10.08	10.10	10.78
MnO wt%	0.17	0.15	0.15	0.15	0.19	0.20	0.19	0.17	0.17	0.22	0.17	0.17	0.17	0.17	0.17	0.19	0.18
MgO wt%	6.94	6.49	9.11	8.91	4.35	5.63	0.94	7.72	7.74	7.98	7.38	7.33	6.92	6.98	7.01	6.88	6.75
CaO wt%	11.74	11.07	11.33	12.57	8.40	10.09	3.08	11.58	11.94	11.34	11.56	11.14	11.75	11.96	11.84	11.72	11.10
Na_2O wt%	2.92	3.04	2.31	2.35	4.14	3.39	5.81	2.73	2.63	2.72	2.92	2.98	2.44	2.35	2.22	2.40	2.49
K_2O wt%	0.34	0.71	0.19	0.13	0.60	0.56	1.18	0.41	0.44	0.47	0.51	0.45	0.39	0.41	0.43	0.40	0.42
P_2O_5 wt%	0.18	0.21	0.08	0.09	0.41	0.24	0.13	0.16	0.16	0.18	0.26	0.24	0.17	0.17	0.21	0.16	0.18
Total	99.35	99.03	99.73	99.55	98.84	99.07	99.25	99.20	99.73	99.49	99.07	98.32	99.00	99.18	98.51	98.66	98.71
Mg#	53.46	57.45	63.02	63.39	40.37	47.02	18.67	59.08	56.90	57.44	60.16	59.70	54.05	54.56	55.34	54.81	52.74
Li	4.49	5.07	3.76	3.97	8.46	6.63	23.65	4.31	4.32	4.20	4.52	4.44	5.44	5.77	5.18	4.86	5.45
Be	0.71	0.94	0.41	0.29	1.20	0.89	3.18	0.71	0.78	0.81	0.92	0.86	0.64	0.59	0.66	0.56	0.67
Na (BCR)	3.08	3.29	2.50	2.56	4.51	3.56	6.90	2.83	2.77	2.90	3.08	3.13	2.50	2.54	2.34	2.50	2.51
Na	3.00	3.10	2.34	2.43	4.40	3.45	6.65	2.72	2.71	2.81	3.01	3.01	2.49	2.47	2.27	2.40	2.48
Mg (BCR)	6.99	6.70	9.74	9.23	4.46	5.77	0.98	7.98	7.93	8.18	7.52	7.49	6.98	7.17	7.12	7.01	6.74
Mg	6.78	6.34	9.18	8.81	4.37	5.61	0.95	7.69	7.78	7.98	7.32	7.19	6.94	6.98	6.96	6.77	6.67
Al 612	14.30	15.31	16.95	16.30	14.17	14.76	12.97	15.78	16.48	15.73	15.93	15.82	14.27	14.21	14.27	14.12	14.13
Al (BCR)	14.75	15.88	17.81	16.81	14.25	14.86	13.20	16.14	16.34	15.92	16.32	16.52	14.41	14.68	14.60	14.63	14.53
P	724.88	945.09	321.97	343.32	1896.98	1139.52	633.19	730.80	666.22	766.88	1048.61	949.77	735.26	717.81	835.41	669.18	758.46
P (BCR)	756.58	1008.58	345.74	363.70	1952.22	1182.76	659.15	765.38	684.78	790.63	1093.60	1002.02	750.23	746.25	859.36	693.91	771.79
K (BCR)	2906.55	6088.85	1645.20	1096.92	5223.03	4879.16	10399.40	3475.84	3865.66	4064.68	4398.24	3972.64	3323.24	3377.33	3694.16	3337.80	3518.45
Ca	12.04	11.29	11.33	12.38	8.68	10.45	3.12	11.89	12.49	11.60	11.51	10.97	11.84	11.76	11.88	11.55	11.20
Ca (BCR)	11.74	11.07	11.33	12.57	8.40	10.09	3.08	11.58	11.94	11.34	11.56	11.14	11.75	11.96	11.84	11.72	11.10
Sc	44.46	34.82	24.13	39.33	32.15	37.67	13.50	35.85	36.97	34.59	37.57	36.72	41.80	42.02	42.05	43.41	43.17
Ti	10315.45	10821.00	8100.95	5854.47	12248.87	12548.89	4430.83	9115.46	9795.80	10494.52	10771.74	10670.12	8619.65	8475.33	8641.11	8653.74	9577.31
V	314.36	263.04	213.57	255.87	280.96	325.73	26.66	267.75	298.43	312.01	293.82	278.18	330.89	331.41	350.30	322.95	354.76
Cr	242.77	163.01	330.07	325.87	63.29	119.25	10.18	281.26	241.27	269.87	250.48	240.16	186.77	190.75	220.62	168.08	161.78
Mn	1520.10	1225.79	1201.68	1328.03	1683.24	1637.43	1607.69	1330.09	1439.52	1472.87	1354.20	1334.58	1553.25	1557.17	1509.79	1508.65	1574.62
Mn (BCR)	1562.22	1287.12	1272.10	1389.31	1714.80	1683.63	1662.21	1386.67	1472.08	1517.85	1385.65	1389.40	1559.49	1596.30	1550.57	1565.82	1589.94
Co	46.71	37.63	53.60	50.27	36.54	41.88	7.50	44.22	48.65	49.58	40.20	39.28	45.87	46.29	43.31	43.27	44.59
Ni	40.18	46.44	243.46	133.27	29.04	40.37	4.00	110.41	102.86	121.20	98.21	102.05	74.21	74.66	79.66	60.76	63.80

	East Futuna			Sula sula caldera (EFVZ)				Central Futuna Volcanic Zone (CFVZ)			South Futuna (SFVZ)						
	NLTD-15-1	NLTD-16-1	NLTD-17-1	NLTD-18-1-1	NLTD-18-3-1	NLTD-19-16	NLTD-21-1-glass	NLTD-22-14	NLTD-23-7-1	NLTD-23-12-glass	NLTD-24-1-	NLTD-26-7-	NLTD-30-24	NLTD-30-38	NLTD-31-11	NLTD-32-1	NLTD-33-6-glass
Cu	105.26	72.43	79.64	119.75	108.93	83.41	26.19	69.30	81.25	84.15	69.85	66.23	104.30	104.00	93.68	95.67	81.22
Zn	109.52	86.41	102.58	87.16	126.09	126.83	170.65	100.52	100.23	102.39	92.65	94.11	107.54	107.56	104.64	100.77	111.45
Ga	18.96	17.36	17.62	16.89	20.61	19.98	24.32	18.11	18.84	19.14	18.48	18.25	17.77	17.55	16.83	17.02	17.69
As	0.22	0.38	0.13	0.11	0.48	0.32	1.20	0.25	0.23	0.26	0.40	0.35	0.27	0.27	0.30	0.26	0.28
Se	0.34	0.27	0.23	0.22	0.53	0.41	0.55	0.28	0.27	0.32	0.30	0.30	0.42	0.40	0.38	0.34	0.36
Rb	7.44	16.53	3.05	2.32	14.26	12.30	28.16	7.39	6.98	6.82	11.26	9.17	9.32	9.34	12.87	10.62	10.35
Sr	193.73	255.83	174.91	110.17	137.33	192.25	67.14	218.74	269.50	260.85	237.32	215.62	156.00	153.57	141.83	149.58	157.35
Y	23.54	22.90	15.16	21.08	60.40	35.16	138.62	22.58	20.78	22.92	27.97	28.73	24.89	24.68	25.61	24.36	26.47
Zr	104.51	115.57	50.71	48.55	228.98	132.32	753.09	90.17	93.37	105.53	124.50	124.16	92.26	89.23	87.67	82.59	95.90
Nb	6.88	17.37	2.93	2.51	14.18	13.46	21.97	9.84	6.06	7.02	15.84	13.12	10.49	10.67	15.44	11.48	12.22
Mo	0.50	0.91	0.28	0.24	0.87	0.80	2.07	0.67	0.60	0.71	0.81	0.74	0.61	0.60	0.62	0.54	0.63
Ag	0.04	0.02	0.03	0.04	0.04	0.03	0.03	0.02	0.03	0.02	0.03	0.02	0.03	0.03	0.03	0.03	0.03
Cd	0.15	0.14	0.13	0.12	0.16	0.17	0.28	0.14	0.14	0.14	0.14	0.15	0.15	0.15	0.15	0.15	0.15
In	0.08	0.06	0.06	0.06	0.10	0.09	0.16	0.07	0.07	0.07	0.07	0.07	0.08	0.07	0.07	0.07	0.08
Sn	1.97	1.92	1.76	1.74	2.87	2.31	6.33	2.00	2.02	2.19	2.28	2.23	1.87	1.84	1.92	1.89	1.94
Sb	0.02	0.03	0.02	0.02	0.05	0.03	0.12	0.02	0.02	0.02	0.03	0.03	0.02	0.02	0.02	0.02	0.02
Cs	0.07	0.18	0.03	0.03	0.16	0.15	0.31	0.09	0.07	0.07	0.11	0.09	0.11	0.11	0.13	0.11	0.11
Ba	59.70	149.18	24.58	25.22	125.92	120.15	188.94	82.70	54.56	55.85	126.81	100.41	82.90	83.49	130.36	102.54	101.67
La	6.23	12.77	2.56	2.53	13.97	10.90	23.81	8.01	6.44	6.98	12.46	10.61	7.66	7.62	10.58	8.17	8.78
Ce	16.24	27.76	7.09	6.83	34.06	25.20	66.11	18.35	15.94	17.68	27.86	24.54	17.61	17.40	22.05	17.94	19.62
Pr	2.31	3.39	1.10	1.06	4.87	3.45	9.90	2.44	2.26	2.54	3.79	3.43	2.44	2.40	2.87	2.37	2.61
Nd	11.14	14.90	5.95	5.94	24.16	16.61	49.03	11.42	10.94	12.31	17.22	15.90	11.43	11.51	13.16	11.02	12.29
Sm	3.46	3.87	2.08	2.17	7.44	4.88	15.50	3.32	3.31	3.59	4.37	4.11	3.25	3.15	3.41	3.03	3.46
Eu	1.27	1.35	0.83	0.86	2.29	1.76	3.33	1.21	1.23	1.32	1.60	1.55	1.19	1.16	1.25	1.15	1.26
Gd	4.20	4.43	2.64	2.99	9.46	5.91	19.66	3.88	3.94	4.18	4.87	4.79	3.92	3.69	4.15	3.74	4.20
Tb	0.67	0.67	0.43	0.52	1.53	0.97	3.32	0.62	0.60	0.66	0.80	0.82	0.69	0.68	0.70	0.66	0.71
Dy	4.39	4.28	2.85	3.66	10.59	6.57	23.02	4.17	3.99	4.40	5.21	5.30	4.57	4.44	4.64	4.42	4.72
Ho	0.91	0.87	0.59	0.80	2.25	1.34	5.15	0.87	0.82	0.91	1.10	1.09	0.96	0.94	0.99	0.94	1.02
Er	2.63	2.46	1.68	2.36	6.61	3.87	15.70	2.43	2.28	2.55	3.07	3.20	2.73	2.73	2.87	2.73	2.99
Tm	0.36	0.33	0.23	0.34	0.93	0.54	2.34	0.33	0.32	0.35	0.42	0.45	0.39	0.38	0.41	0.40	0.42
Yb	2.59	2.39	1.54	2.39	6.71	3.72	17.16	2.39	2.11	2.44	2.86	2.96	2.65	2.65	2.75	2.65	2.94
Lu	0.36	0.33	0.21	0.35	0.97	0.52	2.52	0.33	0.30	0.35	0.43	0.45	0.38	0.39	0.43	0.40	0.44
Hf	2.50	2.81	1.47	1.44	6.14	3.47	19.05	2.41	2.41	2.56	3.32	3.30	2.47	2.44	2.34	2.23	2.47
Ta	0.44	1.07	0.21	0.15	0.85	0.83	1.32	0.59	0.39	0.46	0.89	0.80	0.62	0.62	0.88	0.65	0.71
W	0.069	0.198	0.023	0.028	0.192	0.158	0.391	0.125	0.044	0.054	0.209	0.165	0.129	0.129	0.211	0.155	0.155
Re	0.0012	0.0009	0.0006	0.0012	0.0013	0.0012	0.0004	0.0006	0.0013	0.0011	0.0010	0.0008	0.0013	0.0015	0.0017	0.0014	0.0013
Pt	0.0006	0.0002	0.0008	0.0028	0.0018	0.0004	0.0008	0.0003	0.0006	0.0004	0.0009	0.0007	0.0015	0.0023	0.0041	0.0010	0.0012
Au	0.0004	0.0008	0.0006	0.0017	0.0023	0.0008	0.0024	0.0006	0.0004	0.0009	0.0010	0.0009	0.0015	0.0015	0.0029	0.0014	0.0015
Tl	0.0178	0.0335	0.0103	0.0092	0.0464	0.0338	0.0985	0.0234	0.0251	0.0271	0.0320	0.0280	0.0213	0.0207	0.0225	0.0201	0.0228
Pb	0.88	1.24	0.40	0.38	1.32	1.21	3.13	0.97	0.96	1.03	1.34	1.20	0.87	0.86	0.98	0.88	0.95
Bi	0.0149	0.0089	0.0069	0.0068	0.0187	0.0140	0.0396	0.0088	0.0114	0.0096	0.0109	0.0095	0.0115	0.0111	0.0100	0.0113	0.0102
Th	0.4379	1.3358	0.1732	0.2232	1.8430	1.0631	3.4901	0.7998	0.3998	0.4539	1.3191	1.0742	0.8685	0.8662	1.3578	0.9946	1.0016
U	0.1373	0.4000	0.0572	0.0710	0.5794	0.2985	1.4677	0.2224	0.1373	0.1623	0.3512	0.2907	0.2217	0.2229	0.3145	0.2167	0.2307

	East Futuna			Sula sula caldera (EFVZ)				Central Futuna Volcanic Zone (CFVZ)			South Futuna (SFVZ)						
	NLTD-15-1	NLTD-16-1	NLTD-17-1	NLTD-18-1-j	NLTD-18-3-j	NLTD-19-16	NLTD-21-1-glass	NLTD-22-14	NLTD-23-7-j	NLTD-23-12-glass	NLTD-24-1	NLTD-26-7	NLTD-30-24	NLTD-30-38	NLTD-31-11	NLTD-32-1	NLTD-33-6-glass
CO2	57.68	16.34	110.49	74.07	12.19	58.00	3.06	43.49	18.39	16.01	30.52	81.53	115.01	113.04	111.21	84.72	110.55
+/-	0.59	0.26	0.95	0.91	0.14	0.73	0.36	0.33	0.27	0.59	0.40	0.66	0.97	1.19	1.10	1.16	1.15
H2O	0.44	0.83	0.26	0.19	0.93	0.86	0.80	0.47	0.40	0.47	0.66	0.63	0.52	0.51	0.53	0.50	0.54
+/-	0.00	0.00	0.00	0.00	0.00	0.00	0.03	0.00	0.00	0.00	0.00	0.00	0.00	0.00	0.00	0.00	0.00
F	247.39	401.04	157.46	106.87	530.75	396.08	930.72	280.59	235.03	280.75	433.16	395.60	274.43	275.12	343.75	282.30	308.49
+/-	0.49	0.49	0.28	0.26	0.67	1.20	3.35	1.30	1.07	1.35	1.57	2.40	1.59	1.16	1.35	1.24	1.01
P	748.08	981.44	298.74	341.76	1996.31	1202.28	635.49	728.09	673.59	787.04	1109.59	1008.62	769.06	766.71	872.49	699.58	815.24
+/-	1.83	2.58	24.31	0.90	4.61	2.83	2.47	2.16	1.12	2.51	1.88	3.11	2.30	2.08	3.10	1.99	2.33
S	1431.43	822.62	1130.98	946.14	1122.50	1392.44	228.67	1060.67	1078.75	1078.61	910.62	965.40	1162.50	1159.30	994.10	1093.89	1175.89
+/-	8.12	1.97	1.75	2.40	2.30	2.66	1.06	3.56	2.83	2.71	2.61	3.97	2.88	2.44	3.10	3.57	2.97
Cl	114.26	266.22	32.79	236.00	3535.34	490.80	7745.71	118.29	60.38	75.54	168.29	120.77	248.33	247.75	223.26	136.49	141.79
+/-	0.46	0.87	0.11	0.59	11.76	1.55	27.97	0.36	0.15	0.23	0.42	0.44	0.70	0.71	0.58	0.49	0.40

	NE Fiji Triple Junction (caldera)									NEFTJ (S. arm)				NEFTJ (NE arm)						Fi1 (?)
	NLTD-39-5-1	NLTD-40-1	NLTD-41-8	NLTD-42-1	NLTD-43-1	NLTD-49-1	NLTD-50-1	NLTD-50-2	NLTD-50-3-glass	NLTD-44-1	NLTD-45-1	NLTD-45-2	NLTD-46-1-glass	NLTD-47-1	NLTD-47-2	NLTD-47-3	NLTD-47-4-1	NLTD-47-5	NLTD-48-1-glass	NLTD-38-1
SiO_2 wt%	50.02	47.73	49.31	50.13	50.16	49.99	50.34	49.58	49.61	50.14	48.60	50.45	50.12	50.39	50.11	50.43	50.51	50.66	49.02	50.47
TiO_2 wt%	1.23	2.29	2.81	2.22	1.16	1.38	1.34	1.73	1.71	1.49	1.88	0.99	1.53	1.59	1.64	1.43	1.58	1.50	2.11	1.08
Al_2O_3 wt%	15.19	18.02	15.79	15.69	14.90	15.28	15.42	16.04	16.05	14.97	17.60	15.05	15.19	14.70	14.69	14.81	14.71	14.67	17.73	15.12
FeO wt%	9.33	7.67	9.01	8.97	9.72	9.81	9.44	8.67	8.65	10.37	8.11	9.67	10.28	10.61	10.45	10.28	10.52	10.37	7.30	9.43
MnO wt%	0.17	0.14	0.18	0.17	0.18	0.16	0.17	0.17	0.16	0.19	0.13	0.18	0.18	0.20	0.20	0.16	0.21	0.21	0.14	0.18
MgO wt%	7.96	7.63	5.87	6.31	7.89	7.75	8.14	7.92	8.03	7.45	7.60	8.03	7.69	7.19	7.22	7.19	7.17	7.20	7.38	8.14
CaO wt%	12.24	10.59	10.18	11.07	12.64	12.31	12.42	11.72	11.68	12.05	11.20	13.05	12.01	12.10	12.11	12.06	12.16	12.07	11.00	12.86
Na_2O wt%	2.71	3.17	3.57	3.36	2.75	2.91	2.69	2.83	2.83	2.72	2.95	2.51	2.71	3.01	2.95	3.03	2.99	2.97	3.18	2.25
K_2O wt%	0.22	0.87	1.13	0.80	0.09	0.11	0.12	0.44	0.45	0.14	0.69	0.08	0.12	0.14	0.13	0.13	0.14	0.14	0.91	0.08
P_2O_5 wt%	0.15	0.42	0.49	0.39	0.11	0.13	0.10	0.23	0.24	0.13	0.31	0.08	0.14	0.14	0.13	0.13	0.15	0.14	0.43	0.09
Total	99.21	98.53	98.34	99.10	99.61	99.83	100.19	99.33	99.41	99.65	99.06	100.09	99.97	100.06	99.64	99.66	100.14	99.93	99.19	99.69
Mg#	60.34	63.95	53.73	55.62	59.12	58.49	60.56	61.94	62.32	56.14	62.56	59.67	57.14	54.72	55.19	55.47	54.82	55.28	64.31	60.62
Li	4.84	4.70	6.21	5.65	5.38	4.70	5.03	5.01	5.14	4.94	5.06	5.10	5.22	5.70	5.30	5.97	5.16	5.70	4.60	4.06
Be	0.43	1.05	1.37	1.15	0.33	0.47	0.35	0.71	0.65	0.44	0.90	0.27	0.49	0.47	0.47	0.47	0.52	0.51	1.07	0.29
Na (BCR)	2.88	3.37	3.74	3.46	2.88	2.96	2.75	2.87	2.87	2.82	3.11	2.60	2.82	3.05	3.08	3.05	3.11	3.08	3.34	2.41
Na	2.72	3.19	3.62	3.39	2.74	2.92	2.70	2.86	2.84	2.73	2.96	2.53	2.78	3.02	2.98	3.00	3.04	3.06	3.23	2.22
Mg (BCR)	8.14	7.82	5.96	6.39	8.09	8.10	8.23	8.14	8.17	7.50	7.81	8.19	7.77	7.23	7.30	7.22	7.33	7.24	7.51	8.51
Mg	7.68	7.33	5.70	6.17	7.59	7.95	8.12	8.08	8.06	7.15	7.43	7.93	7.67	7.12	7.06	7.10	7.15	7.16	7.22	7.83
Al 612	14.27	17.04	14.68	14.65	13.93	14.90	15.20	15.86	15.58	13.85	16.51	14.45	14.75	14.30	14.19	14.25	14.20	14.31	16.68	14.19
Al (BCR)	15.25	18.46	15.85	15.69	15.24	15.16	15.29	15.90	15.75	15.00	17.21	14.89	14.89	14.46	14.58	14.42	14.50	14.43	17.30	15.37
P	596.72	1780.60	2148.13	1702.75	430.28	531.68	470.97	956.70	949.86	589.56	1363.31	357.12	609.91	600.05	590.03	593.18	598.43	603.22	1807.19	387.36
P (BCR)	617.89	1857.32	2192.86	1717.57	445.59	545.25	480.40	965.36	969.32	603.04	1442.38	369.63	614.74	608.83	611.47	599.07	611.20	605.69	1882.24	414.39
K (BCR)	1847.97	7745.69	9774.92	6777.42	827.07	938.40	975.38	3823.28	3757.99	1217.23	5975.40	736.18	919.39	1139.57	1144.41	1132.55	1156.70	1150.22	7896.87	692.77
Ca	11.92	10.29	9.87	10.89	12.32	12.45	12.36	11.59	11.61	11.89	11.09	12.99	12.07	12.07	11.99	12.17	12.15	12.12	10.81	12.38
Ca (BCR)	12.24	10.59	10.18	11.07	12.64	12.31	12.42	11.72	11.68	12.05	11.20	13.05	12.01	12.10	12.11	12.06	12.16	12.07	11.00	12.86
Sc	40.73	25.34	34.04	37.56	43.11	44.52	43.69	38.81	37.32	41.91	30.88	44.79	43.93	45.84	45.15	45.30	45.38	45.81	30.51	42.28
Ti	7446.14	12950.84	15322.03	12491.46	6582.90	8029.95	7277.64	9666.26	9554.25	8663.32	11195.38	6168.26	8901.86	8624.73	8568.73	8718.03	8586.17	8606.96	11701.26	6110.11
V	270.58	211.49	294.39	289.71	273.14	287.42	278.71	262.46	259.35	311.62	234.62	276.57	315.33	311.18	309.50	311.26	312.13	314.83	221.26	285.07
Cr	235.21	167.27	88.87	110.47	160.25	324.67	301.48	310.40	310.36	309.91	232.81	327.66	283.80	137.12	140.82	137.80	142.16	144.99	227.30	433.95
Mn	1387.98	1056.61	1321.33	1345.91	1444.64	1498.25	1424.68	1313.84	1292.57	1526.26	1159.35	1448.24	1542.61	1576.23	1561.38	1566.92	1566.64	1579.09	1086.42	1392.88
Mn (BCR)	1459.18	1118.27	1368.23	1377.56	1522.13	1510.27	1435.56	1313.11	1300.93	1585.49	1214.92	1489.32	1559.93	1596.46	1618.92	1594.50	1611.88	1603.27	1125.15	1503.16
Co	44.67	36.94	34.58	36.96	46.62	46.17	45.78	42.62	42.38	44.37	38.33	46.43	46.71	46.30	45.72	46.03	46.43	46.53	35.78	44.06
Ni	74.37	127.85	33.55	45.51	49.66	76.12	77.41	96.84	97.52	65.68	107.99	58.70	67.93	48.28	47.52	47.43	48.75	47.93	98.65	92.11

	NE Fiji Triple Junction (caldera)									NEFTJ (S. arm)				NEFTJ (NE arm)						Fi1 (?)
	NLTD-39-5-1	NLTD-40-1	NLTD-41-8	NLTD-42-1	NLTD-43-1	NLTD-49-1	NLTD-50-1	NLTD-50-2	NLTD-50-3-glass	NLTD-44-1	NLTD-45-1	NLTD-45-2	NLTD-46-1-glass	NLTD-47-1	NLTD-47-2	NLTD-47-3	NLTD-47-4-1	NLTD-47-5	NLTD-48-1-glass	NLTD-38-1
Cu	90.32	47.70	57.45	72.38	102.62	99.50	93.81	80.28	81.17	90.86	64.23	115.67	88.26	102.36	102.65	103.90	103.33	104.59	68.71	95.68
Zn	95.10	84.74	100.93	96.41	94.16	95.44	92.18	90.13	88.70	108.10	83.02	91.98	107.35	104.74	101.47	104.46	102.65	105.33	74.57	95.35
Ga	16.79	19.81	20.26	19.14	16.46	17.53	17.12	17.86	17.69	17.76	18.82	16.74	17.83	17.94	17.78	18.11	18.32	18.15	18.95	16.04
As	0.20	0.53	0.65	0.50	0.12	0.14	0.15	0.30	0.29	0.17	0.43	0.13	0.15	0.15	0.16	0.14	0.17	0.15	0.58	0.11
Se	0.30	0.28	0.36	0.36	0.33	0.30	0.30	0.29	0.32	0.33	0.29	0.30	0.35	0.31	0.34	0.36	0.37	0.34	0.31	0.31
Rb	4.64	21.29	28.52	20.49	1.68	1.98	2.28	10.48	10.02	2.67	16.87	1.62	1.89	2.40	2.34	2.37	2.39	2.49	23.97	1.30
Sr	130.71	348.15	273.68	218.23	107.29	125.33	125.20	224.20	218.35	116.76	277.16	94.28	122.42	129.91	129.08	128.93	129.83	130.62	271.12	85.32
Y	23.19	22.31	30.41	29.66	22.95	26.85	25.02	25.46	24.18	28.84	22.74	23.54	32.24	29.21	28.89	29.15	28.91	29.44	24.09	21.40
Zr	71.44	153.95	195.14	162.04	58.98	77.11	65.01	106.83	106.41	85.91	128.54	55.31	92.65	85.08	84.71	86.04	84.07	85.43	160.85	50.94
Nb	6.06	31.60	39.82	27.72	2.34	2.62	2.98	13.23	12.62	3.45	24.37	2.18	2.70	3.41	3.37	3.46	3.49	3.43	32.43	1.78
Mo	0.38	1.53	1.96	1.43	0.22	0.25	0.25	0.72	0.72	0.30	1.18	0.21	0.27	0.31	0.30	0.30	0.30	0.31	1.67	0.18
Ag	0.03	0.02	0.02	0.02	0.03	0.03	0.03	0.02	0.03	0.03	0.02	0.04	0.03	0.03	0.03	0.03	0.03	0.03	0.02	0.03
Cd	0.14	0.13	0.17	0.16	0.15	0.15	0.14	0.13	0.13	0.16	0.13	0.15	0.15	0.17	0.16	0.16	0.16	0.17	0.13	0.13
In	0.07	0.07	0.08	0.08	0.07	0.07	0.07	0.07	0.07	0.08	0.07	0.07	0.08	0.08	0.08	0.08	0.08	0.08	0.06	0.06
Sn	1.65	2.38	2.66	2.38	1.38	1.57	1.47	1.89	1.97	1.78	2.22	1.50	1.89	1.86	1.87	1.79	1.76	1.79	2.37	1.44
Sb	0.02	0.05	0.06	0.05	0.01	0.02	0.02	0.03	0.03	0.01	0.04	0.01	0.01	0.01	0.01	0.01	0.01	0.01	0.05	0.01
Cs	0.05	0.22	0.31	0.23	0.02	0.02	0.03	0.10	0.11	0.03	0.18	0.02	0.02	0.03	0.03	0.02	0.03	0.02	0.26	0.01
Ba	49.94	245.96	297.94	207.35	18.96	20.13	24.52	109.78	105.06	26.97	195.72	17.38	18.96	25.84	25.31	25.71	25.95	25.90	245.19	13.79
La	4.62	18.97	23.83	17.29	2.52	3.12	3.09	9.34	8.87	3.63	15.07	2.39	3.54	3.74	3.67	3.74	3.67	3.73	19.71	2.02
Ce	11.57	39.42	48.88	36.27	7.51	9.21	8.51	20.68	20.33	10.74	31.79	6.87	10.67	10.69	10.54	10.84	10.71	10.74	40.02	6.10
Pr	1.67	4.86	6.09	4.62	1.23	1.53	1.41	2.97	2.84	1.68	4.04	1.11	1.84	1.74	1.73	1.75	1.74	1.76	4.86	0.99
Nd	8.50	21.55	26.54	20.23	6.71	8.58	7.87	14.05	13.54	9.30	17.72	6.37	10.09	9.54	9.46	9.49	9.45	9.41	21.35	5.78
Sm	2.83	5.30	6.48	5.33	2.47	3.06	2.72	3.79	3.75	3.29	4.57	2.35	3.46	3.29	3.29	3.41	3.33	3.33	5.12	2.21
Eu	1.09	1.81	2.17	1.83	0.99	1.19	1.07	1.54	1.42	1.22	1.63	0.95	1.31	1.29	1.31	1.27	1.28	1.27	1.80	0.88
Gd	3.58	5.15	6.47	5.77	3.34	4.17	3.66	4.08	4.38	4.39	4.71	3.23	4.50	4.22	4.35	4.40	4.09	4.21	4.93	3.10
Tb	0.64	0.77	0.97	0.91	0.61	0.70	0.66	0.77	0.70	0.77	0.72	0.60	0.83	0.78	0.78	0.76	0.78	0.78	0.79	0.55
Dy	4.05	4.45	5.93	5.57	4.01	4.83	4.39	4.72	4.54	5.04	4.48	4.00	5.66	5.27	5.15	5.13	5.10	5.27	4.73	3.73
Ho	0.89	0.85	1.17	1.15	0.89	1.04	0.99	0.99	0.93	1.11	0.89	0.92	1.22	1.12	1.12	1.12	1.12	1.13	0.92	0.84
Er	2.56	2.24	3.20	3.14	2.55	2.96	2.81	2.73	2.67	3.18	2.35	2.62	3.47	3.30	3.30	3.29	3.23	3.23	2.50	2.45
Tm	0.37	0.31	0.43	0.42	0.35	0.41	0.40	0.37	0.36	0.46	0.33	0.38	0.51	0.47	0.45	0.46	0.44	0.46	0.34	0.33
Yb	2.52	2.05	2.90	3.05	2.46	2.96	2.66	2.45	2.45	3.32	2.21	2.66	3.44	3.17	3.11	3.21	3.11	3.14	2.32	2.42
Lu	0.37	0.30	0.40	0.42	0.36	0.43	0.40	0.38	0.34	0.48	0.31	0.39	0.52	0.45	0.47	0.47	0.45	0.48	0.33	0.36
Hf	1.85	3.60	4.84	3.91	1.67	2.07	1.91	2.90	2.77	2.30	3.13	1.63	2.54	2.39	2.27	2.28	2.36	2.27	3.81	1.42
Ta	0.34	1.74	2.17	1.52	0.13	0.16	0.17	0.78	0.72	0.19	1.35	0.12	0.16	0.20	0.20	0.19	0.20	0.19	1.77	0.10
W	0.089	0.454	0.581	0.415	0.031	0.032	0.035	0.166	0.160	0.044	0.351	0.030	0.033	0.044	0.041	0.042	0.042	0.042	0.496	0.022
Re	0.0010	0.0005	0.0009	0.0010	0.0006	0.0010	0.0007	0.0008	0.0009	0.0015	0.0003	0.0010	0.0011	0.0009	0.0009	0.0010	0.0021	0.0007	0.0005	0.0015
Pt	0.0004	0.0002	0.0006	0.0010	0.0003	0.0003	0.0006	0.0005	0.0000	0.0005	0.0004	0.0001	0.0003	0.0005	0.0004	0.0004	0.0007	0.0003	0.0007	
Au	0.0005	0.0009	0.0019	0.0016				0.0005	0.0007	0.0005	0.0007	0.0003	0.0008	0.0007	0.0005	0.0012	0.0004	0.0007	0.0018	0.0007
Tl	0.0111	0.0271	0.0402	0.0303	0.0083	0.0082	0.0085	0.0173	0.0182	0.0112	0.0255	0.0081	0.0129	0.0126	0.0124	0.0122	0.0128	0.0145	0.0354	0.0059
Pb	0.56	1.49	1.82	1.44	0.40	0.47	0.44	0.89	0.87	0.55	1.22	0.37	0.55	0.54	0.54	0.54	0.55	0.55	1.51	0.32
Bi	0.0080	0.0086	0.0098	0.0084	0.0089	0.0066	0.0079	0.0086	0.0081	0.0088	0.0072	0.0087	0.0081	0.0093	0.0086	0.0085	0.0082	0.0082	0.0088	0.0073
Th	0.4938	2.5158	3.2665	2.3421	0.1911	0.2106	0.2345	1.0567	1.0020	0.2826	1.9335	0.1846	0.2315	0.2703	0.2723	0.2774	0.2714	0.2748	2.7293	0.1343
U	0.1227	0.5918	0.8069	0.5710	0.0510	0.0589	0.0647	0.2550	0.2562	0.0729	0.4797	0.0537	0.0645	0.0742	0.0772	0.0763	0.0755	0.0753	0.6924	0.0386

	NE Fiji Triple Junction (caldera)									NEFTJ (S. arm)				NEFTJ (NE arm)			
	NLTD-39-5-glass	NLTD-40-1-glass	NLTD-41-8-glass	NLTD-42-1-glass	NLTD-43-1-glass	NLTD-49-1-glass	NLTD-50-1-glass	NLTD-50-2-glass	NLTD-50-3-glass	NLTD-44-1-glass	NLTD-45-1-glass	NLTD-45-2-glass	NLTD-46-1-glass	NLTD-47-1-glass	NLTD-47-2-glass	NLTD-47-3-glass	NLTD-47-4-glass	NLTD-47-5-glass	NLTD-48-1-glass	NLTD-38-1-glass
CO2	265.16	125.90	165.82	181.33	318.11	200.33	163.29	359.77	391.20	140.81	94.66	113.08	226.05						80.43	185.27
+/-	2.18	0.63	1.10	1.27	1.32	0.76	0.92	2.35	1.07	1.13	0.60	0.56	0.91						0.61	0.97
H2O	0.25	0.84	0.96	0.76	0.18	0.23	0.19	0.48	0.48	0.25	0.67	0.16	0.25						0.74	0.17
+/-	0.00	0.00	0.00	0.00	0.00	0.00	0.00	0.00	0.00	0.00	0.00	0.00	0.00						0.00	0.00
F	165.38	523.84	625.38	444.24	118.09	145.38	135.07	294.78	295.83	167.60	427.62	107.00	167.59						471.79	107.15
+/-	0.64	1.59	1.66	1.92	0.26	0.63	0.64	0.94	1.16	0.32	1.85	0.49	0.66						1.94	0.27
P	612.36	1910.51	2301.44	1802.75	433.75	545.71	477.18	1020.20	1014.59	602.21	1497.21	357.82	616.75						1959.60	377.47
+/-	1.85	4.25	4.32	2.81	1.00	1.00	1.39	2.62	2.28	1.04	3.09	1.69	1.20						2.96	1.59
S	1088.06	826.65	1102.89	1119.34	1162.75	1203.21	1109.06	1033.91	1046.05	1264.32	939.96	1159.41	1283.55						819.78	1061.26
+/-	3.02	2.60	3.50	6.92	2.45	3.57	3.24	2.94	4.18	4.62	2.51	4.94	4.84						2.40	2.94
Cl	54.31	258.33	321.90	298.18	51.40	129.61	43.51	116.52	101.75	42.80	206.34	70.99	135.12						280.41	17.73
+/-	0.13	0.82	0.90	1.09	0.20	0.80	0.26	0.41	0.60	0.15	1.27	0.42	0.65						1.37	0.09

A

B

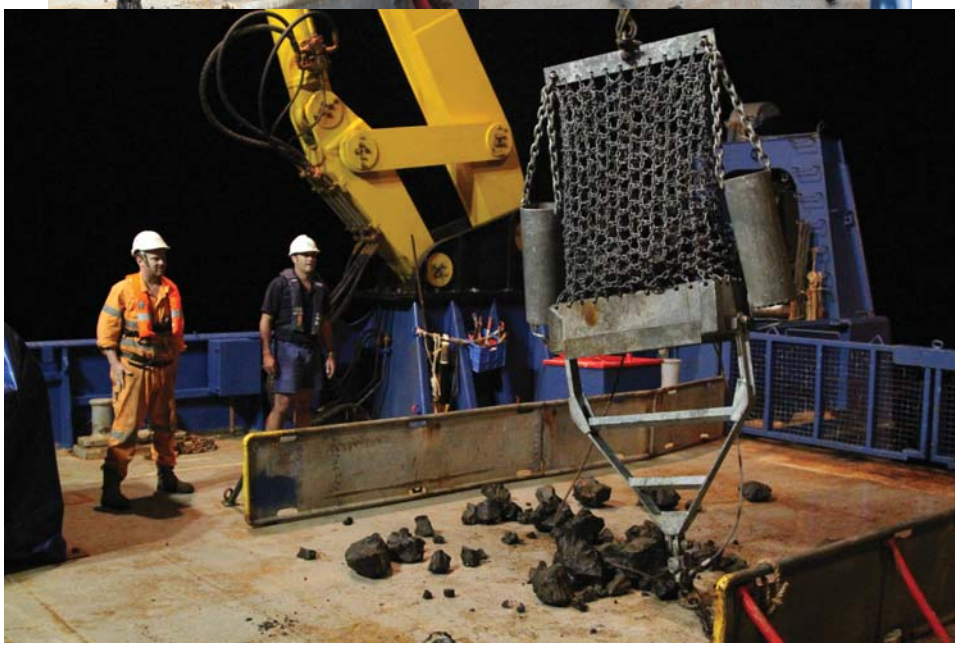


C
D
E

Figure 5 Photos of the research cruise ss2012_v02 (NoLauTe) (A) R/V Southern Surveyor. (B) Dredge which consisted of a mesh net and two trailing buckets. (C) Dredge hauls on the ship deck. (D) Sifting through the samples separating out the fresh volcanic glass. (E) Categorizing the samples and picking fresh glasses for geochemical analyses. (F) The samples recovered from the research cruise were a mixture of aphyric or porphyritic basalts with volcanic glass rinds. The visible phenocrysts were plagioclase.

B. Lithium isotope variations in Tonga-Kermadec arc – Lau back-arc lavas and DSDP Site 204 sediments

Author's Preface

The following manuscript is the lithium manuscript that has been submitted for peer-review. It is included in my appendix because it has been re-written in a format for a shorter journal article and differs in content included for discussion. Here we show that lava from one island does appear to carry a signature from the subducting sediment, while most of the other lithium signatures from the other lavas in the arc have equilibrated in the mantle.

Abstract

The relatively compatible but fluid-mobile nature of Li and its fractionation in low-temperature environments has long fostered the possibility that Li isotopes might provide a complementary or new tracer of subducted materials in arc lavas. The Tonga-Kermadec arc – Lau back-arc provides an end-member of subduction zones with the coldest thermal structure on Earth. Here we report Li isotope data for 14 lavas from the arc front and 7 back-arc lavas as well as 12 pelagic and volcaniclastic sediments along a profile through the sedimentary sequence at DSDP site 204. The arc and back-arc lavas range from basalts to dacites in composition with SiO_2 = 48.3-65.3 wt. % over which Li concentrations increase from 2 to 16 ppm. The majority have δ^7Li that ranges from 2.5 to 5.0 ‰ with an average of 3.6 ± 0.7 ‰, similar to that reported from other arcs. The pelagic sediments have variable Li concentrations (33-133 ppm), and δ^7Li that ranges from 1.2 to 10.2 ‰ whilst the volcaniclastic sediments have an even greater range of Li concentrations (3.6 to 165 ppm) and generally higher δ^7Li values (8-14 ‰). Lava from Niuatoputapu at the northern end of the arc seems to show a clear contribution from the volcaniclastics. However, fluid versus sediment signatures are not readily distinguished for most of the lavas, and sediment mass-balance models require an order of magnitude

more sediment than previous estimates based on Th-Nd-Be isotopes. This is taken as evidence that fluids provide a significant proportion of the total Li budget in the lavas from the subducting sediments and altered oceanic crust. We infer that subsequent diffusive equilibration overprints much of this signature with the ambient mantle wedge.

Keywords: Li isotopes; Tonga-Kermadec arc; Lau back-arc; recycling; sediment profile

1. INTRODUCTION

Subduction recycles altered oceanic crust and overlying sediments into the mantle, and there is much interest in the extent to which these components influence the composition of arc lavas and mantle that may much later be sampled at mid-ocean ridges and oceanic islands. Lithium is a light, fluid-mobile trace element that has also been widely evaluated as potential tracer of subduction zone recycling (Brenan et al., 1998; Elliott et al., 2004; Penniston-Dorland et al., 2012; Ryan and Langmuir, 1987; Tang et al., 2014; You et al., 1996). The utility of Li in this regard reflects low temperature isotopic fractionation that occurs during weathering and the uptake of seawater into sediments and the altered oceanic crust (e.g., Brant et al., 2012; Chan et al. 1992; Gao et al., 2012; Liu et al., 2013, 2015; Rudnick et al., 2004; Liu and Rudnick, 2011). Accordingly, Li isotope variations in mid-ocean ridge basalts have been taken as evidence for long-term "pollution" of the mantle by subducted components (Elliott et al., 2006). Given this variation, it is surprising that studies of arc lavas have frequently been frustrated by the lack of clear Li isotope signatures of subducted components and the ubiquitous range of δ^7Li = 3-4 being widely attributed to diffusive interaction between rising melts and the mantle wedge (e.g., Elliott et al., 2004; Penniston-Dorland et al., 2012; Tang et al., 2014). Nevertheless, some workers have found evidence for sediment-derived lithium isotope signals in arc lavas (Chan et al., 2002; Moriguti and Nakamura, 1998; Tang et al., 2014).

In light of these on-going investigations, we present here Li concentration and isotope data from well-characterised samples from the oceanic Tonga-Kermadec arc and Lau back-arc as well as the sediment profile at DSDP Site 204 (Fig. 1). This arc encompasses the largest variation in subduction rates (24 to 6 cm/yr) worldwide (Bevis et al., 1995) and affords the opportunity to provide new insights into the debates outlined above because it erupts lavas which carry (1) a strong trace element (e.g. high

Ba/Th, U/Th) fluid signature (Ewart et al., 1998; Turner et al., 2003), (2) very low HFSE concentrations indicative of a depleted wedge that is highly sensitive to slab contributions (Ewart et al, 1998; Turner et al., 1997), (3) ^{226}Ra evidence for rapid melt transport (Turner et al., 2000), (4) ^{10}Be evidence for pelagic sediment addition (George et al, 2005), and (5) a unique tracer of subducted sediment in the Louisville volocaniclastics (Regelous et al., 1997; Turner et al, 1997). The back-arc lavas from the Fonualei Spreading Centre, the Mangatolo Triple Junction and Niuafo'ou offer a contrast to the arc front lavas as sediment- and fluid-related signatures become increasingly muted and the melting regime changes from fluid-fluxed to decompression dominated (Caulfield et al., 2012).

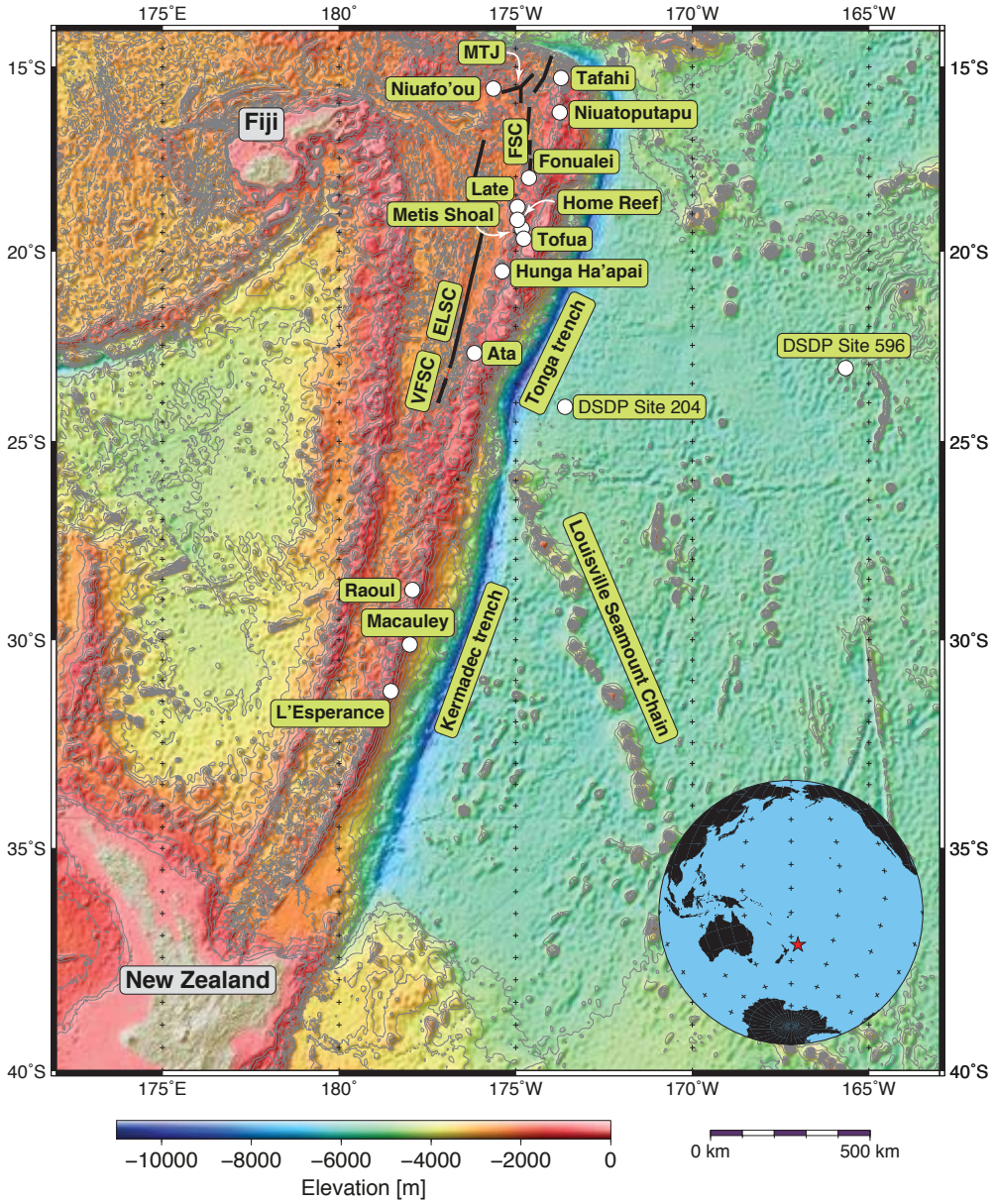

Fig. 1 Map of the Tonga-Kermadec arc – Lau back-arc region showing the localities of the samples analysed. Also shown are the DSDP Sites 204 and 596. VFSC – Valu Fa Spreading Centre, ELSC – Eastern Lau Spreading Centre, FSC – Fonualei Spreading Centre, MTJ – Mangatolo Triple Junction.

2. GEOLOGICAL SETTING AND SAMPLE DETAILS

The 2,800-km long Tonga-Kermadec island arc extends from the Taupo Volcanic Zone in New Zealand to the Vitiaz strike-slip fault south of Samoa and results from subduction of the Pacific plate beneath the Australian plate (Fig. 1). The arc is composed of more than 80 volcanoes, both above and below sea level (Stoffers et al.,

2006; Wright et al., 2006). The Louisville seamount chain, an aseismic ridge, intersects the arc, effectively splitting it into the Tonga segment to the north, and the Kermadec segment to the south. The subducting Pacific plate is 85-144 Ma old (Billen and Stock, 2000; Sutherland and Hollis, 2001) based on biostratigraphy of radiolarian chert and dating of ferrobasalts near to and from DSDP Holes 595/595A and 596/596A (Fig. 1). Both the dip of the slab and the convergence rate increase from south to north. The plate dips at an angle of 30^{o} to a depth of ~120-130 km beneath both segments of the Tonga-Kermadec arc and steepens to $55\text{-}60^{o}$ in the Kermadec segment and $43\text{-}45^{o}$ in the Tonga segment (Isacks and Barazangi, 1977). Convergence rate along the Kermadec segment is 5 cm/yr, while in the Tonga segment the rate increases to 16-24 cm/yr (Bevis et al., 1995). The Tonga-Kermadec lavas consist predominantly of low-K basalts, basaltic andesites, andesites and minor dacites (see Ewart et al., 1998 for a summary).

The composition of the sediments on the Pacific plate are well constrained and dominated by pelagic clays (Burns et al., 1973; Plank and Langmuir, 1998; Turner et al., 1997). Close to the Louisville Ridge, these are underlain by volcaniclastics derived from this seamount chain. The thickness of sediment decreases northwards from 200 – 70 m (Plank and Langmuir, 1998) and it is thought that the full sediment packet is subducted beneath this arc (Bloomer and Fisher, 1986). Mass balance calculations show that only a minor amount (~ 0.25-1 %) of the pelagic sediment is recycled into the lavas (George et al., 2005; Turner et al., 1997). Enrichment in $^{206}Pb/^{204}Pb$ is observed in the volcanoes at the northern end of the arc (Tafahi and Niuatoputapu), and this has been interpreted to reflect the incorporation of the Louisville Ridge volcaniclastic sediments (Regelous et al., 2010; Turner et al., 2007; Wendt et al., 1997).

Westward of the Tonga-Kermadec arc lies two active back-arc basins, the Havre Trough to the south, and the Lau Basin to the north (Fig. 1). The rate of spreading increases northward from 6 cm/yr the Havre Trough to 16 cm/yr in the northern Lau

Basin (Bevis et al., 1995). In the northeast section of the Lau Basin, the Fonualei Spreading Center (FSC) is an active spreading center that extends obliquely away from the active volcanic front northward to the Mangatolu Triple Junction (MTJ) and is punctuated by a series of transform faults that extend into the MTJ (Fig. 1). The Lau back-arc basin basalts (BABB) range from near MORB-like compositions (Hawkins, 1995) when erupted far from the arc, to arc-like compositions when erupted close to the arc (Pearce et al., 1995). BABB, such as those erupted along the Fonualei Spreading Center and Valu Fa Ridge, show subduction signatures that are characterized by enrichment in LILE, volatile elements (e.g., they have up to 2.5 wt.% H_2O), and show depletion in HFSE (Caulfield et al., 2012; Keller et al., 2008; Langmuir et al., 2006; Pearce and Stern, 2006).

The arc lavas analyzed range from basalt to dacite in composition and include some pumaceous samples, while the back-arc lavas are basalt to basaltic andesite in composition. Full petrographic and geochemical data for these samples can be found elsewhere (Acland, 1996; Caulfield et al., 2012; Ewart and Hawkesworth, 1987; Ewart et al., 1998; George et al., 2005; Keller et al., 2008; Leeman et al., 2017; Turner et al., 1997, 2000; 2009). The sediments samples come from DSDP Site 204 which has been subdivided into three units (Burns et al., 1973). Unit 1 is comprised of pelagic clay and ash and dates from the Quaternary to early Miocene or Oligocene. Two samples analysed from the top of the clay unit are composed of dark brown clay that contains plagioclase (andesine), glass shards, mica, quartz, montmorillonite, zeolite, augite, and secondary clay phillipsite. Two samples from the bottom of the clay unit are dark reddish-brown iron-oxide clay composed of montmorillonite, potash feldspar, quartz, amorphous iron oxide, glass shards, and some authigenic carbonate layers. The bottom two units are comprised of volcanogenic sediments derived from the Louisville Seamount Chain. Unit 2, from which three samples were analyzed, is a tuffaceous

sandstone and conglomerate of early Cretaceous age. The clasts are composed of glass shards, andesine, calcite, pumice, and andesitic and basaltic rock fragments. The matrix is mainly altered ash with secondary minerals of epidote, zeolites, calcite, chloritic minerals, serpentine, and amorphous iron oxide. Unit 3, from which two samples were analyzed, is a vitric tuff composed of basaltic to andesitic glass with pyroxene and feldspar crystals in a glass matrix.

3. ANALYTICAL METHODS

The samples analysed were splits of powders for which major and trace element, and radiogenic isotope data have been reported previously (Turner et al., 1997; Ewart et al., 1998; Keller et al., 2008; Caulfield et al., 2012). Both samples and standards were prepared for Li isotopic analysis at the University of Maryland by digesting the powders with a 3:1 mixture of concentrated HF and HNO_3 in Savillex® screw top beakers on a hot plate (T~ 120 ^{o}C). This was followed by addition of concentrated HNO_3 and HCl, with drying between each stage of acid addition. The residue was then re-dissolved in 4 N HCl in preparation for chromatographic separation.

Lithium separation was achieved through ion-exchange chromatography, adapted from Moriguti and Nakamura (1998), where four chromatographic columns were used. For each column, 1 ml of cation exchange resin of AG50w-X12, 200-400 mesh (Bio-Rad) was cleaned with HCl and Milli-Q water followed by conditioning, chemical separation and sample collection using an eluent mixture of HCl and ethanol. The first two columns remove major element cations with 2.5M HCl and subsequently 0.15M HCl. The third and fourth columns separate Na from Li with 30% ethanol in 0.5M HCl through a N_2 pressurized ion exchange column (Rudnick et al., 2004).

The samples were analyzed for ^{6}Li and ^{7}Li on a Nu Plasma multi-collector inductively coupled mass spectrometer (MC-ICP-MS) using faraday cups. Li isotopic

compositions were analyzed by bracketing the sample, before and after, with the L-SVEC standard. The δ^7Li value ($\delta^7Li = [[^7Li/^6Li]_{sample} / [^7Li/^6Li]_{standard} - 1 \times 1000]$) is expressed as per mil deviations from the L-SVEC standard (Flesch et al., 1973). External reproducibility of the isotopic compositions is ≤ ±1.0 ‰ (2σ) based on repeat runs of pure Li standard solutions: in-house standard UMD-1 (δ^7Li = 0.10 ‰, n = 5) and international standard reference material IRMM-016 (δ^7Li = 55.14 ‰, n = 5) (Liu et al., 2010, 2013; Teng et al., 2006). The in-house and the international standard reference materials were analyzed at the beginning and end of each session and often a third time between runs in which more than eight samples were analyzed.

Comparing signal intensities for the whole rock with that measured for the 50 ppb L-SVEC standard and then adjusting for sample weight determined lithium concentrations. These measurements have a 2σ uncertainty of ≤ 10‰ (Teng et al., 2006). Results for USGS international rock standards BHVO-1, AGV-2, and BCR-2 are reported in Table 1. The results are within analytical error of the recommended values from the U.S. Geological Survey and within the ranges for published data (Bouman et al., 2004; Chan and Frey, 2003; Gladney and Goode, 1981; Govindaraju, 1994; James and Palmer, 2000; Liu et al., 2015; Penniston-Dorland et al., 2012; Ryan and Langmuir, 1987; Rudnick et al., 2004; Shihong et al., 2012; Tang et al., 2014). The only exception is BHVO-1 that initially had slightly lower values than published data (Magna et al., 2004). Replicating the analysis produced a value within the accepted range (Tian et al., 2012).

Table 1. Lithium concentrations and isotope ratios for lavas and standards analyzed

Location	Sample ID	SiO_2 (wt. %)	Li (ppm)	δ^7Li (‰)
North Tonga trench	Stn. 25 Boninite	54.72	4.7	2.9
Arc Front Lavas:				
Tafahi	T116	52.81	3.1	4.2
Niuatoputapu	NTT 29/3	60.13	5.8	6.4
Replicate				*7.9*
Fonualei	FON 39	65.34	16.0	4.5
Late	Late 7	53.19	3.3	3.5
Metis Shoal	TLi7	64.25	9.5	4.3
Home Reef	HR06	64.45	8.1	3.3
Tofua	26835	53.94	4.4	2.9
Tofua	26833	54.56	5.0	3.8
Hunga Ha'apai	HHTop	55.35	5.7	3.7
Ata	ATA 8-1	51.90	4.5	1.9
Replicate				*1.6*
Raoul	7125	49.52	3.7	2.5
Macauley	45658	48.30	2.1	3.7
L'Esperance	14831	52.66	1.9	0.3
Rear Arc Lavas:				
Fonualei Spreading Centre	ND-46	53.17	4.1	3.1
Fonualei Spreading Centre	ND-40	52.71	2.9	5.0
Fonualei Spreading Centre	ND-58	54.18	4.8	3.5
Fonualei Spreading Centre	ND-61	54.88	6.2	4.4
Fonualei Spreading Centre	ND-67	52.31	3.8	3.0
Mangatolo Triple Junction	ND-69	49.73	5.6	3.3
Niuafo'ou	31461	49.43	7.8	2.9
Standards:	BHVO-1		4.9	3.6
	BHVO-1		4.8	3.2
	AGV-2		11.1	5.2
	AGV-2		10.5	5.6
	BCR-2		10.3	2.1

4. RESULTS

The new lava results are presented in Table 1. The lavas range from basalts to dacites in composition with SiO_2 = 48.3-65.3 wt. % (Caulfield et al., 2012; Ewart et al., 1998; Keller et al., 2008; Turner et al., 1997). They have Li concentrations that range

from 2 to 16 ppm and overlap the global arc array on Fig. 2a. As a moderately incompatible element Li concentrations increase with increasing SiO_2 (Fig. 2a) but there is no clear correlation between δ^7Li and SiO_2 (Fig.2b). The majority have δ^7Li that ranges from 2.5 to 5.0 ‰ with an average of 3.6 ± 0.7 ‰ that is similar to those reported from other arcs (Bouman et al., 2004; Moriguti and Nakamura, 1998; Tang et al., 2014; Tomascak et al. 2000, 2002). However, there are three notable outliers. For the former two we replicated the data: Niuatoputapu with δ^7Li = 6.4 and 7.9 ‰, ‘Ata with δ^7Li = 1.6 and 1.9 ‰. However, there was insufficient sample from the L’Esperance sample to undertake a replicate analysis (δ^7Li = 0.3 ‰, see Table 1). Thus, it is possible that the range of δ^7Li in this arc may be slightly larger than reported elsewhere (see Fig. 2b and discussion below). The back-arc lavas cluster at the low Li, low SiO_2 end of the arrays on Fig. 2a and overlap the median δ^7Li ratio of the arc lavas (Fig. 2b).

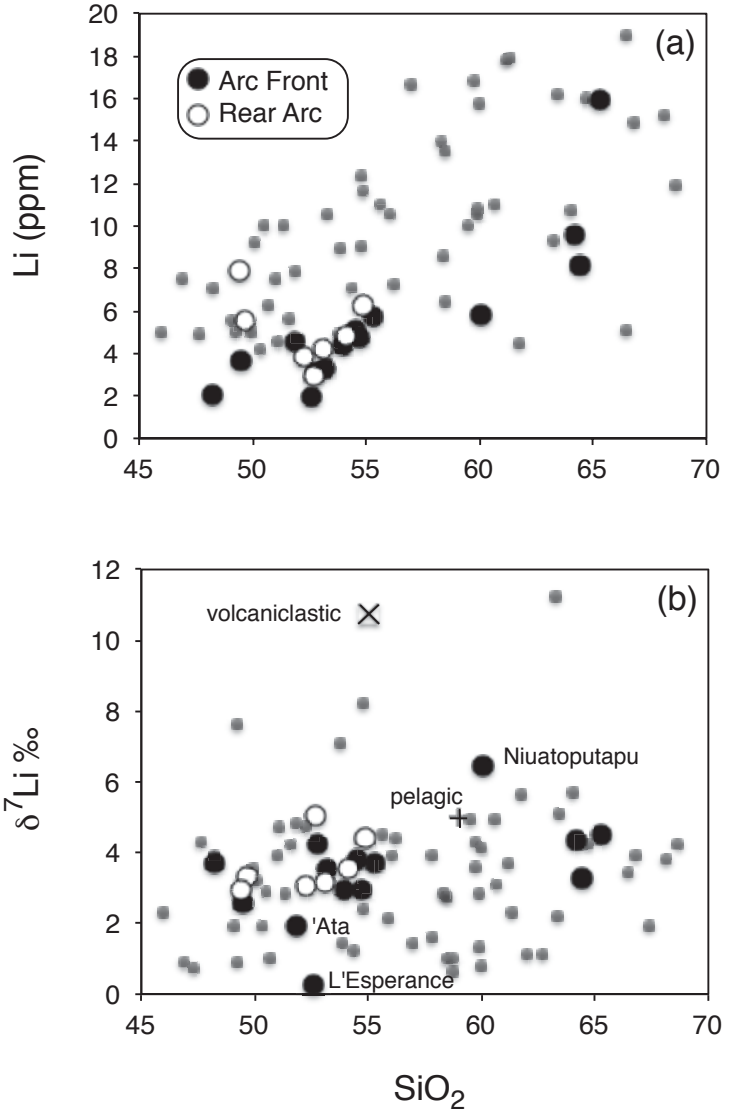

Fig. 2. Plots of Li concentration (a) and δ^7Li (b) versus SiO_2 for Tonga-Kermadec-Lau lavas. The average compositions of the DSDP Site 204 pelagic and volcaniclastic sediments are also shown. Small grey circles are literature data for lavas from other arcs (Moriguti and Nakamura, 1998; Tang et al., 2014; Tomascak et al. 2000, 2002).

The sediment profile at DSDP site 204 is presented in Table 2 and consists of ~ 100 m of pelagic sediments underlain by volcaniclastic sediments from the Louisville seamount chain (Burns et al., 1973). The pelagic sediments have quite variable Li concentrations (33-133 ppm) and δ^7Li that ranges from 1.2 to 10.2 ‰ (Fig. 3) similar to equivalent pelagic sediments analysed by Chan et al. (2006) from DSDP Site 596 further to the east of the trench (see Fig. 1). The volcaniclastic sediments have an even

greater range of Li concentrations (3.6 to 165 ppm) and generally heavier δ^7Li values (8-14 ‰). Overall the range is similar to that reported previously for a wide range of marine sediments (Chan et al., 2006) and the average δ^7Li values are higher than that inferred for the depleted mantle (e.g. Elliott et al., 2004).

Table 2. Li concentrations and isotope ratios in DSDP Site 204 Sediments

Sample ID	Type	Depth (m)	Li (ppm)	δ^7Li (‰)
204-1R-3W-60-61	pelagic	3.6	34.5	1.2
204-2R-1W-109-110	pelagic	8.6	64.1	7.3
204-2R-4W-60-61	pelagic	12.6	47.9	3.8
204-3R-2W-59-60	pelagic	50.9	38.8	10.2
204-4R-1W-75-76	pelagic	85.8	133.3	3.2
204-4R-4W-140-141	pelagic	90.9	32.9	5.2
204-5R-4W-60-61	pelagic	100.6	38.8	3.9
204-6R-3W-48-50	volcaniclastic	106.5	102.6	8.0
204-7R-1W-92-93	volcaniclastic	112.9	4.4	7.2
204-8R-3W-86-87	volcaniclastic	124.9	165.3	11.2
204-9R-1W-108-110	volcaniclastic	142.1	5.2	12.8
204-9R-3W-24-27	volcaniclastic	144.2	3.6	14.4

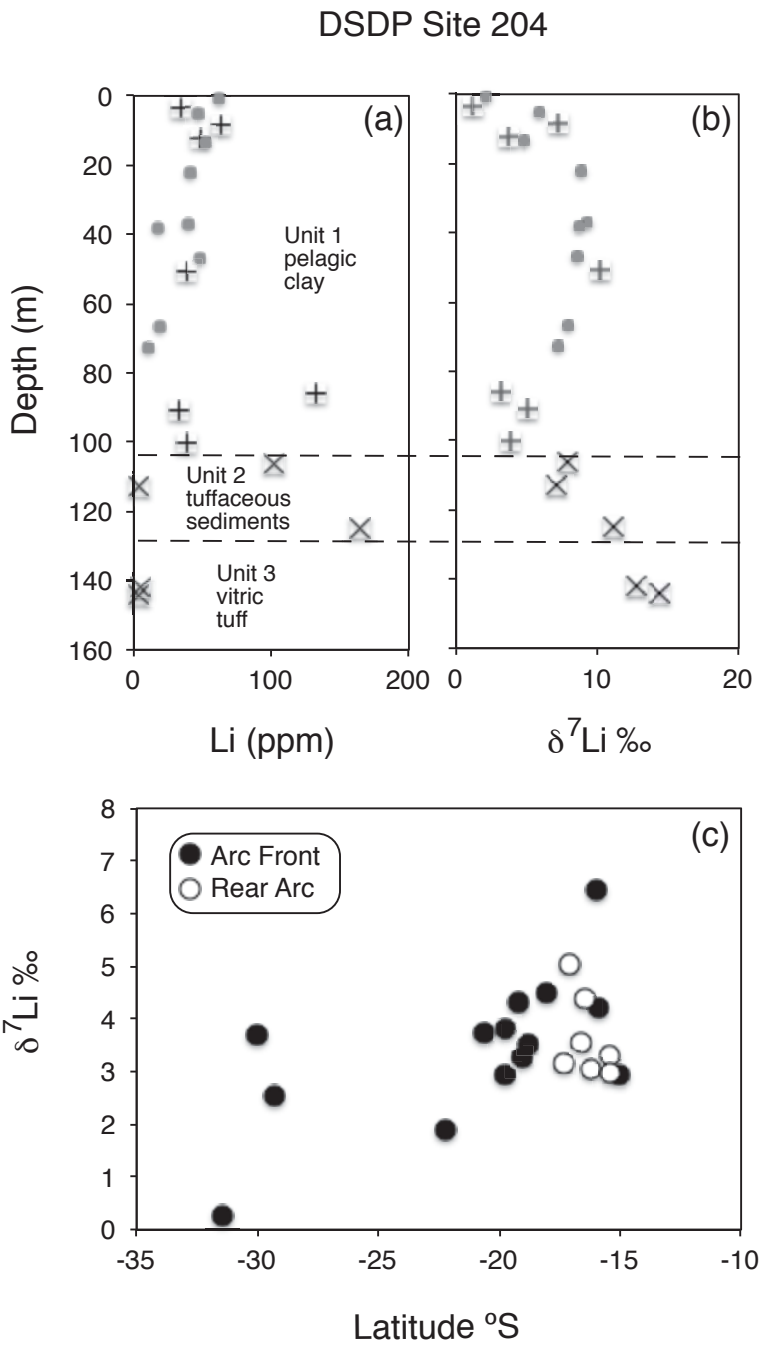

Fig. 3. Profiles of Li concentration (a) and δ^7Li (b) versus depth in the subducting sediment sequence. The crosses are DSDP Site 204 data from Table 2 and the grey circles are pelagic sediments from DSDP Site 596 (Chan et al., 2006). Note that the Louisville volcaniclastic sediments of Units 2 and 3 at Site 204, that include some of the highest Li concentrations and δ^7Li values, are not present at Site 596. (c) Plot of δ^7Li ‰ versus southern Latitude. The occurrence of some elevated values at the northern end of the arc may reflect addition of a Louisville volcaniclastic component to the source of the lavas here (Regelous et al., 1997; Turner et al., 1997).

5. DISCUSSION

In the following sub-sections, we first assess the possible significance of the outlier lavas and then explore possible links to independent tracers of subducted components.

5.1. Lava and sediment data in terms of global distribution and outliers

As shown in Fig. 2, the lavas broadly overlap the global array in terms of both Li concentrations and δ^7Li. Within this broad overlap, the elevated δ^7Li ratio of the Niuatoputapu lava could be explained by addition of a Louisville volcaniclastic component at ~ 4 Ma (Regelous et al., 1997; Turner et al., 1997), though it is unclear why an equivalent signature is not observed in the Tafahi lava since both carry the elevated ^{206}Pb/^{204}Pb Louisville signature. The low δ^7Li ratio from the ‘Ata sample seems to reflect the odd isotopic signature of lavas from this island in general (Ewart et al., 1998; Leeman et al., 2017). Finally, the very low δ^7Li ratio from the L’Esperance lava may reflect alteration since this sample has a chemical index of alteration (CIA) = 64 (Nesbitt and Young, 1982). As noted above the sediments become broadly heavier in δ^7Li with increasing depth in the profile and are on the higher end of sediment values globally.

5.2. Controls on Li isotopic composition

Many studies have utilized U/Th and Th/Ce ratios as tracers of fluid and sediment components in arc lavas (e.g. Turner et al., 1997; Plank and Langmuir, 1998). On Fig. 4a we plot δ^7Li against U/Th as a tracer of fluid contributions from the subducting plate. Overall there is a weak positive correlation, but the majority of the lavas lie between likely average compositions of the mantle wedge (DMM) and altered oceanic crust (AOC) which can have a very large range in δ^7Li (Gao et al., 2012). Here

the Niuatoputapu lava is clearly displaced from the remaining lavas towards the average volcaniclastic sediment composition. No correlation is observed when the δ^7Li data from the Togna-Kermadec lavas is plotted against indices of sediment addition such as Th/Ce (Fig. 4b) unlike the findings of Moriguti and Nakamura (1998) or Chan et al. (2002). The back-arc lavas lie at the low U/Th, low Th/Ce end of the data, consistent with lesser overall contributions from the slab (Caulfield et al., 2012).

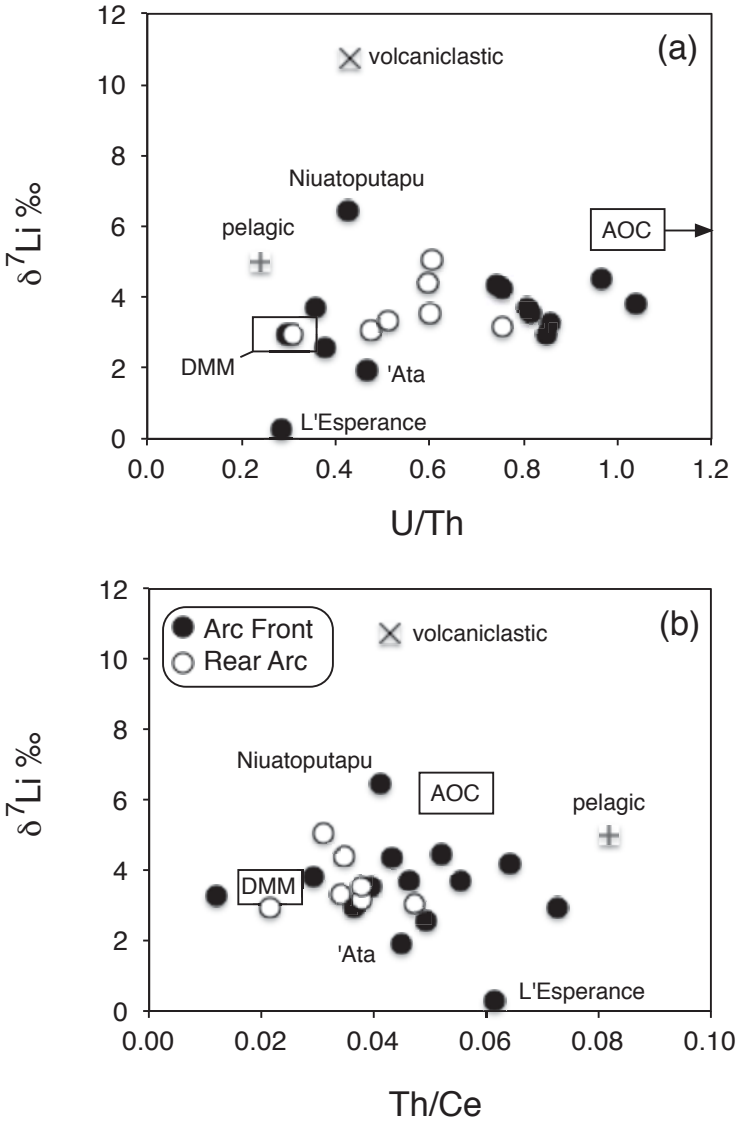

Fig. 4. Plots of δ^7Li versus U/Th a fluid-sensitive index (a) and Th/Ce a sediment-sensitive index (b). The average compositions of the DSDP Site 204 pelagic and volcaniclastic sediments are also shown along with average estimates for depleted MORB mantle (DMM) and altered oceanic crust (AOC) – data from

Elliott et al. (2004), Gao et al. (2012), Kelley et al. (2003), Salters and Stracke (2004).

On Fig. 5 we investigate variations between δ^7Li and two other isotope systems that tend to be track sub-arc fluid additions since both B and Sr are fluid mobile (Brenan et al., 1998). There is no correlation between δ^7Li and ^{87}Sr/^{86}Sr though, as in Fig. 4a, both the arc front and back-arc lavas generally fall between DMM and AOC and the average sediment compositions. Although there is less data, we plot δ^7Li versus δ^{11}B on Fig. 5b. Once again, there is no correlation though the diagram does highlight the unusually light B in the ‘Ata sample that may reflect complex mantle wedge circulation caused by the locus of present-day subduction of the Louisville seamounts (Leeman et al., 2017).

The conclusion from Figs. 4 and 5 (and similar diagrams not shown) has to be that there are no trends that unambiguously distinguish between sediment and fluid addition as the main control on the variations in δ^7Li in the Tonga-Kermadec-Lau lavas. It is highly likely that diffusive equilibration with non-subduction modified mantle wedge has erased much of any putative initial subduction-derived signatures (e.g., Elliott et al., 2004; Tang et al., 2014; Penniston-Dorland et al., 2012). Nevertheless, some δ^7Li signals do appear to survive such as that of the Louisville volcaniclastics in the case of the lava from Niuatoputapu. Conversely, the lack of an equivalent signal in similar lavas from neighboring Tafahi testifies to just how fragile they are in the face of diffusive interaction with the wedge.

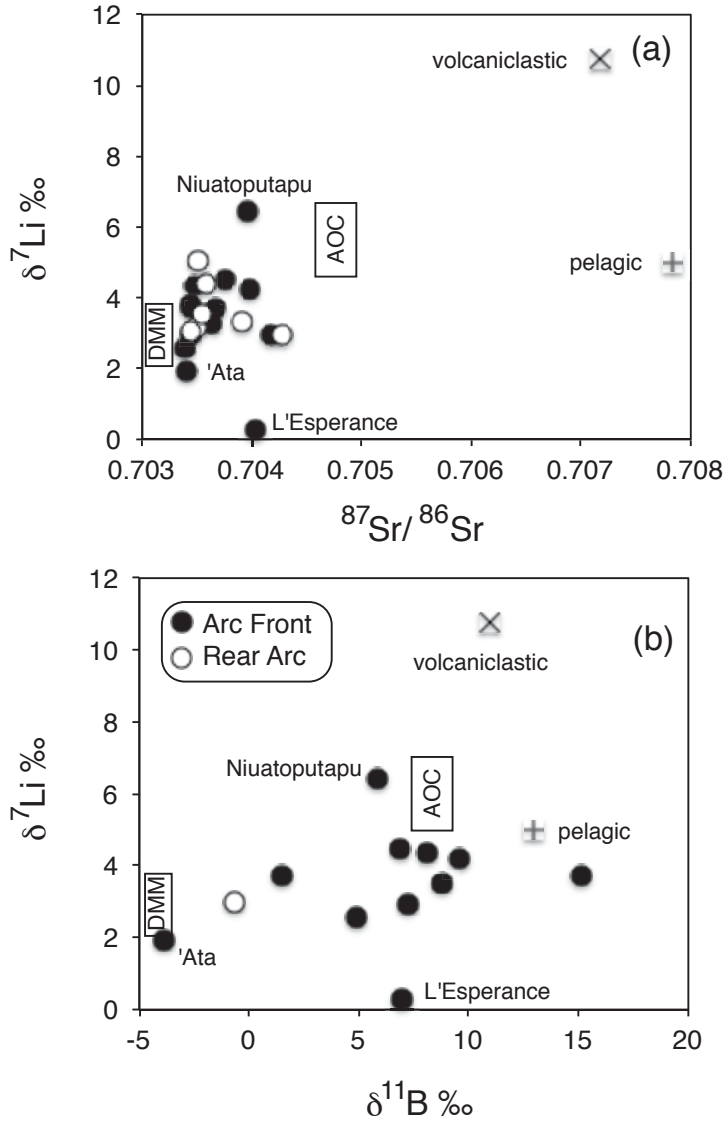

Fig. 5. Plots of δ^7Li versus (a) ^{87}Sr/^{86}Sr and (b) δ^{11}B. Boron data from Leeman et al. (2017), other symbols and data sources as for Fig. 4.

5.3. Quantification of sediment mixing

As an end-member model, we assessed the likelihood that all of the δ^7Li – Y/Li variation reflects bulk sediment addition on Fig. 6. This shows the results of a Monte Carlo simulation involving bulk sediment addition to a depleted mantle wedge allowing the full range of sediment compositions from Table 2 to be involved. Given the range in δ^7Li in the local sediments, it is an unsurprising outcome that the resultant envelope of solutions encompasses the full variation observed in the lavas (see Fig. 6). However, the

implied amounts of sediment addition required (1-3%) exceed, by almost an order of magnitude, those estimated (0.1-0.5%) on the basis of Th-Nd-Be isotopes (Turner et al., 1997; George et al., 2005). This is best explained by the enrichment of Li (Brenan et al., 1998) where the implication that fluid addition of Li must have played a significant role in controlling the Li isotope variations. Though we accept that three-component models will necessarily be non-unique, Leeman et al. (2017) have recently argued that, because the Tonga slab lies at the cold end of the global thermal structure spectrum (Syracuse et al. 2010), fluid addition (from both sediments and AOC) may be the principal means of slab-derived elemental transport beneath this arc. Certainly, the relationships on Figs. 4 and 5 are consistent with such models from the Li isotope perspective. Further development of this will require better knowledge of when and at what temperatures fluids are driven off the sediments and AOC in the Tonga slab.

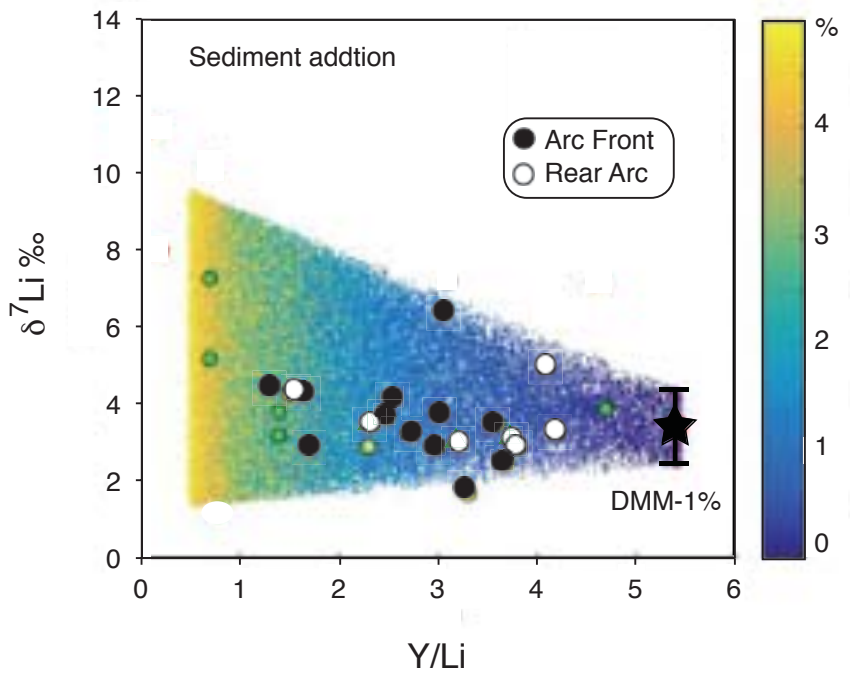

Fig. 6. Plot of δ^7Li versus Y/Li to appraise the ability of addition of bulk sediment addition to a depleted mantle source (DMM-1%) explain the range of δ^7Li in the Tonga-Kermadec-Lau lavas. The gradation of coloured dots in the background represent random mixing results using a Monte Carlo simulation, the bar to the right of each panel represents the amount of sediment (%) required to attain that value in the simulation (small coloured circles are sediment analysed that fall within the Monte Carlo envelope). The DMM-1%

source has Li = 0.7 ppm, Y = 4.1 ppm and δ^7Li = +3.4 ‰. See text for discussion.

6. CONCLUSIONS

We have undertaken a reconnaissance study of Li isotopes in the oceanic Tonga-Kermadec arc and Lau back-arc as well as the sediment profile at DSDP Site 204. Like many arc lavas, the range in δ^7Li appears to have been muted by diffusive equilibration with ambient mantle. Nevertheless, lava from Niuatoputapu Island appears to carry a signature from the subducting Louisville volcaniclastic sediments. Lavas from ‘Ata and L’Esperance Islands have unusually low δ^7Li of unknown origin. For the remaining arc front and back-arc lavas, δ^7Li = 3.6 ± 0.7 ‰. Modelled δ^7Li – Y/Li relationships require 1-3% bulk sediment addition to explain the range in observed ratios. This is an order of magnitude higher than required by Th-Nd-Be isotope systematics suggesting an important role for fluid addition of Li from both the subducting sediments and altered oceanic crust beneath this arc – back-arc system.

REFERENCES

Acland S. (1996) Magma genesis in the northern Lau Basin, S.W. Pacific. Ph.D. dissertation. University of Durham.

Bevis, M., Taylor, F.W., Schutz, B.E., Recy, J. and Isacks, B.L., Helu, S., Singh, R., Kendrick, E., Stowell, J. (1995) Geodetic observations of very rapid convergence and back-arc extension at the Tonga arc. *Nature* **374**, 249-251.

Billen, M. I. and Stock, J. (2000) Morphology and origin of the Osbourn Trough. *Journal of Geophysics Research* **105**, 13481-13489.

Bloomer, S.H. and Fisher, R.L. (1986) Petrology and geochemistry of igneous rocks from the Tonga trench – A non-accreting plate boundary. *Journal of Geology* **95**, 469-495.

Bouman, C., Elliott, T. and Vroon, P.Z. (2004) Lithium inputs to subduction zones. *Chemical Geology* **212**, 59-79.

Brant, C., Coogan, L.A., Gillis, K.M., Seyfried, W.E., Pester, N.J. and Spence, J. (2012) Lithium and Li-isotopes in young altered upper oceanic crust from the East Pacific Rise. *Geochimica et Cosmochimica Acta* **96**, 272-293.

Brenan, J.M., Ryerson, F.J. and Shaw, H.F. (1998) The role of aqueous fluids in the slab-to-mantle transfer of boron, beryllium, and lithium during subduction; experiments and models. *Geochimica et Cosmochimica Acta* **62**, 19-20, 3337-3347.

Burns, R. E., Andrews, J. E., van der Lingen, G. J., Churkin, M., Jr., Galehouse, J. S., Packham, G., Davies, T. A., Kennett, J. P., Dumitrica, P., Edwards, A. R. and Von Herzen, R. P. (1973) Site 204. *Initial Reports of the Deep Sea Drilling Project* **21**, 33-56.

Caulfield, J., Turner, S., Arculus, R., Dale, C., Jenner, F., Pearce, J., Macpherson, C. and Handley, H. (2012) Mantle flow, volatiles, slab‐surface temperatures and melting dynamics in the north Tonga arc–Lau back‐arc basin. *Journal of Geophysical Research: Solid Earth*, **117** (B11).

Chan, L.H. and Frey, F.A. (2003) Lithium isotope geochemistry of the Hawaiian plume: results from the Hawaii Scientific Drilling Project and Koolau Volcano, *Geochemistry, Geophysics, Geosystems - G3*, **4**, 8707.

Chan, L.H., Edmond, J.M., Thompson, G. and Gillis, K. (1992) Lithium isotopic composition of submarine basalts; implications for the lithium cycle in the oceans. *Earth and Planetary Science Letters* **108**, 1-3, 151-160.

Chan, L.H., Leeman, W.P. and You, C.F. (2002) Lithium isotopic composition of Central American Volcanic Arc lavas: Implications for modification of the subarc mantle by slab-derived fluids: Correction. *Chemical Geology* **182**, 293-300.

Chan, L.H., Leeman, W.P. and Plank, T. (2006) Lithium isotopic composition of marine sediments. *Geochemistry, Geophysics, Geosystems*, **7**, *Q06005*.

Elliott, T., Jeffcoate, A. and Bouman, C. (2004). The terrestrial Li isotope cycle: light-weight constraints on mantle convection. *Earth and Planetary Science Letters* **220**, 231–245.

Elliott, T., Thomas, A., Jeffcoate, A. and Niu, Y. (2006). Lithium isotope evidence for subduction-enriched mantle in the sources of mid-ocean ridge basalts. *Nature* **443**, 565-568.

Ewart, A. and Hawkesworth, C.J. (1987) The Pleistocene-Recent Tongan-Kermadec arc lavas: interpretation of new isotope and rare earth data in terms of a depleted mantle source model. *Journal of Petrology* **28**, 295-330.

Ewart, A., Collerson, K.D., Regelous, M., Wendt, J.I. and Niu, Y. (1998) Geochemical evolution within the Tonga-Kermadec-Lau arc-back-arc systems; the role of

varying mantle wedge composition in space and time. *Journal of Petrology* **39**, 3, 331-368.

Flesch, G., Anderson, A.R. and Svec, H.J. (1973) A secondary isotopic standard for $^{6}Li/^{7}Li$ determinations. *International Journal of Mass Spectrometry and Ion Physics* **12**, 265-272.

Gao, Y., Vils, F., Cooper, K. M., Banerjee, N., Harris, M., Hoefs, J., Teagle, D. A. H., Casey, J. F., Elliott, T., Laverne, C., Alt, J. C. and Muechlenbachs (2012). Downhole variation of lithium and oxygen isotopic compositions of oceanic crust at East Pacific Rise, ODP Site 1256. *G Geochemistry, Geophysics, Geosystems*, **13**, Q10001.

George, R., Turner, S., Morris, J., Plank, T., Hawkesworth, C.J. and Ryan, J. (2005) Pressure-temperature-time paths of sediment recycling beneath the Tonga-Kermadec arc. *Earth and Planetary Science Letters* **233**, 1-2, 195-211.

Gladney, E.S. and Goode, W.E. (1981) Elemental concentrations in eight new United States Geological Survey rock standard: a review. *Geostandards Newsletter* **5**, 31-64.

Govindaraju, K. (1994) Compilation of working values and sample descriptions for 383 geostandards. *Geostandards Newsletter* **5**, 31-64.

Hawkins, J.W. (1995) *The geology of the Lau Basin. In Backarc Basins: Tectonics and Magmatism*, p. 63-138, edited by Brian Taylor, Plenum Press, New York

Isacks, B.L. and Barazangi, M. (1977) Geometry of Benioff zones: Lateral segmentation and downwards bending of the subducted lithosphere. In: *Island Arcs Deep Sea Trenches and Back-Arc Basins* Maurice Ewing Ser. **1**, 99-114.

James, R.H., and Palmer, M.R. (2000) The Li isotope composition of international rock standards. *Chemical Geology* **166**, 319-326.

Keller, N.S., Arculus, R.J., Hermann, J. and Richards, S. (2008) Submarine back-arc lava with arc signature: Fonualei Spreading Center, northeast Lau Basin, Tonga. *Journal of Geophysical Research: solid earth*, **113**, 1-28.

Kelley, K.A., Plank, T., Ludden, J. and Staudigel, H. (2003). Composition of altered oceanic crust at ODP Sites 801 and 1149. *Geochemistry, Geophysics, Geosystems, **4**, 8910.*

Langmuir, C.H., Bézos, A., Escrig, S. and Parman, S.W. (2013) Chemical Systematics and Hydrous Melting of the Mantle in Back-Arc Basins, in *Back-Arc Spreading Systems: Geological, Biological, Chemical, and Physical Interactions* (eds D. M. Christie, C. R. Fisher, S.-M. Lee and S. Givens), American Geophysical Union, Washington, D. C.

Leeman, W. P., Tonarini, S. and Turner, S. (2017) Boron isotope variations in Tonga-Kermadec-New Zealand arc lavas: implications for origin of subduction components and mantle influences. *Geochem. Geophys. Geosys.* **18**, doi:10.1002/2016GC006523.

Liu, X.M., Rudnick, R.L. (2011) Constraints on continental crustal mass loss via chemical weathering using lithium and its isotopes. *Proceedings of the National Academy of Sciences of the United States of America* **108**, 20873-20880.

Liu, X.M., Rudnick, R.L., Hier-Majumder, S. and Sirbescu, M.C. (2010) Processes controlling lithium isotopic distribution in contact aureoles; a case study of the Florence County pegmatites, Wisconsin. *Geochemistry, Geophysics, Geosystems - G3*, **11**, Q08014.

Liu, X.M., Rudnick, R.L., McDonough, W.F. and Cummings, M.L. (2013) Influence of chemical weathering on the composition of the continental crust; insights from Li and Nd isotopes in bauxite profiles developed on Columbia River basalts. *Geochimica et Cosmochimica Acta* **115**, 73-91.

Liu, X.M., Wanner, C., Rudnick, R.L. and McDonough, W.F. (2015) Processes controlling δ^7Li in rivers illuminated by study of streams and groundwaters draining basalts. *Earth and Planetary Science Letters* **409**, 212-224.

Moriguti, T. and Nakamura, E. (1998) Across-arc variation of Li isotopes in lavas and implications for crust/mantle recycling at subduction zones. *Earth and Planetary Science Letters* **163**, 167-174.

Nesbitt, H.W. and Young, G.M. (1982) Early Proterozoic climates and plate motions inferred from the major element chemistry of lutites. *Nature* **299**, 715-717.

Pearce, J.A. and Stern, R.J. (2006) Origin of back-arc basin magmas; trace element and isotope perspectives. *Geophysical Monograph* **166**, 63-86.

Pearce, J.A., Ernewein, M., Bloomer, S. H., Parson, L. M., Murton, B. J. and Johnson, L.E. (1995) Geochemistry of Lau Basin volcanic rocks: Influence of ridge segmentation and arc proximity, in *Volcanism Associated With Extension at Consuming Plate Margins*, edited by J. L. Smellie, *Geological Society, London, Special Publications* **81**, 53-75.

Penniston-Dorland, S.C., Bebout, G.E., Pogge von Strandmann, P.A., Elliott, T. and Sorensen, S.S. (2012) Lithium and its isotopes as tracers of subduction zone fluids and metasomatic processes: Evidence from the Catalina Schist, California, USA. *Geochimica et Cosmochimica Acta* **77**, 530-545.

Plank, T. and Langmuir, C.H. (1998) The chemical composition of subducting sediment and its consequences for the crust and mantle. *Chemical Geology* **145**, 325-394.

Regelous, M., Collerson, K.D., Ewart, A. and Wendt, J.I. (1997) Trace element transport rates in subduction zones; evidence from Th, Sr and Pb isotope data for Tonga-Kermadec Arc lavas. *Earth and Planetary Science Letters* **150**, 3-4, 291-302.

Regelous, M., Gamble, J.A. and Turner, S.P. (2010) Mechanism and timing of Pb transport from subducted oceanic crust and sediment to the mantle source of arc lavas. *Chemical Geology* **273**, 46-54.

Rudnick, R.L., Tomascak, P.B., Heather, B.N. and Gardner, L.R. (2004) Extreme lithium isotopic fractionation during continental weathering revealed in saprolites from South Carolina. *Chemical Geology* **212**, 45-57.

Ryan, J.G. and Langmuir, C.H. (1987) The systematics of lithium abundance in young volcanic rocks. *Geochimica et Cosmochimica Acta* **51**, 1727-1741.

Salters, V. J. M. and Stracke, A. (2004). Composition of the depleted mantle. *Geochemistry, Geophysics, Geosystems*, **5**, doi:10.1029/2003GC000597.

Stoffers, P., Worthington, T.J., Schwarz-Schampera, U., Hannington, M.D., Massoth, G.J., Hekinian, R., Schmidt, M., Lundsten, L.J., Evans, L.J., Vaiomo'unga, R. and Kerby, T. (2006) Submarine volcanoes and high-temperature hydrothermal venting on the Tonga arc, southwest Pacific. *Geology* **34**, 453–456.

Sutherland, R. and Hollis, C. (2001) Cretaceous demise of the Moa plate and strike-slip motion at the Gondwana margin. *Geology* **29**, 279-282.

Syracuse, E. M., van Keken, P. E. and Abers, G. A. (2010) The global range of subduction zone thermal models. *Phys. Earth Planet. Int.* **183**, 73-90.

Tang, M., Rudnick, R.L., Chauvel, C. (2014) Sedimentary input to the source of Lesser Antilles lavas: A Li perspective. *Geochimica et Cosmochimica Acta* 144, 43-58.

Teng, F.Z., McDonough, W.F., Rudnick. R.L., Walker, R.J.and Sirbescu, M.L.C. (2006) Lithium isotopic systematics of granites and pegmatites from the Black Hills, South Dakota. *American Mineralogist* **91**, 1488-1498.

Tian, S.H., Hou, Z.Q., Su, A.N., Hou, K.J., Hu, W.J., Li, Z.Z., Zhao, Y., Gao, Y.G., Li, Y.H., Yang, D., and Yang, Z.S. (2012) Separation and Precise Measurement of Lithium Isotopes in Three Reference Materials Using Multi Collector-Inductively Coupled Plasma Mass Spectrometry. *Acta Geologica Sinica* **86**, 1297-1305.

Tomascak, P.B., Ryan, J.G. and Defant, M.J. (2000) Lithium isotope evidence for light element decoupling in the Panama subarc mantle. *Geology* **28**, 507-510.

Tomascak, P.B., Widom, E., Benton, L.D., Goldstein, S.L. and Ryan, J.G. (2002) The control of lithium budgets in island arcs. *Earth and Planetary Science Letters* **196**, 227-238.

Turner, S., Hawkesworth, C., Rogers, N., Bartlett, J., Worthington, T., Hergt, J., Pearce, J. and Smith, I. (1997) ^{238}U- ^{230}Th disequilibria, magma petrogenesis, and flux rates beneath the depleted Tonga-Kermadec island arc, *Geochimica et Cosmochimica Acta* **61**, 4855-4884.

Turner, S., Bourdon, B., Hawkesworth, C., Evans, P. (2000) ^{226}Ra-^{230}Th evidence for multiple dehydration events, rapid melt ascent and the time scales of differentiation beneath the Tonga-Kermadec island arc. Earth and Planetary Science Letters **179**, 581-593.

Turner, S., Handler, M., Bindeman, I. and Suzuki, K. (2009) New insights into the origin of O-Hf-Os isotope signatures in arc lavas from Tonga-Kermadec. *Chemical Geology* **266**, 196-202.

Wendt, J.I., Regelous, M., Collerson, K.D., and Ewart, A. (1997) Evidence for a contribution from two mantle plumes to island-arc lavas from northern Tonga. *Geology*, ***25***, 611-614.

Wright, I.C., Worthington, T.J. and Gamble, J.A. (2006) New multibeam mapping and geochemistry of the 30–35 S sector, and overview, of southern Kermadec arc volcanism. *Journal of Volcanology and Geothermal Research* **149**, 263-296.

You, C.F., Castillo, P.R., Gieskes, J.M., Chan, L.H. and Spivac A.J. (1996) Trace element behavior in hydrothermal experiments: Implications for fluid processes at shallow depths in subduction zones. *Earth and Planetary Science Letters* **140**, 41-52.

C. Supporting Information for Lau and North Fiji Basins

Introduction

In Figure S1 we show a silica versus total alkali plot, with subdivisions for different rock classifications based on Le Bas et al. (1986), that includes the new Rotuman and Fijian lavas in this study. In Figure S2 we show primitive mantle-normalized trace element patterns for the Fijian and Rotuman lavas in this study.

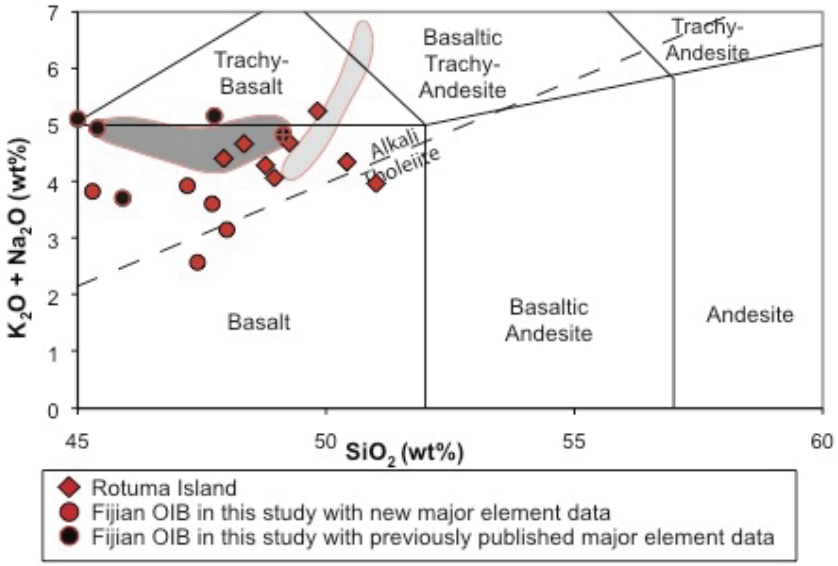

Figure S1. Silica versus total alkali plot, with subdivisions for different rock classifications based on Le Bas et al. (1986). The alkali-tholeiite line is from Macdonald and Katsura (1964). Previous published major element data for Fijian OIB looked at in this study are from Gill and Whelan (1989) and Pearce et al. (2007). The one Fijian lava with a + represents the Type II lava (WQ7b), while all other Fijian lavas are Type I (see section 3.3.7 of the paper for more information). The dark grey field represents previously published Fijian OIB major element data for lavas not studied here and are from Gill (1984). The light grey field represents previously published Rotuma major

element data for lavas not studied here and are from Price et al. (1990).

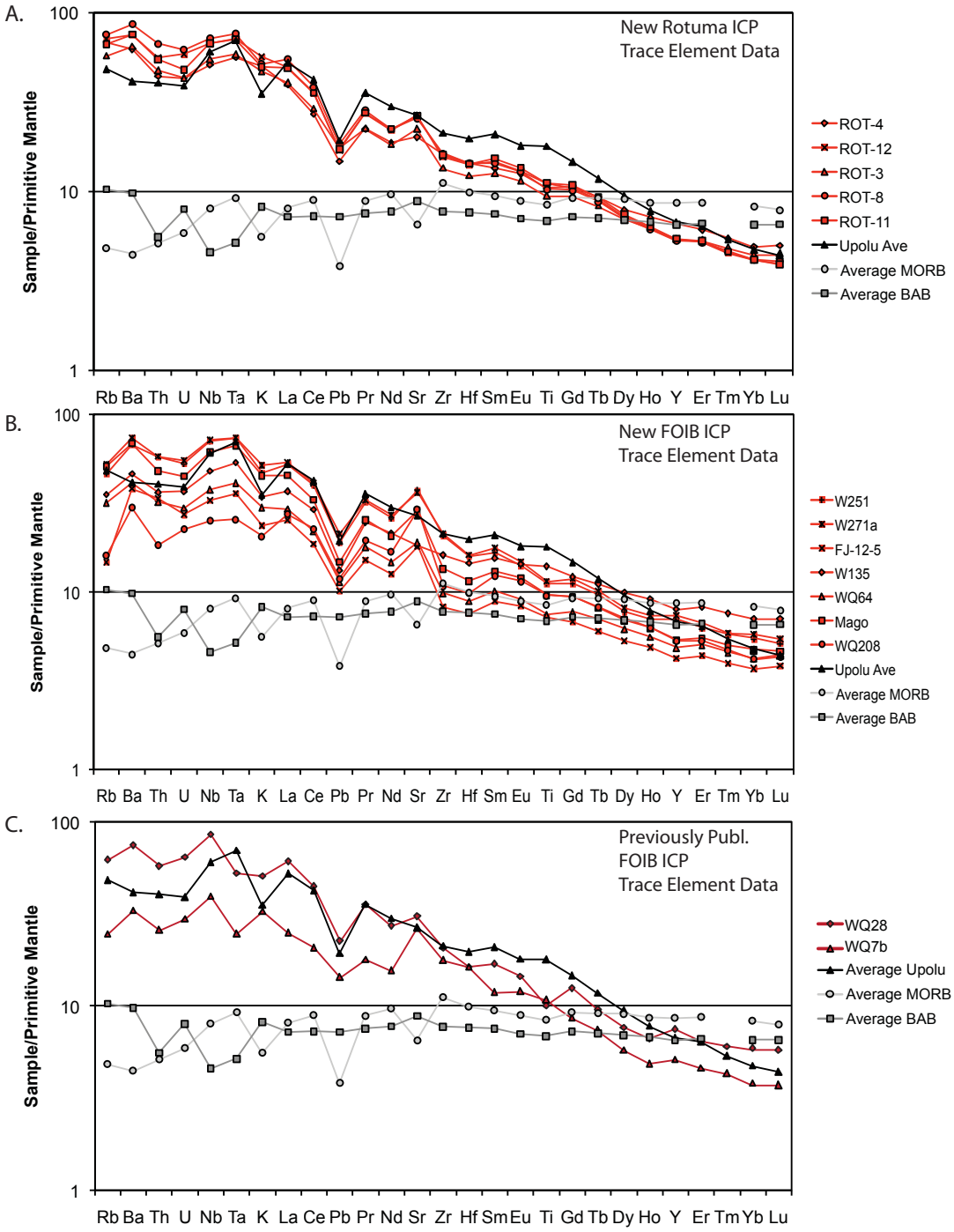

Figure S2. Primitive mantle-normalized trace element patterns for the lavas examined in this and previous studies. Panel A shows new data from Rotuma Island lavas, panel B shows new data from young Fijian lavas, and panel C shows lavas previously published

young (FOIB) Fijian lavas (Pearce et al (2007)). Average Upolu, which was calculated from Upolu shield data with MgO > 6.5 wt. %, is shown on all plots in black. All plots also show average MORB (mid-ocean ridge basalt) and average BABB (backarc basin basalt) from Gale et al. (2013) and are plotted as light and dark grey, respectively. The primitive mantle composition is from McDonough and Sun (1995).

References

Carpentier, M., Weis, D., & Chauvel, C. (2013) Large U loss during weathering of upper continental crust: The sedimentary record. *Chemical Geology*, *340*, 91-104.

Chauvel, C., Maury, R. C., Blais, S., Lewin, E., Guillou, H., Guille, G., & Gutscher, M. A. (2012). The size of plume heterogeneities constrained by Marquesas isotopic stripes. *Geochemistry, Geophysics, Geosystems*, *13*(7).

Gale, A., Dalton, C. A., Langmuir, C. H., Su, Y., & Schilling, J. G. (2013) The mean composition of ocean ridge basalts. *Geochemistry, Geophysics, Geosystems*, *14*(3), 489-518.

Gill JB (1984) Sr-Pb-Nd isotopic evidence that both MORB and OIB sources contribute to ocean island arc magmas in Fiji. Earth and Planetary Science Letters 68:443–458.

Gill, J., & Whelan, P. (1989) Postsubduction ocean island alkali basalts in Fiji. *Journal of Geophysical Research: Solid Earth*, *94*(B4), 4579-4588.

Le Bas, M. J., Le Maitre, R. W., Streckeisen, A., & Zanettin, B. (1986) A chemical classification of volcanic rocks based on the total alkali-silica diagram. *Journal of petrology*, *27*(3), 745-750.

MacDonald, G. A., & Katsura, T. (1964) Chemical composition of Hawaiian lavas1. *Journal of petrology*, *5*(1), 82-133.

Marx, S. K., & Kamber, B. S. (2010). Trace-element systematics of sediments in the Murray–Darling Basin, Australia: Sediment provenance and palaeoclimate implications of fine scale chemical heterogeneity. *Applied Geochemistry*, *25*(8), 1221-1237.

McDonough, W. F., & Sun, S. S. (1995) The composition of the Earth.*Chemical geology*, *120*(3), 223-253.

Pearce JA, Kempton PD, Gill JB (2007) Hf-Nd evidence for the origin and distribution of mantle domains in the SW Pacific. Earth and Planetary Science Letters 260:98–114.

Price, R. C., Johnson, L. E., & Crawford, A. J. (1990) Basalts of the North Fiji Basin: the generation of back arc basin magmas by mixing of depleted and enriched mantle sources. *Contributions to Mineralogy and Petrology*, *105*(1), 106-121.

Raczek, I., Stoll, B., Hofmann, A. W., & Peter Jochum, K. (2001) High-Precision Trace Element Data for the USGS Reference Materials BCR-1, BCR-2, BHVO-1, BHVO-2, AGV-1, AGV-2, DTS-1, DTS-2, GSP-1 and GSP-2 by ID-TIMS and MIC-SSMS. *Geostandards Newsletter*, *25*(1), 77-86.

Tollstrup, D., Gill, J., Kent, A., Prinkey, D., Williams, R., Tamura, Y., & Ishizuka, O. (2010). Across-arc geochemical trends in the Izu-Bonin arc: Contributions from the subducting slab, revisited. *Geochemistry, Geophysics, Geosystems*, *11*(1).

Supporting Information Dataset S2 . Trace element analyses of lavas examined in this study; trace element data shown here are only for lavas that are characterized for radiogenic isotopic compositions in this study.

Method	V (ppm)	Ba (ppm)	Sr (ppm)	Zr (ppm)	Y (ppm)	Ga (ppm)	Cu (ppm)	Zn (ppm)	Cs (ppm)	Rb (ppm)	Ba (ppm)	Th (ppm)	U (ppm)	Nb (ppm)	Ta (ppm)	La (ppm)	Ce (ppm)
Sample Name	XRF	XRF	XRF	XRF	XRF	XRF	XRF	XRF	ICP	ICP	ICP	ICP	ICP	ICP	ICP	ICP	ICP
ROT-4	232	440	412	178	28.4	20.9	59	89	0.46	45.0	433	3.90	0.90	34.47	2.20	27.24	47.93
ROT-12	231	550	555	182	23.6	20.7	43	83	0.75	46.3	534	4.75	1.24	46.82	2.85	33.26	61.47
ROT-13	237	526	449	188	23.8	18.9	45	71									
ROT-3	230	455	471	158	22.4	19.5	51	67	0.38	36.9	461	4.14	0.89	39.16	2.39	28.03	51.19
ROT-15	220	479	438	162	23.7	16.8	49	72									
ROT-6	213	674	482	224	24.9	20.9	38	83									
ROT-8	233	585	534	189	22.5	18.6	47	83	0.74	46.2	598	5.73	1.27	49.91	3.05	37.37	67.18
ROT-11	240	496	510	174	21.1	20.5	44	79	0.66	41.9	530	4.64	0.98	46.20	2.79	32.83	60.82
FJ-12-3	221	277	519	134	24.6	16.8	63	79									
FJ-12-5	229	303	421	108	21.3	14.5	79	71	0.07	9.8	301	2.58	0.58	26.06	1.64	19.62	37.66
W135 [2]	367	319	376	184	34.0	20.4	56	95	0.13	22.5	320	3.15	0.73	33.47	2.16	24.93	50.78
WQ64	240	295	404	111	21.9	16.2	82	70	0.19	19.8	297	2.73	0.61	27.38	1.73	20.64	39.67
WQ7b [3]	212	217	523	185	21.9	21.9	33	92		14.7	217	2.05	0.60	25.87	0.91	4.5	19.4
Mago	217	461	583	153	22.6	14.7	63	65	0.20	31.9	478	4.15	0.93	43.67	2.73	31.77	59.62
WQ208 [2]	252	214	596	131	23.1	19.0	78	97	0.09	10.2	211	1.62	0.47	17.39	1.04	19.19	41.08
W251 [4]	238	453	783	230	27.5	17.1	64	83		27.7	444	4.57	1.06	46.33	2.72	8.1	32.3
WQ28 [3]	216	492	609	217	32.2		96	97		37.2	492	4.56	1.30	56.04	1.94	9.0	34.0
WQ271a [4]	222	461	693	227	25.6	18.5	50	77		31.1	485	4.58	1.11	46.80	2.73	8.3	33.6
Reference Material Comparisons: [5]																	
BCR-2 (new from this study)									1.13	45.8	678	6.23	1.60	11.47	0.77	25.52	53.18
BCR-2 (new from this study)	413	675	340	186	35.3	22.6	21	133									
Marx and Kamber, 2010 BCR-2	*420*	*680*	*340*	*185*	*33.7*	*21.9*	*19*	*135*	*1.15*	*47.0*	*680*	*5.80*	*1.69*	*12.40*	*0.77*	*25.1*	*53.0*
Carpentier et al., 2013 BCR-2	*440*	*660*	*374*	*188*	*37.0*		*17*	*134*	*1.16*	*46.0*	*660*	*5.90*	*1.63*	*12.50*	*0.79*	*25.0*	*52.0*
AGV-2 (new from this study)	120	1129	675	252	19.2	20.1	53	91									
Marx and Kamber, 2010 AGV-2	*116*	*1150*	*660*	*231*	*18.3*	*20.4*	*50*	*89*									
Carpentier et al., 2013 AGV-2	*115*	*1140*	*650*	*240*	*19.6*		*51*	*100*									

cont'd	Pb (ppm) ICP	Pr (ppm) ICP	Nd (ppm) ICP	Sr (ppm) ICP	Zr (ppm) ICP	Hf (ppm) ICP	Sm (ppm) ICP	Eu (ppm) ICP	Gd (ppm) ICP	Tb (ppm) ICP	Dy (ppm) ICP	Ho (ppm) ICP	Y (ppm) ICP	Er (ppm) ICP	Tm (ppm) ICP	Yb (ppm) ICP	Lu (ppm) ICP	Sc (ppm) ICP
ROT-4	2.03	5.96	24.57	407	175	3.99	5.81	1.98	5.94	0.96	5.56	1.10	29.37	2.81	0.38	2.32	0.35	23.7
ROT-12	2.54	7.16	28.21	545	174	3.97	6.30	2.09	5.98	0.92	5.10	0.96	23.63	2.35	0.32	1.91	0.28	22.4
ROT-13																		
ROT-3	2.02	5.92	23.39	465	152	3.56	5.25	1.80	5.31	0.85	4.94	0.96	23.79	2.44	0.34	2.11	0.31	29.1
ROT-15																		
ROT-6																		
ROT-8	2.64	7.56	28.75	517	183	4.12	6.11	2.02	5.67	0.87	4.93	0.93	23.11	2.30	0.31	1.88	0.29	26.3
ROT-11	2.46	7.04	27.64	537	174	3.94	6.21	2.05	5.86	0.90	5.11	0.94	23.47	2.37	0.31	1.89	0.28	23.2
FJ-12-3																		
FJ-12-5	1.40	4.61	18.65	413	107	2.48	4.24	1.49	4.34	0.71	4.25	0.85	21.52	2.24	0.32	2.00	0.31	34.6
W135[2]	1.94	6.56	27.96	375	185	4.32	6.85	2.32	7.02	1.16	7.10	1.43	35.95	3.77	0.54	3.35	0.52	32.2
WQ64	1.54	4.84	19.53	403	112	2.57	4.46	1.54	4.56	0.74	4.52	0.90	22.36	2.36	0.33	2.08	0.32	35.3
WQ7b[3]	2.14	4.51	19.4	523	185	4.57	4.80	1.84	4.67	0.73	3.86	0.72	21.9	2.00	0.29	1.67	0.25	24.1
Mago	1.96	7.01	27.45	596	152	3.33	5.87	1.95	5.38	0.85	5.06	0.99	24.57	2.57	0.36	2.24	0.35	28.5
WQ208[2]	1.69	5.30	22.50	611	123	2.95	5.39	1.85	5.42	0.87	5.10	0.97	24.30	2.44	0.34	2.04	0.30	30.2
W251[4]	2.84	8.14	32.3	740	217	4.46	6.73	2.16	6.04	0.95	5.18	1.03	29.8	2.73	0.39	2.40	0.35	28.3
WQ28[3]	3.38	9.00	34.0	609	217	4.59	6.87	2.22	6.79	0.95	5.15	0.99	32.2	2.81	0.41	2.60	0.39	29.7
WQ271a[4]	3.16	8.29	33.6	718	222	4.54	7.15	2.27	6.43	0.99	5.44	1.09	31.6	2.90	0.40	2.53	0.37	27.2
Reference Material Comparisons:[5]																		
BCR-2 (new from this study)	10.07	6.87	28.72	337	188	4.83	6.93	2.10	7.01	1.15	7.03	1.42	35.86	3.75	0.54	3.37	0.52	33.1
BCR-2 (new from this study)																		
Marx and Kamber, 2010 BCR-2	*9.70*	*6.90*	*28.7*	*350*	*185*	*4.85*	*6.60*	*1.96*	*6.80*	*1.06*	*6.40*	*1.33*	*33.7*	*3.65*	*0.540*	*3.40*	*0.50*	*34.0*
Carpentier et al., 2013 BCR-2	*10.24*	*6.70*	*28.5*	*340*	*188*	*4.90*	*6.50*	*1.92*	*6.70*	*1.05*	*6.31*	*1.30*	*37.0*	*3.70*		*3.39*	*0.49*	*34.9*
AGV-2 (new from this study)																		
Marx and Kamber, 2010 AGV-2																		
Carpentier et al., 2013 AGV-2																		

[1] Major elements and V, Ba, Sr, Zr, Y, Ga, Cu, and Zn were measured by XRF. A subset of these trace elements, and a suite of additional trace elements, were measured by ICP-MS.

[2] New ICP and XRF data are presented here. Previously published XRF trace element data are available on a subset of these elements in Gill and Whelan [1989], and we present new

[3] These ICP and XRF trace element data were published previously in Pearce et al. [2007]; these elemental concentration analyses were made on a different aliquot of powder (obtained from a different portion of the same whole rock) than the aliquot of powder used to obtain the isotopic data reported in Table 1.

[4] New ICP trace element data were measured at UCSC following the methods of Tollstrup et al. [2010]. These trace element analyses were made on a different aliquot of powder (obtained from a different portion of the same whole rock) than the aliquot of powder used for the XRF (this table) and the isotopic analyses (Table 1) reported here.

[5] USGS reference material BCR-2 was run together with the samples as an unknown. This analysis is reported together with trace element compositions for BCR-2 reported in Marx and Kamber [2010], Carpentier et al. [2013], and Chauvel et al. [2012].

Supplementary Information Data Set S3. Parameters for Mixing Models shown in Supplementary Information Figure S3

	Pb (ppm)	Sr (ppm)	Nd (ppm)	Hf (ppm)	$^{206}Pb/^{204}Pb$	$^{207}Pb/^{204}Pb$	$^{208}Pb/^{204}Pb$	$^{87}Sr/^{86}Sr$	$^{143}Nd/^{144}Nd$	$^{176}Hf/^{177}Hf$
Lau and N. Fiji Basin Depleted End-Member #1:										
Sample 162-1 from Yasawa-Yadua Volcanic Zone	0.14	60	3.2	0.9	18.269	15.490	38.094	0.702892	0.513218	0.283510
data sources	*Price et al. [2014]*	*Price et al. [2014]*	*Price et al. [2014]*	*Price et al. [2014]*	*Price et al. [2014]*	*Price et al. [2014]*	*Price et al. [2014]*	*Price et al. [2014]*	*Price et al. [2014]*	*Price et al. [2014]*
Lau and N. Fiji Basin Depleted End-Member #2:										
Sample ST14-DT7-2 from the North Fiji Basin,N-S Segment	0.35	78	7.0	1.8	18.045	15.499	37.807	0.702890	0.513111	0.283218
data sources	*Peate et al. [1997]*	*Peate et al. [1997]*	*Peate et al. [1997]*	*Peate et al. [1997]*	*Peate et al. [1997]*	*Peate et al. [1997]*	*Peate et al. [1997]*	*Nohara et al. [1994]*	*Nohara et al. [1994]*	*Pearce et al. [2007]*
Lau and N. Fiji Basin Depleted End-Member #3:										
Sample ST15-11-1 from the North Fiji Basin,N-S Segment	0.46	117	11.2	2.7	18.043	15.462	37.696	0.703090	0.513011	0.283186
data sources	*Peate et al. [1997]*	*Peate et al. [1997]*	*Peate et al. [1997]*	*Peate et al. [1997]*	*Peate et al. [1997]*	*Peate et al. [1997]*	*Peate et al. [1997]*	*Nohara et al. [1994]*	*Nohara et al. [1994]*	Pearce et al. [2007]
Lau and N. Fiji Basin Depleted End-Member #4:										
Sample ST53 9-1-7 from the North Fiji Basin, N160 Segment	1.17	243	12.0	2.0	18.389	15.522	38.223	0.703350	0.512903	0.283139
data sources	*Peate et al. [1997]*	*Peate et al. [1997]*	*Peate et al. [1997]*	*Peate et al. [1997]*	*Peate et al. [1997]*	*Peate et al. [1997]*	*Peate et al. [1997]*	*Nohara et al. [1994]*	*Nohara et al. [1994]*	*Pearce et al. [2007]*
Samoa End-Member #1 (Samoan EM2 component):										
Sample ALIA-D115-18 from Savai'I Island, Shield Series	11.3	511	55.9	8.9	18.957	15.643	39.399	0.718592	0.512314	0.282635
data sources	*Jackson et al. [2007a]*	*Jackson et al. [2007a]*	*Jackson et al. [2007a]*	*Jackson et al. [2007a]*	*Jackson et al. [2007a]*	*Jackson et al. [2007a]*	*Jackson et al. [2007a]*	*Jackson et al. [2007a]*	*Jackson et al. [2007a]*	*Salters et al. [2011]*
Samoa End-Member #2 (Samoan EM1 component):										
Sample Sample U35M from Upolu Island, Rejuvenated Series	2.75	524	37.8	6.0	18.681	15.606	38.883	0.705631	0.512668	0.282929
data sources	*Workman et al. [2004]*	*Workman et al. [2004]*	*Workman et al. [2004]*	*Workman et al. [2004]*	*Workman et al. [2004]*	*Workman et al. [2004]*	*Workman et al. [2004]*	*Workman et al. [2004]*	*Workman et al. [2004]*	*Pfänder et al. [2007]*
Samoa End-Member #3 (Samoan HIMU component):										
Sample AVON3-70-9 from Vailulu'u Seamount	2.64	430	32.4	5.2	19.396	15.633	39.719	0.705352	0.512753	0.282925
data sources	*Workman et al. [2004]*	*Workman et al. [2004]*	*Workman et al. [2004]*	*Workman et al. [2004]*	*Workman et al. [2004]*	*Workman et al. [2004]*	*Workman et al. [2004]*	*Workman et al. [2004]*	*Workman et al. [2004]*	*Salters et al. [2011]*
Samoa End-Member #4 (Samoan High $^{3}He/^{4}He$ component):										
Sample OFU-04-06 from Ofu Island	2.60	599	44.1	7.6	19.189	15.571	39.202	0.704584	0.512827	0.282980
data sources	*Jackson et al. [2008]*	*Jackson et al. [2008]*	*Jackson et al. [2008]*	*Jackson et al. [2008]*	*Jackson et al. [2007a]*	*Jackson et al. [2007a]*	*Jackson et al. [2007a]*	*Jackson et al. [2007a]*	*Jackson et al. [2007a]*	*Salters et al. [2011]*
Samoa End-Member #5 (Samoan Depleted Mantle component):										
Sample U43F from Upolu Island, Shield Series	3.15	552	42.3	7.6	18.848	15.564	38.783	0.705179	0.512883	0.283070
data sources	*Workman et al. [2004]*	*Workman et al. [2004]*	*Workman et al. [2004]*	*Workman et al. [2004]*	*Workman et al. [2004]*	*Workman et al. [2004]*	*Workman et al. [2004]*	*Workman et al. [2004]*	*Workman et al. [2004]*	*Pfänder et al. [2007]*

D. DATA FOR LATE EXPERIMENTS

Introduction

The follow sub-section contains the data acquired for the Late experiments at pressure and one-atmopheric. The data in red have been omitted from the results in Chapter 5.

Experiment	Condition	Name	Phase	SiO2	TiO2	Al2O3	Cr2O3	FeO	MnO	MgO	CaO	Na2O	K2O	P2O5	NiO	Total
B01-14	1atm, 1080 °C	01/04/14 Glass 1	Gl	64.39	0.11	21.04	*BDL*	2.11	*BDL*	0.32	11.57	2.01	0.16	*BDL*	*BDL*	**101.71**
		01/04/14 Glass 1	Gl	65.05	0.29	14.57	*BDL*	4.92	0.18	4.02	10.32	1.08	0.17	0.1	*BDL*	**100.7**
		01/04/14 Glass 1	Gl	36.46	2.49	7.76	0.04	35.81	0.21	1.51	3.42	0.99	0.05	0.05	*BDL*	**88.79**
		01/04/14 Glass 1	Gl	77.26	0.24	11.17	*BDL*	0.94	*BDL*	0.13	5.49	1.44	0.1	*BDL*	*BDL*	**96.77**
		01/04/14 Glass 1	Gl	74.97	0.21	13.56	*BDL*	1.52	*BDL*	0.42	7.1	1.43	0.13	*BDL*	*BDL*	**99.34**
		01/04/14 Glass 2	Gl	56.39	1.73	18.74	*BDL*	13.19	0.09	0.42	9.36	2.12	0.12	*BDL*	*BDL*	**102.16**
		01/04/14 Glass 2	Gl	59.61	2.17	11.22	0.09	20.3	0.11	0.4	4.56	1.32	0.08	*BDL*	*BDL*	**99.86**
		01/04/14 Glass 2	Gl	55.08	1.32	18.48	*BDL*	8.41	0.21	2.31	11.43	1.87	0.62	0.5	*BDL*	**100.23**
		01/04/14 Glass 2	Gl	52.15	0.44	23.73	*BDL*	4.13	0.12	1.84	13.99	2.38	0.27	0.09	*BDL*	**99.14**
		01/04/14 Glass 2	Gl	51.35	0.27	22.05	*BDL*	5.46	0.15	3.08	14.63	1.68	0.29	0.1	*BDL*	**99.06**
		1/4/14 Glass	Gl	59.93	1.08	11.62	0	11.73	0.27	3.08	8.22	1.53	0.93	0.17	*BDL*	**98.56**
		1/4/14 Glass	Gl	56.75	0.71	7.46	*BDL*	14.78	0.47	11.37	6.71	0.89	0.63	0.09	*BDL*	**99.86**
		1/4/14 Glass	Gl	56.31	0.54	5.99	*BDL*	14.68	0.46	12.59	9.8	0.77	0.43	*BDL*	*BDL*	**101.57**
		1/4/14 Glass	Gl	60.9	1.07	12.02	*BDL*	11.32	0.24	3	8.09	1.89	1.07	0.16	*BDL*	**99.76**
		1/4/14 Glass	Gl	61.07	1.09	11.66	*BDL*	11.36	0.27	3.04	7.92	1.81	1.06	0.18	*BDL*	**99.46**
		1/4/14 Plag	Gl	55.32	0.53	21.52	*BDL*	5.68	0.11	1.39	11.61	2.38	0.56	*BDL*	*BDL*	**99.1**
		1/4/14 pyroxene	Gl	50.29	0.25	16.22	*BDL*	10.29	0.25	8.71	10.36	1.82	0.25	*BDL*	*BDL*	**98.44**
		1/4/14 Plag	Pl	53.19	0.19	25.67	*BDL*	3.03	*BDL*	0.69	13.21	2.94	0.28	*BDL*	*BDL*	**99.2**
		1/4/14 Plag	Pl	53.01	0.11	27	*BDL*	2.78	*BDL*	0.55	13.77	2.75	0.25	*BDL*	*BDL*	**100.22**
		1/4/14 Plag	Pl	54.21	0.28	24.77	*BDL*	3.72	0.09	0.85	13.1	2.39	0.37	*BDL*	*BDL*	**99.78**
		1/4/14 Plag	Pl	53.26	0.11	26.83	*BDL*	2.8	*BDL*	0.56	13.76	2.69	0.22	*BDL*	*BDL*	**100.23**
		1/4/14 pyroxene	Cpx	51.2	0.37	2.67	*BDL*	14.97	0.5	17.21	13.73	0.17	*BDL*	*BDL*	*BDL*	**100.82**
		1/4/14 pyroxene	Cpx	51.56	0.34	2.91	*BDL*	17.02	0.55	20.18	8.16	0.11	*BDL*	*BDL*	*BDL*	**100.83**
		1/4/14 pyroxene	Cpx	49.17	0.5	3.33	*BDL*	13.6	0.38	14.43	18.42	0.24	*BDL*	*BDL*	*BDL*	**100.07**
		1/4/14 pyroxene	Cpx	51.14	0.36	2.82	*BDL*	16.99	0.54	19.96	8.4	*BDL*	*BDL*	*BDL*	*BDL*	**100.21**
		1/4/14 pyroxene	Cpx	49.9	0.39	3.07	*BDL*	14.76	0.45	16.11	15.63	0.13	*BDL*	*BDL*	*BDL*	**100.44**
		1/4/14 pyroxene	Cpx	49.85	0.61	3.35	*BDL*	12.76	0.41	13.97	19.58	0.19	*BDL*	*BDL*	*BDL*	**100.72**
		1/4/14 pyroxene	Cpx	52.79	0.27	2.25	*BDL*	18.6	0.58	21.04	5.2	0.2	0.08	*BDL*	*BDL*	**101.01**
		1/4/14 pyroxene	Cpx	51.19	0.37	3.12	*BDL*	16.94	0.57	18.93	9.08	0.12	0.03	*BDL*	*BDL*	**100.35**
		1/4/14 pyroxene	Cpx	51	0.37	3.2	0.07	16.32	0.43	17.67	12.42	0.13	*BDL*	*BDL*	*BDL*	**101.61**
		1/4/14 pyroxene	Cpx	50.39	0.35	3.28	*BDL*	15.28	0.5	17.15	13.07	0.18	*BDL*	*BDL*	*BDL*	**100.2**
		1/4/14 oxide	Ilmenite	4.94	4.36	3.84	0.05	81.06	0.35	2.85	0.57	0.2	0.07	*BDL*	*BDL*	**98.29**
		1/4/14 oxide	Ilmenite	0.25	4.47	3.33	0.06	81.23	0.33	2.94	0.37	*BDL*	*BDL*	*BDL*	*BDL*	**92.98**
		1/4/14 oxide	Ilmenite	0.27	4.5	3.3	0.1	81.21	0.31	2.88	0.32	*BDL*	*BDL*	*BDL*	*BDL*	**92.89**
		1/4/14 oxide	Ilmenite	1.16	4.54	3.42	0.09	79.92	0.29	2.77	0.44	*BDL*	*BDL*	*BDL*	*BDL*	**92.63**
		1/4/14 oxide	Ilmenite	0.29	4.13	3.32	*BDL*	81.83	0.32	2.78	0.33	*BDL*	*BDL*	*BDL*	*BDL*	**93**

Experiment	Condition	Name	Phase	SiO2	TiO2	Al2O3	Cr2O3	FeO	MnO	MgO	CaO	Na2O	K2O	P2O5	NiO	Total
B29-14	1atm, 1099 °C	29/03/14 Pyroxene 1	Gl	57.94	0.74	16.77	*BDL*	9.13	0.23	2.34	10.55	1.67	0.68	0.16	*BDL*	**100.21**
		29/03/14 Pyroxene 1	Gl	59.43	0.92	14.26	*BDL*	10.1	0.19	2.63	9.55	1.69	0.81	0.14	*BDL*	**99.72**
		29/03/14 Pyroxene 1	Gl	59.9	1.11	11.36	*BDL*	11.81	0.24	3	8.43	1.71	0.96	0.18	*BDL*	**98.7**
		29/03/14 Pyroxene 1	Gl	60.55	1.08	12.03	*BDL*	11.94	0.24	3.05	8.59	1.57	0.87	0.17	*BDL*	**100.09**
		29/03/14 Pyroxene 1	Gl	61.05	1.07	11.6	*BDL*	11.58	0.25	3	8.3	1.53	0.99	0.17	*BDL*	**99.54**
		29/03/14 Glass 1	Gl	59.57	0.92	14.22	*BDL*	10.73	0.23	2.68	9.47	1.73	0.76	0.16	*BDL*	**100.47**
		29/03/14 lt/med grey 2B	Gl	59.68	1.2	11.41	*BDL*	10.58	0.25	2.99	7.98	1.74	1.09	0.19	*BDL*	**97.11**
		29/03/14 lt/med grey 2B	Gl	61.32	1.23	11.8	*BDL*	10.35	0.22	2.94	8.12	1.71	1.07	0.17	*BDL*	**98.93**
		29/03/14 lt/med grey 2B	Gl	61.15	1.05	11.49	*BDL*	10.2	0.24	2.69	7.49	1.8	1.11	0.16	*BDL*	**97.38**
		29/03/14 Glass 2B	Gl	60.24	1.03	12.9	*BDL*	10.19	0.26	2.72	8.38	1.91	1	0.16	*BDL*	**98.79**
		29/03/14 Glass 2B	Gl	59.37	0.84	15.99	*BDL*	9.79	0.18	2.35	10.09	1.6	0.86	0.18	*BDL*	**101.25**
		29/03/14 Glass 1	Gl	54.59	0.47	22.59	*BDL*	5.5	0.16	1.2	13.05	2.09	0.44	0.08	*BDL*	**100.17**
		29/3/14 dark glass	Gl	65.54	0.14	19.7	*BDL*	1.46	*BDL*	0.23	10.37	1.63	0.15	*BDL*	*BDL*	**99.22**
		29/3/14 glass	Gl	57.96	0.42	21.29	*BDL*	4.37	0.07	0.84	10.77	2.44	1.05	0.17	*BDL*	**99.38**
		29/3/14 glass	Gl	56.86	0.29	22.92	*BDL*	3.57	*BDL*	0.76	11.88	2.45	0.83	*BDL*	*BDL*	**99.56**
		29/3/14 glass	Gl	65.15	0.8	13.95	*BDL*	6.2	0.2	1.43	6.42	2.06	2.07	0.28	*BDL*	**98.56**
		29/3/14 glass	Gl	60.09	0.52	18.7	*BDL*	5.33	0.12	1.16	9.44	2.41	1.29	0.15	*BDL*	**99.21**
		29/3/14 pyroxene	Gl	55.23	0.29	19.82	*BDL*	4.26	0.1	2.83	12.33	2.58	0.71	0.1	*BDL*	**98.25**
		29/3/14 pyroxene	Gl	60.28	0.76	7.57	*BDL*	10.2	0.36	7.68	10.71	0.98	1.08	0.15	*BDL*	**99.77**
		29/3/14 plag	Gl	60.76	0.13	19.81	*BDL*	1.78	*BDL*	0.23	10.13	1.91	0.1	*BDL*	*BDL*	**94.85**
		29/3/14 plag	Gl	64.39	*BDL*	22.01	*BDL*	2.36	*BDL*	0.51	11.36	2.14	0.11	*BDL*	*BDL*	**102.88**
		29/3/14 plag	Gl	58.71	0.25	18.72	0.03	6.34	0.18	4.79	12.15	1.99	0.14	0.07	*BDL*	**103.37**
		29/3/14 plag	Gl	57.42	0.27	14.26	0.03	5.84	0.17	4.35	10.48	1.56	0.11	*BDL*	*BDL*	**94.49**
		29/3/14 plag	Gl	62.85	0.18	17.24	*BDL*	2.58	0.06	1.11	9.48	1.96	0.17	0.07	*BDL*	**95.7**
		29/3/14 plag	Gl	60.37	0.18	18.97	*BDL*	3.48	0.07	1.89	11.01	1.91	0.15	0.06	*BDL*	**98.09**
		29/3/14 plag	Gl	55.82	0.4	19.68	*BDL*	5.31	0.14	2.81	12.1	1.91	0.23	0.27	*BDL*	**98.67**
		29/3/14 plag	Gl	52.8	0.25	16.07	0.04	8.96	0.27	7.71	12.6	1.45	0.09	0.06	*BDL*	**100.3**
		29/3/14 plag	Gl	57.9	0.21	20.71	*BDL*	4.45	0.12	2.28	12.2	2.02	0.12	*BDL*	*BDL*	**100.01**
		29/3/14 plag	Gl	52.75	0.33	17.82	*BDL*	7.81	0.22	5.49	12.65	1.82	0.18	0.12	*BDL*	**99.19**
		29/3/14 pyroxene	Gl	68.13	0.9	7.34	*BDL*	11.23	0.2	3.54	5.62	0.86	0.15	0.14	*BDL*	**98.11**
		29/3/14 ilmenite?	Gl	59.44	0.71	18.8	*BDL*	5.74	0.17	0.86	9.51	1.99	1.4	0.12	*BDL*	**98.74**
		29/3/14 pyroxene	Gl	59.54	0.15	20.08	*BDL*	3.22	0.09	1.85	11.71	1.9	0.14	*BDL*	*BDL*	**98.68**
		29/3/14 pyroxene	Gl	55.51	0.45	19.81	*BDL*	5.06	0.1	1.4	10.68	2.23	0.83	0.08	*BDL*	**96.15**
		29/3/14 glass	Gl	55.43	0.65	20.09	*BDL*	4.18	0.14	2.13	11.39	2.53	0.82	0.11	*BDL*	**97.47**
		29/3/14 glass	Gl	53.85	0.52	19.61	*BDL*	4.97	0.16	3.5	12.82	2.23	0.57	0.1	*BDL*	**98.33**
		29/3/14 glass	Gl	56.89	0.7	17.9	*BDL*	5.52	0.16	2.65	10.51	2.47	1.03	0.1	*BDL*	**97.93**
		29/3/14 glass	Gl	55.37	0.8	16.84	*BDL*	6.92	0.21	3.35	10.87	2.3	0.94	0.15	*BDL*	**97.75**
		29/3/14 glass	Gl	56.31	0.55	17.62	*BDL*	6.07	0.2	3.2	10.72	2.23	0.93	0.11	*BDL*	**97.94**
		29/3/14 ilmenite?	Gl	54.15	0.46	17.9	*BDL*	6.33	0.17	4.08	12.03	2.21	0.67	0.08	*BDL*	**98.08**
		29/3/14 ilmenite?	Gl	55.19	0.47	20.83	*BDL*	5.07	0.11	1.7	11.09	2.39	0.79	0.08	*BDL*	**97.72**
		29/3/14 ilmenite?	Gl	55.99	0.57	17.94	*BDL*	7.16	0.19	3.42	10.56	2.21	0.81	0.13	*BDL*	**98.98**
		29/3/14 ilmenite?	Gl	54.86	0.5	16.09	*BDL*	7.42	0.25	5.4	11.59	1.99	0.68	0.08	*BDL*	**98.86**
		29/3/14 ilmenite?	Gl	54.92	0.4	18.4	*BDL*	6.06	0.18	4.1	12.06	2.12	0.62	0.08	*BDL*	**98.94**

Experiment	Condition	Name	Phase	SiO2	TiO2	Al2O3	Cr2O3	FeO	MnO	MgO	CaO	Na2O	K2O	P2O5	NiO	Total
		29/03/14 Glass 1	Pl	53.32	0.25	24.79	*BDL*	3.7	*BDL*	0.82	13.72	2.67	0.26	0.05	*BDL*	**99.58**
		29/03/14 Glass 1	Pl	52.58	0.06	27.03	*BDL*	2.55	*BDL*	0.44	14.47	2.76	0.14	*BDL*	*BDL*	**100.03**
		29/03/14 Glass 1	Pl	53.46	0.04	26.69	*BDL*	2.37	*BDL*	0.42	14.35	2.89	0.13	*BDL*	*BDL*	**100.35**
		29/03/14 lt/med grey 2B	Pl	53.46	0.18	25.44	*BDL*	2.35	*BDL*	0.73	13.84	2.53	0.23	*BDL*	*BDL*	**98.76**
		29/03/14 Glass 2B	Pl	55.39	0.33	23.84	*BDL*	3.53	*BDL*	0.96	12.81	2.58	0.36	0.07	*BDL*	**99.87**
		29/03/14 Glass 2B	Pl	51.88	0.07	26.57	*BDL*	2.33	*BDL*	0.88	14.47	2.31	0.18	*BDL*	*BDL*	**98.69**
		29/03/14 Glass 2B	Pl	52.67	0.07	26.66	*BDL*	2.09	*BDL*	0.4	13.67	2.92	0.17	0.04	*BDL*	**98.69**
		29/3/14 glass	Pl	52.01	0.04	27.4	*BDL*	2.48	*BDL*	0.43	14.39	2.83	0.2	*BDL*	*BDL*	**99.78**
		29/03/14 lt/med grey 2B	Cpx	51.37	0.5	3.85	0.09	9.72	0.49	15.46	17.77	0.3	0.06	*BDL*	*BDL*	**99.61**
		29/3/14 pyroxene	Cpx	53.06	0.42	2.77	*BDL*	15.89	0.58	16.91	9.87	0.24	0.22	*BDL*	*BDL*	**99.96**
		29/3/14 pyroxene	Cpx	51.74	0.37	3.48	*BDL*	16.54	0.65	17.12	10.89	0.14	0.08	*BDL*	*BDL*	**101.01**
		29/3/14 pyroxene	Cpx	54.6	0.33	2.32	*BDL*	18.08	0.67	17.98	8.22	0.1	*BDL*	*BDL*	*BDL*	**102.3**
		29/3/14 pyroxene	Cpx	50.38	0.49	7.43	*BDL*	14.54	0.52	14.87	12.59	0.29	*BDL*	*BDL*	*BDL*	**101.11**
		29/3/14 pyroxene	Cpx	51.08	0.41	2.62	*BDL*	16.96	0.67	19.06	8.77	0.11	*BDL*	*BDL*	*BDL*	**99.68**
		29/3/14 pyroxene	Cpx	51.04	0.37	2.44	*BDL*	16.03	0.66	17.34	12.03	*BDL*	*BDL*	*BDL*	*BDL*	**99.91**
		29/3/14 pyroxene	Cpx	50.34	0.42	3.26	*BDL*	17.18	0.58	16.65	11.43	0.13	*BDL*	*BDL*	*BDL*	**99.99**
		29/3/14 pyroxene	Cpx	51.91	0.61	14.6	*BDL*	8.37	0.29	7.51	15.9	1.12	0.26	0.28	*BDL*	**100.85**
		29/3/14 pyroxene	Cpx	54.26	0.54	17.61	*BDL*	7.46	0.19	4.02	11.59	2.01	0.61	0.12	*BDL*	**98.41**
		29/3/14 pyroxene	Cpx	49.76	1.08	18.34	*BDL*	13.87	0.19	2.8	9.76	2.03	0.61	0.08	*BDL*	**98.52**
		29/3/14 dark glass	Gl/Qtz	82.02	0.26	8.54	*BDL*	0.65	*BDL*	0.08	4.06	1	0.08	*BDL*	*BDL*	**96.69**
		29/3/14 dark glass	Gl/Qtz	85.82	0.3	3.94	*BDL*	0.65	*BDL*	0.07	2.32	0.78	0.06	*BDL*	*BDL*	**93.94**
		29/3/14 dark glass	Gl/Qtz	92.06	0.32	3.76	*BDL*	0.51	*BDL*	0.17	1.62	0.73	0.06	*BDL*	*BDL*	**99.23**
		29/3/14 dark glass	Gl/Qtz	89.29	0.24	5.78	*BDL*	0.56	*BDL*	0.06	2.39	0.82	0.07	*BDL*	0.06	**99.27**
		29/3/14 ilmenite?	Ilmenite	68.16	0.81	5.6	*BDL*	9.13	0.16	3.98	6.04	0.57	0.05	*BDL*	*BDL*	**94.5**
		29/3/14 ilmenite?	Ilmenite	14.98	5.3	8.31	*BDL*	68.51	0.34	2.46	2.03	0.29	*BDL*	*BDL*	*BDL*	**102.22**
		29/3/14 ilmenite?	Ilmenite	41.98	5.48	6.13	*BDL*	62.11	0.43	2.13	1.57	1.99	1.38	*BDL*	*BDL*	**123.2**
B26-14	1atm, 1117 °C	26/03/14 Glass 1	Gl	54.56	0.6	16.57	0.04	9.11	0.16	4.35	11.14	1.86	0.46	0.09	*BDL*	**98.94**
		26/03/14 Glass 1	Gl	54.84	0.6	16.69	*BDL*	8.99	0.22	4.38	11.07	1.85	0.47	0.09	*BDL*	**99.2**
		26/03/14 Glass 1	Gl	54.74	0.59	16.63	*BDL*	8.48	0.19	4.05	10.98	1.94	0.5	0.1	*BDL*	**98.2**
		26/03/14 Glass 1	Gl	55.25	0.6	16.6	*BDL*	8.49	0.17	4.24	10.92	1.9	0.46	0.06	*BDL*	**98.69**
		26/03/14 Glass 1	Gl	54.82	0.59	16.75	*BDL*	8.92	0.24	4.25	11.15	1.9	0.53	0.08	*BDL*	**99.23**
		26/03/14 Glass 2	Gl	57.03	1.08	11.56	*BDL*	12.75	0.32	4.15	9.47	1.74	0.68	0.18	*BDL*	**98.96**
		26/03/14 Glass 2	Gl	56.49	1.09	11.49	*BDL*	12.88	0.27	4.18	9.47	1.6	0.68	0.17	*BDL*	**98.32**
		26/3/14 glass	Gl	55.45	0.69	17.43	*BDL*	9.3	0.17	3	11.53	1.72	0.57	0.13	*BDL*	**99.99**
		26/3/14 glass	Gl	56.67	1.02	11.71	*BDL*	13.36	0.29	4.26	9.58	1.49	0.73	0.1	*BDL*	**99.21**
		26/3/14 glass	Gl	53.76	0.51	19.62	*BDL*	8.05	0.15	2.5	12.54	1.76	0.38	*BDL*	*BDL*	**99.27**

Experiment	Condition	Name	Phase	SiO2	TiO2	Al2O3	Cr2O3	FeO	MnO	MgO	CaO	Na2O	K2O	P2O5	NiO	Total
		26/3/14 glass	Gl	55.07	1.03	11.73	*BDL*	13.26	0.26	4.16	9.59	1.54	0.72	0.14	*BDL*	**97.5**
		26/3/14 glass	Gl	56.11	1.03	11.67	*BDL*	12.99	0.27	4.16	9.61	1.61	0.71	0.21	*BDL*	**98.37**
		26/3/14 glass	Gl	56.38	1.01	11.56	*BDL*	13.43	0.29	4.25	9.63	1.42	0.67	0.17	*BDL*	**98.81**
		26/3/14 glass	Gl	56.37	1.02	11.66	*BDL*	13.31	0.25	4.24	9.6	1.69	0.69	0.23	*BDL*	**99.06**
		26/3/14 glass	Gl	56.44	1.04	11.66	*BDL*	13.54	0.27	4.19	9.54	1.49	0.7	0.15	*BDL*	**99.02**
		26/3/14 glass	Gl	51.72	0.37	22.55	*BDL*	6.37	0.13	1.9	13.59	1.97	0.27	0.11	*BDL*	**98.98**
		26/3/14 plag	Gl	58.13	1.02	12.08	0.04	11.39	0.25	3.99	9.19	1.68	0.77	0.2	*BDL*	**98.74**
		26/3/14 proxene	Gl	55.63	0.52	20.46	*BDL*	6.04	0.14	2.2	12.24	2.28	0.52	0.16	*BDL*	**100.19**
		26/3/14 proxene	Gl	54.82	0.59	20.23	*BDL*	6.13	0.15	2.86	11.89	2.2	0.45	0.12	*BDL*	**99.44**
		26/3/14 proxene	Gl	59.65	0.73	22.11	*BDL*	1.61	0.08	1.31	11.28	2.66	0.82	0.16	*BDL*	**100.41**
		26/3/14 proxene	Gl	58.91	0.82	14.56	*BDL*	9.69	0.2	3.15	9.26	2.12	0.84	0.1	*BDL*	**99.65**
		26/03/14 Glass 2	Pl	52.16	0.35	22.6	*BDL*	4.78	0.11	1.53	13.73	2.11	0.32	0.06	*BDL*	**97.75**
		26/03/14 Glass 2	Pl	49.95	0.05	27.95	*BDL*	2.28	*BDL*	0.43	15.53	2.19	0.12	*BDL*	*BDL*	**98.5**
		26/3/14 glass	Pl	51.18	0.17	26.74	*BDL*	2.72	*BDL*	0.79	14.91	2.3	0.27	*BDL*	*BDL*	**99.08**
		26/3/14 plag	Pl	50.8	0.04	27.74	*BDL*	2.5	*BDL*	1.28	14.71	2.48	0.12	*BDL*	*BDL*	**99.67**
		26/3/14 plag	Pl	51.96	0.17	26.73	*BDL*	3.23	*BDL*	0.91	14.97	2.13	0.19	*BDL*	*BDL*	**100.29**
		26/3/14 proxene	Pl	53.2	0.09	27.08	*BDL*	2.18	*BDL*	0.56	14	2.96	0.21	*BDL*	*BDL*	**100.28**
		26/3/14 proxene	Pl	52.37	0.09	28.3	*BDL*	0.97	*BDL*	0.77	15.12	2.64	0.13	*BDL*	*BDL*	**100.39**
		26/3/14 proxene	Pl	47.88	0.08	24.47	*BDL*	2.08	*BDL*	0.54	12.95	2.3	0.18	*BDL*	*BDL*	**90.48**
		26/3/14 proxene	Pl	52.03	0.06	23.99	*BDL*	3.52	0.09	3.79	13.24	2.28	0.11	*BDL*	*BDL*	**99.11**
		26/3/14 proxene	Pl	50.55	0.18	27.31	*BDL*	3.07	*BDL*	0.79	15.04	1.98	0.19	*BDL*	*BDL*	**99.11**
		26/03/14 Glass 2	Cpx	53.26	0.21	1.71	0.04	16.46	0.48	23.71	4.84	*BDL*	*BDL*	*BDL*	*BDL*	**100.71**
		26/3/14 plag	Cpx	52.67	0.16	1.48	0.04	16.52	0.55	22.8	5.66	0.08	*BDL*	*BDL*	*BDL*	**99.96**
		26/3/14 plag	Cpx	53.26	0.28	1.73	*BDL*	13.01	0.44	20.12	12.07	0.08	*BDL*	*BDL*	*BDL*	**100.99**
		26/3/14 proxene	Cpx	52.97	0.12	11.93	*BDL*	11.68	0.4	16.01	7.98	0.72	*BDL*	*BDL*	*BDL*	**101.81**
B29-12	1atm, 1120 °C	B29-A1-glass	Gl	52.50	0.42	22.93	0.00	6.06	0.10	1.74	13.12	2.44	0.39	0.08	0.00	**99.78**
		B29-A2-glass	Gl	53.21	0.55	20.07	0.01	7.71	0.13	2.24	11.91	2.47	0.50	0.14	0.00	**98.94**
		B29-A3-glass	Gl	54.84	0.78	16.21	0.04	10.11	0.17	3.19	10.51	2.14	0.64	0.12	0.00	**98.76**
		B29-A4-glass	Gl	54.44	0.71	17.42	0.00	9.99	0.20	2.92	11.13	2.10	0.58	0.09	0.02	**99.61**
		B29-A5-glass	Gl	55.15	0.97	12.38	0.02	13.29	0.20	3.94	9.47	1.82	0.78	0.17	0.01	**98.20**
		B29-A6-glass	Gl	52.12	0.40	23.62	0.00	6.13	0.09	1.66	13.20	2.46	0.37	0.06	0.03	**100.12**
		B29-A1-unk2	Gl	56.69	0.93	12.41	0.01	11.88	0.22	3.86	9.03	2.50	1.03	0.15	0.03	**98.72**
		B29-A2-unk3	Gl	57.20	0.64	19.61	0.02	9.77	0.14	3.15	10.27	2.75	0.59	0.08	0.00	**104.23**
		B29-A3-unk3	Gl	53.95	0.53	21.10	0.00	7.94	0.12	2.28	12.01	2.44	0.51	0.10	0.00	**100.97**
		B29-B1-glass	Gl	56.05	0.99	13.24	0.01	12.80	0.22	3.82	9.71	1.92	0.73	0.19	0.05	**99.71**
		B29-B2-glass	Gl	54.20	0.67	19.07	0.01	8.76	0.16	2.42	11.62	2.36	0.53	0.10	0.01	**99.91**

Experiment	Condition	Name	Phase	SiO2	TiO2	Al2O3	Cr2O3	FeO	MnO	MgO	CaO	Na2O	K2O	P2O5	NiO	Total
		B29-B3-glass	Gl	54.26	0.45	21.36	0.00	6.61	0.09	1.87	12.15	2.62	0.47	0.08	0.00	**99.95**
		B29-B4-glass	Gl	54.53	0.64	19.48	0.00	8.57	0.11	2.36	11.53	2.38	0.58	0.09	0.00	**100.26**
		B29-B5-glass	Gl	56.01	0.99	12.18	0.00	13.61	0.17	3.94	9.57	1.87	0.75	0.13	0.05	**99.26**
		B29-B6-glass	Gl	55.89	1.00	12.12	0.05	13.50	0.23	3.98	9.63	1.91	0.73	0.13	0.03	**99.20**
		B29-B1-unk3	Gl	55.63	0.80	16.25	0.00	11.59	0.20	3.33	10.12	2.23	0.86	0.12	0.00	**101.11**
		B29-B1-unk4	Gl	56.67	0.69	17.83	0.00	9.74	0.17	2.93	10.90	2.49	0.67	0.09	0.00	**102.19**
		B29-B3-unk5	Gl	51.03	0.24	21.69	0.01	7.06	0.17	5.21	12.30	2.24	0.19	0.05	0.02	**100.19**
		29/10/2012 Glass1-A	Gl	56.57	0.97	11.51	*BDL*	12.06	0.26	3.98	9.28	1.68	0.80	0.09	*BDL*	**97.20**
		29/10/2012 Glass1-A	Gl	56.59	1.01	11.72	*BDL*	12.01	0.20	3.93	9.29	1.56	0.77	0.16	*BDL*	**97.24**
		29/10/2012 Glass1-A	Gl	57.40	0.99	11.69	*BDL*	12.20	0.25	4.01	9.37	1.65	0.76	0.15	*BDL*	**98.47**
		29/10/2012 Glass1-B	Gl	57.38	0.99	11.95	*BDL*	12.11	0.25	3.86	9.38	1.63	0.72	0.11	*BDL*	**98.38**
		29/10/2012 Glass1-B	Gl	55.96	0.83	14.57	*BDL*	10.22	0.19	3.34	10.35	1.81	0.68	0.12	*BDL*	**98.07**
		29/10/2012 Glass2	Gl	55.10	0.93	11.66	0.05	13.81	0.27	4.36	9.70	1.59	0.68	0.14	*BDL*	**98.29**
		29/10/2012 Glass2	Gl	55.17	0.94	11.70	*BDL*	13.83	0.29	4.21	9.73	1.40	0.68	0.12	*BDL*	**98.07**
		29/10/2012 Glass2	Gl	54.61	0.97	11.48	*BDL*	13.76	0.21	4.31	9.72	1.45	0.70	0.15	*BDL*	**97.36**
		29/10/2012 Glass2	Gl	55.00	0.94	11.63	*BDL*	13.96	0.26	4.25	9.71	1.48	0.67	0.15	*BDL*	**98.05**
		29/10/2012 Glass2	Gl	54.92	0.96	11.37	*BDL*	13.76	0.24	4.27	9.70	1.51	0.68	0.13	*BDL*	**97.54**
		B29/10/12 Plag 1	Gl	55.35	0.76	15.05	*BDL*	10.23	0.23	3.23	10.48	1.76	0.68	0.10	*BDL*	**97.87**
		B29/10/12 Plag 1	Pl	51.6	0.16	25.78	*BDL*	3.27	*BDL*	0.89	14.21	2.54	0.22	*BDL*	*BDL*	**98.67**
		B29/10/12 Plag 1	Pl	50.49	0.03	27.04	*BDL*	1.86	*BDL*	0.46	14.48	2.70	0.12	*BDL*	*BDL*	**97.18**
		B29/10/12 Plag 1	Pl	51.17	0.10	26.33	*BDL*	2.67	*BDL*	0.76	14.60	2.39	0.21	0.05	*BDL*	**98.28**
		B29/10/12 Plag 1	Pl	50.71	0.14	25.95	*BDL*	2.96	*BDL*	0.76	14.34	2.50	0.18	*BDL*	*BDL*	**97.54**
		B29/10/12 Plag 2	Pl	50.44	*BDL*	28.05	*BDL*	1.40	*BDL*	0.44	14.67	3.03	0.11	*BDL*	*BDL*	**98.14**
		B29/10/12 Plag 2	Pl	50.71	0.03	29.06	*BDL*	1.26	*BDL*	0.37	15.30	2.42	0.11	*BDL*	*BDL*	**99.26**
		B29/10/12 Plag 2	Pl	50.91	0.04	27.55	*BDL*	1.78	*BDL*	0.48	14.56	2.79	0.14	*BDL*	*BDL*	**98.25**
		B29/10/12 Plag 2	Pl	50.55	0.14	26.20	*BDL*	2.62	*BDL*	0.74	14.44	2.67	0.22	*BDL*	*BDL*	**97.58**
		B29/10/12 Plag 2	Pl	50.56	0.04	28.18	*BDL*	1.25	*BDL*	0.39	14.85	2.76	0.12	*BDL*	*BDL*	**98.15**
		B29-A1-unk4	cpx	51.89	0.30	4.66	0.09	16.11	0.42	18.36	5.97	0.64	0.20	0.03	0.11	**98.77**
		B29-A2-unk4	cpx	51.44	0.13	14.74	0.08	10.16	0.21	11.49	9.69	1.62	0.13	0.00	0.08	**99.77**
		B29-B1-unk1	cpx	50.69	0.16	7.41	0.05	13.76	0.36	16.34	9.07	0.64	0.07	0.00	0.03	**98.58**
		B29-B2-unk1	cpx	52.69	0.47	6.18	0.00	15.19	0.35	13.96	8.11	0.94	0.36	0.09	0.03	**98.36**
		B29-B3-unk1	cpx	52.03	0.16	10.42	0.05	13.13	0.33	15.95	8.48	1.19	0.17	0.04	0.00	**101.94**
		B29-B1-unk2	cpx	54.46	0.30	3.61	0.04	16.31	0.43	19.80	5.34	0.72	0.28	0.08	0.00	**101.36**
		B29-B2-unk2	cpx	56.70	0.20	2.93	0.03	16.15	0.44	25.27	4.98	0.36	0.10	0.03	0.03	**107.23**

Experiment	Condition	Name	Phase	SiO2	TiO2	Al2O3	Cr2O3	FeO	MnO	MgO	CaO	Na2O	K2O	P2O5	NiO	Total
B22-12	1atm, 1139 °C	B22-A1-glass	Gl+Pl mix	51.06	0.16	26.12	0.00	3.71	0.04	1.34	13.94	2.85	0.25	0.02	0.02	**99.51**
		B22-A2-glass	Gl	54.11	0.86	12.69	0.02	12.42	0.24	5.08	9.57	1.92	0.68	0.10	0.00	**97.68**
		B22-A3-glass	Gl	54.25	0.87	12.73	0.00	12.35	0.21	4.88	9.41	1.88	0.69	0.19	0.01	**97.46**
		B22-A4-glass	Gl+Pl mix	51.11	0.22	25.61	0.00	3.53	0.04	1.37	13.72	3.00	0.25	0.03	0.00	**98.88**
		B22-A5-glass	Gl+Pl mix	52.01	0.38	23.56	0.00	5.59	0.09	1.94	12.97	2.62	0.36	0.03	0.00	**99.55**
		B22-A6-glass	Gl+Pl mix	53.04	0.45	21.55	0.00	6.76	0.12	2.31	12.11	2.45	0.44	0.02	0.05	**99.29**
		B22-B1-unk1	Gl	53.61	0.76	12.66	0.03	12.98	0.22	5.76	9.87	1.69	0.57	0.13	0.00	**98.28**
		B22-B2-unk1	Gl	53.77	0.79	12.69	0.00	12.96	0.25	5.71	10.03	1.67	0.57	0.14	0.00	**98.58**
		B22-B3-unk1	Gl	53.70	0.82	12.68	0.00	12.78	0.27	5.69	9.91	1.73	0.56	0.11	0.00	**98.25**
		B22-B3-glass	Gl	54.50	0.82	12.81	0.02	12.76	0.24	5.63	9.96	1.79	0.55	0.16	0.00	**99.23**
		B22-B4-glass	Gl	54.55	0.80	12.88	0.02	12.72	0.28	5.66	9.87	1.76	0.55	0.16	0.00	**99.25**
		B22-B5-glass	Gl	54.27	0.85	12.84	0.02	12.66	0.26	5.64	9.95	1.76	0.60	0.11	0.00	**98.96**
		B22-B6-glass	Gl	54.30	0.82	12.71	0.03	12.93	0.28	5.57	9.89	1.75	0.56	0.10	0.00	**98.93**
		22/10/2012 Glass1	Gl	54.88	0.78	12.48	*BDL*	12.54	0.28	5.66	9.63	1.53	0.55	0.13	0.06	**98.52**
		22/10/2012 Glass1	Gl	54.56	0.77	12.38	*BDL*	12.68	0.26	5.71	9.58	1.51	0.58	0.11	*BDL*	**98.14**
		22/10/2012 Glass1	Gl	55.33	0.78	12.27	*BDL*	12.47	0.26	5.72	9.60	1.55	0.63	0.13	*BDL*	**98.74**
		22/10/2012 Glass1	Gl	55.33	0.75	12.35	*BDL*	12.32	0.29	5.62	9.56	1.56	0.59	0.13	*BDL*	**98.50**
		22/10/2012 Glass1	Gl	55.32	0.78	12.39	0.05	12.40	0.28	5.61	9.53	1.61	0.58	0.11	*BDL*	**98.66**
		22/10/2012 Glass2	Gl	54.71	0.78	12.22	*BDL*	12.76	0.26	5.81	9.94	1.65	0.51	0.12	*BDL*	**98.76**
		22/10/2012 Glass2	Gl	54.41	0.77	12.19	*BDL*	12.78	0.30	5.89	9.80	1.51	0.51	0.15	*BDL*	**98.31**
		22/10/2012 Glass2	Gl	54.88	0.77	12.23	*BDL*	12.76	0.27	5.86	9.87	1.50	0.54	0.11	*BDL*	**98.79**
		22/10/2012 Glass2	Gl	54.84	0.76	12.12	*BDL*	12.45	0.29	5.78	9.85	1.47	0.53	0.08	*BDL*	**98.17**
		22/10/2012 Glass2	Gl	55.29	0.80	12.14	*BDL*	12.37	0.28	5.85	9.81	1.61	0.53	0.12	*BDL*	**98.80**
		B22-B1-unk2	Pl	50.52	0.03	29.06	0.01	1.56	0.02	0.41	14.86	3.19	0.11	0.03	0.00	**99.80**
		B22-B2-unk2	Pl	50.29	0.06	29.30	0.01	1.59	0.03	0.49	15.11	3.02	0.12	0.03	0.07	**100.12**
		B22-B3-unk2	Pl	50.56	0.03	29.15	0.00	1.64	0.03	0.39	14.95	3.25	0.11	0.01	0.05	**100.16**
		B22-B2-unk3	Pl	50.17	0.05	28.87	0.00	1.46	0.00	0.45	14.69	3.15	0.13	0.00	0.04	**98.99**
		B22-B3-unk3	Pl	50.22	0.09	27.85	0.00	2.92	0.04	0.93	14.80	2.76	0.15	0.00	0.00	**99.77**
		B22/10/12 Plag 1	Gl+Pl mix	53.4	0.51	18.88	*BDL*	7.78	0.17	3.53	11.60	2.14	0.48	0.07	*BDL*	**98.56**
		B22/10/12 Plag 1	Pl	51.26	0.03	28.52	*BDL*	1.37	*BDL*	0.41	14.89	2.82	0.09	*BDL*	*BDL*	**99.39**
		B22/10/12 Plag 1	Pl	51.06	0.04	28.24	*BDL*	1.49	*BDL*	0.43	14.77	2.69	0.12	*BDL*	*BDL*	**98.84**
		B22/10/12 Plag 1	Pl	52.33	*BDL*	28.43	*BDL*	1.45	*BDL*	0.39	14.75	2.93	0.13	*BDL*	*BDL*	**100.41**
		B22/10/12 Plag 1	Pl	51.17	*BDL*	28.39	*BDL*	1.46	*BDL*	0.38	14.99	2.56	0.10	*BDL*	*BDL*	**99.05**
		B22/10/12 Plag 2	Pl	51.95	0.03	28.67	*BDL*	1.35	*BDL*	0.41	14.76	2.59	0.15	*BDL*	*BDL*	**99.91**
		B22/10/12 Plag 2	Pl	51.13	0.05	27.84	*BDL*	1.60	*BDL*	0.61	14.90	2.54	0.10	*BDL*	*BDL*	**98.77**
		B22/10/12 Plag 2	Pl	51.94	0.03	28.04	*BDL*	1.52	*BDL*	0.40	14.84	2.85	0.09	*BDL*	*BDL*	**99.71**
		B22/10/12 Plag 2	Pl	51.15	*BDL*	28.76	*BDL*	1.58	*BDL*	0.41	15.06	2.51	0.09	*BDL*	*BDL*	**99.56**
		B22/10/12 Plag 2	Pl	50.79	0.04	28.43	*BDL*	1.49	*BDL*	0.48	15.10	2.43	0.10	0.04	*BDL*	**98.90**

Experiment	Condition	Name	Phase	SiO2	TiO2	Al2O3	Cr2O3	FeO	MnO	MgO	CaO	Na2O	K2O	P2O5	NiO	Total
B17-12	1atm, 1158 °C	B17-A1-glass	Gl	54.10	0.72	13.61	0.02	12.01	0.22	5.22	9.95	1.85	0.58	0.17	0.02	**98.46**
		B17-A2-glass	Gl	54.56	0.74	13.62	0.01	12.00	0.25	5.29	9.84	1.81	0.54	0.10	0.00	**98.76**
		B17-A3-glass	Gl	55.38	0.73	13.60	0.02	11.44	0.20	5.15	9.75	1.97	0.59	0.12	0.01	**98.97**
		B17-A4-glass	Gl	55.03	0.76	13.51	0.02	11.43	0.21	5.12	9.63	1.88	0.60	0.11	0.00	**98.30**
		B17-A5-glass	Gl	54.64	0.78	13.63	0.01	11.86	0.27	5.33	9.99	1.81	0.57	0.08	0.01	**98.97**
		B17-A6-glass	Gl	55.52	0.77	13.68	0.00	11.10	0.22	4.97	9.66	1.97	0.63	0.10	0.00	**98.63**
		B17-A1-unk4	Gl	55.04	0.71	13.56	0.01	11.36	0.21	5.00	9.67	2.20	0.66	0.16	0.00	**98.58**
		B17-B1-glass	Gl	53.91	0.72	13.58	0.05	12.18	0.26	5.17	9.77	1.91	0.59	0.17	0.06	**98.38**
		B17-B2-glass	Gl	53.71	0.72	13.47	0.00	11.99	0.24	5.15	9.77	1.90	0.58	0.08	0.05	**97.67**
		B17-B3-glass	Gl	53.70	0.73	13.49	0.04	11.90	0.20	5.15	9.69	1.93	0.57	0.11	0.01	**97.54**
		B17-B4-glass	Gl	53.89	0.75	13.48	0.02	11.61	0.23	5.16	9.63	1.92	0.59	0.11	0.01	**97.40**
		B17-B5-glass	Gl	55.13	0.71	13.60	0.02	11.60	0.18	5.11	9.70	1.97	0.63	0.08	0.01	**98.74**
		B17-B6-glass	Gl	55.40	0.73	13.62	0.04	11.34	0.25	5.00	9.47	1.99	0.63	0.11	0.03	**98.60**
		B17-B1-unk4	Gl	53.01	0.74	13.56	0.01	12.15	0.25	5.22	9.72	1.88	0.57	0.11	0.04	**97.27**
		17/10/2012 Glass1	Gl	54.8	0.76	13.06	*BDL*	11.57	0.28	5.47	9.79	1.71	0.60	0.10	*BDL*	**98.14**
		17/10/2012 Glass1	Gl	55.2	0.73	13.33	0.04	11.50	0.24	5.53	9.71	1.80	0.60	0.12	*BDL*	**98.80**
		17/10/2012 Glass1	Gl	54.34	0.74	12.98	0.04	12.03	0.21	5.70	9.99	1.49	0.53	0.11	*BDL*	**98.16**
		17/10/2012 Glass1	Gl	54.42	0.74	12.85	*BDL*	11.90	0.28	5.60	9.89	1.62	0.56	0.12	*BDL*	**97.98**
		17/10/2012 Glass1	Gl	54.29	0.77	12.98	*BDL*	12.08	0.27	5.62	9.95	1.68	0.59	0.09	*BDL*	**98.32**
		17/10/2012 Glass2	Gl	54.79	0.73	12.84	*BDL*	11.96	0.24	5.73	9.97	1.68	0.53	0.11	*BDL*	**98.58**
		17/10/2012 Glass2	Gl	54.8	0.77	12.80	*BDL*	11.82	0.24	5.72	10.10	1.54	0.51	0.08	*BDL*	**98.38**
		17/10/2012 Glass2	Gl	53.53	0.72	12.51	*BDL*	11.96	0.27	5.67	10.00	1.59	0.56	0.11	*BDL*	**96.92**
		17/10/2012 Glass2	Gl	55.11	0.75	13.01	*BDL*	11.86	0.25	5.71	9.97	1.60	0.58	0.12	*BDL*	**98.96**
		17/10/2012 Glass2	Gl	55.41	0.73	12.89	*BDL*	12.01	0.24	5.72	10.01	1.71	0.54	0.11	*BDL*	**99.37**
		B17-A1-unk1(pl)	Pl	50.61	0.31	24.47	0.01	5.23	0.12	2.11	13.53	2.34	0.27	0.02	0.00	**99.01**
		B17-A2-unk1(pl)	Pl	49.51	0.00	30.43	0.00	1.11	0.01	0.29	15.49	2.65	0.10	0.00	0.00	**99.59**
		B17-A3-unk1(pl)	Pl	48.69	0.01	30.70	0.01	1.22	0.01	0.30	15.86	2.75	0.12	0.00	0.01	**99.68**
		B17-A1-unk2(pl)	Pl	50.35	0.01	29.95	0.01	1.03	0.01	0.34	14.96	3.20	0.11	0.00	0.00	**99.97**
		B17-A2-unk2(pl)	Pl	49.98	0.03	30.17	0.00	1.10	0.00	0.30	15.05	3.17	0.11	0.02	0.00	**99.94**
		B17-A3-unk2(pl)	Pl	49.78	0.02	30.03	0.00	1.07	0.03	0.32	15.15	3.14	0.09	0.01	0.03	**99.67**
		B17-A2-unk4	Pl	50.69	0.23	26.11	0.01	3.66	0.09	1.52	14.04	2.89	0.28	0.09	0.00	**99.62**
		B17-B1-unk1	Pl	50.02	0.07	29.17	0.00	2.06	0.02	0.71	14.72	2.90	0.13	0.03	0.00	**99.83**
		B17-B2-unk1	Pl	49.39	0.04	30.28	0.02	1.36	0.00	0.38	15.48	2.88	0.10	0.01	0.00	**99.93**
		B17-B3-unk1	Pl	50.47	0.02	29.60	0.00	1.35	0.01	0.38	14.70	3.19	0.14	0.00	0.00	**99.86**
		B17-B2-unk2	Pl	50.39	0.04	29.64	0.02	1.36	0.04	0.43	14.71	3.16	0.14	0.00	0.04	**99.97**
		B17-B1-unk2	Pl	50.08	0.03	29.69	0.00	1.29	0.01	0.39	14.99	3.09	0.13	0.04	0.02	**99.76**
		B17-B3-unk2	Pl	49.87	0.03	30.14	0.00	1.35	0.02	0.36	15.12	3.07	0.12	0.00	0.00	**100.08**
		B17-B1-unk3	Pl	49.77	0.02	29.67	0.03	1.21	0.01	0.33	14.96	3.18	0.12	0.00	0.00	**99.29**
		B17-B2-unk3	Pl	49.64	0.05	29.66	0.00	1.15	0.00	0.35	15.00	3.16	0.11	0.00	0.05	**99.18**
		B17-B3-unk3	Pl	49.80	0.02	30.00	0.00	1.21	0.03	0.32	14.97	3.14	0.10	0.00	0.01	**99.61**
		B17-B1-unk5	Pl	48.15	0.02	31.18	0.00	0.98	0.00	0.27	15.77	2.64	0.11	0.00	0.01	**99.12**
		B17-B2-unk5	Pl	49.86	0.05	30.18	0.02	1.09	0.03	0.32	15.13	2.97	0.10	0.02	0.02	**99.77**
		B17-B3-unk5	Pl	52.54	0.51	19.65	0.04	8.91	0.15	3.75	11.87	2.01	0.45	0.09	0.01	**99.98**

Experiment	Condition	Name	Phase	SiO2	TiO2	Al2O3	Cr2O3	FeO	MnO	MgO	CaO	Na2O	K2O	P2O5	NiO	Total
B26-12	1atm, 1177 °C	B26-A1-glass	Gl	54.63	0.69	14.42	0.01	11.45	0.23	4.94	10.03	1.95	0.58	0.11	0.05	**99.10**
		B26-A2-glass	Gl	54.27	0.70	14.45	0.02	11.47	0.20	4.96	9.90	1.91	0.58	0.10	0.02	**98.58**
		B26-A3-glass	Gl	53.98	0.72	14.51	0.05	11.33	0.16	5.08	10.13	1.92	0.57	0.11	0.00	**98.56**
		B26-A4-glass	Gl	54.31	0.75	14.48	0.01	11.31	0.23	5.07	10.12	1.96	0.57	0.12	0.04	**98.97**
		B26-A1-unk1	Gl	53.88	0.75	14.10	0.00	10.97	0.20	4.88	9.93	1.93	0.57	0.09	0.02	**97.32**
		B26-A2-unk1	Gl	53.45	0.71	13.98	0.04	10.79	0.20	4.88	9.92	1.89	0.59	0.12	0.01	**96.58**
		B26-A3-unk1	Gl	53.79	0.72	14.09	0.04	10.71	0.21	4.96	9.87	1.94	0.58	0.11	0.01	**97.03**
		B26-B1-glass	Gl	54.09	0.73	14.15	0.00	10.78	0.22	5.12	9.80	1.89	0.54	0.10	0.00	**97.42**
		B26-B2-glass	Gl	53.59	0.71	13.97	0.04	10.95	0.19	5.13	9.83	1.91	0.56	0.06	0.00	**96.94**
		B26-B3-glass	Gl	53.52	0.70	13.99	0.00	10.64	0.24	5.08	9.87	1.91	0.52	0.11	0.00	**96.58**
		26/10/2012 Glass1	Gl	55.36	0.71	13.57	*BDL*	10.69	0.24	5.15	10.05	1.76	0.57	0.11	*BDL*	**98.21**
		26/10/2012 Glass1	Gl	55.9	0.69	13.73	*BDL*	11.03	0.19	5.33	10.15	1.79	0.50	0.09	*BDL*	**99.40**
		26/10/2012 Glass1	Gl	55.46	0.68	13.54	*BDL*	10.92	0.21	5.34	10.17	1.67	0.56	0.14	*BDL*	**98.69**
		26/10/2012 Glass1	Gl	55.09	0.70	13.67	*BDL*	11.00	0.26	5.55	10.32	1.66	0.51	0.12	*BDL*	**98.88**
		26/10/2012 Glass1	Gl	55.6	0.71	13.79	*BDL*	10.22	0.20	5.32	10.02	1.89	0.58	0.09	*BDL*	**98.42**
		26/10/2012 Glass2	Gl	55.18	0.68	13.74	*BDL*	11.24	0.22	5.26	10.13	1.65	0.51	0.12	*BDL*	**98.73**
		26/10/2012 Glass2	Gl	54.45	0.69	13.78	*BDL*	11.16	0.22	5.19	10.09	1.79	0.57	0.09	*BDL*	**98.03**
		26/10/2012 Glass2	Gl	54.1	0.67	13.75	*BDL*	11.20	0.21	5.15	10.11	1.75	0.52	0.07	0.06	**97.59**
		26/10/2012 Glass2	Gl	53.49	0.68	13.46	*BDL*	11.37	0.25	5.20	10.15	1.76	0.52	0.10	*BDL*	**96.98**
		26/10/2012 Glass2	Gl	54.94	0.69	13.92	*BDL*	10.90	0.22	5.14	9.99	1.88	0.57	0.09	*BDL*	**98.34**
		B26/10/12 Plag 1	Pl	49.67	*BDL*	29.07	*BDL*	1.07	*BDL*	0.29	15.69	2.26	0.08	*BDL*	*BDL*	**98.13**
		B26/10/12 Plag 1	Pl	48.97	*BDL*	28.47	*BDL*	1.06	*BDL*	0.31	15.29	2.40	0.08	*BDL*	*BDL*	**96.58**
		B26/10/12 Plag 1	Pl	49.6	0.03	29.36	*BDL*	1.16	*BDL*	0.40	15.70	2.52	0.07	*BDL*	*BDL*	**98.84**
		B26/10/12 Plag 1	Pl	50.49	0.03	29.46	*BDL*	1.13	*BDL*	0.32	15.83	2.41	0.09	*BDL*	*BDL*	**99.76**
		B26/10/12 Plag 1	Pl	49.15	0.03	29.36	*BDL*	1.11	*BDL*	0.30	15.64	2.52	0.12	*BDL*	*BDL*	**98.23**
		B26/10/12 Plag 2	Pl	49.83	*BDL*	28.79	*BDL*	1.04	*BDL*	0.29	15.29	2.59	0.11	*BDL*	*BDL*	**97.94**
		B26/10/12 Plag 2	Pl	50.33	*BDL*	28.87	*BDL*	1.08	*BDL*	0.30	15.27	2.86	0.09	*BDL*	*BDL*	**98.80**
		B26/10/12 Plag 2	Pl	48.71	*BDL*	29.49	*BDL*	0.98	*BDL*	0.29	15.80	2.49	0.10	*BDL*	*BDL*	**97.86**
		B26/10/12 Plag 2	Pl	49.32	0.03	28.93	*BDL*	1.03	*BDL*	0.32	15.37	2.51	0.09	*BDL*	*BDL*	**97.60**
		B26/10/12 Plag 2	Pl	48.75	*BDL*	29.83	*BDL*	0.95	*BDL*	0.25	16.13	2.28	0.06	*BDL*	*BDL*	**98.25**

Experiment	Condition	Name	Phase	SiO2	TiO2	Al2O3	Cr2O3	FeO	MnO	MgO	CaO	Na2O	K2O	P2O5	NiO	Total
B02-12	1atm, 1196 °C	B02-A1-glass	Gl	53.44	0.60	17.00	0.04	9.56	0.20	4.14	10.83	2.11	0.58	0.14	0.00	**98.62**
		B02-A2-glass	Gl	53.60	0.62	16.96	0.06	9.47	0.18	4.24	11.04	2.03	0.59	0.10	0.04	**98.92**
		B02-A3-glass	Gl	53.40	0.60	17.02	0.02	9.71	0.18	4.18	11.01	2.02	0.58	0.08	0.01	**98.83**
		B02-A4-glass	Gl	53.05	0.61	17.03	0.02	9.69	0.16	4.19	10.94	1.99	0.55	0.14	0.02	**98.39**
		B02-A5-glass	Gl	53.65	0.58	17.11	0.02	9.76	0.22	4.18	11.02	2.01	0.57	0.07	0.01	**99.21**
		B02-A6-glass	Gl	54.10	0.57	17.06	0.00	9.56	0.17	4.17	10.97	2.00	0.58	0.10	0.03	**99.30**
		B02-A1-unk4	Gl	53.48	0.63	16.63	0.01	9.68	0.17	4.24	11.02	1.86	0.58	0.08	0.01	**98.39**
		B02-A1-unk6	Gl	53.45	0.61	17.06	0.00	9.62	0.22	4.21	10.93	2.01	0.55	0.09	0.04	**98.80**
		B02-A2-unk6	Gl	53.88	0.58	17.07	0.01	9.97	0.18	4.26	10.93	1.97	0.58	0.08	0.03	**99.54**
		B02-B1-glass	Gl	54.79	0.68	15.30	0.01	10.31	0.19	4.65	10.34	1.99	0.73	0.09	0.03	**99.11**
		B02-B2-glass	Gl	54.43	0.67	15.11	0.01	10.22	0.25	4.66	10.26	2.01	0.70	0.13	0.00	**98.46**
		B02-B3-glass	Gl	54.72	0.68	15.39	0.02	10.01	0.21	4.61	10.25	2.02	0.74	0.08	0.00	**98.74**
		B02-B4-glass	Gl	54.87	0.67	15.11	0.00	10.33	0.21	4.65	10.42	2.01	0.69	0.02	0.02	**99.00**
		B02-B5-glass	Gl	55.05	0.67	15.12	0.00	10.02	0.21	4.66	10.43	2.01	0.69	0.11	0.00	**98.98**
		B02-B6-glass	Gl	54.88	0.69	15.19	0.00	10.03	0.18	4.63	10.48	2.00	0.71	0.15	0.00	**98.92**
		B02-B1-unk2	Gl	54.97	0.67	14.94	0.03	9.95	0.21	3.67	10.21	1.90	0.71	0.10	0.01	**97.37**
		B02-B2-unk2	Gl	55.10	0.67	15.06	0.02	10.26	0.21	4.75	10.27	1.98	0.70	0.09	0.03	**99.16**
		B02-B1-unk3	Gl	55.37	0.68	15.09	0.01	9.70	0.22	4.69	10.35	1.99	0.74	0.14	0.04	**99.02**
		B02-B2-unk3	Gl	54.92	0.65	15.32	0.00	9.53	0.17	4.65	10.51	2.02	0.73	0.15	0.02	**98.67**
		B02-B2-unk4	Gl	54.77	0.67	15.06	0.00	10.19	0.19	4.71	10.41	1.99	0.71	0.08	0.03	**98.81**
		02/10/2012 Glass1	Gl	53.24	0.58	16.02	*BDL*	9.50	0.16	4.37	11.05	1.71	0.54	0.08	*BDL*	**97.25**
		02/10/2012 Glass1	Gl	54.11	0.58	16.52	*BDL*	9.39	0.19	4.34	11.04	1.79	0.55	0.08	*BDL*	**98.59**
		02/10/2012 Glass1	Gl	53.61	0.57	16.19	*BDL*	9.34	0.23	4.33	10.98	1.62	0.54	0.08	*BDL*	**97.49**
		02/10/2012 Glass1	Gl	54.23	0.58	16.47	*BDL*	9.40	0.23	4.32	10.89	1.86	0.53	0.10	*BDL*	**98.61**
		02/10/2012 Glass1	Gl	53.82	0.58	16.43	*BDL*	9.34	0.18	4.33	10.94	1.70	0.53	0.10	*BDL*	**97.95**
		02/10/2012 Glass2	Gl	55.43	0.67	14.86	*BDL*	9.84	0.22	4.88	10.44	1.72	0.63	0.08	*BDL*	**98.77**
		02/10/2012 Glass2	Gl	55.34	0.66	15.06	*BDL*	9.62	0.25	4.79	10.35	1.91	0.69	0.10	*BDL*	**98.77**
		02/10/2012 Glass2	Gl	55.57	0.66	14.56	*BDL*	10.05	0.26	4.95	10.30	1.71	0.69	0.11	*BDL*	**98.86**
		02/10/2012 Glass2	Gl	55.53	0.66	14.65	*BDL*	10.11	0.25	4.91	10.38	1.82	0.70	0.12	*BDL*	**99.13**
		02/10/2012 Glass2	Gl	55.65	0.63	15.12	*BDL*	9.72	0.21	4.77	10.36	1.84	0.71	0.07	*BDL*	**99.08**
		B02/10/12 Plag 1	Pl	48.97	0.04	29.61	*BDL*	0.92	*BDL*	0.25	15.76	2.39	0.10	*BDL*	*BDL*	**98.04**
		B02/10/12 Plag 1	Pl	49.8	*BDL*	29.57	*BDL*	0.96	*BDL*	0.25	15.85	2.41	0.08	*BDL*	*BDL*	**98.92**
		B02/10/12 Plag 1	Pl	49.85	0.03	29.56	*BDL*	0.89	*BDL*	0.28	15.70	2.34	0.12	*BDL*	*BDL*	**98.77**
		B02/10/12 Plag 1	Pl	48.5	*BDL*	29.59	*BDL*	0.93	*BDL*	0.28	15.92	2.31	0.10	*BDL*	*BDL*	**97.63**
		B02/10/12 Plag 1	Pl	48.97	*BDL*	29.22	*BDL*	0.85	*BDL*	0.27	15.78	2.39	0.09	*BDL*	*BDL*	**97.57**

Experiment	Condition	Name	Phase	SiO2	TiO2	Al2O3	Cr2O3	FeO	MnO	MgO	CaO	Na2O	K2O	P2O5	NiO	Total
B16-12	1atm, 1242 °C	B16-A1-glass	Gl	53.81	0.61	17.10	0.00	9.76	0.17	4.30	11.16	1.98	0.49	0.09	0.04	**99.50**
		B16-A2-glass	Gl	54.00	0.63	17.07	0.00	9.66	0.21	4.20	11.17	1.99	0.47	0.05	0.03	**99.48**
		B16-A3-glass	Gl	53.69	0.60	17.05	0.01	9.79	0.23	4.28	11.05	1.99	0.48	0.10	0.05	**99.32**
		B16-A4-glass	Gl	54.35	0.62	16.96	0.00	9.57	0.19	4.08	10.98	2.04	0.48	0.14	0.02	**99.42**
		B16-A5-glass	Gl	54.01	0.58	17.01	0.01	9.44	0.23	4.20	10.97	2.03	0.49	0.12	0.00	**99.09**
		B16-A6-glass	Gl	54.27	0.57	16.93	0.00	9.48	0.17	4.19	11.01	2.04	0.52	0.10	0.00	**99.25**
		B16-A2-unk1	Gl	54.09	0.57	16.39	0.03	9.41	0.17	4.13	11.04	1.85	0.47	0.07	0.02	**98.26**
		B16-A1-unk2	Gl	54.06	0.61	17.02	0.00	9.66	0.17	4.12	11.07	2.05	0.52	0.06	0.00	**99.34**
		B16-A2-unk2	Gl	53.99	0.55	17.07	0.00	9.56	0.17	4.15	11.07	2.07	0.49	0.12	0.00	**99.24**
		B16-A3-unk2	Gl	54.06	0.57	17.10	0.00	9.57	0.17	4.16	11.06	2.07	0.48	0.07	0.01	**99.32**
		B16-A3-unk3	Gl	53.87	0.64	16.94	0.02	9.63	0.21	4.26	11.11	1.99	0.47	0.10	0.05	**99.28**
		B16-B1-glass	Gl	53.40	0.60	17.08	0.00	9.75	0.19	4.17	10.81	2.04	0.52	0.11	0.06	**98.73**
		B16-B2-glass	Gl	53.85	0.60	17.06	0.04	9.78	0.17	4.12	10.84	2.06	0.53	0.09	0.01	**99.15**
		B16-B3-glass	Gl	53.38	0.60	17.01	0.02	9.72	0.17	4.10	10.88	2.09	0.48	0.09	0.03	**98.56**
		B16-B4-glass	Gl	53.39	0.62	17.04	0.01	9.95	0.15	4.15	10.68	2.06	0.52	0.11	0.05	**98.73**
		B16-B5-glass	Gl	54.16	0.56	17.08	0.03	9.67	0.16	4.13	10.76	2.10	0.50	0.10	0.00	**99.26**
		B16-B6-glass	Gl	53.44	0.60	16.94	0.00	9.76	0.18	4.18	10.91	2.05	0.52	0.06	0.06	**98.71**
		B16-B1-unk1	Gl	52.93	0.56	16.98	0.06	9.97	0.18	4.20	10.87	2.04	0.50	0.11	0.04	**98.45**
		B16-B1-unk2	Gl	53.25	0.59	16.51	0.00	9.78	0.21	4.12	10.73	1.91	0.49	0.11	0.04	**97.75**
		B16-B1-unk4	Gl	53.32	0.60	16.64	0.00	9.93	0.17	4.06	10.89	1.97	0.50	0.08	0.07	**98.24**
		B16-B2-unk4	Gl	53.50	0.59	16.98	0.01	9.85	0.19	4.13	10.84	2.04	0.52	0.10	0.02	**98.77**
		B16-B3-unk4	Gl	53.26	0.61	16.86	0.01	9.75	0.13	4.07	10.87	2.04	0.52	0.11	0.04	**98.25**
		16/10/2012 Glass1	Gl	55.09	0.57	16.80	*BDL*	9.21	0.16	4.25	10.92	1.83	0.45	0.10	*BDL*	**99.38**
		16/10/2012 Glass1	Gl	54.66	0.59	16.98	*BDL*	9.15	0.17	4.26	10.99	1.84	0.47	0.06	*BDL*	**99.17**
		16/10/2012 Glass1	Gl	54.8	0.57	16.68	*BDL*	9.28	0.16	4.31	10.92	1.86	0.55	0.07	*BDL*	**99.20**
		16/10/2012 Glass1	Gl	54.8	0.60	16.71	*BDL*	9.52	0.21	4.44	11.08	1.78	0.47	0.09	*BDL*	**99.70**
		16/10/2012 Glass1	Gl	54.06	0.56	16.85	*BDL*	9.41	0.21	4.33	11.09	1.73	0.46	0.09	*BDL*	**98.79**
		16/10/2012 Glass2	Gl	55.17	0.58	16.73	*BDL*	9.61	0.20	4.34	10.91	1.96	0.50	0.10	*BDL*	**100.10**
		16/10/2012 Glass2	Gl	54.23	0.58	16.58	*BDL*	9.65	0.16	4.30	10.82	1.83	0.51	0.08	*BDL*	**98.74**
		16/10/2012 Glass2	Gl	54.62	0.60	16.62	0.04	9.35	0.19	4.27	10.77	1.63	0.50	0.09	*BDL*	**98.68**
		16/10/2012 Glass2	Gl	54.48	0.58	16.71	*BDL*	9.17	0.19	4.23	10.76	1.96	0.52	0.08	*BDL*	**98.68**
		16/10/2012 Glass2	Gl	54.54	0.57	16.53	*BDL*	9.51	0.21	4.19	10.86	1.94	0.51	0.09	*BDL*	**98.95**
		B16/10/12 Plag 1	Pl	49.87	0.12	27.14	*BDL*	2.41	*BDL*	0.95	15.17	2.40	0.21	*BDL*	*BDL*	**98.27**
		B16/10/12 Plag 1	Pl	50.35	*BDL*	29.07	*BDL*	1.30	*BDL*	0.41	15.36	2.48	0.08	*BDL*	*BDL*	**99.05**
		B16/10/12 Plag 1	Pl	51.26	0.03	28.74	*BDL*	1.12	*BDL*	0.38	15.07	2.66	0.12	*BDL*	*BDL*	**99.38**
		B16/10/12 Plag 1	Pl	50.74	*BDL*	27.91	*BDL*	1.24	*BDL*	0.35	14.98	2.90	0.09	*BDL*	*BDL*	**98.21**
		B16/10/12 Plag 1	Pl	50.27	*BDL*	28.48	*BDL*	1.18	*BDL*	0.36	15.04	2.71	0.09	0.04	*BDL*	**98.17**
		B16/10/12 Plag 2	Pl	49.96	0.03	29.36	*BDL*	1.22	*BDL*	0.34	15.48	2.37	0.10	*BDL*	*BDL*	**98.86**
		B16/10/12 Plag 2	Pl	50.32	0.03	28.71	*BDL*	1.16	*BDL*	0.35	15.26	2.44	0.08	*BDL*	*BDL*	**98.35**
		B16/10/12 Plag 2	Pl	51	0.04	28.48	*BDL*	1.24	*BDL*	0.39	14.95	2.72	0.11	*BDL*	*BDL*	**98.93**
		B16/10/12 Plag 2	Pl	50.48	*BDL*	28.71	*BDL*	1.21	*BDL*	0.37	15.25	2.85	0.10	*BDL*	*BDL*	**98.97**
		B16/10/12 Plag 2	Pl	50.12	0.03	28.50	*BDL*	1.24	*BDL*	0.42	15.21	2.83	0.09	*BDL*	*BDL*	**98.44**

Experiment	Condition	Name	Phase	SiO2	TiO2	Al2O3	Cr2O3	FeO	MnO	MgO	CaO	Na2O	K2O	P2O5	NiO	Total
2008	2.5kb, 1000 °C	Run 2008 Glass	Gl	99.12	0.18	1.11	*BDL*	0.64	*BDL*	0.07	0.33	0.12	*BDL*	*BDL*	*BDL*	**101.57**
		Run 2008 Glass	Gl	91.76	0.3	3.16	*BDL*	2.4	0.06	0.19	1.22	0.57	0.69	0.11	*BDL*	**100.46**
		Run 2008 Glass	Gl	62.26	0.68	21.07	*BDL*	4.11	*BDL*	0.17	11.03	2.55	0.15	*BDL*	*BDL*	**102.02**
		Run 2008 Glass	Gl	97.63	0.19	1.05	*BDL*	0.68	*BDL*	0.1	0.27	0.14	0.16	*BDL*	*BDL*	**100.22**
		Run 2008 Glass	Gl	81.69	0.13	12.4	*BDL*	1.02	*BDL*	0.13	6.32	1.03	0.09	*BDL*	*BDL*	**102.81**
		2008 Plag	Pl	50.67	*BDL*	30.22	*BDL*	1.18	*BDL*	0.24	14.92	3.07	0.08	*BDL*	*BDL*	**100.38**
		2008 Plag	Pl	47.52	*BDL*	32.74	*BDL*	1.25	*BDL*	0.17	17.42	1.53	*BDL*	*BDL*	*BDL*	**100.63**
		2008 Plag	Pl	51.52	0.04	29.38	*BDL*	1.6	*BDL*	0.25	14.46	3.13	0.11	*BDL*	*BDL*	**100.49**
		2008 Plag	Pl	50.75	*BDL*	30.24	*BDL*	1.52	*BDL*	0.23	15.08	2.73	0.11	*BDL*	*BDL*	**100.66**
		2008 Plag	Pl	46.6	*BDL*	33.58	*BDL*	1.14	*BDL*	0.16	17.96	1.34	0.05	*BDL*	*BDL*	**100.83**
		2008 Plag	Pl	46.28	*BDL*	33.69	*BDL*	1.26	*BDL*	0.14	18.05	1.34	0.05	*BDL*	*BDL*	**100.81**
		2008 Plag	Pl	46.78	*BDL*	33.03	*BDL*	1.13	*BDL*	0.18	17.5	1.44	0.05	*BDL*	*BDL*	**100.11**
		2008 Plag	Pl	48.24	*BDL*	32.3	*BDL*	1.18	*BDL*	0.19	16.81	2.01	0.05	*BDL*	*BDL*	**100.78**
		2008 Plag	Pl	45.84	*BDL*	33.61	*BDL*	1.18	*BDL*	0.14	18.04	1.27	*BDL*	*BDL*	*BDL*	**100.08**
		2008 Plag	Pl	46.11	*BDL*	33.09	*BDL*	1.18	*BDL*	0.17	17.62	1.21	0.05	*BDL*	*BDL*	**99.43**
		2008 Pyroxene	Cpx	52.97	0.21	1.92	0.06	10.11	0.33	17.02	18.72	0.07	*BDL*	*BDL*	*BDL*	**101.41**
		2008 Pyroxene	Cpx	53.51	0.13	0.84	0.04	19.32	0.54	21.84	4.77	*BDL*	*BDL*	*BDL*	*BDL*	**100.99**
		2008 Pyroxene	Cpx	53	0.15	1.11	*BDL*	19.44	0.52	21.56	5.15	*BDL*	*BDL*	*BDL*	*BDL*	**100.93**
		2008 Pyroxene	Cpx	53.1	0.18	1.18	*BDL*	19.18	0.53	21.27	5.69	*BDL*	*BDL*	*BDL*	*BDL*	**101.13**
		2008 Pyroxene	Cpx	53.88	0.11	0.82	*BDL*	19.46	0.54	21.83	4.54	*BDL*	*BDL*	*BDL*	*BDL*	**101.18**
		2008 Pyroxene	Cpx	53.5	0.15	1	*BDL*	19.65	0.49	21.37	5.18	0.09	*BDL*	*BDL*	*BDL*	**101.43**
		2008 Pyroxene	Cpx	53.3	0.12	0.81	*BDL*	19.38	0.44	21.94	4.94	*BDL*	*BDL*	*BDL*	*BDL*	**100.93**
		2008 Pyroxene	Cpx	52.79	0.11	0.75	*BDL*	19.56	0.52	21.89	4.72	0.07	*BDL*	*BDL*	*BDL*	**100.41**
		2008 Pyroxene	Cpx	54.01	0.12	1.24	*BDL*	16.55	0.45	26.22	2.23	0.06	*BDL*	*BDL*	*BDL*	**100.88**
		2008 Pyroxene	Cpx	53.3	0.14	0.92	*BDL*	19.7	0.6	21.62	4.79	*BDL*	*BDL*	*BDL*	*BDL*	**101.07**
		2008 Pyroxene Transect	Cpx	59.62	0.55	7.66	*BDL*	19.14	0.35	2.86	5.89	1.57	1.84	0.15	*BDL*	**99.63**
		2009 Pyroxene Transect	Cpx	47.69	0.76	2.91	*BDL*	30.01	0.63	8.27	8.9	0.11	0.04	*BDL*	*BDL*	**99.32**
		2010 Pyroxene Transect	Cpx	47.75	0.73	2.63	*BDL*	29.43	0.69	9.25	8.93	*BDL*	0.04	*BDL*	*BDL*	**99.45**
		2011 Pyroxene Transect	Cpx	47.86	0.66	2.43	*BDL*	28.17	0.69	10.58	8.68	0.1	*BDL*	*BDL*	*BDL*	**99.17**
		2012 Pyroxene Transect	Cpx	48.79	0.51	2.26	*BDL*	27.46	0.62	11.78	8.23	0.09	*BDL*	*BDL*	*BDL*	**99.74**
		2013 Pyroxene Transect	Cpx	49.62	0.39	2.15	*BDL*	26.87	0.62	13.43	7.17	0.09	*BDL*	*BDL*	*BDL*	**100.34**
		2014 Pyroxene Transect	Cpx	49.44	0.35	2.1	*BDL*	25.69	0.58	14.4	6.95	0.14	*BDL*	*BDL*	*BDL*	**99.65**
		2015 Pyroxene Transect	Cpx	50.03	0.31	2.07	*BDL*	24.12	0.58	15.39	6.78	*BDL*	*BDL*	*BDL*	*BDL*	**99.28**
		2016 Pyroxene Transect	Cpx	50.38	0.31	1.98	*BDL*	23.07	0.59	16.49	6.64	*BDL*	*BDL*	*BDL*	*BDL*	**99.46**
		2017 Pyroxene Transect	Cpx	50.8	0.3	1.9	*BDL*	21.81	0.53	17.24	6.52	0.12	*BDL*	*BDL*	*BDL*	**99.22**
		2018 Pyroxene Transect	Cpx	51.84	0.26	1.72	*BDL*	21	0.45	18.32	6.31	*BDL*	*BDL*	*BDL*	*BDL*	**99.9**
		2019 Pyroxene Transect	Cpx	52.58	0.21	1.48	*BDL*	20.05	0.52	19.38	6.02	*BDL*	*BDL*	*BDL*	*BDL*	**100.24**
		2020 Pyroxene Transect	Cpx	52.36	0.17	1.28	*BDL*	19.06	0.51	20.23	5.9	*BDL*	*BDL*	*BDL*	*BDL*	**99.51**
		2021 Pyroxene Transect	Cpx	52.53	0.18	1.18	*BDL*	18.87	0.51	20.78	5.99	*BDL*	*BDL*	*BDL*	*BDL*	**100.04**
		2022 Pyroxene Transect	Cpx	53.05	0.15	1.18	*BDL*	19.1	0.49	20.89	5.95	0.1	*BDL*	*BDL*	*BDL*	**100.91**
		2023 Pyroxene Transect	Cpx	52.91	0.18	1.12	*BDL*	19.04	0.51	21.06	5.82	*BDL*	*BDL*	*BDL*	*BDL*	**100.64**
		2024 Pyroxene Transect	Cpx	52.75	0.16	1.13	*BDL*	18.86	0.52	21.1	5.78	*BDL*	*BDL*	*BDL*	*BDL*	**100.3**
		2025 Pyroxene Transect	Cpx	53.35	0.16	1.07	*BDL*	18.96	0.58	20.97	5.89	0.06	*BDL*	*BDL*	*BDL*	**101.04**
		2026 Pyroxene Transect	Cpx	47.97	0.16	0.97	*BDL*	21.87	0.52	19.07	6.25	0.12	*BDL*	*BDL*	*BDL*	**96.93**
		2027 Pyroxene Transect	Cpx	52.55	0.15	1.08	*BDL*	18.8	0.54	21.18	5.45	*BDL*	*BDL*	*BDL*	*BDL*	**99.75**
		2028 Pyroxene Transect	Cpx	52.93	0.15	1.07	*BDL*	18.98	0.47	21.2	5.36	*BDL*	*BDL*	*BDL*	*BDL*	**100.16**
		2029 Pyroxene Transect	Cpx	53.12	0.18	1.04	0.04	19.22	0.49	21.32	5.26	0.09	*BDL*	*BDL*	*BDL*	**100.76**
		2030 Pyroxene Transect	Cpx	53.27	0.15	1.02	*BDL*	18.98	0.52	21.28	5.18	0.11	*BDL*	*BDL*	*BDL*	**100.51**
		2031 Pyroxene Transect	Cpx	52.86	0.14	1.01	*BDL*	18.97	0.49	21.34	5.09	0.07	*BDL*	*BDL*	*BDL*	**99.97**

Experiment	Condition	Name	Phase	SiO2	TiO2	Al2O3	Cr2O3	FeO	MnO	MgO	CaO	Na2O	K2O	P2O5	NiO	Total
		2032 Pyroxene Transect	Cpx	52.97	0.14	1.05	*BDL*	19.24	0.5	21.39	5.04	*BDL*	*BDL*	*BDL*	*BDL*	**100.33**
		2033 Pyroxene Transect	Cpx	52.94	0.14	0.99	*BDL*	19.39	0.48	21.38	4.92	*BDL*	*BDL*	*BDL*	*BDL*	**100.24**
		2034 Pyroxene Transect	Cpx	53.37	0.16	0.97	*BDL*	19.21	0.49	21.51	4.85	*BDL*	*BDL*	*BDL*	*BDL*	**100.56**
		2035 Pyroxene Transect	Cpx	52.6	0.14	0.91	*BDL*	19.03	0.54	21.4	4.81	*BDL*	*BDL*	*BDL*	*BDL*	**99.43**
		2036 Pyroxene Transect	Cpx	53.17	0.14	0.87	*BDL*	19.07	0.49	21.36	4.87	*BDL*	*BDL*	*BDL*	*BDL*	**99.97**
		2037 Pyroxene Transect	Cpx	52.5	0.14	0.92	*BDL*	19.26	0.49	21.52	4.96	*BDL*	*BDL*	*BDL*	*BDL*	**99.79**
		2038 Pyroxene Transect	Cpx	53.42	0.14	0.94	*BDL*	19.23	0.49	21.37	4.92	0.07	*BDL*	*BDL*	*BDL*	**100.58**
		2039 Pyroxene Transect	Cpx	53.29	0.14	0.9	*BDL*	19.1	0.49	21.66	4.86	*BDL*	*BDL*	*BDL*	*BDL*	**100.44**
		2040 Pyroxene Transect	Cpx	52.86	0.15	0.94	*BDL*	19.12	0.48	21.67	4.97	0.09	*BDL*	*BDL*	*BDL*	**100.28**
		2041 Pyroxene Transect	Cpx	52.62	0.14	0.93	*BDL*	18.99	0.51	21.43	5	*BDL*	*BDL*	*BDL*	*BDL*	**99.62**
		2042 Pyroxene Transect	Cpx	53.51	0.14	0.95	*BDL*	19.49	0.48	21.47	4.86	*BDL*	*BDL*	*BDL*	*BDL*	**100.9**
		2043 Pyroxene Transect	Cpx	53.2	0.16	2.29	*BDL*	19.3	0.53	19.71	5.15	0.16	*BDL*	*BDL*	*BDL*	**100.5**
M10-39	25kb, 1000 °C	M10-39 Glass	Gl	64.23	0.26	13.67	*BDL*	2.16	*BDL*	0.74	4.99	0.74	2.46	*BDL*	*BDL*	**89.25**
		M10-39 Glass	Gl	64.49	0.25	13.96	*BDL*	2.04	*BDL*	0.64	4.81	0.59	0.8	0.12	*BDL*	**87.7**
		M10-39 Glass	Gl	65.11	0.27	13.61	*BDL*	2.12	*BDL*	0.71	4.88	1.23	0.89	0.09	*BDL*	**88.91**
		M10-39 Glass	Gl	65.16	0.25	13.4	*BDL*	1.99	*BDL*	0.67	4.75	0.74	0.85	0.12	*BDL*	**87.93**
		M10-39 Glass	Gl	64.52	0.25	13.71	*BDL*	2.21	*BDL*	0.92	5.33	0.9	0.76	*BDL*	*BDL*	**88.6**
		M10-39 Pyroxene	Cpx	55.38	0.19	9.79	*BDL*	5.02	*BDL*	8.41	16.53	1.79	0.26	*BDL*	*BDL*	**97.37**
		M10-39 Pyroxene	Cpx	51.88	0.24	10.26	0.05	6.23	0.1	10.49	19.64	2.31	0.03	*BDL*	*BDL*	**101.23**
		M10-39 Pyroxene	Cpx	52.2	0.17	8.77	*BDL*	5.84	0.09	11.02	20.14	1.95	*BDL*	*BDL*	*BDL*	**100.18**
		M10-39 Pyroxene	Cpx	52.4	0.19	9.59	*BDL*	6.5	0.08	10.89	20.05	1.88	0.04	*BDL*	*BDL*	**101.62**
		M10-39 Pyroxene	Cpx	52.28	0.26	10.74	*BDL*	6.08	*BDL*	9.89	19.41	2.18	0.03	*BDL*	*BDL*	**100.87**
M10-40	10kb, 900 °C	M10-40 Glass	Gl	57.17	0.42	17.58	*BDL*	4.95	0.08	1.2	6.57	2.33	0.73	0.14	*BDL*	**91.17**
		M10-40 Glass	Gl	53.59	0.4	15.86	*BDL*	5.79	0.08	2.66	9.14	1.52	0.64	0.12	*BDL*	**89.8**
		M10-40 Glass	Gl	53.06	0.48	15.18	*BDL*	6.91	*BDL*	4.02	9.92	1.48	0.52	0.12	*BDL*	**91.69**
		M10-40 Glass	Gl	51.94	0.55	13.05	*BDL*	9.81	0.12	6.05	12.87	0.98	0.4	*BDL*	*BDL*	**95.77**
		M10-40 Glass	Gl	57.04	0.44	17.62	*BDL*	5.41	*BDL*	1.44	6.77	1.65	0.71	0.16	*BDL*	**91.24**
		M10-40 Pyroxene	Cpx	50.98	0.44	7.05	*BDL*	12.7	0.22	10.27	17.84	1.14	0.13	*BDL*	*BDL*	**100.77**
		M10-40 Pyroxene	Cpx	49.52	0.59	7.57	0.05	10.25	0.15	10.9	19.59	0.47	0.11	*BDL*	*BDL*	**99.2**
		M10-40 Pyroxene	Cpx	55.36	0.4	17.2	*BDL*	5.34	0.08	1.42	7.22	1.74	0.79	0.09	*BDL*	**89.64**
		M10-40 Pyroxene	Cpx	56.69	0.39	16.88	*BDL*	4.46	*BDL*	1.75	7.35	1.79	0.76	0.12	*BDL*	**90.19**
		M10-40 Pyroxene	Cpx	53.04	0.46	12.28	*BDL*	7.62	0.1	5.48	12.99	0.71	0.4	0.15	*BDL*	**93.23**

Experiment	Condition	Name	Phase	SiO2	TiO2	Al2O3	Cr2O3	FeO	MnO	MgO	CaO	Na2O	K2O	P2O5	NiO	Total
M10-41	25kb, 1060 °C	M10-41 Glass	Gl	59.14	0.48	15.81	*BDL*	4.23	0.13	2.14	8.48	3.15	0.69	0.17	*BDL*	**94.42**
		M10-41 Glass	Gl	58.17	0.49	15.72	*BDL*	4.37	0.07	2.18	8.68	2.11	0.74	0.18	*BDL*	**92.71**
		M10-41 Glass	Gl	58.95	0.47	15.75	*BDL*	4.14	0.12	2.12	8.59	2.36	0.66	0.13	*BDL*	**93.29**
		M10-41 Glass	Gl	58.34	0.49	15.88	*BDL*	3.97	0.1	2.13	8.51	2.04	0.66	0.11	*BDL*	**92.23**
		M10-41 Glass	Gl	62.14	0.37	14.85	*BDL*	2.96	*BDL*	1.42	7.57	2.04	0.89	*BDL*	*BDL*	**92.24**
		M10-41 Pyroxene	Cpx	51	0.23	10.39	*BDL*	6.12	0.11	9.88	19.01	1.72	0.16	*BDL*	*BDL*	**98.62**
		M10-41 Pyroxene	Cpx	39.13	1.05	21.03	*BDL*	19.22	0.6	7.23	12.11	*BDL*	*BDL*	*BDL*	*BDL*	**100.37**
		M10-41 Pyroxene	Cpx	53.78	0.51	14.66	*BDL*	7.13	0.12	3.79	14.26	1.93	0.29	0.08	*BDL*	**96.55**
		M10-41 Pyroxene	Cpx	59.78	0.5	15.53	*BDL*	3.67	0.09	1.53	7.33	2.29	0.71	0.16	*BDL*	**91.59**
		M10-41 Pyroxene	Cpx	51.8	0.17	6.41	*BDL*	7.2	0.11	12.32	21.37	1.26	*BDL*	*BDL*	*BDL*	**100.64**
M10-42	20kb, 1140 °C	M10-42 Glass	Gl	55.12	0.55	17.09	*BDL*	5.96	0.18	3.27	9.61	2.28	0.59	0.18	*BDL*	**94.83**
		M10-42 Glass	Gl	55.25	0.57	17.15	*BDL*	5.86	0.14	3.36	9.76	2.55	0.59	0.14	*BDL*	**95.37**
		M10-42 Glass	Gl	54.55	0.58	17.22	*BDL*	5.99	0.17	3.4	9.61	2.31	0.58	0.15	*BDL*	**94.56**
		M10-42 Glass	Gl	54.31	0.57	17.16	*BDL*	6.01	0.18	3.3	9.55	2.14	0.5	*BDL*	*BDL*	**93.72**
		M10-42 Glass	Gl	55.09	0.54	17.18	*BDL*	6	0.17	3.36	9.52	2.12	0.57	0.15	*BDL*	**94.7**
		M10-42 Pyroxene	Cpx	49.28	0.69	16.34	*BDL*	7.23	0.24	5.69	16.03	1.21	0.24	0.12	*BDL*	**97.07**
		M10-42 Pyroxene	Cpx	50.18	0.67	13.03	*BDL*	10.19	0.33	8.16	18.32	1.26	0.09	*BDL*	*BDL*	**102.23**
		M10-42 Pyroxene	Cpx	50.72	0.26	8.57	*BDL*	6.41	0.19	12.62	21.23	0.78	*BDL*	0.09	*BDL*	**100.87**
		M10-42 Pyroxene	Cpx	60.56	0.37	18.47	*BDL*	2.48	*BDL*	0.61	5.65	3.02	1.06	0.13	*BDL*	**92.35**
		M10-42 Pyroxene	Cpx	50.88	0.22	7.52	*BDL*	6.66	0.18	12.77	21.34	0.84	*BDL*	*BDL*	*BDL*	**100.41**
M10-43	25kb, 1200 °C	M10-43 Glass	Gl	54.64	0.56	16.27	*BDL*	6.42	0.18	4.59	13.73	1.45	0.45	0.13	*BDL*	**98.42**
		M10-43 Glass	Gl	55.07	0.58	16.84	*BDL*	4.72	0.13	3.3	9.41	2.18	0.53	0.12	*BDL*	**92.88**
		M10-43 Glass	Gl	55.09	0.6	16.78	*BDL*	4.93	0.18	3.45	9.95	2.09	0.56	0.1	*BDL*	**93.73**
		M10-43 Glass	Gl	55.51	0.61	16.83	*BDL*	4.88	0.13	3.43	9.73	1.87	0.56	0.12	*BDL*	**93.67**
		M10-43 Glass	Gl	56.43	0.53	16.45	*BDL*	4.42	0.13	2.89	9.24	2.37	0.68	*BDL*	*BDL*	**93.14**
		M10-43 Pyroxene	Cpx	53.12	0.56	15.41	*BDL*	6.18	0.18	4.48	14.2	1.88	0.4	*BDL*	*BDL*	**96.41**
		M10-43 Pyroxene	Cpx	55.29	0.47	16.24	*BDL*	2.59	0.12	1.73	8.06	2.08	0.58	*BDL*	*BDL*	**87.16**
		M10-43 Pyroxene	Cpx	58.19	0.6	17.21	*BDL*	3.58	0.11	2.13	6.62	1.93	0.64	0.14	*BDL*	**91.15**
		M10-43 Pyroxene	Cpx	55.94	0.58	16.6	*BDL*	4.92	0.12	3.26	9.38	2.45	0.52	0.12	*BDL*	**93.89**
		M10-43 Pyroxene	Cpx	56.56	0.58	16.63	*BDL*	4.84	0.15	2.94	9.07	2.15	0.54	0.11	*BDL*	**93.57**
		M10-43 Pyroxene	Cpx	57.73	0.59	17.08	*BDL*	4.26	0.13	2.22	8.65	2.59	0.68	0.15	*BDL*	**94.08**

Experiment	Condition	Name	Phase	SiO2	TiO2	Al2O3	Cr2O3	FeO	MnO	MgO	CaO	Na2O	K2O	P2O5	NiO	Total
M10-47	5kb, 900 °C	M10-47 Glass	Gl	51.9	0.72	14.43	*BDL*	12.57	0.26	4.74	8.63	1.18	0.48	*BDL*	*BDL*	**94.91**
		M10-47 Glass	Gl	54.01	0.64	15.51	*BDL*	8.97	0.16	2.18	7.56	1.54	0.69	0.09	*BDL*	**91.35**
		M10-47 Glass	Gl	55.86	0.47	18.86	*BDL*	6.53	0.12	1.23	9.18	1.27	0.65	0.09	*BDL*	**94.26**
		M10-47 Glass	Gl	55.7	0.71	16.32	*BDL*	8.17	0.18	1.55	6.98	1.51	0.62	0.11	*BDL*	**91.85**
		M10-47 Glass	Gl	55.44	0.68	15.44	*BDL*	7.99	0.16	1.54	6.43	1.17	0.66	*BDL*	*BDL*	**89.51**
		M10-47 Plag	Gl	53.86	0.58	17.02	*BDL*	6.79	0.14	1.46	7.71	1.39	0.77	0.13	*BDL*	**89.85**
		M10-47 Plag	Gl	54.97	0.71	17.84	*BDL*	7.26	0.16	1.17	7.72	1.57	0.62	0.12	*BDL*	**92.14**
		M10-47 Plag	Gl	51.24	0.43	23.9	*BDL*	4.99	0.07	0.66	9.88	1.47	0.47	0.12	*BDL*	**93.23**
		M10-47 Plag	Gl	47.99	0.12	23.13	*BDL*	9.44	0.22	5.09	12.58	1.1	*BDL*	*BDL*	*BDL*	**99.67**
		M10-47 Plag	Gl	51.27	0.77	10.12	*BDL*	13.61	0.28	7.47	13.49	0.97	0.32	0.09	*BDL*	**98.39**
		M10-47 Pyroxene	Cpx	52.44	0.37	22.52	*BDL*	4.43	0.14	1.28	12.01	1.81	0.53	0.09	*BDL*	**95.62**
		M10-47 Pyroxene	Cpx	53.56	0.6	12.88	*BDL*	8.73	0.18	4.05	9.02	0.52	0.56	0.13	*BDL*	**90.23**
		M10-47 Pyroxene	Cpx	53.62	0.47	17.27	*BDL*	8.12	0.21	2.61	9.35	1.48	0.6	0.15	*BDL*	**93.88**
		M10-47 Pyroxene	Cpx	50.6	0.42	28.32	*BDL*	5.9	0.08	1.12	8.87	2.48	0.45	0.12	0.06	**98.42**
		M10-47 Pyroxene	Cpx	52.67	0.36	23.34	*BDL*	4.53	0.07	1.26	12.62	1.96	0.43	*BDL*	*BDL*	**97.24**
		M10-47 Pyroxene	Cpx	52.79	0.6	15.06	*BDL*	8.09	0.14	2.81	8.38	1.15	0.66	0.12	*BDL*	**89.8**
		M10-47 Unknown	Cpx	51.98	0.36	13.35	*BDL*	14.01	0.28	6.96	10.11	0.72	0.31	0.09	*BDL*	**98.17**
		M10-47 Unknown	mix	53.45	0.44	20.5	*BDL*	5.93	0.13	0.99	8.37	1.52	0.59	*BDL*	*BDL*	**91.92**
		M10-47 Unknown	mix	49.72	0.57	6.5	*BDL*	16.22	0.38	10.23	12.33	0.46	0.24	*BDL*	*BDL*	**96.65**
		M10-47 Unknown	mix	58.13	0.5	15.89	*BDL*	6.46	0.17	1.13	5.85	1.36	0.94	0.18	*BDL*	**90.61**
M10-48	25kb, 1220 °C	M10-48 Glass	Gl	53.49	0.57	17.54	*BDL*	5.73	0.21	4.24	10.41	2.09	0.58	0.08	*BDL*	**94.94**
		M10-48 Glass	Gl	54.22	0.58	17.38	*BDL*	5.68	0.16	4.2	10	1.74	0.48	*BDL*	*BDL*	**94.44**
		M10-48 Glass	Gl	53.9	0.57	17.43	*BDL*	5.59	0.18	4.37	10.41	2.47	0.5	0.1	*BDL*	**95.52**
		M10-48 Glass	Gl	54.18	0.58	17.43	*BDL*	5.24	0.16	3.99	9.55	2.41	0.49	*BDL*	*BDL*	**94.03**
		M10-48 Glass	Gl	53.79	0.57	17.39	*BDL*	5.18	0.2	4.17	10.27	2.05	0.54	0.12	*BDL*	**94.28**
		M10-48 Pyroxene	Cpx	52.48	0.63	17.31	*BDL*	8.06	0.27	6.43	11.55	1.75	0.5	*BDL*	*BDL*	**98.98**
		M10-48 Pyroxene	Cpx	51.07	0.53	16.99	*BDL*	6.46	0.23	4.88	12.4	1.17	0.33	0.16	*BDL*	**94.22**
		M10-48 Pyroxene	Cpx	44.34	0.47	13.5	*BDL*	3.68	0.1	2.62	7.26	1.23	0.41	0.49	*BDL*	**74.1**
		M10-48 Pyroxene	Cpx	53.57	0.57	17.5	*BDL*	5.11	0.17	3.86	9.64	2.09	0.6	*BDL*	*BDL*	**93.11**
		M10-48 Pyroxene	Cpx	54.64	0.56	15.82	*BDL*	8.22	0.3	6.63	16.97	1.27	0.41	0.1	*BDL*	**104.92**

Experiment	Condition	Name	Phase	SiO2	TiO2	Al2O3	Cr2O3	FeO	MnO	MgO	CaO	Na2O	K2O	P2O5	NiO	Total
M10-50	25kb, 940 °C	M10-50 Glass	Gl	59.6	0.33	11.75	*BDL*	4.61	*BDL*	5.74	15.23	1.73	0.47	*BDL*	*BDL*	**99.46**
		M10-50 Glass	Gl	37.57	1.72	20.57	*BDL*	22.26	0.53	4.8	12.34	*BDL*	*BDL*	0.18	*BDL*	**99.97**
		M10-50 Glass	Gl	39.54	0.82	21.54	*BDL*	17.22	0.32	6.84	14.31	*BDL*	*BDL*	0.11	*BDL*	**100.7**
		M10-50 Glass	Gl	38.65	1.63	20.27	*BDL*	22.09	0.64	5.1	12.18	0.07	*BDL*	0.15	*BDL*	**100.78**
		M10-50 Glass	Gl	39.47	0.74	21.7	*BDL*	18.79	0.38	7.06	13.09	*BDL*	*BDL*	0.12	*BDL*	**101.35**
		M10-50 Pyroxene	Cpx	66.43	0.26	13.4	*BDL*	1.45	*BDL*	0.36	4.6	1.55	0.95	0.11	*BDL*	**89.11**
		M10-50 Pyroxene	Cpx	38.49	1.51	20.61	*BDL*	20.81	0.48	5.37	12.95	0.08	*BDL*	0.19	*BDL*	**100.49**
		M10-50 Pyroxene	Cpx	38.72	1.2	20.76	*BDL*	20.73	0.43	5.59	13.04	*BDL*	*BDL*	0.17	*BDL*	**100.64**
		M10-50 Pyroxene	Cpx	56.89	0.28	11.04	*BDL*	4.92	*BDL*	7.41	15.85	2.41	0.39	*BDL*	*BDL*	**99.19**
		M10-50 Pyroxene	Cpx	66.12	0.27	13.68	*BDL*	1.62	*BDL*	0.52	4.92	2.08	0.96	0.09	*BDL*	**90.26**
		M10-50 Pyroxene	Cpx	66.1	0.23	13.51	*BDL*	1.54	*BDL*	0.46	4.83	1.76	1	*BDL*	*BDL*	**89.43**
M10-60	15kb, 900 °C	M10-60 Glass	Gl	59.43	0.23	14.87	*BDL*	2.33	*BDL*	1.47	6.7	2.09	0.86	0.14	*BDL*	**88.12**
		M10-60 Glass	Gl	61.47	0.27	15.42	*BDL*	2.37	*BDL*	0.63	5.68	1.46	0.9	0.1	*BDL*	**88.3**
		M10-60 Glass	Gl	38.91	1.17	20.67	*BDL*	20.24	0.38	6.57	12.49	*BDL*	*BDL*	0.17	*BDL*	**100.6**
		M10-60 Glass	Gl	60.38	0.23	12.7	*BDL*	2.16	*BDL*	2.35	8.38	1.86	0.66	0.11	*BDL*	**88.83**
		M10-60 Glass	Gl	62.24	0.26	15.73	*BDL*	2.31	*BDL*	0.77	5.61	1.89	0.81	*BDL*	*BDL*	**89.62**
		M10-60 Glass	Gl	62.09	0.25	15.41	*BDL*	1.91	*BDL*	0.54	5.42	2.47	0.95	0.13	*BDL*	**89.17**
		M10-60 Pyroxene	Cpx	62.1	0.24	14.61	*BDL*	2.57	*BDL*	1.53	7.35	1.63	0.87	0.1	*BDL*	**91**
		M10-60 Pyroxene	Cpx	62.04	0.25	15.85	*BDL*	2.1	*BDL*	0.63	5.55	2.63	0.93	*BDL*	*BDL*	**89.98**
		M10-60 Pyroxene	Cpx	54.92	0.3	11.41	*BDL*	5.85	0.1	6.57	14.4	0.97	0.32	0.12	*BDL*	**94.96**
		M10-60 Pyroxene	Cpx	60.94	0.26	14.25	*BDL*	3.28	*BDL*	2.23	8.28	1.44	0.82	*BDL*	*BDL*	**91.5**
		M10-60 Pyroxene	Cpx	60.11	0.3	15.34	*BDL*	3.28	0.07	0.89	6.18	3.29	0.87	*BDL*	*BDL*	**90.33**
		M10-60 Pyroxene	Cpx	38.59	1.34	20.54	*BDL*	21.58	0.49	5.83	12.51	*BDL*	*BDL*	0.12	*BDL*	**101**
M10-62	10kb, 980 °C	M10-62 Glass?Plag?	Gl	53.55	0.52	16.93	*BDL*	8.6	0.19	4.11	11.34	1.94	0.47	0.12	*BDL*	**97.77**
		M10-62 Glass?Plag?	Gl	54.8	0.68	13.39	*BDL*	11.45	0.25	5.17	9.61	0.91	0.67	0.13	*BDL*	**97.06**
		M10-62 Glass?Plag?	Gl	39.13	1.35	20.77	0.05	23.53	0.74	7.14	8.36	*BDL*	*BDL*	0.11	*BDL*	**101.18**
		M10-62 Glass?Plag?	Gl	56.78	0.44	20.31	*BDL*	4.79	0.07	1.15	10.11	2.37	0.67	0.1	*BDL*	**96.79**
		M10-62 Pyroxene	Gl	54.75	0.63	12.88	*BDL*	10.76	0.23	5.16	10.07	1.15	0.72	0.11	*BDL*	**96.46**
		M10-62 Pyroxene	Gl	53.97	0.4	19.95	*BDL*	6.83	0.13	3.01	12	2.4	0.42	*BDL*	*BDL*	**99.11**
		M10-62 Pyroxene	Gl	56.89	0.44	22.21	*BDL*	4.8	*BDL*	0.8	9.68	2.71	0.55	0.11	*BDL*	**98.19**
		M10-62 Pyroxene	Gl	55.97	0.42	20.88	*BDL*	4.86	0.09	1.64	10.61	2.5	0.6	0.11	*BDL*	**97.68**
		M10-62 Pyroxene	Gl	56.67	0.61	13.66	*BDL*	9.35	0.2	3.98	9.34	1.68	0.84	0.15	*BDL*	**96.48**
		M10-62 Glass?Plag?	Cpx	51.58	0.59	8.84	*BDL*	15.42	0.36	9.53	13.12	0.82	0.28	0.11	*BDL*	**100.65**
		M10-62 Glass?Plag?	Cpx	53.05	0.63	11.56	*BDL*	11.53	0.25	6.2	10.44	0.77	0.55	0.09	*BDL*	**95.07**
		M10-62 Unknown	Cpx	55.15	0.62	13.89	*BDL*	11.48	0.22	5.91	10.85	1.66	0.56	0.15	*BDL*	**100.49**
		M10-62 Unknown	Cpx	53.82	0.65	12.27	*BDL*	11.97	0.21	6.03	10.95	1.39	0.59	0.08	*BDL*	**97.96**
		M10-62 Unknown	Cpx	53.8	0.66	12.72	*BDL*	13	0.21	5.62	10.34	1.09	0.5	0.16	*BDL*	**98.1**